Faculty of Science
Palacký University
Olomouc

Quantum nonlinearity constructed from individual photons

Mgr. Petr Marek, Ph. D.

Habilitation thesis

Olomouc 2017

Přírodovědecká fakulta
Univerzita Palackého
Olomouc

Kvantová nelinearita budovaná jednotlivými fotony

Mgr. Petr Marek, Ph. D.

Habilitační práce

Olomouc 2017

Acknowledgements

I would like to express my sincerest gratitude to my colleagues and co-authors, both from the Department of Optics at Palacký University and from the rest of the world. I would especially like to thank Radim Filip for the countless hours spent discussing topics ranging from mundane to bizarre. Last but not least, I would like to thank my family and my friends. They know what they did.

Petr Marek

Declaration of originality

I hereby confirm that I am the sole author of the submitted thesis which, to the best of my knowledge and belief, contains no material previously published by another person, except where due acknowledgement has been made.

The author grants permission to Palacký University in Olomouc to store and display this thesis and its electronic version in the university library and on the official website.

Contents

Chapter 1

Introduction

By the end of the 19$^{\text{th}}$ century, the common sentiment was that nearly all the mysteries of physics were already unraveled. True, there were few inconsistencies in need of ironing out, but after that was done there would be nothing left to do but perform increasingly precise measurements of fundamental constants. Or so was thought. One of these minor quirks was the spectrum of blackbody radiation and its continuous and stubborn refusal to fully match the existing theoretical models. These differences were finally reconciled by introduction of photons [1] which ultimately lead to a completely new field, a completely *new physics* - quantum physics. Originally, the photons were an abstract concept used to model statistical properties of light. Today, more than a century later, we are in an era in which individual photons and their nonlocal properties can be observed and even manipulated with aims of accomplishing a number of intriguing goals.

The research field with the ambition to harness the spooky nature of quantum systems in order to devise new and powerful technologies is called quantum information processing (QIP) and it is an amalgam of physics and information theory. So far, the investigation revealed the exciting possibilities of quantum simulation [2, 3], quantum computation [4, 5, 6, 7], quantum communication [8, 9, 10], and quantum metrology [11, 12], but other paradigm shifting discoveries may be revealed in the future. All of the aforementioned applications require, as one of the elementary build-

ing blocks, quantum nonlinearity which is incompatible with classical and semi-classical descriptions. The nonlinear behavior can be found in natural systems, but it is unfortunately fairly weak and vulnerable to decoherence. Reliably providing desired nonlinear behavior is therefore one of the bottle-necks holding back the development of quantum technologies.

Quantum technologies need to be firmly rooted in real physical systems and many experimental platforms are investigated for this purpose. Photons or, more formally, traveling light are one of the analyzed possibilities. Light is a natural candidate for quantum connection [13] and the associated information processing. Quantum states of light, either of individual photons or more complex multiphoton fields, can be straightforwardly generated already with the present day technology. These states can be also effectively manipulated by linear optical schemes and linear squeezing, and measured by homodyne or single photon detectors [14, 15, 16]. Detectors resolving exact numbers of photons are not yet easily accessible but they are a focus of intensive investigation [17, 18]. One of light's main advantages is its resilience to noise. This is related to the ease with which a mode of light can be prepared in what is effectively the zero temperature state and isolated from a noisy environment during propagation. However, the noninteractibility of light, responsible for this robustness, is also the reason why realizing nonlinear operations for light is a fairly challenging task.

Currently, the most feasible way of obtaining a nonlinear behavior for modes of traveling light lies in inducing it through a suitable measurement. Detectors of discrete quantum qualities, such as numbers of photons, are inherently nonlinear and, when used on a part of an entangled multi-mode field of light, are capable of probabilistically projecting the remaining state into a nonlinear one [19]. This is the traditional way of generating individual photons, but it was also used for creating of more complicated nonlinear states [20] and implementing quantum nonlinear operations [21].

This thesis expands upon this basic principle and shows several different kinds of nonlinearity which can be constructed at the single photon level. The theoretical proposals of the protocols form the the sturdy basis of the thesis. However, from the very first phase of their conception, they were

always motivated by the experimental reality and the tools available. That is why a significant portion of the mainly theoretical thesis is composed of reports of the experiments which took the proposals and turned them into real life devices. The main results of the thesis can be separated into three thematically distinct topics, each one summarized in a separate chapter.

In chapter 3 we will focus on a specific example of quantum nonlinearity - the noiseless amplification. We will introduce the problem and present specific proposals for implementation [A1]. We then demonstrate their feasibility by showcasing the experimental results obtained in collaboration with *Max Planck Institute for Science of Light in Erlangen* [A2, A3]. We will part with the chapter by abstracting the noiseless amplification and pondering its consequences for probabilistic measurements of quantum phase [A4].

In chapter 4 we will abandon the specific example and consider the broader scope of quantum information processing. We will show several ways in which we can manipulate a quantum state of light in an arbitrary way. Specifically, we will show a feasible set of elementary logic gates required for processing of superposed coherent state qubits [A5] and discuss the experimental results obtained in collaboration with *Danish Technical Institute in Lyngby* [A6]. We then present a set of elementary gates suitable for a general transformation of optical field [A8] and discuss the nature of universal quantum resources required by these operations [A7]. As in chapter 3, all the operations considered in this chapter are probabilistic. This makes them unsuitable for universal computation and other protocols aiming for speed-up, but they are well fit for preparation of quantum states and tests of other tools in the quantum optical toolbox [16, 36].

In chapter 5 we will show how to implement a nonlinear quantum gate deterministically. Specifically, we will propose a realization of the cubic gate [A9, A12], which is the lowest order nonlinear gate sufficient for universal processing of quantum information. The key element required by the gate is a nonlinear quantum state used as a source of the nonlinearity. We will show that the required state can be constructed, photon by photon, with help of suitable measurements. We will analyze the experimental results obtained in collaboration with the *University of Tokyo* [A10, A11] and show that the

required nonlinearity is present in the generated states despite the existing experimental imperfections.

Chapter 2

Nuts and bolts of quantum optics

Quantum information processing with quantum optics can be approached from two different angles. In the first one, the relevant physical systems are individual photons, which can be found in distinctive modes and labeled accordingly. The total number of these modes[1], together with the number of photons, then determine the dimension of the Hilbert space used for describing the system. This dimension can be arbitrarily large, but it is always finite and the total number photons of is always limited and well known. This is the historically older Discrete Variable (DV) approach [23], which has been already used for realization of many fundamental tests of quantum mechanics [24, 25, 26, 27], as well as for proof-of-principle test of quantum information protocols [6, 28] and even first commercially available devices [30]. The strength of the DV approach lies in the natural self-correcting ability of the systems - a random loss of a photon can be easily detected and therefore does not introduce errors. However, it is not without weaknesses. There are experimental limits as to how many photons can be utilized at the same time and what operations can be realized by the available detectors. For example, quantum teleportation [31], the quintessential quantum protocol which plays role in many advanced applications, can not be deterministically

---

[1]polarization, spatial, temporal, and so on

realized without nonlinear operations which are currently unavailable in the DV quantum optics [32].

While the DV theory is governed by the algebra of finite Hilbert spaces, the DV experiments are fully determined by the available tools: sources of single photons, single photon detectors, and quantum operations preserving photon numbers. However, there is also a plethora of quantum states and operations which have no place in DV quantum optics, because they violate its basic assumptions. These tools are the focus of the Continuous Variables (CV) quantum optics which studies states of the radiation modes instead of the photons. Each of the distinct modes can contain an arbitrarily large number of photons and is therefore described by infinite dimensional Hilbert space. Aside from the photon number, the light in the modes can be also described by its electric and magnetic intensities which are continuous quantities - hence the name, CV.

The main benefit of the CV approach is that it has naturally broader range of experimental tools at its disposal. In addition to the DV tools, it can employ coherent and squeezed states of light, high efficiency homodyne detection, and squeezing [33]. Many quantum protocols can be realized both in CV and DV and the CV implementation is often beneficial [34, 35]. For example, CV quantum teleportation can be realized deterministically [22] and it can be even used for transmission of a DV state [36]. In this work we focus on quantum information processing with CV quantum optics and show realization of several interesting protocols.

In CV quantum optics, a single mode of field of light is best modeled by a quantum harmonic oscillator [33, 37]. The Hamiltonian of such the system is rather simple,

$$\hat{H} = \hbar\omega\left(\hat{a}^\dagger\hat{a} + \frac{1}{2}\right), \tag{2.1}$$

where ω is the frequency, $\hbar$ is the Planck constant and $\hat{a}$ is the photon number annihilation operator. In the following we will be mainly interested in fundamental properties of the system; we will therefore take some liberties and simplify the description a little bit. We shall consider $\hbar = 1$ and define

quadrature operators

$$\hat{x} = \frac{\hat{a} + \hat{a}^\dagger}{\sqrt{2}}, \quad \hat{p} = \frac{\hat{a} - \hat{a}^\dagger}{\sqrt{2i}} \tag{2.2}$$

with commutation relations $[\hat{x}, \hat{p}] = i$. The physical interpretation of these operators is related to electric and magnetic intensities of the electromagnetic field, but in our description they will be dimensionless and interchangeable. Their main purpose is to enable different ways in which we can describe the harmonic oscillators under our consideration.

The most complete knowledge of a quantum state is given by its quantum state vector $|\psi\rangle$ if it is pure and quantum state density operator $\hat{\rho}$ when it is mixed. However, there are several ways to represent the quantum state and one of the key skills used in CV quantum information lies in choosing the representation best suited for any given task and flexibly changing between them when needed. The Fock representation expresses the state in the term of photon number states $|n\rangle$ which are the eigenstates of the photon number operator $\hat{n} = \hat{a}^\dagger \hat{a}$. Similarly, the quadrature representation employs eigenstates of quadrature operators $\hat{x}$ and $\hat{p}$, always either one of them or their linear combination. This is the consequence of their dual nature arising from their noncommutativity. Representation by Wigner functions is different, because it attempts to combine the incompatible x and p representations and describe the quantum state of a single mode of radiation by a bivariate real function defined as

$$W(x,p) = \frac{1}{2\pi} \int_{-\infty}^{\infty} e^{i2pq} \langle x - q|\hat{\rho}|x + q\rangle dq. \tag{2.3}$$

This function resembles a joint probability distribution of two classical random variables, but it has several differing features arising from the noncommutative nature of the two quantum variables. Most importantly, it can attain negative values. Such values have no place in classical theory of probability and states exhibiting them can be considered distinctively quantum or, as they are oftentimes called, non-classical [38]. In retrospect, it is not surprising that these states can be only produced by quantum nonlinear

operations.

Related to this distinction, tools of quantum optics can be separated into two broad categories: Gaussian and non-Gaussian. Gaussian quantum states have Wigner functions proportional to multivariate Gaussian distribution, Gaussian operations transform Gaussian states into Gaussian states and Gaussian measurements project on Gaussian eigenstates. The Gaussian resources play a significant role in quantum optics experiments, because they can be straightforwardly realized. Passive linear optics elements, together with displacement [39] and the squeezing operation, can be used to implement an arbitrary Gaussian operation [40] and, by extension, used to prepare an arbitrary Gaussian state. The homodyne detection [33], which can be realized with high quantum efficiency, is then the quintessential Gaussian measurement.

Unfortunately, the ease with which Gaussian tools can be processed both theoretically and experimentally comes at a cost. Many desirable quantum protocols, such as quantum computation [41] or distillation of quantum entanglement [42, 43, 44], have been shown to absolutely require non-Gaussian elements to work. This lead to great focus being devoted to obtaining these tools, with differing measures of success. Non-Gaussian operations can be realized in some naturally nonlinear media, such as those exhibiting Kerr nonlinearity [45]. Unfortunately, in practice the nonlinearity in the materials presently available is too weak to be applied to weak signals [2] employed in quantum information protocols. Single photons prepared on demand would be a great source of non-Gaussian states but, even though the technology continuously progresses [46], they are not fully reliable yet. Similar situation is with quantum memories, which have the potential, but still lack the necessary efficiencies [47, 48].

In the end, the most feasible way of obtaining non-Gaussian resources for CV quantum information processing with light currently lies in measurement induced operations. This is enabled by the availability of avalanche photodiodes serving as on-off detectors, discerning either presence or absence of light [20]. In quantum mechanical terms, the two measurement

---

[2]with at most few photons on average

Figure 2.1: Conceptual description of a measurement induced operation.

outcomes are related to POVM elements

$$\hat{\Pi}_{\text{off}} = |0\rangle\langle 0|, \quad \hat{\Pi}_{\text{on}} = \hat{1} - |0\rangle\langle 0|. \tag{2.4}$$

The 'on' element confirming presence of photons is non-Gaussian and can be therefore used for realization of non-Gaussian operations and preparation of non-Gaussian states.

2.1 Measurement induced operations

Measurement induced operations are enabled by one of the basic paradigms of quantum mechanics - observing a quantum system changes it. This is the principle which students of quantum mechanics usually encounter in their first lesson when discussing the Stern-Gerlach experiment. However, the detectors of quantum optics are based on absorption and therefore destroy the system they measure. Measurement induced operations therefore require an additional component - an ancillary system which interacts with the signal and is measured afterwards. This process, illustrated in Fig. 2.1, formally transforms the density matrix of the signal as:

$$\hat{\rho}_s \rightarrow \frac{\text{Tr}_a[\hat{U}_{sa}\hat{\rho}_s \otimes \hat{\rho}_a \hat{U}_{sa}^\dagger \hat{\Pi}_a(q)]}{\text{Tr}[\hat{U}_{sa}\hat{\rho}_s \otimes \hat{\rho}_a \hat{U}_{sa}^\dagger \hat{\Pi}_a(q)]}. \tag{2.5}$$

The subscripts s and a denote the signal and the ancilla, respectively, unitary operator $\hat{U}_{sa}$ represents the coupling between the systems, and $\hat{\Pi}_a(x)$ marks the POVM element related to the measurement outcome q. As a consequence, the state of the signal is altered based on the particular measure-
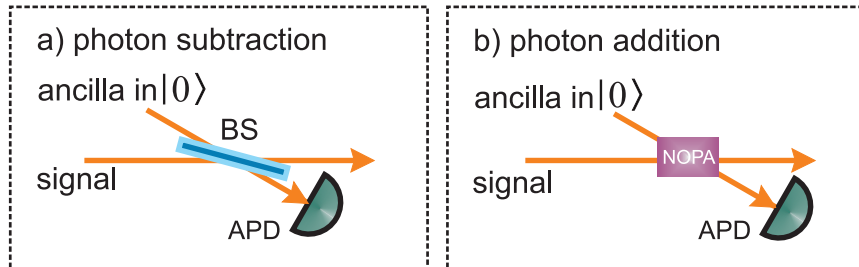
Figure 2.2: Schematic depiction of probabilistic implementation of photon subtraction (a) and photon addition (b). BS - beam splitter, NOPA - non-degenerate optical parametric amplifier, APD - avalanche photo diode.

ment result. We now have the option to only keep the states corresponding to certain measurement outcomes, which results in a probabilistic operation, or to keep all the different situations and treating the resulting state as a statistical mixture with weights equal to the individual probabilities of success. In this case, the information gained by the measurement can be used to drive a feed-forward loop which completes the operation by erasing some of the back-action of the measurement [49].

In quantum optics, this elementary principle has been employed towards realization of a wide range of quantum operations, both probabilistic and deterministic. Possibly the most prominent probabilistic operation is the approximation of the photon number annihilation operator $\hat{a}$, which can be realized by mixing the signal with a vacuum on a weakly transmitting beam splitter and then measuring the reflected light with the avalanche photo-diode, see Fig. 2.2a. When the signal is in a pure state $|\psi\rangle$, the full operation can be approximatively written as

$$|\psi\rangle_s|0\rangle_a \rightarrow \langle 1|_a(1 + \epsilon \hat{a}_s \hat{a}_a^\dagger)|\psi\rangle_s|0\rangle_a \propto \hat{a}_s|\psi\rangle_s. \tag{2.6}$$

We have written the unitary operator for the beam splitter, an operation with effective Hamiltonian $\hat{H} = -i\epsilon(\hat{a}_s\hat{a}_a^\dagger - \hat{a}_s^\dagger\hat{a}_a)$, in the form of the first order Taylor expansion, because we assume the coupling ratio ϵ to be small. Thanks to this approximation, we can also consider the 'on' POVM element (2.4) to be the projector $|1\rangle_s\langle 1|$, which allows us to preserve the purity

of the state. In the end, the subtraction operation is achieved with success probability $P_S = \epsilon^2 \langle\psi|_s \hat{a}_s^\dagger \hat{a}_s |\psi\rangle_s$, which strongly depends on the signal state. For example, for the vacuum state it is zero - a logical conclusion of the inability to remove photons from a state which has none. Photon subtraction realized in this manner has been originally suggested as means for generation of arbitrary quantum states [50] and realization of arbitrary operations [51]. The first experimental realization then demonstrated its ability to transform a Gaussian squeezed state of light into a non-Gaussian state resembling a superposition of coherent states [20], coining its upcoming role as the most prevalent source of non-Gaussian behavior in quantum optics.

Photon addition operation can be realized in a very similar manner by replacing the beam splitter with a Nondegenerate Optical Parametric Amplifier (NOPA) [21], see Fig. 2.2b. This operation, characterized by Hamiltonian $\hat{H} = -i\epsilon(\hat{a}_s^\dagger \hat{a}_a^\dagger - \hat{a}_s \hat{a}_a)$ and widely used for generation of entangled photon pairs, can add a single photon to both the signal and the ancillary mode. A positive detection outcome of the ancilla measurement then confirms implementation of the addition. At the first sight, photon addition may seem to be similar in effect to photon subtraction. From the point of view of non-Gaussian features it is, however, much stronger. In contrast to photon subtraction, which requires states with certain properties [38] to create non-Gaussian states, photon addition produces them always [52]. The cost of this, however, is lower experimental feasibility arising from the need of injecting the signal into an active medium and mode-matching it with the pump.

As far as deterministic measurement induced operations go, the most prevalent examples in this category are actually Gaussian. However, this does not diminish their usefulness as the Gaussian operations are necessary for CV quantum information processing and some of them can not be applied directly [53]. An example of such operation is the squeezing, operation which reduces fluctuations in one quadrature at the cost of increasing fluctuations of the other, represented in Heisenberg picture by transformation relations

$$\hat{x}' = g\hat{x}, \quad \hat{p}' = \frac{1}{g}\hat{p}. \tag{2.7}$$

It is important to note that the aforementioned difficulty is related to squeezing of an arbitrary unknown state. Squeezing a vacuum state, amounting to preparation of the squeezed vacuum state, is a task routinely implemented in quantum optics laboratories [54, 55]. Unfortunately, the process involves active media in optical resonators with low in-coupling and out-coupling efficiencies, making it unsuitable for unknown quantum states. The available squeezed vacuum states can be fortunately used as part of the measurement induced scheme in order to impart the squeezing onto an arbitrary quantum state. Within the scheme shown in Fig. 2.3, the signal s mixes with the ancilla a, prepared in the squeezed vacuum state, on a beam splitter with transmissivity T. In Heisenberg picture this transforms the quadrature operators as

$$\hat{x}'_s = \sqrt{T}\hat{x}_s + \sqrt{1-T}\hat{x}_a \quad \hat{p}'_s = \sqrt{T}\hat{p}_s + \sqrt{1-T}\hat{p}_a,$$
$$\hat{x}'_a = \sqrt{T}\hat{x}_a - \sqrt{1-T}\hat{x}_s \quad \hat{p}'_a = \sqrt{T}\hat{p}_a - \sqrt{1-T}\hat{p}_s. \tag{2.8}$$

Quadrature $\hat{p}'_a$ of the ancillary mode now gets measured by the homodyne detection, producing a classical value $q = \sqrt{T}\hat{p}_a - \sqrt{1-T}\hat{p}_s$. This value can be used to displace the signal as

$$\hat{x}''_s = \hat{x}'_s = \sqrt{T}\hat{x}_s + \sqrt{1-T}\hat{x}_a$$
$$\hat{p}''_s = \hat{p}'_s - \frac{\sqrt{1-T}}{\sqrt{T}}q = \frac{1}{\sqrt{T}}\hat{p}_s. \tag{2.9}$$

We can see, that apart from the term related to $\hat{x}_a$, the relations perfectly follow the ideal relations for squeezing with transmissivity corresponding to the new squeezing parameter. The squeezing of the ancillary mode now comes into play - it manifests as reduced fluctuations of the $\hat{x}_a$ quadrature, meaning that for large squeezing we can use approximation $\hat{x}_a \to 0$. The inline squeezing operation, which has been applied to a range of both Gaussian and non-Gaussian states [56, 57], then serves, together with passive linear optics, as a resource from which all other Gaussian operations can be constructed [40, 58, 59].

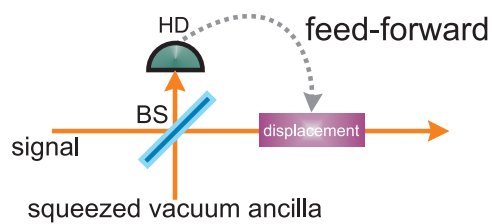These are but few examples of the measurement induced operations used

Figure 2.3: Measurement induced realization of the squeezing operation. BS - beam splitter, HD - homodyne detection

in contemporary quantum optics, but they nicely illustrate the basic benefits of the paradigm. Namely that resources needed for quantum operations can be drawn both from the measurements and the ancillary states. In the following chapters we will take this basic concept and expand it to several possible applications.

Chapter 3

Noiseless Amplification

Amplification is a central concept in classical communication. There, information is being carried by signals which tend to deteriorate during propagation. Long distance communication therefore requires repeater stations, which employ amplification to compensate the losses and other channel imperfections. Similar issues arise in quantum communication and it is intuitive to adapt similar approaches to combat them. Unfortunately, the actual realization of practical quantum amplification is not straightforward as it faces quite a number of specific difficulties.

The main difference between classical and quantum amplification lies in the nature of the amplified entity. The classical signal can be, under realistic conditions, completely measured and the information it carries can be fully extracted. Any classical amplifier can be therefore imagined as a device which measures the signal and then prepares a new, stronger but otherwise identical one. On the other hand, quantum communication aims to transmit quantum states, which have the fundamental property that they carry more information that can be extracted by a single measurement. This is the very feature which enables the quantum key distribution protocols [30, 60], but it also largely prevents amplifiers based on measurement and re-preparation.

Quantum amplifiers therefore need to be actively transforming the quantum state of the signal. While doing so, they must adhere to the fundamental constraints imposed by quantum physics, the most limiting one being the

no-cloning theorem [61], which states that it is impossible to take an un-
known quantum state and create, in any way, several copies of it. After all,
if the main purpose of amplification is to make information carried by the
signal more accessible, creating several copies of the signal works quite well.

Quantum amplification therefore always needs to come with drawbacks,
which ensure that the operation is not too good. As an example, let us
consider amplification of a single mode of light. Such amplification could be
represented by the following transformation of the quadrature operators of
the field:

$$\hat{x}' = \sqrt{G}\hat{x}, \quad \hat{p}' = \sqrt{G}\hat{p}, \tag{3.1}$$

where the parameter G is the amplification gain. However, transforma-
tion relations (3.1) do not preserve the fundamental commutation relations
$[X, P] = i$ and therefore do not represent any physical operation. Operation
(3.1) can not exist. However, we can transition into the realm of possibility
by adding some additional terms. Transformation relations

$$\hat{x}' = \sqrt{G}\hat{x} + \sqrt{G-1}\hat{x}_a \tag{3.2}$$

$$\hat{p}' = \sqrt{G}\hat{p} + \sqrt{G-1}\hat{p}_a \tag{3.3}$$

satisfy the commutation relation under the assumption that operators $\hat{x}_a$
and $\hat{p}_a$ represent quadrature operators of an ancillary system. Transforma-
tion relations (3.2) are used to describe the non-degenerate optical para-
metric amplifier (NOPA), which has been long used in the area of quantum
optics for generation of entangled states of light [62], both discrete states
of entangled photons [6, 28, 31] and continuous two mode squeezed state
[22, 36]. For our purposes it is important that the operation adds photons
into the amplified mode, but for each photon added in this way, a photon
is added also into the ancillary *idler* mode. This creates correlations, even
entanglement, between the signal and the idler modes and when the idler
mode is discarded, part of these correlations turns into noise. And this noise
is the cost we pay for the amplification.

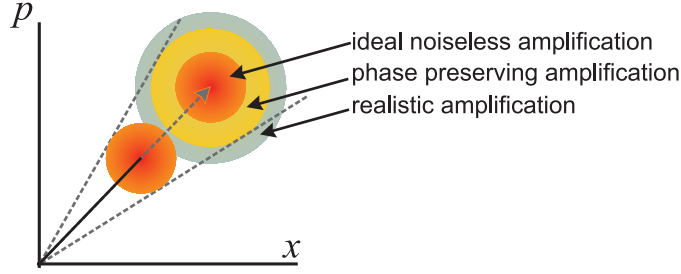We can illustrate this on the example of amplifying a coherent state of

Figure 3.1: Illustration of amplification for coherent states of light. The circles schematically demonstrate profile of the states' Wigner functions in phase space.

light. In the phase space representation, coherent state $|\alpha\rangle$ is represented by its Gaussian Wigner function in the form

$$W_\alpha(x,p) = \frac{1}{\pi}e^{-(x-\alpha_r\sqrt{2})^2-(p-\alpha_i\sqrt{2})^2}, \tag{3.4}$$

where $\alpha = \alpha_r + i\alpha_i$. In the following we will always consider $\alpha > 0$ - this has no bearing on the validity of the presented results and it simplifies their description considerably. In phase space a coherent state can be represented by a circle where its radius corresponds to the uncertainty in measuring $\hat{x}$ or $\hat{p}$. It does not matter which one; the fluctuations are symmetrical. The amplification is schematically illustrated in Fig. 3.1. The important realization is that even though the amplification increases the amplitude, which is represented by displacement of the state disc, it also increases the respective fluctuations, represented by its change in size. What is even more unfortunate is that from the point of view of information carried by the state, the amplification did make the situation worse - the extra fluctuations cancel out any improvement brought in by the amplification of the amplitude. Within this example it can be easily seen that in the Schröedinger picture the ideal operation would take a coherent state $|\alpha\rangle$ and transform it into another coherent state $|g\alpha\rangle$ with $g > 1$. The operation would be therefore represented by operator

$$g^{\hat{n}} = \sum_{k=0}^{\infty} g^k |k\rangle\langle k|. \tag{3.5}$$

The operator (3.5) is unbounded, which is the consequence of the ever increasing values of coefficients g^k. This means that the operator is non-physical and can not be realized. Or, rather, it can not be realized in its ideal form. In fact, the operator is unbounded only when we consider an infinite dimensional Hilbert space. However, in all the potential scenarios in which we deal with quantum amplification, the states of interest are weak, having on average only few quanta of energy. This effectively limits the Hilbert space they live in and enables the noiseless amplification *approximatively*.

It was first realized in [63] that very weak coherent states, which can be effectively represented as a superposition of one and no photons, $|\alpha\rangle \approx |0\rangle + \alpha|1\rangle$, can be used in a quantum scissors protocol to generate another superposition, $|0\rangle + g\alpha|1\rangle$, which closely resembles the desired amplified state if $g|\alpha| \ll 1$. The key feature which enables the noiseless amplification is its non-unit probability of success. There is still a cost to the amplification, but this time it does not manifest as a reduction of quality of the amplified state, but rather as a reduction in the success rate. With the realization that in practical scenarios noiseless amplification is not impossible in principle we can start looking for other effects which can be used to implement it.

3.1 Noise-powered amplification

Interestingly enough, the amplification can be also constructed from the elementary operators of quantum optics - the annihilation and the creation operators $\hat{a}$ and $\hat{a}^\dagger$. These operators are elementary in the theoretical sense, they are the cornerstone for theoretical description of the optical fields. Their experimental realization is made difficult by the fact that they, in their ideal versions, represent non-physical operations. They can be, however, realized approximatively by employing the nonlinearity of detectors capable of resolving individual photons [21, 50, 51, 52].

When the creation and the annihilation operators are applied in this

order to a weak coherent state they transform it as

$$\hat{a}\hat{a}^{\dagger}\left(|0\rangle + \alpha|1\rangle + \frac{\alpha^2}{2}|2\rangle + ...\right)$$

$$= |0\rangle + 2\alpha|1\rangle + \frac{3\alpha^2}{2}|2\rangle + ... \tag{3.6}$$

If the coherent amplitude is small enough, the state closely resembles the coherent state amplified with gain $g = 2$. In comparison with the quantum scissors scheme [63], the scheme has the disadvantage of fixed amplification gain, but the benefit of not throwing away all the higher Fock terms, which means it can provide a meaningful improvement even if the coherent amplitude is not negligible compared to one [A1]. We can also view the operation as implementing operator $1 + \hat{n}$, which is close to the first order Taylor expansion of an ideal noiseless amplification operator $e^{\hat{n}}$. This view can be further expanded into involving other more complicated polynomials of the number operator $\hat{n}$ [64, 65].

Interestingly enough, the first step of the protocol, the coherent addition of photon, can be in certain cases, such as for amplification of coherent states, replaced by addition of incoherent photons. These photons, also appearing, for example, during the Gaussian amplification (3.2), are most often treated as noise. The process of adding them is classical and it is best described as random displacement of the field:

$$|\alpha\rangle\langle\alpha| \rightarrow \int \Theta(\beta)\hat{D}(\beta)|\alpha\rangle\langle\alpha|\hat{D}^{\dagger}(\beta)d^2\beta, \tag{3.7}$$

where $\hat{D}(\beta)$ is the displacement operator [37] and $\Theta(\beta)$ is a classical probability distribution of the complex displacing amplitudes. The second step of the operation, the photon subtraction, then transforms the state into

$$\frac{\int \Theta(\beta)|\alpha + \beta|^2|\alpha + \beta\rangle\langle\alpha + \beta|d^2\beta}{\int \Theta(\beta)|\alpha + \beta|^2 d^2\beta}, \tag{3.8}$$

where the denominator represents the probability of success of the operation and we took advantage of coherent states being eigenstates of the annihila-
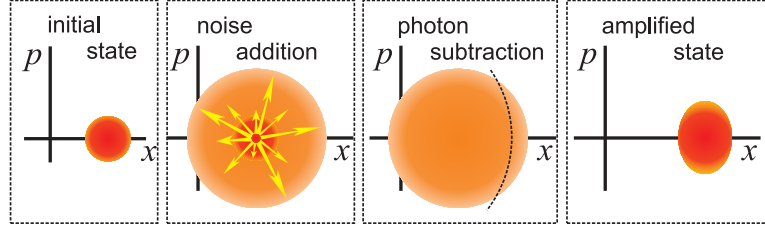
19

Figure 3.2: Phase space illustration of the noise powered amplification of a coherent state of light

tion operator. The subtraction of photons acts as a probabilistic filter. Some coherent states from the initial mixture (3.7) have higher probability of being post-selected and are thus over-represented in the transformed state. This is characteristic for the states with the highest amplitudes, which happens when the phase of the random displacement aligns with the unknown phase of the initial coherent state. See Fig. 3.2 for illustration of the effect. Increasing the number of subtractions makes the filtering more strict, which improves the amplification at the cost of the success rate.

The particular form of $\Theta(\beta)$ depends on the mechanism used for adding the noise. The most common form of noise, which naturally appears during the process of Gaussian amplification (3.2), is represented by thermal chaotic light with

$$\Theta(\beta) = \frac{1}{\pi N_{TH}} e^{-\frac{|\beta|^2}{N_{TH}}}. \tag{3.9}$$

Parameter N_{TH} represents the mean number of added photons and quantifies the strength of the added noise. For any particular scenario, the amount of noise can be optimized in order to achieve the best performance. However, there are other forms of noise which can be considered. In fact, using random displacement operations, any thinkable noise distribution can be achieved in experimental scenario. The only condition, which needs to be satisfied for preventing bias, is phase insensitivity. As an example, one possible way of adding noise consists of performing displacements with fixed

20

amplitude $|\beta| = \sqrt{N_D}$ and random phase;

$$\Theta(\beta) = \frac{1}{2\pi}\delta(|\beta| - N_D), \tag{3.10}$$

where $\delta()$ denotes the singular δ-function.

For evaluating the performance of the amplification we need to introduce quantitative figure of merits. Phase is an important property of coherent states and it is often used for encoding information. It therefore makes sense to see how well any given state can carry a particular phase value and subsequently reveal it in a measurement [66]. The best possible measurement which can be imagined is the so called canonical measurement of phase [66, 67, 68]. It can be mathematically described as a projection on idealized phase states $|\theta\rangle = \sum_{k=0}^{\infty} e^{i\theta k}|k\rangle$. These phase states are not normalized, which makes them similar to eigenstates of continuous operators (such as position and momentum), but they are also not orthogonal. For any quantum state $\hat{\rho}$ the results of the canonical phase measurement can be characterized by probability distribution $P(\theta) = \text{Tr}[\hat{\rho}|\theta\rangle\langle\theta|]$ - the canonical phase distribution. The phase distribution for coherent state has a single peak and it is symmetrical around it, meaning that the encoded phase can be measured without bias. The quality of the phase encoding is given by the width of the peak, which can quantified by the phase variance [67]

$$V_\mu = \frac{1}{|\mu|^2} - 1, \text{ where } \mu = \int_0^\pi e^{i\theta} P(\theta) d\theta. \tag{3.11}$$

We have tested the noise powered amplification experimentally [A2]. Coherent states with initial amplitude $|\alpha|^2 = 0.186$ were amplified by addition of thermal noise with $\langle N_{TH}\rangle = 0.15$ and subsequent photon subtraction. The resulting phase distribution and phase variances of the amplified states relative to the number of subtracted photons is shown in Fig. 3.3. We can see that even though the initial addition of thermal noise reduces quality of the state, subsequent photon measurements improve it beyond the initial level for both the theoretical predictions and the experimental tests.

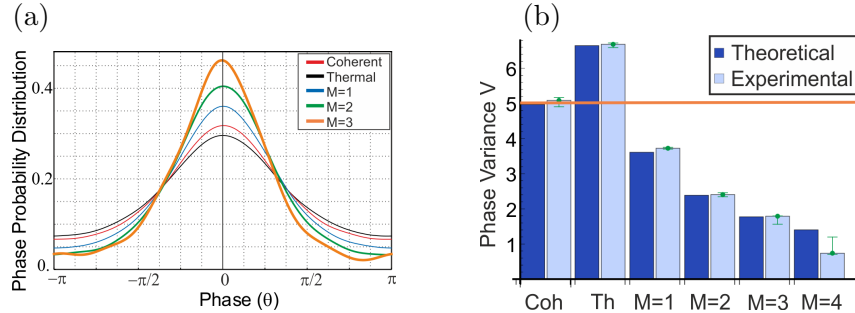Finally, the noise powered amplification can be also considered for per-

Figure 3.3: (a) Phase distributions for the initial coherent state and different levels of amplification. (b) Phase variances for different levels of amplification. Experimental data of [A2].

fect cloning of coherent states. Laws of quantum physics prevent creation of perfect copies [61]. Copies can be created, but they are always burdened by noise [69, 70]. This is very similar to the trade-offs for amplification, especially for coherent states for which cloning is realized by amplification followed by splitting. This also means that, with help of noiseless amplification, coherent states can be cloned almost perfectly, at the cost of reduced success rate. We experimentally tested this possibility by attempting to use the noise-powered amplifier to generate perfect copies of a coherent state with unknown phase [A3]. The Wigner functions of the produced states can be seen in Fig. 3.4 and they clearly show that quality of the copies improves with the number of subtracted photons and approaches the ideal noiseless regime.

3.2   Optimal probabilistic measurement of phase

In the previous section we have shown that noiseless amplification can be used for enhancing phase properties of quantum states. Or, to rephrase that, that probabilistic operations can be used for increasing precision of individual phase measurements. Furthermore, we can leave the distinction between amplification and measurement and simply examine the concept of probabilistic measurements. This is not the first time it appeared. Methods
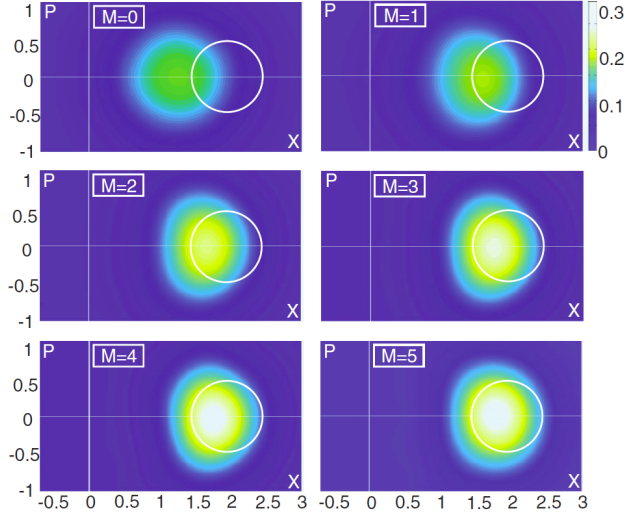
Figure 3.4: Wigner functions of coherent state cloned with help of the noise-powered amplifier. The white contour symbolizes the ideal clone. Experimental data of [A3].

for unambiguous distribution of quantum states [71] profit from the ability to pronounce certain measurement results 'inconclusive' and provide definite certain answers in the scenarios in which they do succeed. However, these methods require a discrete set of states to distinguish and are not directly applicable to measuring continuous set of phase values. So instead of finding a single ultimate measurement which measures the phase perfectly, which is impossible with the exception of zero probability of success, we aim to quantify the trade-offs between the quality of the phase measurement and its probability of success.

Extension of the canonical measurement of phase into the probabilistic regime can be represented by a set of operators $\hat{\Pi}_\phi$, each of them corresponding to a positive detection event of a value ϕ, and a single operator $\hat{\Pi}_0$ representing the inconclusive results. Together these operators form a positive operator valued measure (POVM). For the canonical deterministic measurement of phase these operators are $\hat{\Pi}_\phi^{(D)} = \frac{1}{2\pi}|\phi\rangle\langle\phi|$. Keeping the pure-state projector structure intact, we can express the probabilistic
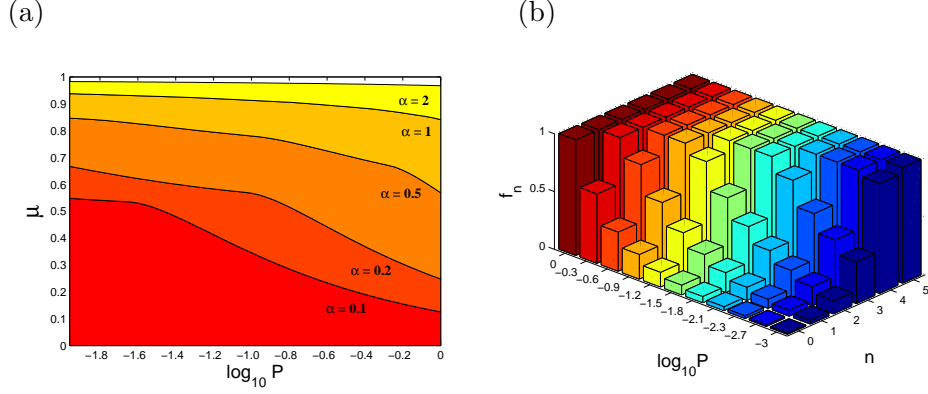
23

Figure 3.5: (a)Value of μ for optimal probabilistic measurement of phase for various coherent states. (b) The optimal filters for coherent state with $\alpha = 0.5$ and range of success probabilities.

POVMs as

$$\hat{\Pi}_\phi^{(P)} = \frac{1}{2\pi}\hat{F}|\phi\rangle\langle\phi|\hat{F}^\dagger, \quad \hat{\Pi}_0^{(P)} = \hat{1} - \int \hat{\Pi}_\phi^{(P)}d\phi. \tag{3.12}$$

Here $\hat{F} = \sum_n f_n |n\rangle\langle n|$, where $|f_n| \leq 1$ for all $n = 0, 1, \cdot$, is operator diagonal in Fock space. It is practical to represent the probabilistic measurement by a filter, transmitting and modifying the quantum state with some limited probability, followed by the deterministic canonical phase measurement. The operator $\hat{F}$ then plays the role of the probabilistic filter and the task of finding the optimal measurement is reduced to finding the optimal operator $\hat{F}$, which minimizes the phase variance and maximizes parameter μ (3.11).

After the first glance at the problem, one issue immediately becomes apparent. For any quantum state $\hat{\rho}$, the probability of successful measurement, $P = 1 - \text{Tr}[\hat{\rho}\hat{\Pi}_0^{(P)}]$ is dependant on the choice of the measured state. The optimal measurement therefore needs to be tailored to a specific state or to a class of states. Fortunately, for the class of coherent states it is possible to find a semi-analytical solution. The results are illustrated in Fig. 3.5. In Fig. 3.5a we show how the chosen success rate of the optimal measurement affect the measured phase variance for a set of coherent states. Fig. 3.5b

24

then shows the exact form filters which realize the optimal operation for one particular coherent state.

3.3 Summary

We have proposed two methods which employ non-Gaussian operations for probabilistic amplification of quantum signals. We have tested one of these methods experimentally, first to confirm the ability to concentrate quantum phase, then to clone coherent states with unknown phase. Finally, we have used the concept of probabilistic amplification to derive general bounds on quality of a probabilistic measurement of phase. This chapter is based on publications:

- P. Marek and R. Filip, *Coherent-state phase concentration by quantum probabilistic amplification*, Physical Review A **81**, 022302 (2010)

- M. A. Usuga, C. R. Müller, C. Wittmann, P. Marek, R. Filip, C. Marquardt, G. Leuchs, and U. L. Andersen, *Noise-powered probabilistic concentration of phase information*, Nature Physics **6**, 767 (2010)

- C. R. Müller, C. Wittmann, P. Marek, R. Filip, C. Marquardt, G. Leuchs, U. L. Andersen, *Probabilistic cloning of coherent states without a phase reference*, Physical Review A **86**, 010305(R) (2012)

- P. Marek, *Optimal probabilistic measurement of phase*, Physical Review A **88**, 045802 (2013)

Chapter 4

Probabilistic Quantum Information Processing

Processing of quantum information ultimately boils down to transforming the physical systems which carry it. The preparation and measurement of the states of the quantum systems are inseparable parts of complete quantum information protocols, but the actual processing consists of transforming mostly unknown quantum states in a well defined manner. The lack of knowledge is an important point: if a pure quantum state is known it can be turned into any other state by a suitable unitary operation. However, without the full information some transformations are inaccessible and some can only be performed with a reduced probability of success. An example of such quantum operation is the noiseless amplification, which was the focus of the previous chapter. Amplitude of a single coherent state can be adjusted at will. But if the phase of the coherent state is unknown, the amplitude can be increased only probabilistically. The significance of the probabilistic methods is exactly in that they enable otherwise impossible operations, which are nevertheless crucial for the rest of the field. State purification [72, 73] and entanglement distillation [74, 75] protocols are but two examples of such techniques.

Apart from overcoming the fundamental limitations, probabilistic operations play a key practical role in quantum information processing with CV

systems of light. Triggering operations by performing projective measurements in Fock basis is the most efficient source of non-Gaussian features [20, 21, 52], which are indispensable in reaching many goals of quantum information science [41, 42, 43, 44].

4.1   Processing with coherent state qubits

States of continuous systems live in an infinite dimensional Hilbert space. However, that does not mean that all of those dimensions need to be used for quantum information processing. Formally, any discrete system with limited dimensionality can be represented by limiting the continuous system to a certain subspace. For example, the discrete quantum information processing based on two dimensional quantum systems - qubits - can be emulated by considering a pair of coherent states with opposite phase, $|\alpha\rangle$ and $|-\alpha\rangle$, and using them as the basis states for the processing [76, 77]. In the limit of large amplitude $|\alpha| \gg 1$, these states are almost completely orthogonal and the representation allows perfect quantum computation. The advantage, these coherent state qubits have over the older approaches employing qubits encoded into polarization of individual photons, lies in the ability to perform measurements. With access to detectors recognizing specific numbers of photons, the full Bell-state measurement, crucial for quantum teleportation, can be implemented only with linear optics elements - a feat impossible for the polarization encoding [32]. However, there is a cost to this fundamental feature: the practical difficulty to prepare or manipulate the required quantum states.

All coherent state qubits $c_+|\alpha\rangle + c_-|-\alpha\rangle$, apart from the two basis states, are non-Gaussian and therefore cannot be prepared by the standard Gaussian tools. The methods of preparation therefore need to rely on non-Gaussian elements, which are most often either photon number resolving measurement [20, A11] or photon number states [78]. Similar difficulty lies in manipulating the qubit. Even the elementary single mode gates, such as the phase gate or the Hadamard gate, have to be realized by non-Gaussian operations, as they can either turn a Gaussian state into a non-Gaussian
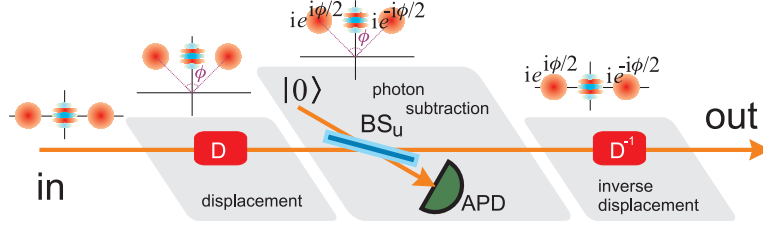
Figure 4.1: (Color online) Schematic representation of the single-mode phase gate. BS stands for a mostly transmitting strongly unbalanced beam splitter, APD stands for avalanche photodiode, and D represents the displacement operation.

(Hadamard gate) or change parity of the state (phase gate). These gates can be realized deterministically, but the implementation requires a sequence of weak operations each one consisting of a displacement and subsequent teleportation [77]. Unfortunately, the current experimental reality is such that it is not feasible to consider more than one of these steps and, as a consequence, the complete gates are out of reach.

To work around the issue, we proposed an alternative way to realize the elementary gates [23] for coherent state qubits [A5]. The gates were probabilistic, which made them unsuitable for scalable quantum information processing, but they were feasible with the contemporary technology. This allowed them to be used in experiments and help in evaluating the performance of other parts of the processing circuits [A6].

In order to clearly convey the basic ideas, let us work in the idealized scenario of perfect superposition of coherent states and perfect photon subtraction. The crux of the method lies in realization that the perfect photon subtraction realizes the annihilation operator and that coherent states are its eigenstates. Subtracting a photon from a superposition of coherent states therefore changes their coefficients relative to the amplitudes of the states, which can be employed for transformative operations.

Specifically, let us consider the single-mode phase gate which is necessary for single qubit manipulations. The gate should transform the basis coherent
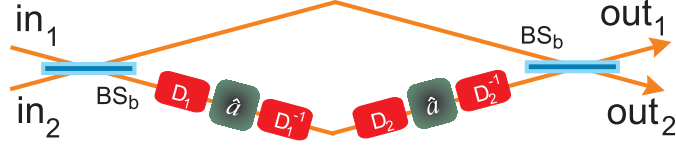
29

Figure 4.2: (Color online) Schematic representation of the two-mode controlled phase gate. BS_b stands for a balanced beam splitter and $D_{1,2}$ represent displacements by $\gamma_{1,2}/\sqrt{2}$. Numbers 1 and 2 distinguish the two participating modes, while labels 'in' and 'out' describe the input and output state of the gate.

states as

$$|\pm\alpha\rangle \rightarrow e^{\pm i\phi/2}|\pm\alpha\rangle, \tag{4.1}$$

and the procedure to implement it is is schematically shown in Fig. 4.1.

An arbitrary qubit in the coherent state basis $|\psi_{\text{in}}$ is first coherently displaced by amplitude γ, $|\psi_{\text{in}}\rangle \rightarrow \hat{D}(\gamma)|\psi_{\text{in}}\rangle$. Subsequently, a single photon is subtracted from the state, which is mathematically described by the action of annihilation operator $\hat{a}$. Finally, the state undergoes an inverse displacement by $-\gamma$, and we have

$$
\begin{aligned}
|\psi_{\text{out}}\rangle &= \hat{D}(-\gamma)\hat{a}\hat{D}(\gamma)|\psi_{\text{in}}\rangle \\
&= c_+(\alpha+\gamma)|\alpha\rangle + c_-(-\alpha+\gamma)|-\alpha\rangle.
\end{aligned} \tag{4.2}
$$

This operation then becomes equivalent to a phase gate, up to a global phase factor, when the complex displacement γ satisfies

$$\frac{\gamma-\alpha}{\gamma+\alpha} = e^{i\phi}, \tag{4.3}$$

which yields $\gamma = i\alpha/\tan(\phi/2)$.

The basic concept can be adapted for the other two gates required for qubit information processing - the controlled phase gate and the Hadamard gate. The controlled phase gate acts on two qubits, transforming their joint

state as

$$c_{11}|\alpha, \alpha\rangle + c_{10}|\alpha, -\alpha\rangle + c_{01}| -\alpha, \alpha\rangle + c_{00}| -\alpha, -\alpha\rangle$$
$$\rightarrow c_{11}|\alpha, \alpha\rangle + c_{10}|\alpha, -\alpha\rangle + c_{01}| -\alpha, \alpha\rangle + c_{00}e^{i\phi}| -\alpha, -\alpha\rangle \qquad (4.4)$$

and is locally equivalent to the C-NOT gate. It can be implemented by performing two displaced single photon subtractions in one arm of a balanced Mach-Zehnder interferometer which mixes the two modes, see Fig. 4.2. We can formally express this operation as

$$
\begin{aligned}
|\Psi_{\text{out}}\rangle &= \hat{U}_{BSb}^{\dagger}\hat{D}_2^{\dagger}\hat{a}\hat{D}_2\hat{D}_1^{\dagger}\hat{a}\hat{D}_1\hat{U}_{BSb}|\Psi_{\text{in}}\rangle \\
&= (\hat{a} + \hat{b} + \gamma_2)(\hat{a} + \hat{b} + \gamma_1)|\Psi_{\text{in}}\rangle, \qquad (4.5)
\end{aligned}
$$

where $\hat{U}_{BSa}$ and $\hat{U}_{BSb}$ are unitary operators of the two beam splitters and γ_1 with γ_2 are the two displacing amplitudes. Straightforward evaluation reveals that the controlled phase gate is realized when the amplitudes satisfy

$$\gamma_{1,2} = -\alpha \left[1 \pm \sqrt{\frac{e^{i\phi} - 9}{e^{i\phi} - 1}} \right]. \qquad (4.6)$$

The final member of the set of elementary gates, the Hadamard gate, requires more than single photon subtractions. This is quite understandable, because the gate is supposed to transform a coherent state $|\alpha\rangle$ into a superposed state $|\alpha\rangle + | -\alpha\rangle$, which is a strongly non-linear process. Therefore an additional superposed coherent state, say $|\alpha\rangle + | -\alpha\rangle$, is required as a resource. The required configuration is illustrated in Fig. 4.3.

The goal is to perform controlled subtraction of a single photon from the ancilla represented by operator $\hat{a} + \beta$, where $\beta = 0$ when the input was in state $|\alpha\rangle$ and $\beta \gg 1$ when the input was in state $| -\alpha\rangle$. This can be realized by first displacing the input state by α to obtain $\hat{D}(\alpha)|\psi_{\text{in}}\rangle = c_+|\beta\rangle + c_-|0\rangle$ where $\beta = 2\alpha$. This is followed by tapping off light from the two participating modes, mixing it on an unbalanced interferometer, and feeding it into a single photon detector. This realizes joint photon
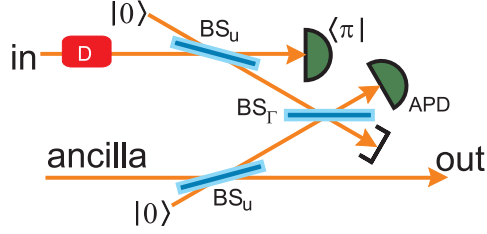
Figure 4.3: (Color online) Schematic representation of the approximate single-mode Hadamard gate. BS_u stands for a highly unbalanced weakly reflecting beam splitter, while BS_Γ is a beam splitter with transmission coefficient t_Γ used to set the parameter Γ. APD stands for a avalanche photodiode and $\langle\pi|$ represents the suitable projective measurement (see text).

subtraction $\Gamma\hat{a} + \hat{b}$, where $\hat{a}$ and $\hat{b}$ are annihilation operators acting on the ancillary and the input mode, respectively. After the input state is then projected onto a chosen pure state $\langle\pi|$, the state of the ancilla remains as

$$c_+\langle\pi|\beta\rangle[(\beta+\Gamma\alpha)|\alpha\rangle+(\beta-\Gamma\alpha)|-\alpha\rangle] + c_-\langle\pi|0\rangle\Gamma\alpha(|\alpha\rangle-|-\alpha\rangle). \quad (4.7)$$

If $|\Gamma\alpha| \ll |\beta|$ holds, we can make approximation $\beta \pm \Gamma\alpha \approx \beta$ and the output state simplifies to

$$c_+\langle\pi|\beta\rangle\beta(|\alpha\rangle+|-\alpha\rangle) + c_-\langle\pi|0\rangle\Gamma\alpha(|\alpha\rangle-|-\alpha\rangle). \quad (4.8)$$

The desired Hadamard operation is then performed if $\langle\pi|\beta\rangle\beta = \langle\pi|0\rangle\Gamma\alpha$. To achieve this, the projective measurement $|\pi\rangle$ needs to be properly chosen. For example, using homodyne detection to project on a $\hat{x}$ eigenstate $\langle\hat{x} = q|$ is appropriate, provided that $\exp[-(q-\sqrt{2}\beta)^2/2] = \exp(-q^2)\alpha\Gamma/\beta$. This can always be done. The value of Γ itself can be set by manipulating the beam splitter of the joint photon subtraction as $\Gamma = t_\Gamma/\sqrt{1-t_\Gamma^2}$. In this way, even if there is a large difference in amplitudes of the two participating states, the Hadamard gate can be implemented with arbitrary precision.

The Hadamard gate was tested experimentally [A6]. The gate was implemented for the base states $|\alpha\rangle$ and $|-\alpha\rangle$ with $\alpha = 0.75$. For these base states the gate was realized with fidelities $F_\alpha = 0.94$ and $F_{-\alpha} = 0.65$. To get
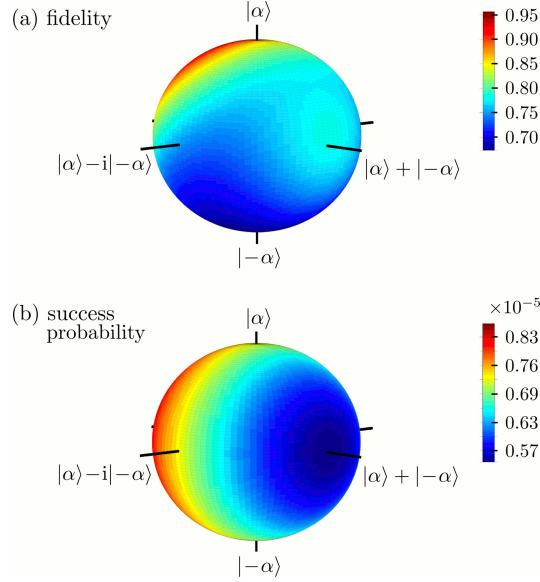
Figure 4.4: Simulation of the Hadamard gate of arbitrary coherent state qubits: a) Fidelity; b) Probability of success.

a greater insight we used the experimental parameters of the setup to simulate the effect of the gate on an arbitrary qubit in the coherent state basis. The fidelities, shown in Fig. 4.4a span the interval $F \in [0.67, 0.96]$ with an average value of $\overline{F} = 0.78$. For the base states $|\alpha\rangle$ and $|-\alpha\rangle$, the fidelities were predicted as $F_\alpha = 0.88$ and $F_{-\alpha} = 0.67$, which agreed well with the observed results. The probabilities of success are shown in Fig. 4.4b. The fidelities and probabilities of success can be also merged into a single figure of merit, the fidelity of process [79, 80], which was found to be $\mathcal{F} = 0.70$.

4.2   Continuous Information Processing

Continuous processing of quantum information tries to take advantage of the full infinite dimension of the Hilbert space of harmonic oscillators [16]. This naturally complicates the required tools, because quantum states and quantum operations employable by the processing tend to have infinite number of potential parameters. However, any practical realization always needs to

be restrained to a finite dimensional subspace, even though the number of dimensions can be chosen arbitrarily high. The arbitrary quantum states and operations required by the processing can be then decomposed into elementary resources, which can be investigated individually.

For optical systems, one such elementary object is the single photon. Together with the set of Gaussian operations, single photon states are sufficient for probabilistic implementation of arbitrary quantum operation on a Hilbert space with arbitrary finite dimension [81]. This is enabled by the ability to use single photon states, together with Gaussian measurements, to implement projective single photon measurements. Such measurement can be realized with help of an ancillary single-photon state, a balanced beam splitter and a pair of homodyne detectors measuring two different quadrature operators $\hat{x}_1$ and $\hat{p}_2$. Successful projection is heralded by outcomes $x_1 = 0$ and $p_2 = 0$. In this case, the two input modes impinging on the balanced beam splitter are projected on the maximally entangled EPR state $|\Psi_{\mathrm{EPR}}\rangle = \sum_{n=0}^{\infty} |n, n\rangle$. This in conjunction with the ancillary single-photon state implements the probabilistic projection on a single-photon state. Single-photon states and single-photon measurements combined with Gaussian operations are sufficient for probabilistic preparation of arbitrary finite dimensional multimode quantum state [81] and implementation of arbitrary transformation on the employed finite Hilbert space, e.g. by exploiting the scheme described in Ref. [51] or simply by quantum teleportation [82].

In [A7] we discovered that single photon states are not unique in this regard. In fact, an arbitrary non-Gaussian state $|\psi_N\rangle = \sum_{k=0}^{N} c_k |k\rangle$ which is finite in Fock basis shares this feature. This is because a supply of such states can be probabilistically transformed, by means of Gaussian operations and Gaussian measurements, into the supply of single photon states. This can be realized by the configuration shown in Fig. 4.5. A single copy of the non-Gaussian state is subjected to a sequence of photon subtraction operations, which can be realized by Gaussian operations and the available non-Gaussian states, see Fig. 4.5b. These subtraction operations transform the state into superposition $c_0 |0\rangle + c_1 |1\rangle$. This state can be then separated
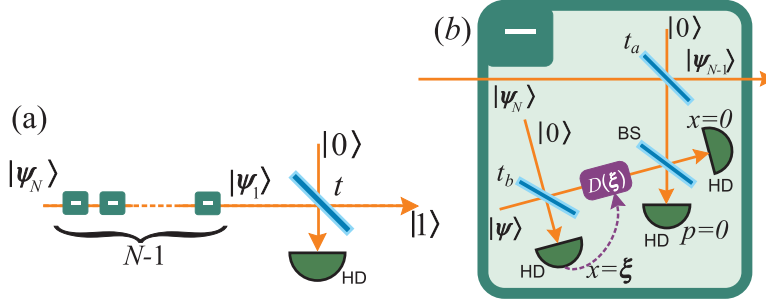
Figure 4.5: (a) Scheme for generating a single photon state from an arbitrary
state with finite dimension. (b) Detailed scheme for a single subtraction step.
t, t_a, and t_b denote transmission coefficients of the respective beam splitters,
BS - balanced beam splitter, HD - homodyne detection, $D(\xi)$ - displacement
driven by the measured value ξ.

on a beam splitter with transmission coefficient t and homodyne detection
is used to project one mode into quadrature eigenstate orthogonal to state
$c_0|0\rangle + c_1\sqrt{1 - t^2}|1\rangle$. This leaves the remaining mode in the single photon
state.

Single photon states are sufficient for realization of an arbitrary operation
on a finite dimensional Hilbert space. However, there are several possible
paths leading towards this goal. Employing the teleportation paradigm [82],
any operation can be probabilistically achieved by preparing a suitable en-
tangled state. Different suitable quantum states can be used to realize any
operation, which can be expressed as a linear superposition of annihilation
and creation operators [51].

However, there is an alternative approach. In [A8] we have shown that
it is possible to decompose certain operations into a sequence of elementary
gates. The problem of realizing an arbitrary operation then shifts to the
problem of reliably implementing these basic gates, which can be realized
one at a time. The elementary gates can be described by operators:

$$\hat{\mathcal{A}}(\lambda_-, \lambda_+) = 1 + \lambda_-\hat{a} + \lambda_+\hat{a}^\dagger, \tag{4.9}$$

where λ_+ and λ_- are arbitrary complex parameters. When $|\lambda_+| = |\lambda_-|$, the

gate realizes an X-gate - an arbitrary superposition of a quadrature operator and unity, $1 + \lambda\hat{x}$. Such gates can be, according to the fundamental theorem of algebra, used to compose an arbitrary polynomial of the quadrature operator. This allows, for example, simulating behavior of a quantum system, in an arbitrary nonlinear potential. The general form (4.9) can be used for construction of more complicated superpositions of annihilation and creation operators, but, due to their non-commutativity, finding the proper decomposition is not always straightforward.

The elementary gate can be realized by mixing the signal s with an ancillary single photon state in mode $a1$ on a beam splitter with transmissivity T and following it by a projective unbalanced heterodyne detection, see Fig. 4.6. The projection consists of splitting the ancilla on a beam splitter with transmission and reflection coefficients $\mathcal{T}$ and $\mathcal{R}$, respectively, and projecting the two emerging modes $a1$ and $a2$ onto specific eigenstates $|x'\rangle$ and $|p'\rangle$ of quadrature operators $\hat{x}$ and $\hat{p}$. The full gate can be represented by operator

$$
{}_{a1}\langle x'|_{a2}\langle p'|\hat{U}_{a1,a2}|0\rangle_{a2}\hat{U}_{a1,s}|1\rangle_{a1}
$$
$$
=_{a1}\langle A,B|\hat{U}_{a1,s}|1\rangle_{a1}
$$
$$
= \exp[A^*\frac{R}{T}\hat{a} + B^*\frac{R^2}{T^2}\hat{a}^2]T^{\hat{n}-1}(A^* + 2B^*R^*\hat{a} + R\hat{a}^\dagger), \qquad (4.10)
$$

where $\langle A,B|$ is shorthand notation for the projective measurement where $A = \sqrt{2}(x'\mathcal{T} - ip'\mathcal{R})$ and $B = \frac{1}{2}(\mathcal{R} - \mathcal{T}^2)$ are complex coefficients with arbitrarily adjustable phases. Operators $\hat{U}_{k,l}$ are unitary operators of beam splitters coupling modes k and l.

The operator (4.10) is composed of three parts: the ideal operation $A^* + 2B^*R^*\hat{a} + R\hat{a}^\dagger$ consisting of the proper superposition of annihilation and creation operators, the error operator $\exp[A^*R\hat{a} + B^*R^2\hat{a}^2]$, and another error operator $T^{\hat{n}-1}$ which corresponds to pure attenuation. These two sources of error need to be considered separately, as each of them possesses very different properties. The error term $\exp[A^*R\hat{a} + B^*R^2\hat{a}^2]$ can be compensated using the principally same configuration as (4.10), only with
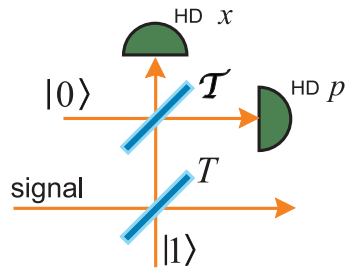
Figure 4.6: Scheme for realizing the X-gate. T and $\mathcal{T}$ denote transmissivities of the respective beam splitters. HD - homodyne detectors.

vacuum in place of the single photon state. On the other hand, term $T^{\hat{n}}$ represents noiseless attenuation and can be removed only by noiseless amplification. It should be noted that in the case of a highly transmissive beam splitter $R \ll 1$, all sorts of errors become less prominent even up to the point when the correction step is not necessary.

4.3 Summary

We have addressed two approaches towards quantum information processing with CV quantum optics. For the first one, employing discrete states encoded into continuous systems, we have designed the full set of measurement induced elementary gates needed for probabilistic simulation of all processing tasks, and we have tested one of these gates experimentally. For the second, fully continuous approach with completely arbitrary quantum states, we have first expanded the definition of required resources from single photons to arbitrary finite dimensional states, and then proposed an elementary non-Gaussian gate from which other, more convoluted operations can be constructed. This chapter is based on the following publications:

- P. Marek and J. Fiurášek, *Resources for universal quantum-state manipulation and engineering*, Physical Review A **79**, 062321 (2009)

- P. Marek and J. Fiurášek, *Elementary gates for quantum information processing with superposed coherent states*, Physical Review A **82**, 014304 (2010)

- A. Tipsmark, R. Dong, A. Laghaout, P. Marek, M. Ježek, and U. L. Andersen, *Experimental demonstration of a Hadamard gate for coherent state qubits*, Physical Review A **84**, 050301(R) (2011)

- K. Park, P. Marek, and R. Filip, *Nonlinear potential of a quantum oscillator induced by single photons*, Physical Review A **90**, 013804 (2014)

Chapter 5

Deterministic Quantum Information Processing

In a sense, processing quantum information probabilistically is more powerful than the deterministic approach - some quantum operations simply can not be realized with unit probability of success [20, 21, 52]. All this power, however, is for naught when it prevents one of the ultimate goals of quantum simulation and computation: the exponential speedup of quantum methods over the classical ones [23]. If individual quantum operations are probabilistic, the overall success probability of quantum networks will be exponentially decaying with the number of systems and individual operations and the improvement will be lost. In order to develop scalable quantum information processing it is necessary to develop quantum operations capable of operating in the deterministic regime.

Such operations are unitary and their respective interaction Hamiltonians can be, in the case of single mode harmonic oscillator, represented as

$$\hat{H} = \sum_{k_1,k_2} (c_{k_1,k_2} \hat{x}^{k_1} \hat{p}^{k_2} + c_{k_1,k_2}^* \hat{p}^{k_2} \hat{x}^{k_1}). \tag{5.1}$$

Such general operation is very difficult to come by, not only because the number of free parameters can be in principle infinite. Even the limited subclass of operations, for which the expansion is finite and the coefficients

c_{k_1,k_2} are time independent, is mostly experimentally unreachable. This is caused by the nature of the CV systems and the restricted set operations available to them. It could be said that the operations naturally available for CV systems are Gaussian [40], with Hamiltonians (5.1) and $k_1 + k_2 \leq 2$. Unfortunately, such operations lead only to linear transformation of quadrature operators and are therefore unsuitable for the desired quantum information processing tasks [41].

These are enabled by operations with Hamiltonians of higher order, also called nonlinear operations. Fortunately, for nearly universal processing we do not need access to wide range of possible operations, it is sufficient to be able to realize *any* one [34]. This is because there are techniques which allow transmogrifying available unitary operations into different ones. Specifically, two quantum unitary operations, represented by Hamiltonians $\hat{A}$ and $\hat{B}$ can be sequentially applied in order to arrive at:

$$e^{i\hat{A}t}e^{i\hat{B}t}e^{-i\hat{A}t}e^{-i\hat{B}t} \approx e^{-[\hat{A},\hat{B}]t^2} + O(t^3). \tag{5.2}$$

The sequence of the non-commuting unitary operators approximatively realizes a new unitary operator with Hamiltonian proportional to the commutator of the two original Hamiltonians. The order of the new Hamiltonian is $N_A + N_B - 2$, where N_A and N_B are the orders of Hamiltonians $\hat{A}$ and $\hat{B}$. If the two operations are Gaussian with N_A, $N_B \leq 2$, the new operation is Gaussian as well. If at least one of the operations is nonlinear, the new operation can be nonlinear as well, and if both $\hat{A}$ and $\hat{B}$ correspond to nonlinear operations, the new operation will be of higher order than any of its constituents.

Unfortunately, deterministic experimental realization of even *any* quantum nonlinear operation is an extremely difficult task. For example, one of the best known nonlinear operations for optical systems, the Kerr nonlinear phase shift represented by Hamiltonian $\hat{H} \propto (\hat{a}^\dagger \hat{a})^2$ can be observed for strong classical signals, but at the quantum level its strength is several orders of magnitude too weak [45]. It is therefore prudent to consider realizing such nonlinear operations artificially. And in doing so, it is sensible to
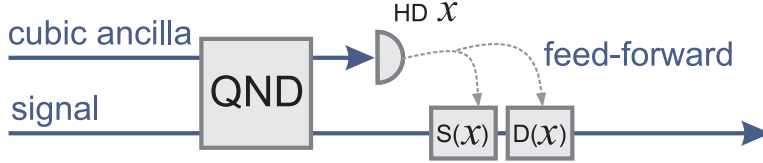
Figure 5.1: Scheme for deterministic implementation of the nonlinear cubic gate. QND - quantum non-demolition interaction, HD - homodyne detector, $S(x)$ and $D(x)$ represent the squeezing and displacement, respectively, driven by the measured value x.

focus on the simplest nonlinear operation sufficient for the task, the cubic operation [83] represented by Hamiltonian $\hat{H} \propto \hat{x}^3$.

5.1   Cubic gate - theoretical concept

In the idealized picture, the deterministic realization of the cubic gate relies on generating the cubic nonlinearity in a specific resource state and later using this state in a measurement-induced scheme to imprint the nonlinearity onto an arbitrary quantum state [83], see Fig. 5.1. The basic principle is best understood in the x-representation, in which the pure state state is given by $|\psi\rangle = \int \psi(x)|x\rangle_s dx$ and the resource state is $|\mathcal{A}\rangle = \int e^{-i\chi y^3}|y\rangle_a dy$ with χ being the strength of the desired nonlinearity and subscripts s and a labeling the modes. These two states are coupled via a quantum non-demolition (QND) coupling, represented by unitary operator $\hat{U}_{QND} = e^{i\hat{x}_s \hat{p}_a}$, which transforms their joint state into

$$\int \psi(x) e^{-iy^3}|x\rangle_s|y-x\rangle_a dxdy. \tag{5.3}$$

The $\hat{x}_a$ quadrature of the ancillary mode now gets measured by a homodyne detection which yields a real value q. This measurement collapses the unknown state of the signal into

$$\int \psi(x) e^{-i(x+q)^3}|x\rangle dx = e^{-iq^3} e^{-i3q^2\hat{x}} e^{-i3q\hat{x}^2}(e^{-i\hat{x}^3}|\psi\rangle). \tag{5.4}$$

We can see that the resulting state consists of the ideally transformed state $e^{-i\hat{x}^3}|\psi\rangle$ warped by presence of additional operations depending on the measured value q. In the probabilistic regime we could condition on the measured value being $q = 0$, but in the deterministic setup the final state is a mixture of all possibilities. Fortunately, of the three terms, e^{iq^3} is inconsequential because it represents a global phase and $e^{-i3q^2\hat{x}}e^{-i3q\hat{x}^2}$ can be removed by Gaussian operations - displacement and squeezing. Such Gaussian feed-forward completely removes the q dependence and results in clean implementation of the cubic gate.

There are several tools necessary for implementation of the cubic gate. The required Gaussian tools consist of the QND coupling, homodyne detection, and dynamically driven feed-forward with displacement and squeezing. All of these can be considered within the reach of contemporary experimental know-how. The biggest hurdle to overcome is the generation of the non-Gaussian resource, field of light in the cubic state

$$|\mathcal{A}\rangle = e^{-\chi\hat{x}^3}|p = 0\rangle = \int e^{-i\chi y^3}|y\rangle dy. \tag{5.5}$$

This state requires both infinite energy, inherent in the quadrature eigenstate, and the otherwise unavailable cubic nonlinearity. For these two reasons we can't really hope to prepare the state in its ideal form. In [A9] we have shown that we can, however, consider an approximation.

Instead of a quadrature eigenstate we can employ a finitely squeezed state $\hat{S}|0\rangle = (\pi g)^{-1/4} \int \exp(-x^2/g)|x\rangle dx$ which allows us to express the ancillary state as $\hat{S}e^{-i\chi'\hat{x}^3}|0\rangle$, where $\chi' = \chi g^{-3/2}$ is the effective nonlinear constant. If we now consider realizations in which the effective nonlinearity is weak, we can expand the unitary operator and arrive at the approximate resource state looking as

$$\hat{S}(1 + \chi'\hat{x}^3)|0\rangle = \hat{S}\left(|0\rangle + \chi'\frac{3}{2\sqrt{2}}|1\rangle + \chi'\frac{\sqrt{3}}{2}|3\rangle\right). \tag{5.6}$$

As squeezing can be considered a well accessible resource, the creation of the suitable ancilla reduces to preparing a suitable superposition of zero, one,
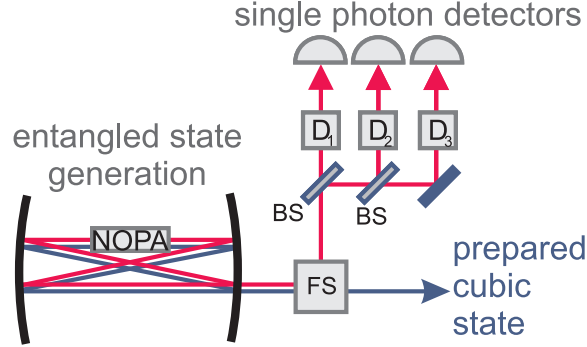
Figure 5.2: Scheme for probabilistic generation of a specific non-Gaussian state.   The entangled two-mode squeezed state is generated in oscillator cavity with nonlinear medium (NOPA). The two frequency modes are separated by the frequency separator (FS) and one of the modes is divided on a sequence of beam splitters (BS), subject to suitable displacements D_1, D_2, and D_3, and measured by single photon detectors.

and three photons. Fortunately, preparation of such state can be in principle done probabilistically, because the prepared state can be stored in quantum memory and released when needed [47, 48]. Quantum memories of sufficient quality are not yet available, but they are the focus of intensive investigation as they are needed for full scale quantum computation no matter which particular architecture wins in the end.

We have shown, in [A10, A11] that the required quantum state can be prepared with help of the setup presented in Fig. 5.2. The basic component is the two mode squeezed vacuum,

$$\psi_{TMS,1,2} \propto \sum_{k=0}^{\infty} \lambda^n |n, n\rangle_{1,2}. \tag{5.7}$$

Sequence of beam splitters is now used to split one of the modes into three, with intensity in these three modes being equal. Each of these three modes is then displaced by coherent amplitude β_j, $j = 1, 2, 3$, and directed towards an avalanche photodiode. In the limit of weak intensity, the avalanche photodiodes act as single photon detectors and project the other mode of the

two-mode squeezed vacuum into

$$
\begin{aligned}
|\psi\rangle_2 \quad &\propto \quad \langle 0|_1 \left(\frac{\hat{a}}{\sqrt{3}} + \beta_1 \right) \left(\frac{\hat{a}}{\sqrt{3}} + \beta_2 \right) \left(\frac{\hat{a}}{\sqrt{3}} + \beta_3 \right) |\psi\rangle_{TMS,1,2} \\
&\propto \quad \beta_1 \beta_2 \beta_3 |0\rangle_2 + \frac{\lambda}{\sqrt{3}} (\beta_1 \beta_2 + \beta_2 \beta_3 + \beta_1 \beta_3) |1\rangle_2 + \\
&\qquad + \frac{\lambda^2 \sqrt{2}}{3} (\beta_1 + \beta_2 + \beta_3) |2\rangle_2 + \frac{\lambda^3 \sqrt{2}}{3} |3\rangle_2.
\end{aligned}
\tag{5.8}
$$

In order to prepare the resource state (5.6), which we can in short express as $|0\rangle + c_1 |1\rangle + c_3 |3\rangle$, the three displacement amplitudes need to satisfy a set of equations:

$$
\begin{aligned}
\beta_1 \beta_2 \beta_3 &= A \\
\beta_1 \beta_2 + \beta_1 \beta_3 + \beta_2 \beta_3 &= \frac{A c_1 \sqrt{3}}{\lambda} \\
\beta_1 + \beta_2 + \beta_3 &= 0 \\
\frac{\sqrt{2} \lambda^3}{3} &= A c_3,
\end{aligned}
\tag{5.9}
$$

where A is a numerical constant related to the normalization factor, which needs to be set in accordance with the required nonlinearity χ' and the available two-mode squeezing λ. The values of displacing amplitudes can be found analytically in the form

$$
\beta_1 = \frac{\xi + \sqrt{\xi^2 - 4\zeta}}{2}, \ \ \beta_2 = \frac{\xi - \sqrt{\xi^2 - 4\zeta}}{2}, \ \ \beta_3 = -\xi,
\tag{5.10}
$$

where ξ and ζ are solutions to the set of equations

$$
\xi \zeta + A = 0, \quad \zeta - \xi^2 - \frac{A c_1 \sqrt{3}}{\lambda},
\tag{5.11}
$$

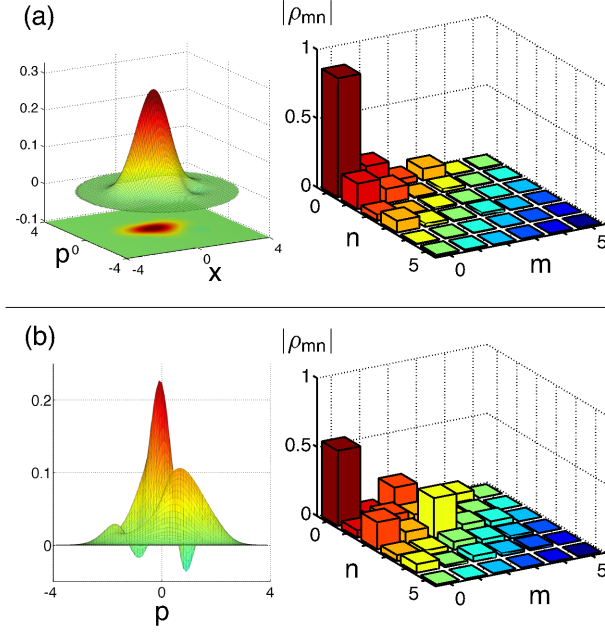which always exist and can be obtained using the Cardan formula.

Figure 5.3: (a) Wigner function and density matrix of the experimentally generated state. (b) Wigner function and density matrix of the experimentally generated state after a single photon is numerically subtracted from the data.

5.2   Experimental cubic states

To test the viability of the setup for state generation we employed it to generate the ancillary resource state $|\psi_{\mathrm{id}}\rangle \propto (1 - i\chi'\hat{x}^3)|0\rangle$ for $\chi' = 0.09$ [A10]. In Fig. 5.3a we can see the reconstructed Wigner function and density matrix. However, deciding whether the preparation was successful didn't turn out to be a straightforward task. The prepared state, represented by density matrix $\hat{\rho}_{\mathrm{exp}}$, had a significant overlap with the target state, $F = \langle \psi_{\mathrm{id}} | \rho_{\mathrm{exp}} | \psi_{\mathrm{id}} \rangle = 0.90$. On the other hand, due to low strength of the nonlinearity, the state had higher overlap with the vacuum state $\langle 0 | \hat{\rho}_{\mathrm{exp}} | 0 \rangle = 0.95$. As a consequence, it was necessary to develop new methods for detecting the presence of cubic nonlinearity in the generated state.
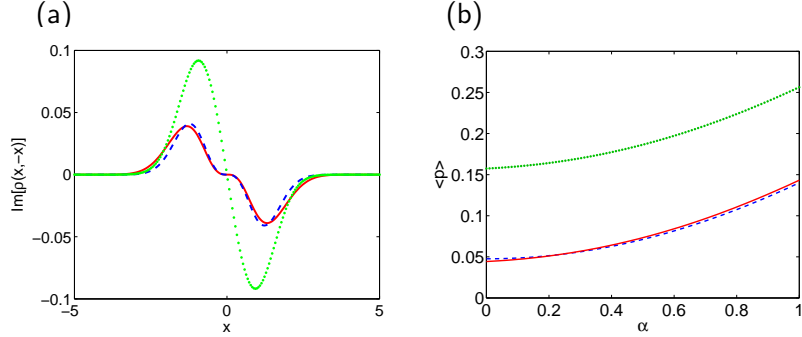
(a) (b)

Figure 5.4: a) Imaginary parts of the anti-diagonal values of coordinate density matrices for the ideal state with $\chi = 0.090$ (dashed blue line), the experimentally generated state (dotted green line) and the experimentally generated state after the suitable displacement $\Delta p = -0.17$ (solid red line). b) First moment of p for various coherent states: ideal state with $\chi = 0.090$ (dashed blue line), experimentally generated state (dotted green line), and experimentally generated state after the suitable displacement $\Delta p = -0.16$ (solid red line).

The first step was looking for the desired features while excluding the dominant contribution of the vacuum term. This was be achieved by transforming the state by a virtual photon subtraction operation resulting in transformation

$$\hat{\rho}_{\text{exp}} \to \hat{\rho}_{\text{1sub}} = \frac{\hat{a}\hat{\rho}_{\text{exp}}\hat{a}^\dagger}{\text{Tr}(\hat{a}\hat{\rho}_{\text{exp}}\hat{a}^\dagger)}. \tag{5.12}$$

For the ideal state, this would result in superposition $|\psi_{\text{id,1sub}}\rangle \propto |0\rangle + \sqrt{2}|2\rangle$. This is a state resembling an even superposition of coherent states and its Wigner function exhibits two regions of negativity. And indeed, as seen in Fig. 5.3, the transformed Wigner function did indeed show this distinctively nonclassical behavior.

Another approach relied on looking for the cubic nonlinearity in the x representation. In this representation, the impure experimental state can be represented by complex function $\rho(x, x') = \langle x|\hat{\rho}_{\text{exp}}|x'\rangle$. The cubic nonlinearity is best visible in the imaginary part of the main antidiagonal which, for the ideal state, equals to $\text{Im}[\rho(x, -x)] = 2\chi' x^3 e^{-x^2}$. The cubic effect should

therefore manifest as as the third order polynomial modulating the overlaying Gaussian function. Unfortunately, this behavior is quite fragile and can be masked by other Gaussian operation, mainly displacement, which modulate the Gaussian envelope by a linear term. This can be seen in Fig. 5.4a, in which the experimental data failed to demonstrate the desired behavior. However, after we numerically compensated the displacement, which in this case corresponded to displacing the $\hat{p}$ quadrature by $\Delta p = -0.17$, the cubic nonlinearity was revealed.

Finally, we also analyzed how would the prepared state perform as part of the full cubic gate. In order to diminish the effects of classical feed-forward, we considered a probabilistic scenario which relied on post-selecting runs in which the measured value was found to be $q = 0$. Based on our knowledge of the resource state ρ_{exp} we numerically simulated the effect of the gate on a set of coherent states $|\alpha\rangle_{\mathrm{in}}$. The behavior we were looking for can be expressed in terms of moments of quadrature operators $\hat{x}_{\mathrm{in}}$ and $\hat{p}_{\mathrm{in}}$ according to $\langle \hat{x}_{\mathrm{out}} \rangle = \langle \hat{x}_{\mathrm{in}} \rangle$, $\langle \hat{p}_{\mathrm{out}} \rangle = \langle \hat{p}_{\mathrm{in}} \rangle + 3\chi \langle \hat{x}_{\mathrm{in}}^2 \rangle$. The first moment of $\hat{x}$ should be preserved, while the first moment of $\hat{p}$ should become linearly dependent on the second moment $\langle \hat{x}^2 \rangle = \mathrm{var}(x) + \langle \hat{x} \rangle^2$. For coherent states with variance not depending on the amplitude, the second moment is a quadratic function of the amplitude. It is this quadratic moment we were looking for in the potentially measurable mean value $\langle \hat{p}_{\mathrm{out}} \rangle$. Fig. 5.4b shows the dependency and we can see that, similarly as in the previous case, there was a constant off-set in the form of $\hat{p}$ quadrature displacement with $\Delta p = -0.16$. These two displacements were obtained by independently optimizing different figures of merit, we can therefore assume that, apart from the displacement, we have indeed progressed towards preparation of the required resource state.

It should be also noted that preparation technique is not limited to preparation of the cubic states. Suitable choice of the coherent amplitudes allows preparation of an arbitrary superposition of Fock states up to number three [A11]. The technique was explicitly used for preparation of isolated Fock state $|3\rangle$, as well as for preparation of odd superposed coherent states $|\alpha\rangle - |-\alpha\rangle$, or three-headed superposed coherent states $|\alpha\rangle + |\alpha e^{i\frac{2\pi}{3}}\rangle + |\alpha e^{-i\frac{2\pi}{3}}\rangle$. All of these states exhibited strong nonclassical feature which
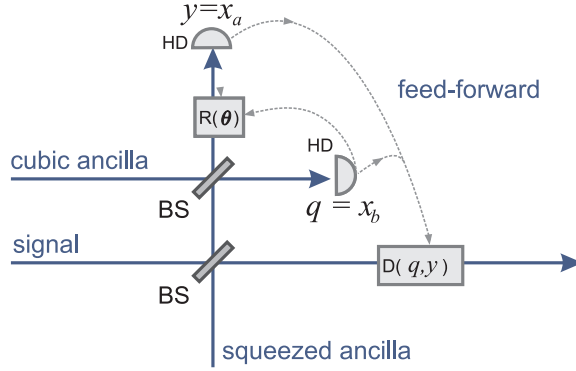
47

Figure 5.5: Scheme of the cubic gate realized by non-Gaussian adaptive measurement. BS - balanced beam splitter, HD - homodyne detection, $R(\theta)$ - phase shift by angle θ, $D(q, y)$ - displacement by value dependant of q and y.

demonstrated suitability of the technique for future quantum information processing protocols other then the deterministic cubic gate.

5.3   Streamlining the scheme

The Gaussian feed-forward, required for the implementation of the cubic gate, can be simplified to only consist of displacement operations. This is advantageous because the displacement is easier to realize and it comes burdened with fewer imperfections. The new configuration, depicted in Fig 5.5, is completely measurement driven and employs a new form of adaptive non-Gaussian measurement. Such measurement, which consist of several steps which can be dynamically changed based on prior measurement results, allows projecting on a non-Gaussian state transformed through arbitrary Gaussian operation. As a consequence, the required squeezing can be already performed during the measurement step and can be left out of the feed-forward.

In the adaptive projective measurement, the signal s is first mixed with ancilla a on a balanced beam splitter, creating a two mode state described by

Wigner function $W_S(x_s, p_s, x_a, p_a)$. The ancillary mode a is then subjected
to the adaptive measurement. As part of the measurement, mode a is mixed
on a balanced beam splitter with an ancillary mode b with Wigner function
$W_A(x_b, p_b)$. The $\hat{x}_b$ quadrature of the second ancilla can be now measured by
homodyne detection, yielding value q. This value can be now used in feed-
forward altering the state of mode a so that the second homodyne detector
measures value y of operator $\hat{p}_a \cos\theta + \hat{x}_a \sin\theta$, where $\theta = \arctan(3\sqrt{2}\chi'q)$.
This leads to the output state of the signal represented by Wigner function

$$W_{out}(x_s, p_s|q, y) \propto \int W_S(x_s, p_s, x_a, p_a) W_M(x_a, p_a; q, y) dx_1 dp_1, \qquad (5.13)$$

where

$$W_M(x, p; q, y) = \frac{2}{|\cos\theta|} W_A\left(-x + \sqrt{2}q, p + 2x\tan\theta - q\sqrt{2}\tan\theta + y\frac{\sqrt{2}}{\cos\theta}\right).$$

$$(5.14)$$

This corresponds to projecting signal onto the state of the ancilla displaced
by the measured values and squeezed (operation with hamiltonian $H \propto \hat{x}^2$)
by a factor related to θ. This squeezing is exactly the operation required by
the feed-forward step of the cubic gate. The remaining dependency on the
measured values can be now removed by a single displacement operation.

Another path towards a more effective operation lies in tailoring the an-
cillary state to the state preparation method. Since the state preparation
always produces a state constrained to a finite Fock subspace, possibly later
adjusted by proper Gaussian operations [84], it is beneficial to try and op-
timize the state preparation to find the best cubic states with regards to
the constraints. As the figure of merit we can use the variance of nonlinear
quadrature $\langle(\hat{p} - 3\chi'\hat{x}^2)^2\rangle$, which should be zero for the ideal cubic resource
state. The mean value of the operator can be freely adjusted by displacing
the state in $\hat{p}$ and it is therefore another parameter which can be optimized
over. For any maximal Fock number N we used numerical methods to find
the optimal approximate state $|\psi_N^{opt}\rangle = \sum_{k=0}^{N} c_k^{opt}|k\rangle$ in the respective re-
stricted Hilbert space. The Wigner functions of optimal states for several
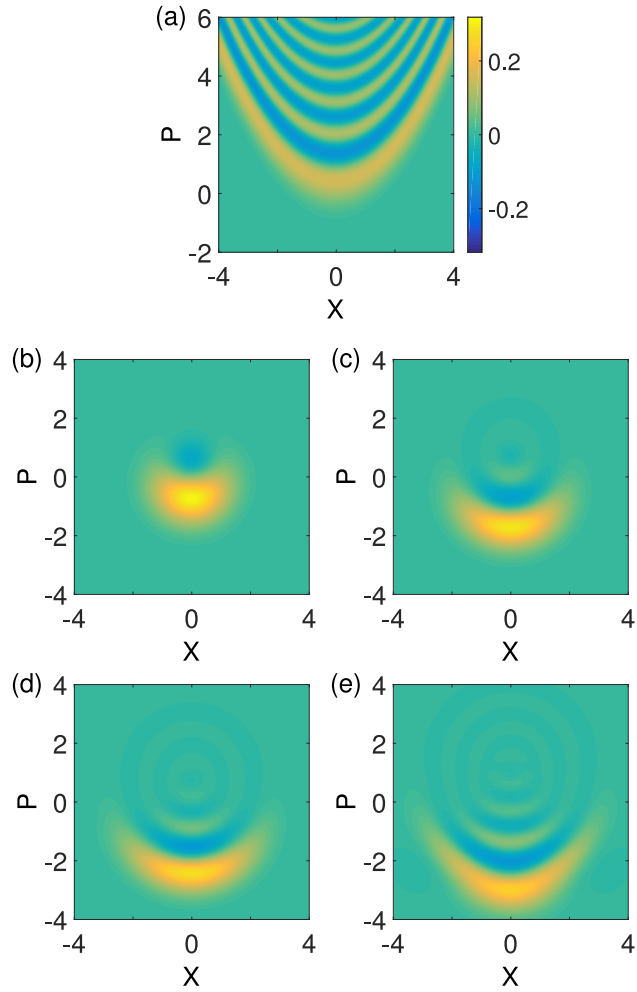
Figure 5.6: Wigner functions of the optimal ancillary states. (a) The ideal cubic state for $\gamma = 0.1$ (normalized over the displayed area), (b) $N = 1$, (c) $N = 3$, (d) $N = 5$, (e) $N = 9$. Note that the approximate states have offsets in the p direction, which can be compensated by p displacement.

possible Fock numbers are illustrated in Fig 5.6.

5.4 Summary

We have proposed a way to deterministically realize cubic nonlinear gate, which uses the measurement induced methodology to imprint the nonlinearity from a suitable ancilla to the target state. We have shown how the required ancilla, as well as other nonlinear quantum states, can be constructed by employing a tailored network of single photon detectors and displacements. Finally, we have presented a general concept of adaptive non-Gaussian measurement and shown how it can be employed in streamlining the original cubic gate into a more feasible form. The content of the chapter draws from the following publications:

- P. Marek, R. Filip, and A. Furusawa, *Deterministic implementation of weak quantum cubic nonlinearity*, Physical Review A **84**, 053802 (2011)

- M. Yukawa, K. Miyata, H. Yonezawa, P. Marek, R. Filip, and A. Furusawa, *Emulating quantum cubic nonlinearity*, Physical Review A **88**, 053816 (2013)

- M. Yukawa, K. Miyata, T. Mizuta, H. Yonezawa, P. Marek, R. Filip, and A. Furusawa, *Generating superposition of up-to three photons for continuous variable quantum information processing*, Optics Express 21, 5529 (2013),

- K. Miyata, H. Ogawa, P. Marek, R. Filip, H. Yonezawa, J. Yoshikawa, and A. Furusawa, *Implementation of a quantum cubic gate by an adaptive non-Gaussian measurement*, Physical Review A **93**, 022301 (2016),

Chapter 6

Conclusion

In this habilitation we addressed one of the key issues of contemporary quantum information processing with light - implementing quantum nonlinearity of sufficiently high order. Such quantum nonlinearity, which is strongly related to non-Gaussian quantum states of light, is required for many advanced applications of quantum information processing, the most prominent example being the quantum computation. The difficulty in implementing it can be traced back to the fundamental nature of light. Photons are bosons, which means that it is very difficult to make them interact. In fact, any interaction can happen only by interacting with other objects, such as atoms of the material used in construction of optical components. By careful manipulation, photons can be made to share modes and bunch together, but when it comes to active transformations, for example in the form of a controlled phase shift, they prefer to not get involved. Years of research in the area of DV QIP with quantum optics were dedicated towards designing tools and tricks to help, or rather to force photons to interact more strongly.

In this thesis we were interested in nonlinear properties of fields of light, rather than individual photons. The basic hurdles, however, were the same. The fields can be straightforwardly manipulated in a linear fashion but the materials capable of facilitating nonlinear behavior were and still mostly are unavailable. Fortunately, we do have access to detectors capable of distinguishing between zero and one photons. Such detectors can be used for

preparation of single photon states, which can then be used as the resources for the nonlinear operations. Alternatively, this intermediate step can be skipped and the detectors can be used for implementing nonlinear operations directly, by means of measurement induced operations.

We have applied this paradigm to several actual problems. The first one, discussed in Chapter 3, was a specific example of quantum nonlinearity tailored to a particular task - the noiseless amplification of quantum coherent states. We have presented two proposals for the noiseless amplifiers [A1] and followed up with analysis of the experimental tests performed in collaboration with *Max-Planck Institute for Science of Light in Erlangen*. The experimental tests demonstrated that the proposals are sound and that they indeed implement amplification with added noise amounting significantly less than required by classical devices [A2, A3]. We have finished the chapter by establishing the bounds on the quality of measuring optical phase, which even limit even the noiseless amplification protocols [A4].

In Chapter 4 we have abandoned the specific example and moved towards a more general picture. The chapter can be still divided into two conceptually differing segments. In the first one, we have considered a general transformation of CV quantum states, but the states themselves were limited. We investigated the possibility of implementing quantum operations for discrete qubits encoded in the basis of continuous coherent states. This encoding has several benefits over its completely DV counterpart, but also several drawbacks. One is, that even operations linear for the qubits become nonlinear due to the encoding into quantum states which can contain many photons on average. We have devised the full set of operations required for universal processing [A5] and, in collaboration with *Danish Technical Institute in Lyngby*, tested one of them in an experimental setting [A6]. In the second part of Chapter 4 we turned our attention to a more general scenario involving arbitrary quantum states of light. We have expanded the definition of universal quantum resource, showing that next to single photons it is also sufficient to have access to any states limited in Fock basis [A7], and we have proposed a way to decompose general operations into sequence of individual elementary quantum gates, which can be independently constructed

from measurements and individual photons [A8].

Finally, in Chapter 5 we have dropped the crutch of the preceding chapters and focused on implementing quantum nonlinearity in a deterministic fashion. This is a significant step towards practical utilization, because it enables scalability of the quantum protocols. Quantum operations implemented in a probabilistic way play an important role in proof-of-principle experiments, but the ultimate consequence of their chancy nature is a probability of success which drops exponentially fast as the number of employed operations increases. We have refined the proposal for the deterministic cubic gate and shown how the required resource states can be constructed from individual photons or single photon measurements [A9]. We have then, in collaboration with the *University of Tokyo* successfully experimentally tested the possibility of preparing the states in this way [A10, A11]. We have also further refined the scheme for the cubic gate, simplifying the experimental implementation considerably [A12]. As a consequence we believe that we could achieve the full deterministic cubic gate soon.

References

[A1] P. Marek and R. Filip, *Coherent-state phase concentration by quantum probabilistic amplification*, Physical Review A 81, 022302 (2010).

[A2] M. A. Usuga, C. R. Müller, C. Wittmann, P. Marek, R. Filip, C. Marquardt, G. Leuchs, and U. L. Andersen, *Noise-powered probabilistic concentration of phase information*, Nature Physics 6, 767 (2010).

[A3] C. R. Müller, C. Wittmann, P. Marek, R. Filip, C. Marquardt, G. Leuchs, U. L. Andersen, *Probabilistic cloning of coherent states without a phase reference*, Physical Review A **86**, 010305(R) (2012).

[A4] P. Marek, *Optimal probabilistic measurement of phase*, Physical Review A 88, 045802 (2013).

[A5] P. Marek and J. Fiurášek, *Elementary gates for quantum information processing with superposed coherent states*, Physical Review A 82, 014304 (2010)

[A6] A. Tipsmark, R. Dong, A. Laghaout, P. Marek, M. Ježek, and U. L. Andersen, *Experimental demonstration of a Hadamard gate for coherent state qubits*, Physical Review A 84, 050301(R) (2011)

[A7] P. Marek and J. Fiurášek, *Resources for universal quantum-state manipulation and engineering*, Physical Review A 79, 062321 (2009)

[A8] K. Park, P. Marek, and R. Filip, *Nonlinear potential of a quantum oscillator induced by single photons*, Physical Review A 90, 013804 (2014)

[A9] P. Marek, R. Filip, and A. Furusawa, *Deterministic implementation of weak quantum cubic nonlinearity*, Physical Review A 84, 053802 (2011)

[A10] M. Yukawa, K. Miyata, H. Yonezawa, P. Marek, R. Filip, and A. Furusawa, *Emulating quantum cubic nonlinearity*, Physical Review A 88, 053816 (2013)

[A11] M. Yukawa, K. Miyata, T. Mizuta, H. Yonezawa, P. Marek, R. Filip, and A. Furusawa, *Generating superposition of up-to three photons for continuous variable quantum information processing*, Optics Express 21, 5529 (2013)

[A12] K. Miyata, H. Ogawa, P. Marek, R. Filip, H. Yonezawa, J. Yoshikawa, and A. Furusawa, *Implementation of a quantum cubic gate by an adaptive non-Gaussian measurement*, Physical Review A 93, 022301 (2016)

[1] M. Planck, *Uber das Gesetz der Energieverteilung im Normalspektrum*, Ann. D. Phys. 4, 553 (1901).

[2] J. Cirac and P. Zoller, *Goals and opportunities in quantum simulation*, Nat. Phys. 8, 246 (2010).

[3] I.M. Georgescu, S. Ashhab, and F. Nori, *Quantum simulation*, Rev. Mod. Phys. 86, 153 (2014).

[4] P. Benioff, *The computer as a physical system: A microscopic quantum mechanical Hamiltonian model of computers as represented by Turing machines*, J. Stat. Phys. 22, 563 (1980).

[5] D. Deutsch, *Quantum Theory, the Church-Turing Principle and the Universal Quantum Computer*, P. Roy. Soc. Lond. A. 400, 97 (1985).

[6] E. Knill, R. Laflamme, and G. J. Milburn, *A scheme for efficient quantum computation with linear optics*, Nature (London) 409, 46 (2001).

[7] J. L. O'Brien, *Optical Quantum Computing*, Science 318, 1567 (2007).

[8] V. Scarani, H. Bechmann-Pasquinucci, N. J. Cerf, M. Dušek, N. Lütkenhaus, and M. Peev, *The Security of Practical Quantum Key Distribution*, Rev. Mod. Phys. 81, 1301 (2009).

[9] H.-K. Lo, M. Curty, and K. Tamaki, *Secure quantum key distribution*, Nature Photonics 8, 595 (2014).

[10] K. Azuma, K. Tamaki, and W. J. Munro, *All-photonic intercity quantum key distribution*, Nature Communications 6, 10171 (2015).

[11] M. W. Mitchell, J. S. Lundeen, and A. M. Steinberg, *Super-resolving phase measurements with a multiphoton entangled state*, Nature 429, 161 (2004).

[12] J. Aasi *et al.*, *Enhanced sensitivity of the LIGO gravitational wave detector by using squeezed states of light*, Nature Photonics 7, 613 (2013).

[13] C. R. Monroe, R. J. Schoelkopf, and M. D. Lukin, *Quantum Connections*, Scientific American 314, 50 (2016).

[14] S. L. Braunstein and P. van Loock, *Quantum information with continuous variables*, Rev. Mod. Phys. 77, 513 (2005).

[15] C. Weedbrook, S. Pirandola, R. Garca-Patrn, N. J. Cerf, T. C. Ralph, J. H. Shapiro, and S. Lloyd, *Gaussian quantum information*, Rev. Mod. Phys. 84, 621 (2012).

[16] U. L. Andersen, J. S. Neergaard-Nielsen, P. van Loock, and A. Furusawa, *Hybrid discrete- and continuous-variable quantum information* Nature Physics 11, 713 (2015).

[17] A. Divochiy *et al.*, *Superconducting nanowire photon-number-resolving detector at telecommunication wavelengths*, Nature Photonics 2, 302 (2008).

[18] O. Thomas, Z.L. Yuan, and A.J. Shields, *Practical photon number detection with electric field-modulated silicon avalanche photodiodes*, Nature Communications 3, 644 (2012)

[19] M. Dakna, T. Anhut, T. Opatrný, L. Knöll, and D.-G. Welsch, *Generating Schrödinger-cat-like states by means of conditional measurements on a beam splitter*, Phys. Rev. A 55, 3184 (1997).

[20] A. Ourjoumtsev, R. Tualle-Brouri, J. Laurat, and P. Grangier, *Generating Optical Schrödinger Kittens for Quantum Information Processing*, Science 312, 83 (2006).

[21] A. Zavatta, S. Viciani, and M. Bellini, *Quantum-to-classical transition with single-photon-added coherent states of light*, Science 306, 660 (2004).

[22] A. Furusawa, J. L. Sorensen, S. L. Braunstein, C. A. Fuchs, H. J. Kimble, and E. S. Polzik, *Unconditional Quantum Teleportation*, Science 282, 706 (1998).

[23] M. A. Nielsen and I. L. Chuang, *Quantum Computation and Quantum Information* (Cambridge University Press, Cambridge, 2000).

[24] A. Aspect, P. Grangier, and G. Roger, *Experimental Realization of Einstein-Podolsky-Rosen-Bohm Gedankenexperiment: A New Violation of Bell's Inequalities*, Phys. Rev. Lett. 49, 914 (1982).

[25] B. Hensen *et al.*, *Loophole-free Bell inequality violation using electron spins separated by 1.3 kilometres*, Nature 526, 682 (2015).

[26] M. Giustina *et al.*, *Significant-loophole-free test of Bell's theorem with entangled photons*, Phys. Rev. Lett. 115, 250401 (2015).

[27] L. K. Shalm *et al*, *A strong loophole-free test of local realism*, Phys. Rev. Lett. 115, 250402 (2015).

[28] C.-Y. Lu, D. E. Browne, T. Yang, and J.-W. Pan, *Demonstration of a Compiled Version of Shors Quantum Factoring Algorithm Using Photonic Qubits* Phys. Rev. Lett. 99, 250504 (2007).

[29] A. Politi, J. C. F. Matthews, and J. L. OBrien, *Shors quantum factoring algorithm on a photonic chip*, Science 325, 1221 (2009).

[30] R. Hughes, J. Nordholt, *Refining Quantum Cryptography*, Science 333, 1584 (2011).

[31] C. H. Bennett, G. Brassard, C. Crépeau, R. Jozsa, A. Peres, and W. K. Wootters, *Teleporting an unknown quantum state via dual classical and Einstein-Podolsky-Rosen channels*, Phys. Rev. Lett. 70, 1895 (1993).

[32] N. Lütkenhaus, J. Calsamiglia, and K.-A. Suominen, *Bell measurements for teleportation*, Phys. Rev. A 59, 3295 (1999).

[33] H.-A. Bachor, T. C. Ralph, *A Guide to Experiments in Quantum Optics, 2nd, Revised and Enlarged Edition* (Wiley-VCH, Weinheim, 2004).

[34] S. Lloyd and S. L. Braunstein, *Quantum Computation over Continuous Variables*, Phys. Rev. Lett. 82, 1784 (1999).

[35] S. L. Braunstein and P. van Loock, *Quantum information with continuous variables*, Rev. Mod. Phys. 77, 513 (2005).

[36] S. Takeda, T. Mizuta, M. Fuwa, P. van Loock, and Akira Furusawa, *Deterministic quantum teleportation of photonic quantum bits by a hybrid technique*, Nature 500, 315 (2013).

[37] U. Leonhardt, *Essential Quantum Optics* (Cambridge University Press, Cambridge 2010).

[38] L. Mandel, *Non-Classical States of the Electromagnetic Field*, Phys. Script. T12, 34 (1986).

[39] M. G. A. Paris, *Displacement operator by beam splitter*, Phys. Lett. A 217, 78 (1996).

[40] S. L. Braunstein, *Squeezing as an irreducible resource* , Phys. Rev. A 71, 055801 (2005).

[41] A. Mari and J. Eisert, *Positive Wigner functions render classical simulation of quantum computation efficient*, Phys. Rev. Lett. 109, 230503 (2012).

[42] G. Giedke and J. I. Cirac, *Characterization of Gaussian operations and distillation of Gaussian states*, Phys. Rev. A 66, 032316 (2002);

[43] J. Eisert, S. Scheel, and M. B. Plenio, *Distilling Gaussian States with Gaussian Operations is Impossible*, Phys. Rev. Lett. 89, 137903 (2002).

[44] J. Fiurášek, *Gaussian Transformations and Distillation of Entangled Gaussian States* Phys. Rev. Lett. 89, 137904 (2002).

[45] A. Sizmann and G. Leuchs, *The Optical Kerr Effect and Quantum Optics in Fibers*, Progress in Optics 39, 373 (1999).

[46] X. Ding, Y. He, Z.-C. Duan, N. Gregersen, M.-C. Chen, S. Unsleber, S. Maier, C. Schneider, M. Kamp, S. Höfling, C.-Y. Lu, and J.-W. Pan, *On-Demand Single Photons with High Extraction Efficiency and Near-Unity Indistinguishability from a Resonantly Driven Quantum Dot in a Micropillar*, Phys. Rev. Lett. 116, 020401 (2016).

[47] A. I. Lvovsky, B. C. Sanders, and W. Tittel, *Optical quantum memory*, Nature Photonics 3, 706 (2009).

[48] Y.-F. Pu, N. Jiang, W. Chang, H.-X. Yang, C. Li, and L.-M. Duan, *Experimental realization of a multiplexed quantum memory with 225 individually accessible memory cells*, Nat. Com. 8, 15359 (2017)

[49] M. O. Scully and K. Drühl, *Quantum eraser: A proposed photon correlation experiment concerning observation and "delayed choice" in quantum mechanics* Phys. Rev. A 25, 2208 (1982).

[50] M. Dakna, J. Clausen, L. Knöll, and D.-G. Welsch, *Generation of arbitrary quantum states of traveling fields* Phys. Rev. A 59, 1658 (1999).

[51] J. Clausen, L. Knöll, and D.-G. Welsch, *Realization of multimode operators with passive linear optics and photodetection*, Phys. Rev. A 68, 043822 (2003).

[52] A. Zavatta, V. Parigi, and M. Bellini, *Experimental nonclassicality of single-photon-added thermal light states* Phys. Rev. A 75, 052106 (2007).

[53] R. Filip, P. Marek, and U. L. Andersen, *Measurement-induced continuous-variable quantum interactions* Physical Review A 71, 042308 (2005).

[54] Y. Takeno, M. Yukawa, H. Yonezawa, and A. Furusawa, *Observation of -9 dB quadrature squeezing with improvement of phase stability in homodyne measurement* Optics Express 15, 4321 (2007).

[55] H. Vahlbruch, M. Mehmet, K. Danzmann, and R. Schnabel, *Detection of 15 dB Squeezed States of Light and their Application for the Absolute Calibration of Photoelectric Quantum Efficiency*, Phys. Rev. Lett. 117, 110801 (2016).

[56] J. Yoshikawa, T. Hayashi, T. Akiyama, N. Takei, A. Huck, U. L. Andersen, and A. Furusawa, *Demonstration of deterministic and high fidelity squeezing of quantum information* Phys. Rev. A 76, 060301(R) (2007).

[57] Y. Miwa, J. Yoshikawa, N. Iwata, M. Endo, P. Marek, R. Filip, P. van Loock, and A. Furusawa, *Exploring a New Regime for Processing Optical Qubits: Squeezing and Unsqueezing Single Photons*, Phys. Rev. Lett 113, 013601 (2014).

[58] J. Yoshikawa, Y. Miwa, A. Huck, U. L. Andersen, P. van Loock, and A. Furusawa, *Demonstration of a Quantum Nondemolition Sum Gate*, Phys. Rev. Lett. 101, 250501 (2008).

[59] J. Yoshikawa, Y. Miwa, R. Filip, and A. Furusawa, *Demonstration of a reversible phase-insensitive optical amplifier* Phys. Rev. A 83, 052307 (2011).

[60] C. H. Bennett and G. Brassard, *Quantum cryptography: Public key distribution and coin tossing*, Proceedings of IEEE International Conference on Computers, Systems and Signal Processing 175, 8 (1984).

[61] W. Wootters, W. Zurek, *A Single Quantum Cannot be Cloned*, Nature 299, 802 (1982).

[62] D. C. Burnham and D. L. Weinberg, *Observation of Simultaneity in Parametric Production of Optical Photon Pairs* Phys. Rev. Lett. 25, 84 (1970).

[63] T. C. Ralph and A. B. Lund (2008), *Quantum Communication Measurement and Computing Proc. 9th Int. Conf.* (ed. A. Lvovsky) 155 (AIP, 2009).

[64] J. Fiurásek, *Engineering quantum operations on traveling light beams by multiple photon addition and subtraction*, Phys. Rev. A 80, 053822 (2009).

[65] A. Zavatta J. Fiurásek, and M. Bellini, *A high-fidelity noiseless amplifier for quantum light states* Nature Phot. 5, 52 (2011).

[66] U. Leonhardt, J. A. Vaccaro, B. Böhmer, and H. Paul, Phys. Rev. A 51, 2169 (1998).

[67] H. M. Wisemann and R. B. Killip, Phys. Rev. A 56, 944 (1997).

[68] H. M. Wisemann and R. B. Killip, Phys. Rev. A 57, 2169 (1998).

[69] S. L. Braunstein, N. J. Cerf, S. Iblisdir, P. van Loock, and S. Massar, *Optimal Cloning of Coherent States with a Linear Amplifier and Beam Splitters*, Phys. Rev. Lett. 86, 4938 (2001).

[70] M. Sabuncu, G. Leuchs, and U. L. Andersen, *Experimental continuous-variable cloning of partial quantum information* Phys. Rev. A 78, 052312 (2008).

[71] I.D. Ivanovic, Phys. Lett. A 123, 257 (1987); D. Dieks, Phys. Lett. A 126, 303 (1988); A. Peres, Phys. Lett. A 128, 19 (1988); S. J. van Enk, Phys. Rev. A 66, 042313 (2002).

[72] L. P. Hughston, R. Jozsa, W. K. Wootters, *A complete classification of quantum ensembles having a given density matrixOriginal Research Article*, Phys. Lett. A 183, 14 (1993).

[73] A. Bassi and G. Ghirardi, *A general scheme for ensemble purification*, Phys. Lett. A 309, 24 (2003).

[74] C. H. Bennett, H. J. Bernstein, S. Popescu, and B. Schumacher, *Concentrating partial entanglement by local operations*, Phys. Rev. A 53, 2046 (1996).

[75] J.W. Pan, C. Simon, Č. Brukner, and A. Zeilinger, *Entanglement purification for quantum communication*, Nature 410, 1067 (2001).

[76] H. Jeong and M. S. Kim, *Efficient quantum computation using coherent states*, Phys. Rev. A 65, 042305 (2002).

[77] T. C. Ralph, A. Gilchrist, G. J. Milburn, W. J. Munro, and S. Glancy, *Quantum computation with optical coherent states* Phys. Rev. A 68, 042319 (2003).

[78] A. Ourjoumtsev, H. Jeong, R. Tualle-Brouri, and P. Grangier, *Generation of optical 'Schrödinger cats' from photon number states* Nature, 448, 784 (2007)/

[79] D. Gottesman, and Isaac L. Chuang, *Demonstrating the viability of universal quantum computation using teleportation and single-qubit operations* Nature 402, 390 (1999).

[80] L. Slodička, M. Ježek, and J. Fiurášek, *Experimental demonstration of a teleportation-based programmable quantum gate* Phys. Rev. A 79, 050304(R) (2009).

[81] J. Fiurášek, S. Massar, and N. J. Cerf, *Conditional generation of arbitrary multimode entangled states of light with linear optics* Phys. Rev. A 68, 042325 (2003).

[82] D. Gottesman and I. L. Chuang, *Demonstrating the viability of universal quantum computation using teleportation and single-qubit operations*, Nature 402, 390 (1999).

[83] D. Gottesman, A. Kitaev, and J. Preskill, *Encoding a qubit in an oscillator*, Phys. Rev. A 64, 012310 (2001).

[84] D. Menzies and R. Filip, *Gaussian-optimized preparation of non-Gaussian pure states* Phys. Rev. A 79, 012313 (2009).

Supplementary material

The thesis draws material from the following twelve articles published between years 2009-2016:

1. P. Marek and R. Filip, *Coherent-state phase concentration by quantum probabilistic amplification*, Physical Review A 81, 022302 (2010).

2. M. A. Usuga, C. R. Müller, C. Wittmann, P. Marek, R. Filip, C. Marquardt, G. Leuchs, and U. L. Andersen, *Noise-powered probabilistic concentration of phase information*, Nature Physics **6**, 767 (2010).

3. C. R. Müller, C. Wittmann, P. Marek, R. Filip, C. Marquardt, G. Leuchs, U. L. Andersen, *Probabilistic cloning of coherent states without a phase reference*, Physical Review A **86**, 010305(R) (2012).

4. P. Marek, *Optimal probabilistic measurement of phase*, Physical Review A 88, 045802 (2013).

5. P. Marek and J. Fiurášek, *Elementary gates for quantum information processing with superposed coherent states*, Physical Review A 82, 014304 (2010)

6. A. Tipsmark, R. Dong, A. Laghaout, P. Marek, M. Jeek, and U. L. Andersen, *Experimental demonstration of a Hadamard gate for coherent state qubits*, Physical Review A 84, 050301(R) (2011)

7. P. Marek and J. Fiurášek, *Resources for universal quantum-state manipulation and engineering*, Physical Review A 79, 062321 (2009)

8. K. Park, P. Marek, and R. Filip, *Nonlinear potential of a quantum oscillator induced by single photons*, Physical Review A 90, 013804 (2014)

9. P. Marek, R. Filip, and A. Furusawa, *Deterministic implementation of weak quantum cubic nonlinearity*, Physical Review A 84, 053802 (2011)

10. M. Yukawa, K. Miyata, H. Yonezawa, P. Marek, R. Filip, and A. Furusawa, *Emulating quantum cubic nonlinearity*, Physical Review A 88, 053816 (2013)

11. M. Yukawa, K. Miyata, T. Mizuta, H. Yonezawa, P. Marek, R. Filip, and A. Furusawa, *Generating superposition of up-to three photons for continuous variable quantum information processing*, Optics Express 21, 5529 (2013)

12. K. Miyata, H. Ogawa, P. Marek, R. Filip, H. Yonezawa, J. Yoshikawa, and A. Furusawa, *Implementation of a quantum cubic gate by an adaptive non-Gaussian measurement*, Physical Review A 93, 022301 (2016)

Coherent-state phase concentration by quantum probabilistic amplification

Petr Marek and Radim Filip

Department of Optics, Palacký University, 17. listopadu 1192/12, CZ-771 46 Olomouc, Czech Republic
(Received 14 July 2009; published 4 February 2010)

We propose a probabilistic measurement-induced amplification for coherent states. The amplification scheme uses a counterintuitive architecture: a thermal noise addition (instead of a single-photon addition) followed by a feasible multiple-photon subtraction using a realistic photon-number-resolving detector. It allows one to substantially amplify weak coherent states and simultaneously reduce their phase uncertainty, which is impossible when using a deterministic Gaussian amplifier.

I. INTRODUCTION

Quantum optics has an extraordinary capability to combine observations of both the wave and the particle phenomena. Information can be encoded both into the intensity and into the phase of an optical field. Although the intensity approach, involving photons, may inherently seem more "quantum" than the phase approach, neither can be described by classical physics in full [1]. In this article, it is the phase aspect of the optical field we are going to focus on. The main aim of the quantum phase information processing is to reduce noise in the system and to compensate for the loss. The classical processing methods, mostly based on measurement and repreparation, are of limited usefulness [2] because of the inherent noise present in all quantum systems. This problem is especially pronounced for optical signals with low intensities, possibly occurring as a consequence of loss. In general, we seek to enhance an unknown phase of an optical signal by deterministic or probabilistic methods, where the main benefit of probabilistic methods lies in their ability to qualitatively overcome the limits of deterministic operations.

A coherent state $|\alpha\rangle$, the approximation of a light from a stabilized laser, is a natural medium for the phase encoding of information. Coherent states are nonorthogonal and very strongly overlapping if the amplitude is small, which can easily happen after a strong attenuation. Therefore, it is highly desirable to reamplify the states in a way that improves the phase information, ideally performing the transformation $|\alpha\rangle \rightarrow |g\alpha\rangle$, where $g > 1$. One might naturally think of the displacement operation, but keep in mind we seek to amplify a coherent state with an unknown phase and therefore we lack the knowledge needed for the correct displacement. Another option is the Gaussian parametric amplification [3,4], which is phase insensitive and it can be applied to an unknown state. However, in this case the phase information of the state does actually get worse due to the fundamental quantum noise penalty [5].

The ideal amplification $|\alpha\rangle \rightarrow |g\alpha\rangle$ is nonphysical, but for small values of $|\alpha|$ it can be implemented approximatively. One approach relies on the quantum scissors paradigm, limiting the dimension of the used Hilbert state [6]. The input coherent state is split into M weak copies, which can be approximated by $(|0\rangle + \alpha/M|1\rangle + \cdots)^{\otimes M}$ and probabilistically amplified to $(|0\rangle + g\alpha/M|1\rangle)^{\otimes M}$. For a small value of $|\alpha|/M$ the subsequent Gaussifying concentration yields a finite Hilbert space approximation of $|g\alpha\rangle$. However, the procedure requires

multiple indistinguishable single-photon sources and high interferometric stability of the multipath interferometer. Another approach is based on a still highly sophisticated cross-Kerr nonlinearity at a single-photon level followed by homodyne detection [7]. This kind of amplification has already been suggested, in Ref. [8], to concentrate entanglement.

In this article we propose a scheme for concentration of an unknown phase of coherent states using a probabilistic highly nonlinear amplifier. Our method is based on the addition of thermal noise to the unknown coherent state, followed by a multiple-photon subtraction using a photon-number-resolving detector. This procedure probabilistically amplifies the coherent state, increasing its mean photon number and simultaneously substantially reducing the phase noise. It leads to a probabilistic concentration of phase information, which cannot be obtained by Gaussian operations alone. Remarkably, the scheme requires neither single-photon sources nor high interferometric stability—the resource for the highly nonlinear amplification is the continual thermal noise injected into the signal mode.

II. PHASE AND AMPLIFICATION

The quality of information carried by the phase is difficult to assess, as the phase is not a quantum mechanical observable and therefore it cannot be directly and ideally measured. However, each measurement devised to obtain the phase of the state can be characterized by a real positive-semidefinite matrix H, which is used in computing the phase distribution $P(\theta) = \text{Tr}[\rho F(\theta)]$, where $F(\theta) = (1/2\pi)\sum_{m,n=0}^{\infty} \exp[i\theta(m-n)]H_{mn}|m\rangle\langle n|$ [9], and $|m\rangle$ stands for the photon number Fock state. The actual form of the matrix H depends on the process used to extract the phase information. For example, for a phase obtained by the most common heterodyne measurement, consisting of a balanced beam splitter and a pair of homodyne detectors measuring conjugate quadratures, the matrix elements are $H_{mn} = \Gamma[(n+m)/2+1]/\sqrt{n!m!}$. Ultimately, for the ideal canonical phase measurement $H_{mn} = 1$ and $F(\theta)$ is a projector on the idealized phase state $|\theta\rangle = \sum_{n=0}^{\infty} e^{i\theta n}|n\rangle$. To obtain a single parameter characterizing the quality of phase encoding, we can use the distribution $P(\theta)$ to calculate the phase variance $V = |\mu|^{-2} - 1$, where $\mu = \langle \exp(i\theta)\rangle$ and subscripts H and C will be used to distinguish between the heterodyne and the canonical measurements, respectively. For calculations of an arbitrary

measurement we can simply use the formula $\langle \exp(i\theta) \rangle = \int_{-\pi}^{\pi} P(\theta) \exp(i\theta) d\theta = \text{Tr}(\sum_{n=0}^{\infty} H_{n,n+1}|n\rangle\langle n+1|\rho)$.

The coherent states can be expressed as $|\alpha\rangle = \exp(-|\alpha|^2/2) \sum_{n=0}^{\infty} \alpha^n/\sqrt{n!}|n\rangle$. For these states, the quality of phase encoding is fully given by the mean number of coherent photons $N = |\alpha|^2$, and the phase variances, obtained with the help of [9]

$$\mu_C = e^{-|\alpha|^2} \alpha \sum_{n=0}^{\infty} \frac{|\alpha|^{2n}}{n!\sqrt{n+1}},$$

$$\mu_H = e^{-|\alpha|^2} \alpha \, _1F_1\left(\frac{3}{2}; 2; |\alpha|^2\right) \frac{\Gamma\left[\frac{3}{2}\right]}{\Gamma[2]}, \quad (1)$$

are both monotonically decreasing functions of the mean photon number N. For weak coherent states with $N < 1$, the variances can be well approximated by

$$V_C(N) \approx N^{-1} + 1 - \sqrt{2} + O(N^2),$$

$$V_H(N) \approx 4/(\pi N) + (-1 + 2/\pi) + O(N^2), \quad (2)$$

if we take only the dominating terms into account. In the following, we focus primarily on the canonical phase variance.

For coherent states the phase variance is directly related to the amplitude $|\alpha|$. The ideal noiseless amplifier, which increases the amplitude while keeping the state coherent, would be therefore a suitable amplification device, if its implementation were not so complicated. On the other hand, the deterministic phase-insensitive (Gaussian) amplifier [3,4] is experimentally quite feasible, but unfortunately it actually worsens the phase variance of the coherent state. To show this, we can use a method similar to the one used in [10] to calculate

$$\mu_C = \frac{\alpha^*}{\pi} \int_0^{\frac{1}{G}} \frac{\exp(-xGN)}{\sqrt{-\ln\frac{1-Gx}{1-(G-1)x}}} dx, \quad (3)$$

where $G = g^2$ is the linear amplification gain. We can now use (3) to obtain the phase variance and numerically verify its increase.

III. AMPLIFICATION BY PHOTON ADDITION AND SUBTRACTION

However, there is another mechanism that can be employed for amplification and phase improvement. Consider a single-photon addition (described by $a^\dagger|n\rangle = \sqrt{n+1}|n+1\rangle$) followed by a single-photon subtraction (described by $a|n\rangle = \sqrt{n}|n-1\rangle$) applied to a weak coherent state (approximately, $|\alpha\rangle = |0\rangle + \alpha|1\rangle$). This corresponds to $aa^\dagger(|0\rangle + \alpha|1\rangle) \rightarrow a(|1\rangle + \sqrt{2}\alpha|2\rangle) \rightarrow |0\rangle + 2\alpha|1\rangle$. For low N this reduces the phase variance roughly by a factor of 4. Note, the canonical variance actually decreases in both the creation and the annihilation process.

For a coherent state transformed in this way, $aa^\dagger|\alpha\rangle$, the total mean photon number $\langle N \rangle = N(4 + 5N + N^2)/(1 + 3N + N^2)$ increases and the canonical variance

$$\mu_C = \exp(-N) \frac{\sqrt{N}}{1 + 3N + N^2} \sum_{n=0}^{\infty} \frac{N^n(n+1)(n+2)}{n!\sqrt{n+1}} \quad (4)$$

is always lower than the Holevo variance from (1). For a lower $N < 1$, the canonical phase variance after the probabilistic

procedure approaches the phase variance for the coherent state with $N = \langle N \rangle$. For a larger N this effect tends to be less pronounced as the relative influence of single-photon operations diminishes. In this scenario it is convenient to consider a generalization, a collective M-photon addition followed by an M-photon subtraction. The phase variance is then determined by

$$\mu_C = e^{-N} \frac{\sqrt{N}}{\mathcal{N}}$$

$$\times \sum_{n=0}^{\infty} \frac{N^n}{n!\sqrt{n+1}} \frac{(n+M)!}{n!}(n+1+M)(n+1)!,$$

$$\mathcal{N} = e^{-N} \sum_{n=0}^{\infty} \frac{N^n}{n!} \left(\frac{(n+M)!}{n!}\right)^2, \quad (5)$$

and it decreases as M grows. Simultaneously, this also leads to an increase of the mean photon number. For sufficiently low values of N, the canonical variance approaches the result of the ideal noiseless amplifier and we can use the approximation

$$V_C(N) \approx \frac{1}{(M+1)^2 N} + 1 - \frac{M+2}{\sqrt{2}(M+1)} + O(N^2). \quad (6)$$

Comparison to the analogous formula for the noiseless amplifier (2) with $N \rightarrow g^2 N$ reveals that $M + 1$ can play a role of the amplification gain g.

For the construction of such a probabilistic phase-insensitive amplifier, the photon addition operation is required. Furthermore, the photons have to be added coherently, perfectly interfering with the incoming coherent state. This task can be performed using a nondegenerate optical parametric amplifier with an avalanche photodiode monitoring the output idler port [11]. This approach has already been used to verify the validity of commutation relations for the annihilation operator [12], and it is therefore fully capable of demonstrating the probabilistic amplification for $M = 1$. However, the procedure is not trivial and adding and subsequently subtracting more than two photons is currently unfeasible, mainly due to low success rates.

IV. AMPLIFICATION WITH NOISE ADDITION

Fortunately, the amplification can be made simpler. Instead of adding single photons separately, we can add a phase-insensitive thermal noise, which is characterized by its mean number of thermal photons N_{th}. The second step is then the same as already discussed—the probabilistic subtraction of M photons. Now the photon subtraction is an operation which can improve the phase properties, but the noise addition is clearly purely destructive. Why does it work then? The main point is that the photon subtraction does nothing when applied to a coherent state. However, for a mixed state the photon subtraction serves as a probabilistic filter, improving the weight of the high amplitude coherent states within the mixture. The first step of the amplification could be explained as a displacement in a random direction. This creates a phase-insensitive mixture of coherent states slightly displaced in the direction given by the initial phase. The second step, the photon subtraction, then "picks" states with the highest intensity and these states are mostly those for which the

displacement had (purely by chance) the same phase as the initial signal. The state after the subtraction is still mixed, with the same mean phase as the initial coherent state, but overall amplitude has been increased by the amplification.

Formally, the density operator of the initial coherent state after the noise addition and M photon subtraction can be represented as $\rho_{\text{amp}} = \sum_{n,m} \rho_{n,m} |n - M\rangle\langle m - M|$, where

$$\rho_{n,m} = \frac{1}{\mathcal{N}} \sqrt{\frac{n!}{m!}} \exp\left(-\frac{|\alpha|^2}{N_{\text{th}} + 1}\right) \frac{(\alpha^*)^{m-n} N_{\text{th}}^n}{(N_{\text{th}} + 1)^{m+1}}$$

$$\times \mathrm{L}_n^{m-n}\left(-\frac{|\alpha|^2}{N_{\text{th}}(N_{\text{th}} + 1)}\right) \sqrt{\frac{n!m!}{(n-M)!(m-M)!}}$$

(7)

for $m \geqslant n$ and $\rho_{m,n} = \rho_{n,m}^*$ otherwise. $L_n^m(x)$ denotes the associated Laguerre polynomial. The normalization factor representing the success rate is

$$\mathcal{N} = \sum_k \exp\left(-\frac{|\alpha|^2}{N_{\text{th}} + 1}\right) \frac{N_{\text{th}}^{k+M}}{(N_{\text{th}} + 1)^{k+M+1}}$$

$$\times \mathrm{L}_{k+M}^0\left(-\frac{|\alpha|^2}{N_{\text{th}}(N_{\text{th}} + 1)}\right) \frac{(k + M)!}{k!}.$$

(8)

It may be surprising that such an incoherent operation preserves and even improves the phase of the initial coherent state. To show that this is really the case we express the density matrix elements (7) as $\rho_{m,n} = \tilde{\rho}_{m,n}(|\alpha|)e^{i\phi(m-n)}$, where we have introduced ϕ as the mean phase of the initial coherent state, $\alpha = |\alpha|e^{i\phi}$. If we formally represent the amplification operation by a mapping $\mathcal{A}$ such that $\rho_{\text{amp}} = \mathcal{A}[|\alpha\rangle\langle\alpha|]$, we can see that it commutes with the unitary phase shift operator $U_\theta = e^{i\theta a^\dagger a}$,

$$U_\theta \mathcal{A}[|\alpha\rangle\langle\alpha|]U_\theta^\dagger = \mathcal{A}[U_\theta|\alpha\rangle\langle\alpha|U_\theta^\dagger].$$

(9)

Consequently, the mean phase of the amplified state is fully given by the phase of the initial coherent state. Also note that the amplification effects are completely covered by the density matrix given by $\tilde{\rho}_{m,n}(|\alpha|)$. In this sense, the amplification procedure is universal with respect to the phase of the initial state. To analyze the phase concentration effect we can calculate the canonical phase variance:

$$\mu_C = \frac{1}{\mathcal{N}} \sum_k \sqrt{\frac{(k+M)!}{(k+M+1)!}} \exp\left(-\frac{|\alpha|^2}{N_{TH} + 1}\right)$$

$$\times \frac{\alpha N_{\text{th}}^{k+M}}{(N_{\text{th}} + 1)^{k+M+2}} \mathrm{L}_{k+M}^1\left(-\frac{|\alpha|^2}{N_{\text{th}}(N_{\text{th}} + 1)}\right)$$

$$\times \sqrt{\frac{(k+M)!(k+1+M)!}{k!(k+1)!}}.$$

(10)

The expression (10) can be calculated numerically and the results are presented in Fig. 1. The probabilistic amplification of the initial coherent state ($M = 0$) results in a visible reduction of the phase variance. The mean number N_{th} of added thermal photons was optimized to minimize the phase variance and it is saturating for larger M. The reduction of the phase variance saturates as well, but already for a somewhat feasible four-photon subtraction the resulting phase
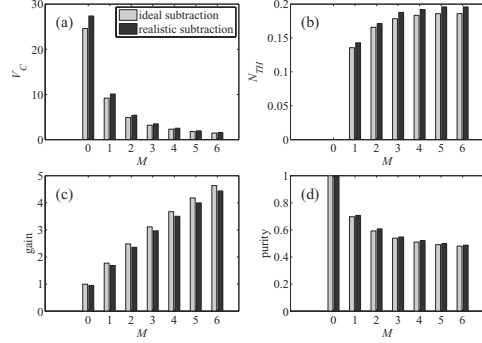

FIG. 1. (Color online) Phase concentration in a highly probabilistic amplification using thermal noise addition and photon subtraction. The separate graphs show the canonical phase variance V_C (a), the optimal number of thermal photons added (b), the gain of the amplification (c), and the purity of the amplified state (d) as a function of the number of subtracted photons M. The different bars correspond to the ideal photon subtraction realized by the annihilation operator (left) and to the realistic photon subtraction employing a beam splitter with $T = 0.9$ and a threshold detector with efficiency $\eta = 0.4$ (right). The color coding given in panel (a) is the same for all the panels.

variance corresponds to the phase variance of a coherent state with $N = 0.36$ (as opposed to the coherent state with $N = 0.04$ before the amplification). This is equivalent to a strong amplification $|\alpha\rangle \rightarrow |g\alpha\rangle$ with gain $g = 3$. We can also look at the process from the amplification perspective and find out how the amplitude of the state increases. If we consider (without loss of generality, because the amplification is phase insensitive) the initial mean phase of $\phi = 0$, the gain of the amplification can be expressed as $\langle(a + a^\dagger)/2\rangle/\sqrt{N}$ and it is shown in Fig. 1(c) for various M. The addition of thermal photons is an incoherent process and the resulting state is therefore not pure. The purity after the amplification can be seen in Fig. 1(d).

The nonlinear nature of the amplification is clearly visible from a change of the contour of Wigner function (taken at full width at a half maximum) in Fig. 2. The contours are
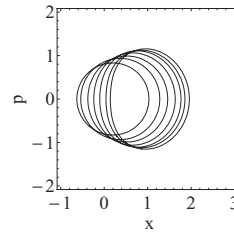

FIG. 2. Contours of Wigner functions of the states amplified by the noise addition and the beam splitter tap, similar to conditions described in Fig. 1. The contours go from left to right as the number of subtractions increases $M = 0, 1, \ldots, 6$.

plotted for an initial state with $\alpha = 0.2$ with a mean phase value of $\phi = 0$. From the contours of the group of amplified states we can see that the mean phase of the state is preserved and the state is displaced in this correct direction. At the same time the initial circular contour gains a "crescent" shape as M increases. This is a difference from the ideal noiseless amplification methods [6,7], which keep the state coherent (in a suitable limit). However, although the change of shape of the Wigner function suggests greater phase uncertainty, the increase of the amplitude of the state results in a smaller phase variance.

For a physical understanding it is illustrative to consider a weak coherent state $|0\rangle + \alpha|1\rangle$ displaced by a weak thermal noise $\rho \rightarrow \rho + \epsilon_{\text{th}}(a^\dagger \rho a + a \rho a^\dagger)$ and followed by a single-photon subtraction. The resulting state is $N|0\rangle\langle 0| + \epsilon_{\text{th}}(|0\rangle + 2\alpha|1\rangle)(\langle 0| + 2\alpha^*\langle 1|)$ up to a normalization $\mathcal{N} = N + \epsilon_{\text{th}} + 4N\epsilon_{\text{th}}$. The canonical phase variance can be determined from $\mu = 2\epsilon_{\text{th}}\alpha/\mathcal{N}$, and for small $N < 0.1$, the reduction approaches $V \propto \frac{1}{4N}$, approximating very well the result for the ideal amplification (2) with $g = 2$, if ϵ_{th} is low enough. More generally, if the thermal noise is approximated as an addition of up to M photons, the M-photon subtraction leads to phase variance $V \propto \frac{1}{(M+1)^2 N}$, which qualitatively matches the results for the ideal amplification with $g = M + 1$ (2), as well as the amplification by coherent addition and subtraction of M photons (6).

The addition of a thermal noise can be realized by mixing the signal with a thermal state on a highly unbalanced beam splitter. The thermal state can be provided either by a thermal source, in which case the sufficient spatial and spectral overlap needs to be ensured by suitable filters, or by creating a mixture of coherent states by a proper random modulation. The benefit of the first approach lies in conceptually lower demand on resources, as there is no need for a coherent source of light. On the other hand, the second approach allows for generation of mixed states with various kinds of distributions (not just thermal), which can be used for a further optimization of the procedure.

A feasible scheme capable of approximately subtracting M photons, which is required for a physical implementation of the procedure, is sketched in Fig. 3. It can be built from a linear coupling (a beam splitter with transmissivity T) to tap a part of the optical signal and a threshold measurement registering at least M_0 photons [13]. The quantum efficiency of the detector can be modeled by a virtual beam splitter with transmissivity η inserted in front of the ideal detector. The quality of the outgoing signal depends on the transmissivity
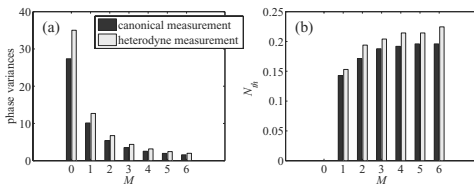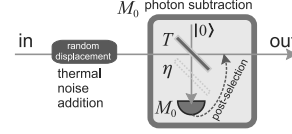

FIG. 4. (Color online) Comparison between the canonical phase measurement and the heterodyne phase measurement after the realistic phase concentration. The respective phase variances are shown in panel (a), while the optimal numbers of thermal photons are shown in panel (b).

T values, $T < 1$ translates as loss, which increases the phase variance. The limited quantum efficiency of the detector only affects the success rate. However, η that is too low may require lower T to achieve sufficiently high success rates.

Generally, the amplified state can be expressed as

$$\rho'_{\text{amp}} = \frac{1}{P_S} \int \Phi\left(\frac{\beta}{\sqrt{T}}\right) \mathcal{P}_\Pi\left(\frac{\beta}{\sqrt{T}}\right) |\beta\rangle\langle\beta| \frac{d^2\beta}{T}, \quad (11)$$

where $\mathcal{P}_\Pi(\beta) = \langle\sqrt{\eta(1-T)}\beta|\Pi|\sqrt{\eta(1-T)}\beta\rangle$ and Π denotes the positive-detection positive operator-valued measure (POVM) element, which in the case of the threshold detector looks like $\Pi = 1 - \sum_{k=0}^{M_0-1} |k\rangle\langle k|$. The initial coherent state with the addition of thermal noise is represented by $\Phi(\beta) = \exp(-|\beta - \alpha|^2/N_{\text{th}})/\pi N_{\text{th}}$. The normalization factor P_S gives the probability of the success: $P_S = \int \Phi(\beta/\sqrt{T}) \mathcal{P}_\Pi(\beta/\sqrt{T}) d^2\beta/T$.

The density operator (11) fully describes the realistically amplified coherent state and its numerical evaluation is straightforward. The results are shown in Fig. 1 and we can see that, although they are quantitatively worse than those for the ideal subtraction, they follow the same qualitative pattern. The realistic multiphoton subtraction, even with the low quantum efficiency $\eta = 0.4$, is therefore a sufficient replacement for the ideal subtraction. Finally, we can check the difference between the canonical and the heterodyne phase measurements. The comparison in Fig. 4 shows a good qualitative agreement and justifies the use of the canonical measurement for the previous analysis.

V. SUMMARY

We have proposed a probabilistic amplifier for coherent states. The amplifier setup, based on a thermal noise addition (instead of a single-photon addition) followed by a feasible multiphoton subtraction allows one to substantially reduce the phase variance of a coherent state. Note that the distribution of the random-noise-like modulation of the signal could be optimized to achieve better performance. There are also several possible applications open for future consideration. In quantum key distribution, the amplifier could be conceivably used in situations when the loss in the quantum channel prevents the secure key generation. At the same time, the amplifier is of no use to the eavesdropper because of its probabilistic nature—any gain in the rare event when the amplification succeeds is lost in the noise produced when it does not. As another possible application one could consider a probabilistic cloning of coherent states. Finally, the amplification itself need

FIG. 3. (Color online) Realistic scheme for the probabilistic amplification of a coherent state.

not be restricted to traveling wave quantum optics. All the necessary components, the thermal field, the coherent field, and the single-photon subtraction are also available in cavity QED [14] and this direction is open for future investigation.

Note added. Recently, a publication appeared that proposed another method for a noiseless amplification of coherent states based on a multiple-photon addition [15].

[1] R. J. Glauber, Phys. Rev. **130**, 2529 (1963).

[2] For an overview, see, for example, U. L. Andersen and R. Filip, *Progress in Optics*, edited by Emil Wolf (Elsevier, Amsterdam/New York, 2009), Vol. 53, p. 365 .

[3] H. A. Haus and J. A. Mullen, Phys. Rev. **128**, 2407 (1962).

[4] V. Josse, M. Sabuncu, N. J. Cerf, G. Leuchs, and U. L. Andersen, Phys. Rev. Lett. **96**, 163602 (2006).

[5] C. M. Caves, Phys. Rev. D **26**, 1817 (1982).

[6] T. C. Ralph and A. P. Lund, AIP Conf. Proc. **1110**, 155 (2009).

[7] D. Menzies and S. Croke (2009), e-print arXiv:0809.0326.

[8] J. Fiurášek, L. Mišta, and R. Filip, Phys. Rev. A **67**, 022304 (2003).

[9] H. M. Wiseman and R. B. Killip, Phys. Rev. A **56**, 944 (1997); **57**, 2169 (1998).

[10] M. Aspachs, J. Calsamiglia, R. Munoz-Tapia, and E. Bagan, Phys. Rev. A **79**, 033834 (2009).

[11] A. Zavatta, S. Viciani, and M. Bellini, Science **306**, 660 (2004); A. Zavatta, V. Parigi, and M. Bellini, Phys. Rev. A **75**, 052106 (2007).

[12] V. Parigi, A. Zavatta, M. S. Kim, and M. Bellini, Science **317**, 1890 (2007).

[13] D. Achilles *et al.*, Opt. Lett. **28**, 2387 (2003); M. J. Fitch, B. C. Jacobs, T. B. Pittman, and J. D. Franson, Phys. Rev. A **68**, 043814 (2003); J. Řeháček, Z. Hradil, O. Haderka, J. Peřina, and M. Hamar, *ibid.* **67**, 061801 (2003); D. Rosenberg, A. E. Lita, A. J. Miller, and S. W. Nam, *ibid.* **71**, 061803(R) (2005); M. Fujiwara and M. Sasaki, Opt. Lett. **31**, 691 (2006); L. Pezze, A. Smerzi, G. Khoury, J. F. Hodelin, and D. Bouwmeester, Phys. Rev. Lett. **99**, 223602 (2007); B. E. Kardynal, Z. L. Yuan, and A. J. Shields, Nature Photonics **2**, 425 (2008); J. S. Lundeen *et al.*, Nature Phys. **5**, 27 (2009); C. F. Wildfeuer *et al.*, Phys. Rev. A **80**, 043822 (2009).

[14] A. Rauschenbeutel, G. Nogues, S. Osnaghi, P. Bertet, M. Brune, J. M. Raimond, and S. Haroche, Phys. Rev. Lett. **83**, 5166 (1999); J. M. Raimond, M. Brune, and S. Haroche, Rev. Mod. Phys. **73**, 565 (2001).

[15] J. Fiurášek, Phys. Rev. A **80**, 053822 (2009).

Noise-powered probabilistic concentration of phase information

Mario A. Usuga[1,2†], Christian R. Müller[1,3†], Christoffer Wittmann[1,3], Petr Marek[4], Radim Filip[4], Christoph Marquardt[1,3], Gerd Leuchs[1,3] and Ulrik L. Andersen[2]★

Phase-insensitive optical amplification of an unknown quantum state is known to be a fundamentally noisy operation that inevitably adds noise to the amplified state[1–5]. However, this fundamental noise penalty in amplification can be circumvented by resorting to a probabilistic scheme as recently proposed and demonstrated in refs 6–8. These amplifiers are based on highly non-classical resources in a complex interferometer. Here we demonstrate a probabilistic quantum amplifier beating the fundamental quantum limit using a thermal-noise source and a photon-number-subtraction scheme[9]. The experiment shows, surprisingly, that the addition of incoherent noise leads to a noiselessly amplified output state with a phase uncertainty below the uncertainty of the state before amplification. This amplifier might become a valuable quantum tool in future quantum metrological schemes and quantum communication protocols.

Besides being the subject of a fundamental discussion going back to Dirac[10], the measurement of phase is at the heart of many quantum metrological and quantum informational applications such as gravitational wave detection, global positioning, clock syncronization, quantum computing and quantum key distribution. In many of these applications, the phase is most often imprinted onto a coherent state of light and subsequently estimated using an interferometric measurement scheme. Such a phase-estimation process[11] is however hampered by the fundamental quantum noise of the coherent state, which plays an increasingly devastating role as the excitation of the coherent state becomes smaller. Small coherent-state excitations and associated large phase uncertainties are typical in real systems such as long-distance coherent-state communication and lossy interferometry.

To reduce the phase uncertainty and thus concentrate the phase information, the state must be amplified noiselessly. This can be done probabilistically using either a highly complicated interferometric set-up of single-photon sources[6–8], a sophisticated sequence of photon-addition and -subtraction schemes[9,12] or a very strong cross-Kerr nonlinearity[13]. However, as we show in this Letter, it is possible to amplify the phase information noiselessly without the use of any non-classical resources or any strong parametric interactions. Remarkably, the supply of energy in our amplifier is simply a thermal-light source.

A schematic of the probabilistic amplifier[9] is shown in Fig. 1a. It is solely based on phase-insensitive noise addition and photon subtraction. To explain in simple terms why the addition of noise can help amplify a coherent state, we consider the phase-space pictures in Fig. 1b. The addition of thermal noise induces random

displacements to the coherent state, thus resulting in a Gaussian mixture of coherent states; some with excitations that are larger than the original excitation and some with smaller excitations. In the photon-subtraction process, the coherent states with large excitations are probabilistically heralded, thereby rendering the state in a mixture consisting of the most excited coherent states from the original Gaussian mixture. As illustrated in Fig. 1b, the resulting state is amplified and possesses a reduced phase uncertainty.

The probabilistic photon-subtraction procedure can be approximated by a largely asymmetric beam splitter combined with a photon-number-resolving detector (PNRD; see Fig. 1a). A small portion of the displaced thermal state is directed to the photon counter and when a pre-specified number of photons is detected, the transmitted state is heralded. Such an approach for photon-number subtraction has also been employed for the generation of coherent-state superpositions[14,15]. However, in contrast to previous implementations that were limited to the demonstration of two-photon subtraction[16], here we subtract up to four photons.

To elucidate the function of the amplifier, theoretically, we consider the amplification of a small-amplitude ($|\alpha| \ll 1$) coherent state that can be approximately described in the two-dimensional Fock space: $|\alpha\rangle \approx |0\rangle + \alpha|1\rangle$. As the amplitude is small, the canonical-phase variance of this state is to a very good approximation given by[17]

$$V_C \approx \frac{1}{|\alpha|^2} \qquad (1)$$

This variance represents the fundamental uncertainty in estimating the phase of the coherent state when a hypothetically ideal phase measurement is employed[18]. The aim is to produce an amplified state with a phase variance reduced with respect to the coherent-state variance in (1), thereby concentrating the phase information. If a conventional phase-insensitive amplifier is used to amplify the coherent state, the resulting variance is larger than (1) (see Supplementary Information). On the other hand, if our amplifier is employed with weak Gaussian noise addition followed by single-photon subtraction, the resulting state is[9]

$$\hat{\rho} \approx \frac{1}{|\alpha|^2 + N_{th} + 4|\alpha|^2 N_{th}}$$
$$\times [|\alpha|^2|0\rangle\langle0| + N_{th}(|0\rangle + 2\alpha|1\rangle)(\langle0| + \langle1|2\alpha^*)]$$

with the canonical-phase variance

$$V_C^{amp} \approx \frac{1}{4|\alpha|^2}\left(1 + \frac{|\alpha|^2}{N_{th}}\right) - 1$$

[1]Max Planck Institute for the Science of Light, Guenther-Scharowsky-Str. 1, 91058 Erlangen, Germany, [2]Department of Physics, Technical University of Denmark, 2800 Kongens Lyngby, Denmark, [3]Institute for Optics, Information and Photonics, University Erlangen-Nuremberg, Staudtstr. 7/B2, 91058 Erlangen, Germany, [4]Department of Optics, Palacký University 17, listopadu 50, 772 07 Olomouc, Czech Republic. [†]These authors contributed equally to this work. *e-mail: ulrik.andersen@fysik.dtu.dk.
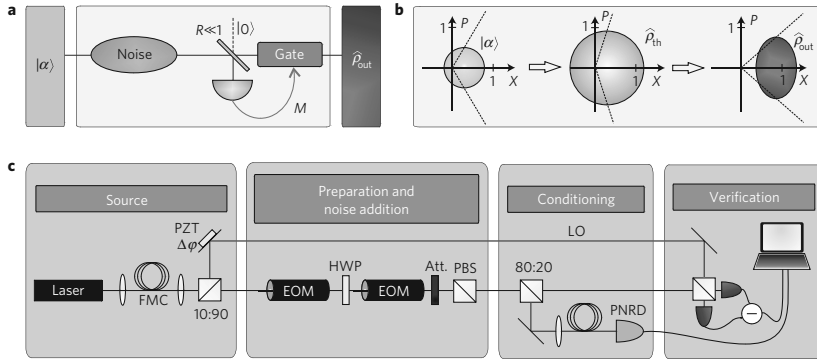
Figure 1 | Basic concept and experimental set-up. a, Principal set-up. Noise is incoherently added to an input state. Subsequently, a part of the beam is tapped off and measured by a PNRD. Results of that measurement that surpass a specified threshold M, herald the output state. **b**, Principal operation in phase space. A coherent state (yellow) serves as the input. The dashed line indicates the phase variance. Thermal noise is added to this input state resulting in a displaced thermal state (green). The output state (blue) is reshaped and the resulting phase variance is reduced compared with the input state. **c**, Experimental set-up. An external-cavity diode laser with fibre mode cleaning (FMC) acts as the source for the experiment and is split into a local oscillator (LO) and an auxiliary oscillator. The signal is prepared by a combination of two electro-optical modulators (EOM), a half-wave plate (HWP) and attenuation (Att.). A polarizing beam splitter (PBS) removes the auxiliary oscillator. Part of the signal is tapped by a 80:20 beam splitter and coupled through a multimode fibre into the PNRD. This measurement is conditioning the output state, which is characterized by a homodyne measurement. The phase of the local oscillator is controlled by a piezoelectric transducer (PZT).
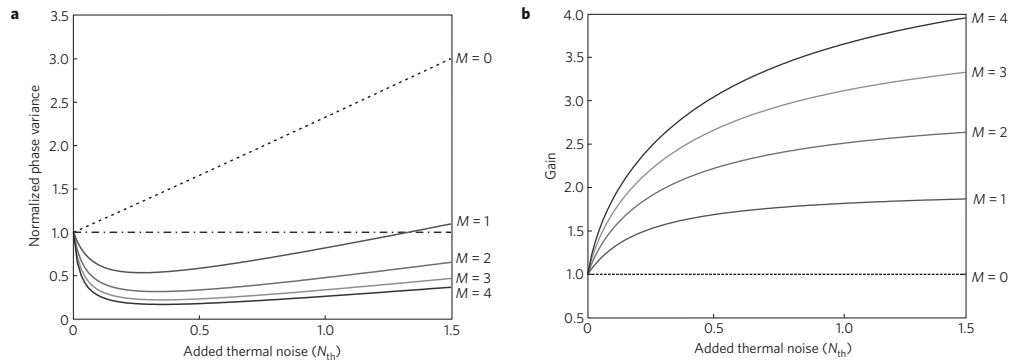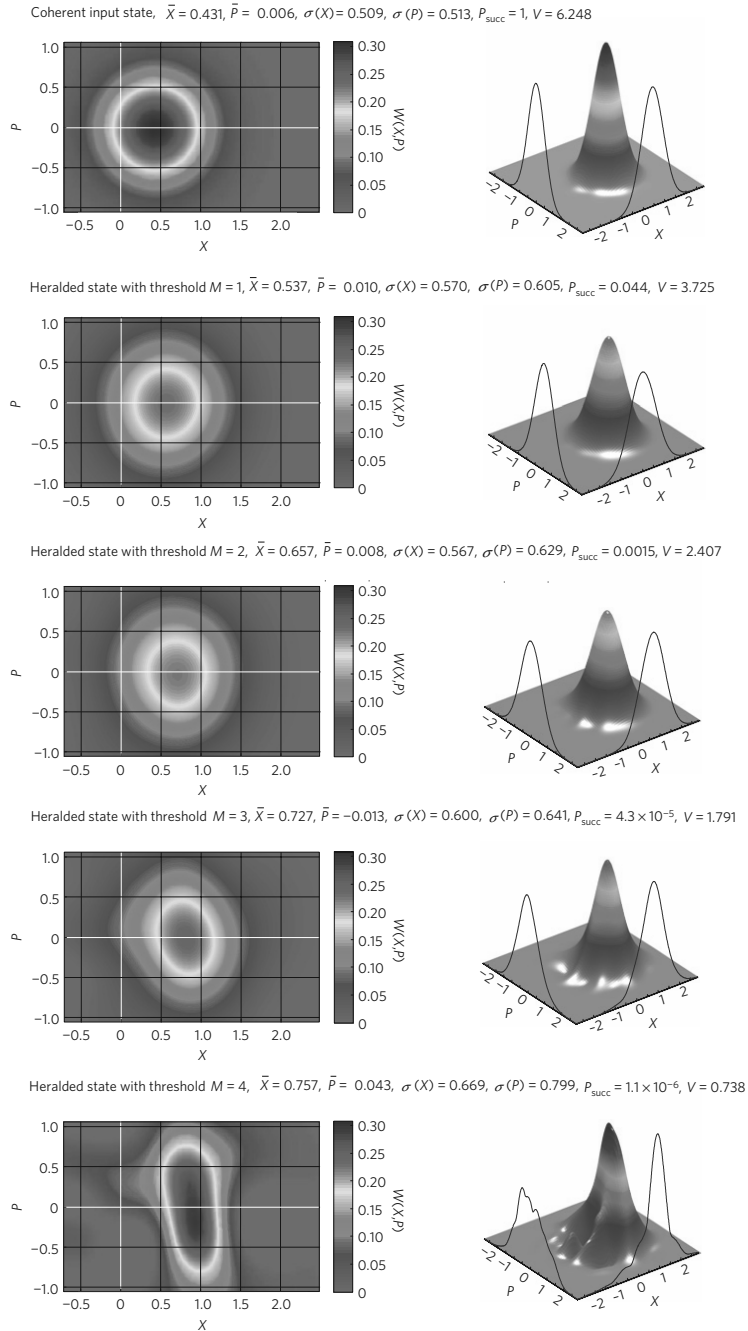

Figure 2 | Theoretical gain and normalized phase variance versus the mean number of added thermal photons. a, The canonical variance normalized to the corresponding variance of the input coherent state. **b**, The gain generally grows with the number of photons in the added thermal noise and the threshold M of added thermal photons for an input coherent state of amplitude $|\alpha| = 0.48$.

where it is assumed that the average number of incoherently added photons is $N_{th} \ll 1$. We quantify the performance of the amplifier by the normalized phase variance, $\Gamma = V_C^{amp}/V_C$, which is smaller than one for a noiseless operation. For the above approximative example, if $|\alpha|^2 \ll N_{th}$, we find that the normalized variance approaches $\Gamma = 1/4$. Another parameter that will be used to evaluate the amplifier is the gain $g = |\beta|/|\alpha|$ (where β is the average amplitude of the output state), being $g = 2$ for the above example. We therefore see that by simply adding a small amount of noise to the input state followed by single-photon subtraction, it is possible to create an output state with twice the amplitude and with a reduced phase variance.

On the basis of a more general model (as presented in the Supplementary Information), in Fig. 2 we plot the normalized phase variance and the gain as a function of the average number

of added thermal photons, where M denotes the threshold for the number of photon subtractions. Figure 2 illustrates three interesting aspects: the phase-noise-reducing operation works even when the parameters go beyond the simple approximation considered above, the effect of the amplification improves with the subtraction of more photons and the amount of noise must be relatively large for the amplification to work well. These aspects also follow the intuitive picture discussed above: large noise addition will partly displace the coherent state in a radial direction in phase space with a correspondingly large magnitude, and the states with the largest amplitude (associated with strongly amplified states) are heralded by high-photon-number subtractions. We also note that the amount of added noise that minimizes the canonical variance depends solely on the magnitude of the input coherent state but not on its phase. The amplifier is thus capable of concentrating an unknown phase of a coherent state.

Coherent input state, $\bar{X} = 0.431$, $\bar{P} = 0.006$, $\sigma(X) = 0.509$, $\sigma(P) = 0.513$, $P_{succ} = 1$, $V = 6.248$

Heralded state with threshold $M = 1$, $\bar{X} = 0.537$, $\bar{P} = 0.010$, $\sigma(X) = 0.570$, $\sigma(P) = 0.605$, $P_{succ} = 0.044$, $V = 3.725$

Heralded state with threshold $M = 2$, $\bar{X} = 0.657$, $\bar{P} = 0.008$, $\sigma(X) = 0.567$, $\sigma(P) = 0.629$, $P_{succ} = 0.0015$, $V = 2.407$

Heralded state with threshold $M = 3$, $\bar{X} = 0.727$, $\bar{P} = -0.013$, $\sigma(X) = 0.600$, $\sigma(P) = 0.641$, $P_{succ} = 4.3 \times 10^{-5}$, $V = 1.791$

Heralded state with threshold $M = 4$, $\bar{X} = 0.757$, $\bar{P} = 0.043$, $\sigma(X) = 0.669$, $\sigma(P) = 0.799$, $P_{succ} = 1.1 \times 10^{-6}$, $V = 0.738$

Figure 3 | Tomographic reconstruction of output states. Wigner functions that were reconstructed from experimental data for the input state and the heralded state for different thresholds M. For each experimental reconstruction, the mean values and standard deviations for the X and P quadratures are given with the corresponding measured success probability and canonical-phase variance.
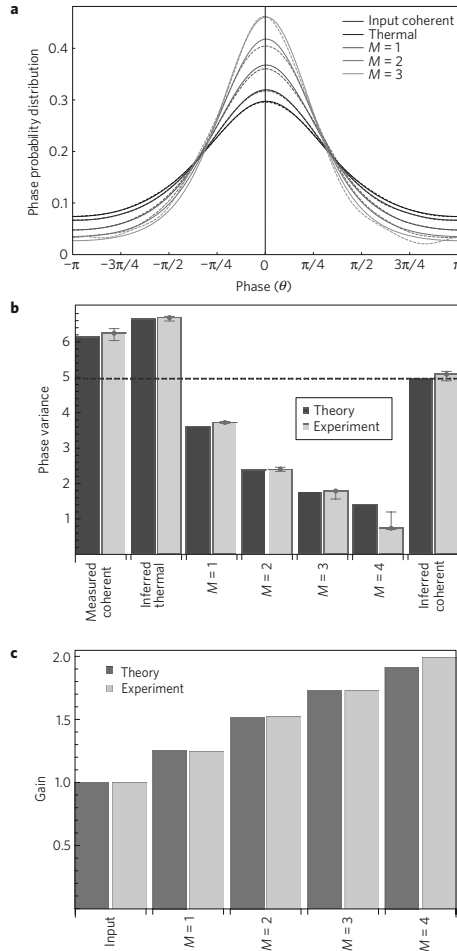
Figure 4 | Comparison between theoretical and experimental results.
a, Phase probability distribution function derived from the experimental data (solid lines) for the measured coherent, the thermal and the conditioned states. Corresponding theoretical functions (dashed lines) were calculated for states fitting to experimentally derived parameters.
b, The canonical-phase variance deduced from the experimental data (light blue) and corresponding theoretical values (dark blue) calculated for states fitting to the experimentally derived parameters. The inferred input coherent state serves as the reference value. The error bars represent the statistical deviations over many different realizations of the experiment.
c, Gain for the input coherent state for different thresholds M.

A laboratory implementation of the amplifier is shown in Fig. 1c. Our source is a grating-stabilized continuous-wave diode laser operating at 809 nm with a coherence time of 1 μs. The laser output is spatially cleaned in an optical fibre, and subsequently split to serve as a local oscillator for homodyne detection and as an auxiliary beam for state preparation. We use a pair of electro-optical modulators for the preparation of the displaced thermal state (corresponding to a coherent state with added thermal

noise) in a polarization mode orthogonal to the polarization of the auxiliary mode (see the Methods section). The duration of the prepared pulses is 800 ns. A portion (20%) of the prepared state is tapped off in an asymmetric beam splitter and measured with an avalanche photo detector operating in an actively gated mode such that the dead time (50 ns) is much shorter than the pulse duration. This means that the avalanche photo detector can be used as a single-photon counter provided that the mean number of photons in the detected pulse is very small. The transmitted part of the state is passed on to the homodyne detector where it interferes with a phase-controlled local oscillator. This provides quadrature measurements of the emerging states under any phase-space angle. The measurement outcome is sent to the computer where it is postselected according to the result of the photon-counting measurement. On the basis of the resulting data points, we reconstruct the density matrix of the heralded state using a maximum-likelihood algorithm[19,20]. We correct the data for the inefficiency of the homodyne detector to reconstruct the actual input state and the amplified output state (see the Methods section).

From the density matrices, we construct the Wigner functions for the input state and the amplified output states for different photon-number subtractions as illustrated in Fig. 3. Here we consider an input state excited along the amplitude quadrature axis with $\langle X \rangle = 0.431$, thus $|\alpha|^2 = 0.186$, and a thermal-noise addition corresponding to $\langle N_{th} \rangle = 0.15$. The amplification factor for this experiment is summarized in Fig. 4c. We also reconstruct the phase distributions (see the Methods section) for different subtractions, the results of which are shown in Fig. 4a. We clearly see that as the number of subtractions increases, the distribution becomes narrower, and thus the phase information is concentrated. These results are summarized in Fig. 4b.

To optimize the performance of the amplifier—that is, to minimize the phase variance—the amount of added thermal noise should be chosen appropriately with respect to the input coherent-state amplitude. Furthermore, we note that having detailed information about the input alphabet, the structure of the noisy displacements can be tailored accordingly, thereby markedly reducing the amount of energy used to drive the amplifier. For example, if the input is a phase-covariant coherent-state alphabet, the optimized structure of the noisy displacement is also phase covariant. Such tailoring of the displacements as well as applications of the amplifier will be interesting directions for future research. Finally, we note that the noise-addition process can also be carried out with a linear amplifier. Such an approach will not only add thermal noise to the input state but will also displace it coherently in the preferred direction, thereby further concentrating the phase information.

We have reduced the phase uncertainty of a coherent state of light through noiseless probabilistic amplification. In contrast to previous approaches to noise-free amplification, the amplifier is based neither on an ample supply of non-classical resources nor on strong parametric interactions, but solely on Gaussian noise addition and photon counting. Owing to its pivotal properties such as simplicity and robustness, we expect that this approach to probabilistic noise-free amplification will be of interest for a large variety of experiments and protocols involving phase estimation such as quantum metrology and quantum communication.

Methods

mode $n_{max} = |\alpha_{AO}|^2$. The signal mode can be chosen to be in an arbitrary mixed state, provided that the state's P-function is positive. We can therefore generate the displaced thermal state applying a suitable modulation sequence to both electro-optical modulators. The state is modelled with a finite set of (more than) 10^3 coherent states, randomly picked from a two-dimensional normal distribution. The random modulation sequence is varied and repeated throughout the measurement.

The tap beam is focused into the fibre coupled PNRD (for details, see refs 22,23). The transmitted part of the beam is sent to a homodyne detector, which measures the signal with a continuously scanned local oscillators' phase. The scanning frequency is chosen to be 21 mHz, leading to an effective phase drift of only 1.6 mrad within the modulation sequence. This value is negligible from an experimental point of view so that the local oscillator's phase is considered constant within a single modulation sequence. The phase angle needed in the tomography was estimated with a series of phase-calibration signals prepended to the modulation sequence. The main source of error in the set-up is the drift of the modulators. To compensate for this drift, the calibration point was continuously adjusted.

As the homodyne detector is not a part of the phase-concentration scheme itself but only implemented in the set-up to prove the effect of the scheme, we do not want to take its imperfections into account in the analysis. We assume therefore perfect detection. The amplitude of the coherent input state $|\alpha|$ is then inferred from the measured mean photon-number values in the imperfect PNRD and the ideal homodyne detector (HD)

$$|\alpha|^2 = |\alpha_{HD}|^2 + \frac{1}{\eta_{PNRD}}|\alpha_{PNRD}|^2$$

where the PNRD's quantum efficiency was calibrated to be $\eta_{PNRD} = 0.63 \pm 3\%$ using the overall quantum efficiency of the homodyne detector. This procedure is preferable as it does not demand an accurate knowledge of the input coherent state's amplitude, the splitting ratio and the losses in the homodyne detector.

Theory. Each measurement procedure devised to estimate a phase of a given quantum state can be characterized by a real semi-definite matrix H. The actual probability distribution of the estimated phase value can be obtained as $P(\theta) = \text{Tr}[\hat{\rho}\hat{F}(\theta)]$, where $\hat{F}(\theta) = 1/2\pi \sum_{m,n=0}^{\infty} \exp(i\theta(m-n))H_{mn}|m\rangle\langle n|$ (ref. 17). To characterize the quality of phase encoding by a single value, we can use the Holevo phase variance[24] $V = |\mu|^{-2} - 1$, where $\mu = \langle\exp(i\theta)\rangle$. The fundamental limit of the phase estimation is obtained for the canonical measurement, in which the operator $\hat{F}(\theta)$ projects onto the idealized phase state $\sum_{n=0}^{\infty} e^{i\theta n}|n\rangle$ and $H \equiv 1$. The canonical-phase variance is therefore given by

$$V_C = \left|\text{Tr}\left\{\sum_{n=0}^{\infty}|n\rangle\langle n+1|\hat{\rho}\right\}\right|^{-2} - 1$$

References

1. Louisell, W. H. *et al.* Quantum fluctuations and noise in parametric processes. I. *Phys. Rev.* **124**, 1646–1654 (1961).
2. Haus, H. A. & Mullen, J. A. Quantum noise in linear amplifiers. *Phys. Rev.* **128**, 2407–2413 (1962).
3. Caves, C. M. Quantum limits on the noise in linear amplifiers. *Phys. Rev. D* **26**, 1817–1839 (1982).
4. Ou, Z. Y., Pereira, S. F. & Kimble, H. J. Quantum noise reduction in optical amplification. *Phys. Rev. Lett.* **70**, 3239–3242 (1993).
5. Josse, V. *et al.* Universal optical amplification without nonlinearity. *Phys. Rev. Lett.* **96**, 163602 (2006).
6. Ralph, T. C. & Lund, A. B. in *Quantum Communication Measurement and Computing Proc. 9th Int. Conf.* (ed. Lvovsky, A.) 155–160 (AIP, 2009).
7. Xiang, G. Y., Ralph, T. C., Lund, A. P., Walk, N. & Pryde, G. J. Heralded noiseless linear amplification and distillation of entanglement. *Nature Photon.* **4**, 316–319 (2010).
8. Ferreyrol, F. *et al.* Implementation of a nondeterministic optical noiseless amplifier. *Phys. Rev. Lett.* **104**, 123603 (2010).
9. Marek, P. & Filip, R. Coherent-state phase concentration by quantum probabilistic amplification. *Phys. Rev. A* **81**, 022302 (2010).
10. Dirac, P. A. M. The quantum theory of the emission and absorption of radiation. *Proc. R. Soc. Lond. A* **114**, 243–265 (1927).
11. Shapiro, J. H., Shepard, S. R. & Wong, N. C. Ultimate quantum limits on phase measurement. *Phys. Rev. Lett.* **62**, 2377–2380 (1989).
12. Fiurášek, J. Engineering quantum operations on travelling light beams by multiple photon addition and subtraction. *Phys. Rev. A* **80**, 053822 (2009).
13. Menzies, D. & Croke, S. Noiseless linear amplification via weak measurements. Preprint at http://arxiv.org/abs/0903.4181v1 (2009).
14. Ourjoumtsev, A., Tualle-Brouri, R., Laurat, J. & Grangier, P. Generating optical Schrödinger kittens for quantum information processing. *Science* **312**, 83–86 (2006).
15. Neergaard-Nielsen, J. S., Melholt Nielsen, B., Hettich, C., Mølmer, K. & Polzik, E. S. Generation of a superposition of odd photon number states for quantum information networks. *Phys. Rev. Lett.* **97**, 083604 (2006).
16. Takahashi, H. *et al.* Generation of large-amplitude coherent-state superposition via ancilla-assisted photon subtraction. *Phys. Rev. Lett.* **101**, 233605 (2008).
17. Wiseman, H. & Kilip, R. B. Adaptive single-shot phase measurements: The full quantum theory. *Phys. Rev. A* **57**, 2169–2185 (1998).
18. Armen, M. A. *et al.* Adaptive homodyne measurement of optical phase. *Phys. Rev. Lett.* **89**, 133602 (2002).
19. Lvovsky, A. I. Iterative maximum-likelihood reconstruction in quantum homodyne tomography. *J. Opt. B: Quantum Semiclass. Opt.* **6**, 556–559 (2004).
20. Hradil, Z. Quantum-state estimation. *Phys. Rev. A* **6**, R1561–R1564 (1997).
21. Wittmann, C. *et al.* Demonstration of near-optimal discrimination of optical coherent states. *Phys. Rev. Lett.* **101**, 210501 (2008).
22. Banaszek, K. *et al.* Direct measurement of the Wigner function by photon counting. *Phys. Rev. A* **60**, 674–677 (1999).
23. Wittmann, C. *et al.* Demonstration of coherent state discrimination using a displacement controlled photon number resolving detector. *Phys. Rev. Lett.* **104**, 100505 (2010).
24. Holevo, A. S. Covariant measurements and imprimitivity systems. *Lect. Notes Math.* **1055**, 153–172 (1982).

Author contributions

M.A.U., C.R.M. and C.W. carried out the experimental work, P.M. and R.F. did the theoretical calculations and all authors discussed the results. U.L.A., M.A.U. and C.R.M. wrote the manuscript and Ch.M., G.L. and U.L.A. coordinated the project.

Probabilistic cloning of coherent states without a phase reference

Christian R. Müller,[1,2] Christoffer Wittmann,[1,2] Petr Marek,[3] Radim Filip,[3] Christoph Marquardt,[1,2]
Gerd Leuchs,[1,2] and Ulrik L. Andersen[1,4]

[1]*Max Planck Institute for the Science of Light, Erlangen, Germany*
[2]*Department of Physics, University of Erlangen-Nuremberg, Erlangen, Germany*
[3]*Department of Optics, Palacký University, Olomouc, Czech Republic*
[4]*Department of Physics, Technical University of Denmark, Kongens Lyngby, Denmark*

We present a probabilistic cloning scheme operating independently of any phase reference. The scheme is based solely on a phase-randomized displacement and photon counting, omitting the need for nonclassical resources and nonlinear materials. In an experimental implementation, we employ the scheme to clone coherent states from a phase covariant alphabet and demonstrate that the cloner is capable of outperforming the hitherto best-performing deterministic scheme. An analysis of the covariances between the output states shows that uncorrelated clones can be approached asymptotically. This simultaneously demonstrates how the effect of loss on coherent states can be compensated via noiseless preamplification.

In classical physics there are no fundamental limits to the performance of an amplifier or to the accuracy of copying a state of the system. The reason is that measurements can, in principle, gain complete knowledge about the classical state, from which it is possible to generate arbitrarily many copies or a perfectly amplified version of the initial state. In general, this does not hold true in the quantum regime, since the laws of quantum mechanics forbid us to gain complete information about all aspects of reality on a single copy of a quantum state. This is widely known as the no-cloning theorem [1]. However, the no-cloning theorem does not prevent the creation of imperfect copies of a state [2]. These can, for instance, be obtained by amplification and subsequent splitting [3]. This situation also emerges naturally when an amplifier is used prior to a lossy channel to compensate for energy loss. In this scenario, one of the clones is lost to the environment [4], while the other clone is preserved.

In general, the amplification of an unknown coherent state $|\alpha\rangle$ is accompanied by the addition of excess noise [5–7]. This noise is responsible for the fundamental bound for deterministic cloning, where the average fidelity of clones is limited to $F \leqslant \frac{2}{3}$. Nevertheless, the excess noise of amplifiers can be drastically reduced by relaxing the constraint of deterministic operation. An ideal amplify-split cloner for coherent states is described by the two-step transformation $|\alpha\rangle |0\rangle \rightarrow |\sqrt{2}\alpha\rangle |0\rangle \rightarrow |\alpha\rangle |\alpha\rangle$. In the probabilistic regime, the amplification can for small amplitudes $|\alpha|$ be achieved with high accuracy as proposed in Refs. [8–11] and experimentally shown in Refs. [12–15]. Yet these approaches require perfect photon number detectors, single-photon ancillary states. and/or high-order nonlinear interactions, thus rendering the physical implementation challenging. Moreover, these approaches rely on additional key ingredients such as interferometric stability, perfect coincidences of single-photon operations, or a phase reference. The physical meaning and necessity of such a phase reference was discussed in an extensive debate [16–21]. It has not been clarified what kind of quantum operations can be realized independently of any of these ingredients.

In this Rapid Communication, we demonstrate a phase covariant cloning scheme capable of probabilistically generating ideal clones of coherent states, without the above-mentioned resources. We experimentally show that the cloner outperforms the bound set by the hitherto best-performing deterministic scheme [22] which is based on an optimal phase measurement. The cloner is of the amplify-split type and consists of solely elementary linear optical elements and a photon number resolving detector. The amplification is achieved probabilistically by first applying an optimally tailored displacement to the input state and subsequently heralding the output depending on the result of a photon number threshold measurement on a part of the displaced state. The probabilistic amplifier may be used as a preamplifier prior to a lossy channel. In contrast to classical amplifiers, the loss is then compensated without introducing correlations to the environment.

Our cloning strategy consists of three steps: displacement, heralding measurement, and splitting, as sketched in Fig. 1(a). First, the input state is randomly displaced in phase space [$\hat{D}(\Phi)$] according to a phase-independent probability distribution Φ. This is followed by probabilistic subtraction of photons via a photon number resolving detector (PNRD). Successful amplification is heralded whenever the detected number of photons surpasses a certain threshold value M. This strategy makes use of the classical correlations among the detected number of photons and the state's amplitude arising from the phase-randomized displacement [15]. The threshold parameter M offers the possibility to tune the trade-off between output fidelity and success rate: Increasing M will result in increased fidelity, however, at the expense of a lower success rate. In the final step the amplified state is split symmetrically to obtain the two copies of the input state. In contrast to other cloning protocols [22,23], our scheme disregards the phase information, as neither an external phase reference, which could be sent along with the quantum states, nor an internal phase reference, e.g., a bright local oscillator, is provided. We merely need the definition of the input state's mode. A detailed demonstration of the cloner's phase-insensitive performance can be found in the Supplemental Material [24].
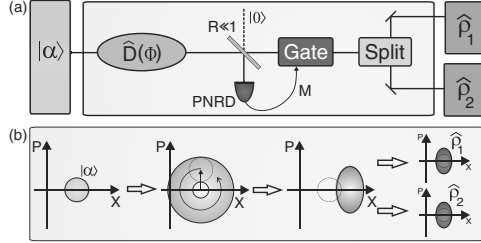
FIG. 1. (Color online) (a) Schematic of the cloning scheme. Two identical clones $\hat{\rho}_{1,2}$ are created by probabilistic amplification and subsequent symmetric splitting. (b) Evolution of a coherent state in phase space during the cloning process.

The phase-insensitive annihilation $\hat{a}$ and creation $\hat{a}^\dagger$ operators constitute the fundamental building blocks of any quantum operation [25]. A specific class of operations that can be realized without a phase reference is described as $\hat{\rho} \rightarrow \sum_n \hat{A}_n \hat{\rho} \hat{A}_n^\dagger$, where the operators $\hat{A}_n$ are proportional to an arbitrary product of $\hat{a}$ and $\hat{a}^\dagger$. An elementary probabilistic amplification can be achieved without a phase reference for $\hat{A}_n = \hat{a}^m \hat{a}^{\dagger m} \delta_{mn}$ [10], which amounts to adding and subtracting a specific number of photons m. However, a perfect coincidence between the additions and the subtractions is required for this operation. This constitutes a requirement in the particle picture, which is similar to providing a phase reference in the wave picture. In our scheme, this constraint is dropped by replacing the single-photon addition by the phase-randomized displacement.

In the following, we discuss the phase covariant cloner for an alphabet with a fixed amplitude and continuous phase. In Ref. [22], it has been shown that for such alphabets fidelities of at least $F \approx 0.85$ can be achieved deterministically, where the prerequisites are unit detection efficiencies, optimal phase measurements, and feed forward. An optimal scheme is not known, but this scheme is to the best of our knowledge the hitherto best-performing deterministic approach. We have specifically tailored the optimal displacement for the cloning of this alphabet. Due to the phase covariance of the alphabet, the task to find the optimal displacement distribution is essentially a one-dimensional problem and we only need to optimize the radial distribution of the displacement. Since the fidelity is linear in the density matrix, the optimal displacement distribution reduces to a fixed amplitude and a random phase. A detailed proof of the optimality of the displacement distribution can be found in the Supplemental Material [24]. Insight into the cloning procedure can be gained by considering a weak coherent state $|\alpha\rangle \propto |0\rangle + \alpha|1\rangle$, with $|\alpha| \ll 1$. The state after the phase-randomized displacement can be expressed as

$$\hat{\rho} \propto \frac{1}{2\pi} \int_0^{2\pi} \hat{D}(|\alpha|e^{i\phi}x)|\alpha\rangle \langle\alpha|\hat{D}^\dagger(|\alpha|e^{i\phi}x)d\phi, \quad (1)$$

where x is the ratio between the amplitude of the displacement and the original state's amplitude. Subtracting a single photon
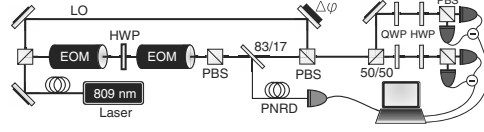

FIG. 2. (Color online) Experimental realization of the cloning scheme.

transforms this state to

$$\hat{\rho}_a \propto |\alpha|^2[|0\rangle\langle 0| + x^2(|0\rangle + 2\alpha|1\rangle)(\langle 0| + 2\alpha^*\langle 1|)], \quad (2)$$

which is a mixture of the vacuum state and the original state approximately amplified with an amplitude gain of two (i.e., four times the original power). A detailed derivation of Eq. (2) can be found in the Supplemental Material [24]. From this state, four clones looking as

$$\hat{\rho}_{\text{clone}} \propto |\alpha|^2[|0\rangle\langle 0| + x^2|\alpha\rangle\langle\alpha|] \quad (3)$$

can be generated, and if the parameters are chosen such that $|\alpha|^2 \ll |x\alpha|^2 \ll 1$, perfect clones are obtained. However, the usability of the cloner is by no means limited only to the extreme values required by the approximation; with the proper choice of x and a multiphoton subtraction, we can achieve a respectable range of gains even for $|\alpha| \approx 1$. Interestingly, for a fixed gain, the required value of x is quasiconstant for several numbers of subtracted photons, which allows for a delayed choice of M and the trade-off between the success rate and the fidelity of the clones.

The experimental setup is sketched in Fig. 2. Our source is a grating-stabilized cw diode laser at 809 nm with a linewidth of 1 MHz. After passing a fiber mode cleaner, the beam is asymmetrically split into two parts, an auxiliary beam for the signal preparation and a local oscillator (LO) used only in the verification stage. The signal states are generated in time windows of 800 ns at a repetition rate of 100 kHz. A combination of two electro-optical modulators (EOMs) and a half-wave plate (HWP) is used to generate and randomly displace a coherent state by transferring photons from the polarization mode of the auxiliary beam to the orthogonal signal polarization mode. A small portion ($\approx$17%) of the state is tapped off via an asymmetric beam splitter and sent to an avalanche photodiode (APD) operated in an actively gated mode. The dead time (50 ns) is much shorter than the pulse duration, allowing to employ the APD as a PNRD [26]. The heralded and effectively amplified state is finally split on a symmetric beam splitter to obtain the two clones. To quantify the fidelity between the input state and the clones, we perform full tomographies of both outputs. For this purpose, the amplified state is spatially mode matched with the LO on a polarizing beam splitter (PBS) but before the state is split into the clones. Up to this stage signal and LO are still residing in orthogonal polarization modes. The outputs of the beam splitter are directed to balanced homodyne detectors embedded in a Stokes measurement setup [27]. The combination of a HWP and a quarter-wave plate (QWP) allows for the adjustment of the relative phase between the clone and the LO and therefore for simultaneous measurements of arbitrary quadratures at each output. To enable tomography, the LO's phase is varied harmonically via a piezoelectric

transducer to provide quadrature measurements of all phase angles. An accurate inference of the measured quadrature is provided by bright phase calibration pulses that are sent in between the signal states. The homodyne data and the number of detected photons are acquired simultaneously by a computer. Finally, we reconstruct the clones' density matrices employing a maximum likelihood algorithm [28,29]. The homodyne detectors are only implemented to determine the performance of the scheme. In order to reconstruct the density matrix—unaffected by any imperfection of the verifying detection system—we assume unit quantum efficiency for the homodyne detectors and determine the performance not using the actual input amplitude but the following inferred value using $\eta_{\mathrm{HD}_{1,2}} = 1$: $|\alpha|^2 = |\alpha_{\mathrm{HD}_1}|^2 + |\alpha_{\mathrm{HD}_2}|^2 + \frac{1}{\eta_{\mathrm{PNRD}}}|\alpha_{\mathrm{PNRD}}|^2$, with $\eta_{\mathrm{PNRD}} = 63 \pm 3\%$. $|\alpha_{\mathrm{HD}_{1,2}}|^2$ and $|\alpha_{\mathrm{PNRD}}|^2$ correspond to the actually measured mean photon numbers in the homodyne detectors and the PNRD, respectively (see the Supplemental Material for details [24]).

The limited fidelity predicted by the no-cloning theorem is, in the case of an amplify-split cloner, due to the addition of excess noise in the amplification step. In our scheme, the excess noise is a remainder of the random displacement. This noise leads to classical correlations among the two clones which can be characterized by measuring the two-mode covariance matrix. Deterministic Gaussian strategies, for instance, add one unit of vacuum noise to the clones, resulting in a uniform covariance of 0.5. Probabilistic strategies are capable of generating ideal clones, having a vanishing covariance, asymptotically. However, in a realistic implementation a certain amount of excess noise is unavoidable.

We measure the covariances for various threshold parameters and compare the results to the theoretical predictions. The results for a coherent state with amplitude $|\alpha| = 1.36$ excited along the X quadrature are presented in Fig. 3. In

the experiment, we lock the LO's phase via a feedback loop and adjust the HWP and QWP at the detector stages to measure four different configurations to attain the in-phase terms $\mathrm{Cov}(X_1, X_2)$, $\mathrm{Cov}(P_1, P_2)$ as well as the out-of-phase terms $\mathrm{Cov}(X_1, P_2)$, $\mathrm{Cov}(P_1, X_2)$. The symmetric copies exit the cloner with identical phases, such that no out-of phase correlations are expected from the theory. This is confirmed by the experiment, apart from statistical fluctuations, which can become more pronounced with increasing threshold parameters and decreasing success rate. Without heralding ($M = 0$), the outputs have equal in-phase covariances. Heralding purifies the mixture by adding a bias to the high-amplitude parts of the mixture. Consequently, both in-phase covariances decrease with rising threshold. We find that the covariance along the direction of the state's excitation in phase space (for the state considered here: the X quadrature) $\mathrm{Cov}(X_1, X_2)$ decreases faster than for the orthogonal quadrature $\mathrm{Cov}(P_1, P_2)$. In a simplified picture, the heralding process cuts off the low-amplitude part of the displaced state, leaving only a segment of the initial ring-shaped displacement, which mainly spreads in the direction orthogonal to the excitation of the input state [see Fig. 1(b)]. We also find this behavior in the full theoretical model, which is in good agreement with the results.

The primary figure of merit for a cloning device is the fidelity. We measure the average fidelity $F = \frac{1}{2}\langle\alpha|(\rho_1 + \rho_2)|\alpha\rangle$ of both clones, to avoid a bias stemming from a possible imbalance of the two outputs. The results for amplitudes in the range of $|\alpha| \in [0.4, 2.1]$ and threshold parameters of up to five photons are shown in Fig. 4 and are compared to our theoretical model for the implementation with realistic parameters. Additionally, the fidelities achievable with the deterministic scheme from Ref. [22] serve as a threshold. For amplitudes of up to $|\alpha| \approx 1.4$ the performance of our probabilistic cloner is comparable to the deterministic scheme at a heralding threshold of $M = 2$ and is superior for $M = 3$ and above. At higher amplitudes, the fidelities of the
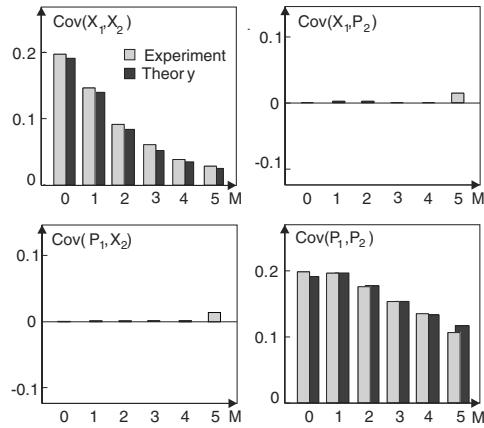
FIG. 3. (Color online) Covariance matrix elements for the clones of a coherent state with initial amplitude $\alpha = 1.36$ for the randomly displaced state ($M = 0$) and threshold parameters from one to five photon subtractions. The displacement parameter was chosen for all M to be $x = 0.5$.
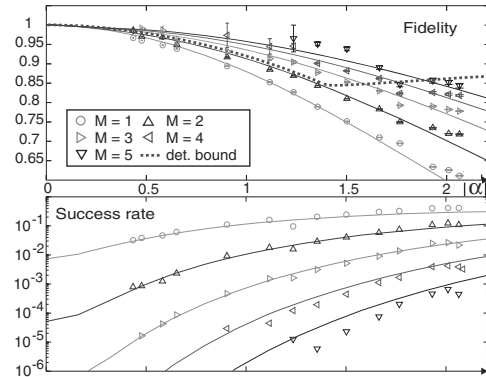
FIG. 4. (Color online) Experimental cloning fidelities and success rates for various input amplitudes and different threshold parameters. The fidelity is maximized in each point over a suitable set of displacement parameters x.
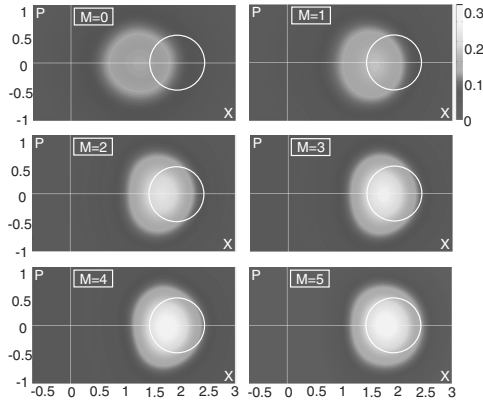
FIG. 5. (Color online) Contour plots of the reconstructed Wigner functions of a single clone for the nonheralded displaced state and for heralding thresholds of up to five detected photons. The coherent input state with $|\alpha| = 1.93$ is indicated by the white contour line, corresponding to the height at the standard deviation. The displacement parameter for all M is $x \approx 0.52$.

deterministic scheme can be surpassed using higher heralding thresholds. We find that the highest fidelities are achieved at effective amplitude gains slightly below unity, where the deficit in amplitude is overcompensated by the reduced residual displacement noise. The error bars represent the statistical fluctuations over repeated realizations of the experiment. The measurements were conducted over a period of several weeks, in which variations of up to $\pm 2\%$ from the average tapping ratio (17%) occurred due to drifts in the setup.

The success probabilities corresponding to the measurements of the presented fidelities are also shown in Fig. 4 and compared to the theoretical predictions. A higher threshold parameter and hence an increased fidelity comes at the price of a lower rate of success. However, with rising amplitude the probability to detect a certain number of photons also

increases. An example for the experimentally generated clones according to different heralding thresholds is presented as reconstructed Wigner functions in Fig. 5 for an input state with $|\alpha| = 1.93$. In this representation the heralding-induced transition from the randomly displaced state ($M = 0$) to a heralded high-fidelity clone ($M = 5$) can clearly be seen. The analysis of a single clone reveals the effect of probabilistic preamplification prior to a 3-dB lossy channel for coherent states. This form of loss compensation, similar in philosophy to Ref. [30], can completely suppress the loss-induced decoherence on a coherent state. In the deterministic regime, the amplification process is necessarily noise afflicted. In the amplification of coherent states this means that classical correlations arise as a consequence of the splitting of the wave. This situation is different from the splitting of a single-photon state, which results in strong particlelike anticorrelation among the output fields [31]. Interestingly, the probabilistic preamplification of coherent states will in principle not introduce any correlations to the environment.

In conclusion, we have proposed and experimentally realized a cloner based on a probabilistic amplifier with minimal resources. In doing so, we have shown that quantum cloning without phase resources is feasible. In good agreement with the theory, we were able to generate high-fidelity clones, beating the hitherto best-performing deterministic approach. We discussed that our scheme allows for a delayed choice between the fidelity and the success rate. Furthermore, the clones exhibit reduced correlations, pointing towards the noiseless nature of the amplification step, which is important if the amplifier is used for loss compensation. After completing our experiment, another form of loss compensation was tested experimentally for very nonclassical particlelike states in Ref. [32].

[1] W. K. Wooters and W. H. Zurek, Nature (London) **299**, 802 (1982).

[2] V. Scarani *et al.*, Rev. Mod. Phys. **77**, 1225 (2005).

[3] N. J. Cerf and J. Fiurášek, Prog. Opt. **49**, 455 (2006).

[4] W. H. Zurek, Rev. Mod. Phys. **75**, 715 (2003).

[5] W. H. Louisell, Phys. Rev. **124**, 1646 (1961).

[6] H. A. Haus and J. A. Mullen, Phys. Rev. **128**, 1240 (1962).

[7] C. M. Caves, Phys. Rev. D **26**, 1817 (1982).

[8] T. C. Ralph and A. P. Lund, in *Proceedings of 9th International Conference on Quantum Communication, Measurement and Computing*, edited by A. Lvovsky, AIP Conf. Proc. No. 1110 (AIP, New York, 2009), pp. 155–160.

[9] D. Menzies and S. Croke, arXiv:0903.4181.

[10] P. Marek and R. Filip, Phys. Rev. A **81**, 022302 (2010).

[11] J. Fiurášek, Phys. Rev. A **80**, 053822 (2009).

[12] F. Ferreyrol *et al.*, Phys. Rev. Lett. **104**, 123603 (2010).

[13] G. Y. Xiang *et al.*, Nat. Photonics **4**, 316 (2010).

[14] A. Zavatta *et al.*, Nat. Photonics **5**, 52 (2011).

[15] M. A. Usuga *et al.*, Nat. Phys. **6**, 767 (2010).

[16] K. Mølmer, Phys. Rev. A **55**, 3195 (1997).

[17] J. Gea-Banacloche, Phys. Rev. A **58**, 4244 (1998).

[18] K. Mølmer, Phys. Rev. A **58**, 4247 (1998).

[19] H. Wiseman, J. Opt. B **6**, S849 (2004).

[20] S. D. Bartlett, T. Rudolph, and R. W. Spekkens, Int. J. Quantum Inf. **4**, 17 (2006).

[21] T. Rudolph and B. C. Sanders, Phys. Rev. Lett. **87**, 077903 (2001).

[22] M. F. Sacchi, Phys. Rev. A **75**, 042328 (2007).

[23] U. L. Andersen, V. Josse, and G. Leuchs, Phys. Rev. Lett. **94**, 240503 (2005).

[24] See Supplemental Material at http://link.aps.org/supplemental/10.1103/PhysRevA.86.010305 contains a prove of the optimality of the displacement distribution and an explicit derivation of equation (3). Furthermore, the applied method to infer the input state is described in detail. Finally, it is proven that the presented cloning operation is indeed truly phase-insensitive.

[25] M. S. Kim, J. Phys. B **41**, 133001, (2008).

[26] C. Wittmann, U. L. Andersen, M. Takeoka, D. Sych, and G. Leuchs, Phys. Rev. Lett. **104**, 100505 (2010).

[27] N. Korolkova, G. Leuchs, R. Loudon, T. C. Ralph, and C. Silberhorn, Phys. Rev. A **65**, 052306 (2002).

[28] A. I. Lvovsky, J. Opt. B **6**, S556 (2004).

[29] Z. Hradil, Phys. Rev. A **55**, R1561 (1997).

[30] T. C. Ralph, Phys. Rev. A **84**, 022339 (2011).

[31] P. Grangier *et al*., Europhys. Lett. **1**, 173 (1986).

[32] M. Micuda *et al*., arXiv:1206.2852.

Optimal probabilistic measurement of phase

Petr Marek

Department of Optics, Palacký University, 17 listopadu 1192/12, 771 46 Olomouc, Czech Republic

When measuring the phase of quantum states of light, the optimal single-shot measurement implements a projection on the unphysical phase states. If we want to improve the precision further we need to accept a reduced probability of success, either by implementing a probabilistic measurement or by probabilistically manipulating the measured quantum state by means of noiseless amplification. We analyze the limits of this approach by finding the optimal probabilistic measurement that, for a given rate of success, maximizes the precision with which the phase can be measured.

Phase is a central concept in both classical and quantum optics. It was, however, a matter of lengthy dialogue before the quantum description of phase was established. The initial attempts of Dirac to treat phase as a canonical conjugate to photon number failed because it is impossible to represent phase by a quantum mechanical observable [1]. As a consequence, phase cannot be projectively measured; it can only be estimated (or guessed) by analyzing the results of other measurements. Despite this, phase states do exist [2] (even if they are not orthogonal) and they were eventually used to construct a well-behaved phase operator [3]. Other attempts to describe phase properties of quantum states relied on the measurement-related phase distribution [4]. Both approaches were later reconciled with the fundamental canonical phase distribution [5].

The canonical phase distribution characterizes phase properties of a quantum state and it is completely independent of its photon number distribution. It can be used to obtain a wide range of quantities related to phase estimation, but it also determines how much information about the phase of the state can be obtained by performing a measurement only on a single copy of it. True, the ideal canonical phase measurement does not and cannot exist, but several approximative approaches have been suggested [6,7].

Aside from improving the actual detector scheme, the overall performance of phase measurement can be enhanced also by specific alteration of the measured quantum state. A highly nonclassical quantum state can in principle lead to an unparalleled precision [8], while weakly nonclassical states are both beneficial and experimentally feasible [9]. However, if the state is unaccessible prior to phase encoding, we need to rely on operations that can enhance the amount of phase information already carried by the scrutinized state. Such operations are commonly referred to as noiseless amplifiers and a great deal of attention was recently devoted both to the concept [10] and to the experimental realizations [11]. The cost of this improvement comes in the reduced success rate of the operation. The amplification is therefore not very practical when the measurements can be repeated, but it may be useful when the event to be detected is rare and we need to be certain that the only measurement outcome obtained corresponds to the theoretical value as closely as possible.

However, even in the scenarios in which the probabilistic approach is worth considering, it would be more prudent to design an actual probabilistic measurement of phase. Such a measurement would be conceptually similar to methods of unambiguous discrimination of quantum states [12], except that a truly errorless detection would be possible only in the limit of zero probability. Rather than this regime of limited interest, the question is how does reducing the success rate of the measurement help us measure the phase more precisely. Maybe even more importantly, we ask what the theoretical limits of this approach are. In this paper we attempt to answer these questions.

Let us start by reviewing what we actually mean by the term "phase measurement." Phase has a well-defined meaning only in the context of an interferometric setup, where it expresses the relative length difference between the two optical paths. In the context of continuous-variable (CV) quantum optics [13], phase is often considered a stand-alone property. However, this is only because the other path in the interferometer, represented by the local oscillator, is taken for granted. In a sense this is justified, as the local oscillator is intense enough to be, for all intents and purposes, just a classical reference framing the associated quantum system. Measuring the phase of the quantum system is then equivalent to discerning a value of the parameter ϕ, which is encoded into the quantum state by means of an operator $\exp(i\phi\hat{n})$, where $\hat{n}$ is the photon number operator. Apart from special cases it is impossible to determine the parameter ϕ perfectly. Rather than complete knowledge, the result of the measurement provides the observer just with the best guess of the parameter, where the quality of the guess depends on both the state of the measured system and the phase measurement employed.

The simplest single-shot measurement of the phase of optical signals relies on simultaneous measurement of quadrature operators X and P, corresponding to the Hermitian and the anti-Hermitian part of the annihilation operator. The phase can be then deduced from the measurement results x' and p' by taking $\phi = \tan^{-1}(p'/x')$. Of course, in addition to knowledge of the phase, this particular measurement also provides us with knowledge of the energy of the state. Therefore, the obtained phase information is not as complete as it could be.

The best possible measurement that can be imagined is the so-called canonical measurement of phase. It can be mathematically described as a projection on idealized phase states $|\theta\rangle = \sum_{k=0}^{\infty} e^{i\theta k}|k\rangle$. These phase states are not normalized, which makes them similar to eigenstates of continuous

operators (such as position and momentum), but they are also not orthogonal. The nonorthogonality is actually responsible for the impossibility of measuring phase completely because a single measured value of θ is not exclusive just to a single phase state. For any quantum state $\hat{\rho}$ the results of the canonical phase measurement can be characterized by the probability distribution $P(\theta) = \text{Tr}[\hat{\rho}|\theta\rangle\langle\theta|]$, i.e., the canonical phase distribution. The shape of the distribution is solely given by the employed quantum state; the encoded phase value is represented only as a linear displacement. For a particular measured value θ the value $P(\theta)$ is related to the probability that the measured value is the encoded value. Simplistically, we can say that for any quantum state, the quality of phase encoding is given by the width of the canonical distribution. This can be formally expressed by evaluating the variance of the phase distribution, but it is actually more convenient to use a different quantity that takes into account the periodicity of the phase in the interval $|0,2\pi\rangle$ [14]. The new quantity is the phase variance $V = |\mu|^{-2} - 1$, where $\mu = \langle\exp i\theta\rangle$ [15]. The phase variance is completely independent of displacement in θ and therefore is completely determined by the state $\hat{\rho}$. We can also see that the phase variance solely depends on the value of the parameter μ, which we are going to use from now on.

For an arbitrary pure quantum state

$$|\psi\rangle = \sum_{n=0}^{\infty} c_n |n\rangle, \tag{1}$$

the value of μ can be found as

$$\mu = \sum_{n=0}^{\infty} c_n c_{n+1}^*. \tag{2}$$

If we fix the magnitudes of the individual coefficients, μ will be maximized when all the coefficients are real and positive. For quantum states from a limited-dimensional Hilbert space, the parameter μ can be straightforwardly maximized and optimal states for phase encoding can be found [6,16,17]. The existence of such ideal states tells us that there are limits to how well the phase can be encoded in a limited-dimensional Hilbert space. In contrast, if the Hilbert space is infinite, which is the case in CV quantum optics communication, it is in principle possible to encode the phase perfectly, in such the way that $\mu = 1$ and consequently the phase variance is zero. As this is obviously the case in classical communication, where phase can be encoded and decoded with arbitrary precision, the inability to measure phase in quantum physics stems from employing quantum states that are so weak their Hilbert space is effectively limited. However, there is a key difference between these states and states from a Hilbert space with factually limited dimension. The difference is that the infinite-dimensional Hilbert space offers a possibility of measuring the state arbitrarily well if we accept a reduced probability of success.

The idea that measurement can be improved when we accept a reduced probability of success is not a new one. When discriminating quantum states drawn from a finite ensemble, one can accept the existence of inconclusive results (reduced success rate) in order to reduce the probability of erroneous result to zero [12]. Similarly, when measuring a continuous parameter such as phase, it is possible to conditionally

transform the quantum states in such a way that the subsequent measurement leads to more precise results [10,11]. Taken as whole, the combination of probabilistic operation and measurement is essentially a probabilistic measurement. In the following we develop a unified picture describing the probabilistic measurement of the phase of a quantum state and derive bounds for the optimal one. Namely, we will look for such a measurement that, for a given probability of success, yields the best possible result.

The extension of the canonical measurement of phase into the probabilistic regime can be represented by a set of operators Π_ϕ, each of them corresponding to a positive detection event of value ϕ and a single operator Π_0 representing the inconclusive results. Together these operators form a positive-operator-valued measure (POVM). For the canonical deterministic measurement of phase these operators are $\Pi_\phi^{(D)} = \frac{1}{2\pi}|\phi\rangle\langle\phi|$. Keeping the pure-state projector structure intact, we can express the probabilistic POVMs as

$$\Pi_\phi^{(P)} = \frac{1}{2\pi} F|\phi\rangle\langle\phi|F^\dagger, \quad \Pi_0^{(P)} = 1 - \int \Pi_\phi^{(P)} d\phi. \tag{3}$$

Here $F = \text{diag}(f_0, f_1, \ldots)$, where $|f_j| \leqslant 1$ for all $j = 0, 1, \ldots$, is an operator diagonal in Fock space. It is practical to represent the probabilistic measurement by a filter, transmitting and modifying the quantum state with some limited probability, followed by the deterministic canonical phase measurement. The operator F then plays the role of the probabilistic filter and the task of finding the optimal measurement is reduced to finding the optimal operator F.

After the first glance at the problem, one issue immediately becomes apparent. For any quantum state ρ, the probability of successful measurement $P = 1 - \text{Tr}[\rho\Pi_0^{(P)}]$ is dependent on the choice of the measured state. The optimal measurement therefore needs to be tailored to a specific state or to a class of states. However, let us first approach the task in a general way. Suppose we have an input quantum state (1). For phase encoding it is best when all the coefficients c_n are real and positive, so we will assume this is the case [18]. The act of the filter transforms this state into a new one

$$|\psi_f\rangle = \frac{1}{\sqrt{P}} \sum_{n=0}^{\infty} f_n c_n |n\rangle, \tag{4}$$

where $P = \sum_{n=0}^{\infty} f_n^2 c_n^2$ is the probability of success and the filter parameters f_n are also considered real and positive. For any given probability P, the act of finding the optimal filter relies on maximization of

$$\mu = \sum_{n=0}^{\infty} f_n f_{n+1} c_n c_{n+1} \tag{5}$$

under the condition $\sum_{n=0}^{\infty} c_n^2 f_n^2 = P$. The problem can be reduced to solving the system of equations

$$f_{n-1} a_{n-1} + f_{n+1} a_n = \lambda f_n x_n,$$
$$n = 0, 1, \ldots, \tag{6}$$
$$\sum_{n=0}^{\infty} x_n f_n^2 = P,$$

where $a_n = c_n c_{n+1}$, $x_n = c_n^2$, $f_{-1} = 0$ by convention, and λ is the Lagrange multiplier. Finding the solution under the most general conditions is not an easy task. Fortunately, there are some simplifications that can be made, provided we are applying the filtration to the practically significant coherent states.

A coherent state $|\alpha\rangle = e^{-|\alpha|^2/2} \sum_{k=1}^{\infty} \frac{\alpha^k}{\sqrt{k!}} |k\rangle$ can be considered a quantum version of a classical complex amplitude of light. It can be used to describe the state of light produced by a well-stabilized laser and it has a place both in classical communication [19] and in quantum cryptography [20], both of which can employ phase encoding. Coherent states are fairly well localized in the Fock space: For any coherent state there always exists a finite N-dimensional Fock subspace such that the probability of the state manifesting outside of it can be made arbitrarily small. As a consequence, those higher Fock dimensions do not significantly contribute to the state's properties and the values of the respective filters can be set to one, i.e., $f_n = 1$ for all $n \geqslant N$. Of course, with severe filtering leading to extremely low success rates, some previously dismissable Fock numbers can start being relevant, but this can be remedied by choosing an even higher photon number N' as the new threshold of significance.

This dramatically simplifies the process of finding the optimal filter. All the filter coefficients for $n = 0, \ldots, N$ can be now expressed in the form

$$f_n = f_0 \mathcal{P}_n(\lambda), \quad (7)$$

where $\mathcal{P}_n(\lambda)$ is a polynomial of λ defined by the recursive relation

$$P_{n+1}(\lambda) = \frac{\lambda x_n \mathcal{P}_n(\lambda) - a_{n-1} \mathcal{P}_{n-1}(\lambda)}{a_n}, \quad (8)$$

with $\mathcal{P}_0(\lambda) \equiv 1$ and $\mathcal{P}_1(\lambda) = x_0/a_0$. Since f_0 can be obtained from the condition $f_N = f_0 \mathcal{P}_N(\lambda) = 1$, getting the full solution is reduced to finding the correct value of the Lagrange multiplier λ, which is one of the roots of the polynomial equation

$$\sum_{n=0}^{N} x_n \mathcal{P}_n(\lambda)^2 = \left(P - 1 + \sum_{n=0}^{N} x_n \right) \mathcal{P}_N(\lambda)^2. \quad (9)$$

To be of physical relevance, the obtained λ needs to be real and it has to lead to a filter with parameters, which are all positive and bounded by one. Among the values of λ satisfying those condition, the one corresponding to the global extreme, rather than just a local one, needs to be selected by directly checking the respective value of μ.

Interestingly enough, not all combinations of α, P, and N lead to physical filters. In fact, for any specific pair of values of α and P, there are only a handful of values of N providing physically relevant filters. This is illustrated in Fig. 1, where it can be seen that for $\log_{10} P = -1.3$ both $N = 2$ and 3 provide a physical filter ($N = 3$ is optimal). There is no filter for $N = 1$ because it is just impossible to reach such a low probability by damping only a single coefficient. There are also no physical filters for $N \geqslant 4$: All the obtained values of λ are either complex or lead to filters that are not bounded by one. This could be resolved by adding additional boundary conditions for the set of equations, but it turns out that it
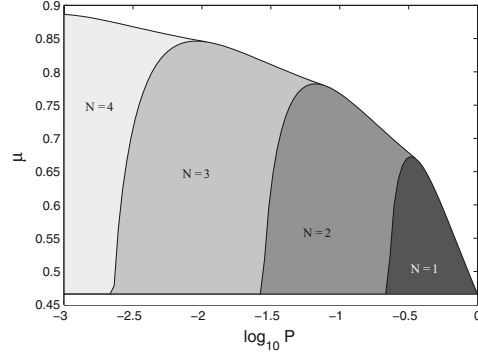

FIG. 1. (Color online) Value of μ for the optimal probabilistic measurement of the phase of the coherent state with $\alpha = 0.5$ dependent on the probability of success. Differently colored areas correspond to filters with different filter parameters N.

is not necessary, as in these cases the optimal filter can be obtained for a different value of N. The particular optimal N needs to be found numerically. Fortunately this is a simple matter of checking a range of values of N and finding the one that leads to positive results. For illustration, several values of N optimal for some range of α and P are depicted in Fig. 2. As another illustration, Fig. 3 shows improvement of the probabilistic measurement for several coherent states with different amplitudes. Finally, the optimal filters for a specific coherent state and a range of success probabilities are depicted in Fig. 4.

We have introduced the concept of optimal probabilistic measurement of quantum phase and shown how such a measurement can be constructed. The approach can be used for any quantum state, but we have mainly focused on practically relevant coherent states, for which we have managed to obtain
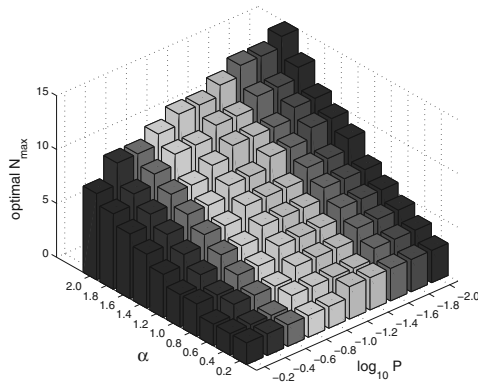

FIG. 2. (Color online) Optimal filter parameters N dependent on the coherent amplitude of the coherent state α and the probability of the successful measurement P.
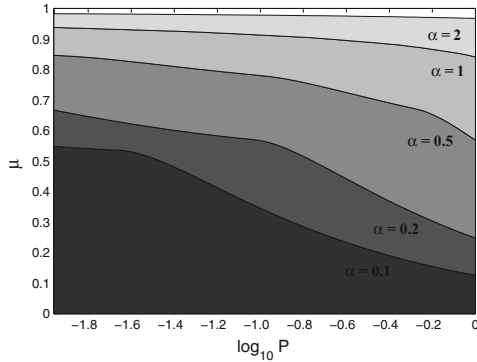
FIG. 3. (Color online) Value of μ for the optimal probabilistic measurement of the phase for various coherent states.

FIG. 4. (Color online) Optimal filters for the coherent state with $\alpha = 0.5$ and a range of success probabilities.

the form of the optimal measurement in a semianalytic form. The probabilistic aspect of the measurement can be represented by a filter transmitting various Fock space elements with different amplitudes. The derived optimal measurement sets an upper bound on the trade-off between the quality and the probability of success of phase measurements. The filter required
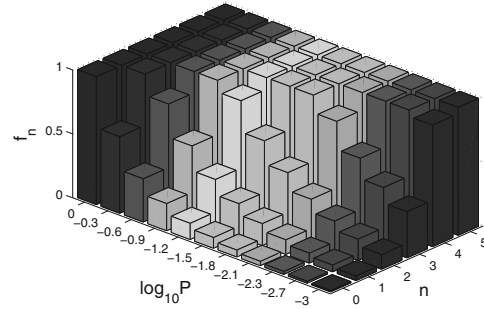
for such a measurement is a highly nonlinear operation, but in light of the recent advent of manipulating light on the individual photon level [11], it might be within experimental reach.

[1] P. A. M. Dirac, Proc. R. Soc. London Ser. A **114**, 243 (1927); W. H. Louisell, Phys. Lett. **7**, 60 (1963); L. Susskind and J. Glogower, Physics **1**, 49 (1964); P. Carruthers and M. M. Nieto, Rev. Mod. Phys. **40**, 411 (1968).

[2] R. Loudon, *The Quantum Theory of Light* (Oxford University Press, New York, 2000).

[3] D. T. Pegg and S. M. Barnett, Phys. Rev. A **39**, 1665 (1989).

[4] C. W. Helsrom, Int. J. Theor. Phys. **11**, 357 (1974); J. H. Shapiro and S. R. Shepard, Phys. Rev. A **43**, 3795 (1991).

[5] U. Leonhardt, J. A. Vaccaro, B. Böhmer, and H. Paul, Phys. Rev. A **51**, 84 (1995).

[6] H. M. Wiseman and R. B. Killip, Phys. Rev. A **56**, 944 (1997); **57**, 2169 (1998).

[7] K. L. Pregnell and D. T. Pegg, Phys. Rev. Lett. **89**, 173601 (2002).

[8] P. Kok, A. N. Boto, D. S. Abrams, C. P. Williams, S. L. Braunstein, and J. P. Dowling, Phys. Rev. A **63**, 063407 (2001).

[9] H. Yonezawa, D. Nakane, T. A. Wheatley, K. Iwasawa, S. Takeda, H. Arao, K. Ohki, K. Tsumura, D. W. Berry, T. C. Ralph, H. M. Wiseman, E. H. Huntington, and A. Furusawa, Science **337**, 1514 (2012).

[10] T. C. Ralph and A. B. Lund, in *Proceedings of the Ninth International Conference on Quantum Communications Measurement and Computing*, edited by A. Lvovsky, AIP Conf. Proc. No. 155 (AIP, New York, 2009); P. Marek and R. Filip, Phys. Rev. A **81**, 022302 (2010); J. Fiurášek, *ibid.* **80**, 053822 (2009).

[11] G. Y. Xiang, T. C. Ralph, A. P. Lund, N. Walk, and G. J. Pryde, Nat. Photon. **4**, 316 (2010); F. Ferreyrol, M. Barbieri,

R. Blandino, S. Fossier, R. Tualle-Brouri, and P. Grangier, Phys. Rev. Lett. **104**, 123603 (2010); M. A. Usuga, C. R. Müller, C. Wittmann, P. Marek, R. Filip, C. Marquardt, G. Leuchs, and U. L. Andersen, Nat. Phys. **6**, 767 (2010); A. Zavatta, J. Fiurášek, and M. Bellini, Nat. Photon. **5**, 52 (2011); C. R. Müller, C. Wittmann, P. Marek, R. Filip, C. Marquardt, G. Leuchs, and U. L. Andersen, Phys. Rev. A **86**, 010305(R) (2012).

[12] I. D. Ivanovic, Phys. Lett. A **123**, 257 (1987); D. Dieks, *ibid.* **126**, 303 (1988); A. Peres, *ibid.* **128**, 19 (1988); S. J. van Enk, Phys. Rev. A **66**, 042313 (2002).

[13] U. Leonhardt, *Essential Quantum Optics* (Cambridge University Press, Cambridge, 2010).

[14] Z. Hradil, Phys. Rev. A **46**, R2217 (1992).

[15] C. W. Helstrom, *Quantum Detection and Estimation Theory* (Academic, New York, 1974).

[16] Expression (2) can also be maximized with the help of Lagrange multipliers and the symmetry condition $c_n = c_{N-n}$.

[17] G. S. Summy and D. T. Pegg, Opt. Commun. **77**, 75 (1990).

[18] If this were not the case and some of the coefficients were negative or complex, the situation could be remedied by using complex filter coefficients with $|f_n| = 1$, which could improve phase properties at no cost in success rate.

[19] V. Giovannetti, S. Guha, S. Lloyd, L. Maccone, J. H. Shapiro, and H. P. Yuen, Phys. Rev. Lett. **92**, 027902 (2004).

[20] F. Grosshans and P. Grangier, Phys. Rev. Lett. **88**, 057902 (2002); V. Scarani, H. Bechmann-Pasquinucci, N. J. Cerf, M. Dušek, N. Lütkenhaus, and M. Peev, Rev. Mod. Phys. **81**, 1301 (2009).

Elementary gates for quantum information with superposed coherent states

Petr Marek and Jaromír Fiurášek

Department of Optics, Palacký University, 17. Listopadu 1192/12, CZ-771 46 Olomouc, Czech Republic
(Received 30 April 2010; published 27 July 2010)

We propose an alternative way of implementing several elementary quantum gates for qubits in the coherent-state basis. The operations are probabilistic and employ single-photon subtractions as the driving force. Our schemes for single-qubit PHASE gate and two-qubit controlled PHASE gate are capable of achieving arbitrarily large phase shifts with currently available resources, which makes them suitable for the near-future tests of quantum-information processing with superposed coherent states.

Quantum computation offers several advantages over its classical counterpart, namely an exponential speedup for some computational tasks. Currently, the most advanced approach to actually building the quantum computer relies on the use of two-level quantum systems: qubits. Their quantum optical implementation relied initially on states of single photons [1], but recently there were proposals to use superpositions of two "macroscopical" objects, two coherent states of light differing by phase [2,3]. Since then there has been considerable attention focused on obtaining such superposed coherent states [4] or even arbitrary qubits in the coherent-state basis [5].

Any quantum computer needs to be constructed from basic building blocks, from quantum gates. In principle, two types of gates are required. Single-mode gates are needed to control quantum states locally, while two-mode gates serve to provide entanglement. The original proposal for quantum computing with coherent states [3] suggested that these gates could be implemented by coherent displacements and interference on unbalanced beam splitters followed by projection back onto the computational subspace. This approach looks fine in theory, but with regards to currently available experimental resources, there is hardly any interesting effect that can be observed.

This statement requires some clarification. The scheme put forward in Ref. [3] relies on the phase shift that occurs when a coherent state gets displaced, $\hat{D}(\beta)|\alpha\rangle = e^{(\alpha\beta^* - \alpha^*\beta)/2}|\alpha + \beta\rangle$. If $|\beta| \ll |\alpha|$, the displaced state strongly resembles the original one, differing mainly in the phase shift of the basis coherent state. The displacement could be driven classically, providing the single-mode phase-shift operation, or by another quantum state to implement a two-qubit gate. However, the need for the low value of the displacement results in a low value of the implemented phase shift, considering the currently achievable size of superposed coherent states, $|\alpha| \approx 1$. Consequently, a large number of operations (at least ten) would be required to achieve a π phase shift. Furthermore, an indispensable part of the operation is quantum teleportation, which projects the displaced state back onto the computational basis $|\alpha\rangle$, $|-\alpha\rangle$ and which should be implemented after each step. Without it, the actual nature of transformations is revealed to be that of a trivial displacement or a beam splitter. Unfortunately, the teleportation requires the entangled superposed coherent state as a resource, which, together with the need for photon number resolving detectors, renders it either unavailable or highly probabilistic.

All in all, the operations of [3] allow, in principle, deterministic interactions of arbitrary strength. In reality though,

the single step produces only a very weak effect, and the need to teleport the states afterward means that presently the full gate is probabilistic anyway and that there probably will not be more steps in the foreseeable future. Therefore, if we wish to test the principles of quantum-information processing with the superposed coherent states, we need to devise alternative, more feasible, approaches.

In the following, we are going to present an alternative way of performing several of the elementary gates: the single-mode PHASE gate, the two-mode controlled PHASE gate, and the single-mode Hadamard gate. The gates are probabilistic, relying on projective measurements (photon subtractions, in particular) to deliver the nonlinear effect.

To clearly convey the basic ideas let us work in the idealized scenario of perfect superposition of coherent states and perfect photon subtraction. We start with the single-mode PHASE gate which is necessary for single qubit manipulations. The procedure is schematically shown in Fig. 1. An arbitrary qubit in the coherent-state basis,

$$|\psi_{\text{in}}\rangle = x|\alpha\rangle + y|-\alpha\rangle, \tag{1}$$

is first coherently displaced by γ, $|\psi_{\text{in}}\rangle \rightarrow \hat{D}(\gamma)|\psi_{\text{in}}\rangle$. This operation can be easily performed by mixing the signal beam with an auxiliary strong coherent field on a highly unbalanced beam splitter [6]. Subsequently, a single photon is subtracted from the state, which is mathematically described by the action of annihilation operator $\hat{a}$. Finally, the state undergoes an inverse displacement by $-\gamma$, and we have

$$\begin{aligned}|\psi_{\text{out}}\rangle &= \hat{D}(-\gamma)\hat{a}\hat{D}(\gamma)|\psi_{\text{in}}\rangle \\ &= x(\alpha + \gamma)|\alpha\rangle + y(-\alpha + \gamma)|-\alpha\rangle. \end{aligned} \tag{2}$$

This operation becomes equivalent to a PHASE gate provided that the complex displacement γ satisfies

$$\frac{\gamma - \alpha}{\gamma + \alpha} = e^{i\phi}, \tag{3}$$

which yields $\gamma = i\alpha/\tan(\phi/2)$. The output state after PHASE gate then reads

$$|\psi_{\text{out}}\rangle = i(xe^{-i\phi/2}|\alpha\rangle + ye^{i\phi/2}|-\alpha\rangle), \tag{4}$$

and it can be seen that, up to a global phase factor, any nonzero phase shift ϕ may be performed in this way.

Another important gate for quantum-information processing is the two-qubit controlled PHASE gate, which is, up to local operations, equivalent to the controlled-NOT (CNOT) gate, and
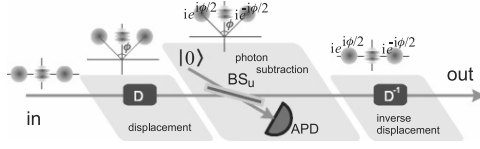
FIG. 1. (Color online) Schematic representation of the single-mode PHASE gate. BS stands for a mostly transmitting strongly unbalanced beam splitter, APD stands for avalanche photodiode, and D represents the displacement operation.

which is used to establish entanglement in cluster states. It can be implemented in a manner similar to the single-qubit PHASE gate, also employing displacements and photon subtractions as the driving force. However, to achieve interaction between the two modes 1 and 2 while preserving the computational basis, the operations take place in one arm of a Mach-Zehnder interferometer, see Fig. 2. For the input two-qubit state written in the coherent-state basis

$$|\Psi_{\text{in}}\rangle = c_{11}|\alpha,\alpha\rangle + c_{10}|\alpha,-\alpha\rangle + c_{01}|-\alpha,\alpha\rangle + c_{00}|-\alpha,-\alpha\rangle, \tag{5}$$

the controlled PHASE gate is symmetric and preserves the structure of the state, only providing the term $|-\alpha\rangle|-\alpha\rangle$ with a phase factor $e^{i\phi}$, where ϕ is the phase shift introduced by the gate. A normalized output state of the gate corresponding to input state (5) thus reads

$$\begin{aligned}|\Psi_{\text{out}}\rangle = c_{11}|\alpha,\alpha\rangle + c_{10}|\alpha,-\alpha\rangle + c_{01}|-\alpha,\alpha\rangle \\ + e^{i\phi}c_{00}|-\alpha,-\alpha\rangle,\end{aligned} \tag{6}$$

which is a new state with coefficients c'_{mn} related to c_{mn} as

$$\frac{c'_{11}}{c_{11}} = \frac{c'_{01}}{c_{01}} = \frac{c'_{10}}{c_{10}} = \frac{c'_{00}}{c_{00}}e^{-i\phi}. \tag{7}$$

The implementation of the gate requires a Mach-Zehnder interferometer with two single-photon subtractions accompanied by suitable displacements placed in one of the arms, which can be formally expressed as

$$\begin{aligned}|\Psi_{\text{out}}\rangle &= \hat{U}_{\text{BSb}}^{\dagger}\hat{D}_2^{\dagger}\hat{a}\hat{D}_2\hat{D}_1^{\dagger}\hat{a}\hat{D}_1\hat{U}_{\text{BSb}}|\Psi_{\text{in}}\rangle \\ &= (\hat{a}+\hat{b}+\gamma_2)(\hat{a}+\hat{b}+\gamma_1)|\Psi_{\text{in}}\rangle.\end{aligned} \tag{8}$$

Here, $\hat{a}$ and $\hat{b}$ represent the annihilation operators of modes 1 and 2, respectively, $\hat{D}_{1,2}$ stand for the displacement operators acting as $\hat{D}_{1,2}^{\dagger}\hat{a}\hat{D}_{1,2} = \hat{a} + \gamma_{1,2}/\sqrt{2}$, and $\hat{U}_{\text{BSb}}$ is the unitary evolution operator of a balanced beam splitter, $\hat{U}_{\text{BSb}}^{\dagger}\hat{a}\hat{U}_{\text{BSb}} = (\hat{a}+\hat{b})/\sqrt{2}$.

FIG. 2. (Color online) Schematic representation of the two-mode controlled PHASE gate. BS$_b$ stands for a balanced beam splitter and $D_{1,2}$ represent displacements by $\gamma_{1,2}/\sqrt{2}$. Numbers 1 and 2 distinguish the two participating modes, while labels "in" and "out" describe the input and output states of the gate.

After the transformation, the composition of the state remains the same, only the coefficients are transformed to

$$\begin{aligned}c'_{11} &= c_{11}[4\alpha^2 + 2\alpha(\gamma_1+\gamma_2) + \gamma_1\gamma_2], \\ c'_{10} &= c_{10}\gamma_1\gamma_2, \\ c'_{01} &= c_{01}\gamma_1\gamma_2, \\ c'_{00} &= c_{00}[4\alpha^2 - 2\alpha(\gamma_1+\gamma_2) + \gamma_1\gamma_2].\end{aligned} \tag{9}$$

To achieve the controlled PHASE gate transformation given by (7) one needs to attune the displacements γ_1 and γ_2 in such a way that

$$\begin{aligned}\gamma_1 + \gamma_2 &= -2\alpha, \\ \gamma_1\gamma_2 &= \frac{8\alpha^2}{e^{i\phi}-1}.\end{aligned} \tag{10}$$

An explicit calculation provides closed analytical formulas for the required displacements

$$\gamma_{1,2} = -\alpha\left[1 \pm \sqrt{\frac{e^{i\phi}-9}{e^{i\phi}-1}}\right]. \tag{11}$$

Again, the phase shift ϕ can attain an arbitrary nonzero value.

It is important to stress, and it holds for both the PHASE gates, that although we have used direct displacements of the participating modes, it is actually more feasible to apply all the required displacement operations only on the ancillary modes used for the photon subtraction, just before the avalanche photodiode (APD) measurement. To explain the procedure we consider an arbitrary two-mode coherent state $|\alpha',\beta'\rangle$ and subject it to the evolution sketched in Fig. 3. First, the two modes are separately split on strongly unbalanced beam splitters with transmission coefficients $t \approx 1$ and reflection coefficients $r \ll 1$, which leads to a joint state $|\alpha',\beta'\rangle|r\alpha',r\beta'\rangle$. The two ancillary modes are now mixed on a balanced beam splitter and one of the modes is traced out. Since r is very small, this does not significantly reduce the purity and we can keep working with the state vector. The remaining mode is then split on another balanced beam splitter and two displacement operations are performed, arriving at the premeasurement state

$$|\alpha',\beta'\rangle\left|\frac{r}{2}(\alpha'+\beta')+\gamma'_1, \frac{r}{2}(\alpha'+\beta')+\gamma'_2\right\rangle. \tag{12}$$
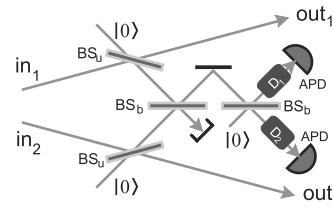
FIG. 3. (Color online) Alternative architecture of the two-mode controlled PHASE gate. BS$_b$ stands for a balanced beam splitter, while BS$_u$ represents a strongly unbalanced weakly reflective one. APD represents avalanche photodiode and D_1 and D_2 are the displacement operations. Numbers 1 and 2 distinguish the two participating modes, while labels "in" and "out" describe the input and output states of the gate.

In the limit of small r, the APD detectors can be represented by projection onto the single-photon Fock state $\langle 1|$ and if the displacements are chosen so $\gamma'_{1,2} = \gamma_{1,2}r/2$ the final state looks as

$$(\alpha' + \beta' + \gamma_1)(\alpha' + \beta' + \gamma_2)|\alpha', \beta'\rangle, \qquad (13)$$

which is exactly what we want.

Note that a similar approach was already used for generation of an arbitrary coherent-state qubit [5], which also demonstrated, albeit in a limited way, the core principle behind the single-mode PHASE gate.

Finally, to complete the set of gates necessary for implementation of an arbitrary single-qubit operation, we present a feasible implementation of the Hadamard gate. Unlike the two previous gates, the Hadamard gate requires more than single-photon subtractions. This is quite understandable because the gate is supposed to transform a coherent state $|\alpha\rangle$ into a superposed state $|\alpha\rangle + |-\alpha\rangle$, which is a strongly nonlinear process. Therefore an additional superposed coherent state, let us say $|\alpha\rangle + |-\alpha\rangle$, is required.

The core principle is simple and it employs the previously described controlled PHASE gate. This gate, with $\phi = \pi$, transforms the initial and the ancillary state to

$$x|\alpha\rangle(|\alpha\rangle + |-\alpha\rangle) + y|-\alpha\rangle(|\alpha\rangle - |-\alpha\rangle). \qquad (14)$$

The gate is finalized by using a projective measurement $\langle \pi|$ such that $\langle \pi|\alpha\rangle = \langle \pi|-\alpha\rangle$. An example of such a measurement is the homodyne detection of the $\hat{p}$ quadrature, postselecting the state only if a specific value is detected, or a photon number resolving detector projecting on an arbitrary even-number Fock state.

This kind of Hadamard gate requires three projective operations. Two photon subtractions for implementation of the controlled gate and one additional measurement to confine the state into a single mode. There is another possibility, illustrated in Fig. 4, which reduces the number of operations to two. This improvement is compensated by imperfection of the operation, as it works only approximatively, even though the quality may be made arbitrarily large.

Here too we need another superposed coherent state $|\alpha\rangle + |-\alpha\rangle$. If we consider a displacement by some amplitude β, a single-photon subtraction, and the inverse displacement, the state would be transformed to

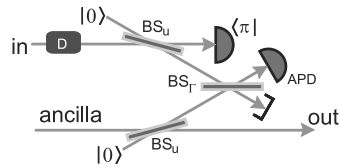$$(\alpha + \beta)|\alpha\rangle + (-\alpha + \beta)|-\alpha\rangle. \qquad (15)$$

FIG. 4. (Color online) Schematic representation of the approximate single-mode Hadamard gate. BS_u stands for a highly unbalanced weakly reflecting beam splitter, while BS_Γ is a beam splitter with transmission coefficient t_Γ used to set the parameter Γ. APD stands for a avalanche photodiode and $\langle \pi|$ represents the suitable projective measurement (see text).

We can now see that for $\beta = 0$ we have obtained an odd cat state, while for $\beta \gg \alpha$ the cat state remained even. If we could correlate the displacement with the basis states of the initial state $x|\alpha\rangle + y|-\alpha\rangle$, we would have obtained the required transformation. So how to do it?

Let us start with the initial state (1) and displace it by α. The complete state of the initial mode and the resource mode then looks as

$$(x|\beta\rangle + y|0\rangle) \otimes (|\alpha\rangle + |-\alpha\rangle), \qquad (16)$$

where $\beta = 2\alpha$, but its value could be different if the initial state had a different amplitude than the ancillary resource. The next step is to apply a joint single-photon subtraction, similarly as for the controlled PHASE gate, represented by operator $\Gamma\hat{a} + \hat{b}$ (where $\hat{a}$ and $\hat{b}$ are annihilation operators acting on the ancillary and the input mode, respectively) and a projection of the initial mode onto a certain pure state $\langle \pi|$ that will be specified in the following. The resulting single-mode output state then reads

$$x\langle \pi|\beta\rangle[(\beta + \Gamma\alpha)|\alpha\rangle + (\beta - \Gamma\alpha)|-\alpha\rangle]$$
$$+ y\langle \pi|0\rangle\Gamma\alpha(|\alpha\rangle - |-\alpha\rangle). \qquad (17)$$

If $|\Gamma\alpha| \ll |\beta|$ holds, we can make the approximation $\beta \pm \Gamma\alpha \approx \beta$ and the output state simplifies to

$$x\langle \pi|\beta\rangle\beta(|\alpha\rangle + |-\alpha\rangle) + y\langle \pi|0\rangle\Gamma\alpha(|\alpha\rangle - |-\alpha\rangle). \qquad (18)$$

The desired Hadamard operation is then performed if

$$\langle \pi|\beta\rangle\beta = \langle \pi|0\rangle\Gamma\alpha. \qquad (19)$$

To achieve this, the projective measurement $|\pi\rangle$ needs to be properly chosen. For example, using homodyne detection to project on an $\hat{x}$ eigenstate $\langle \hat{x} = q|$ is appropriate, provided that $\exp[-(q - \sqrt{2}\beta)^2/2] = \exp(-q^2)\alpha\Gamma/\beta$. This can always be done. The value of Γ itself can be set by manipulating the beam splitter of the joint photon subtraction as $\Gamma = t_\Gamma/\sqrt{1 - t_\Gamma^2}$. In this way, even if there is a large difference in amplitudes of the two participating states, the Hadamard gate can be implemented with arbitrary precision. Note that the standard way of generating an odd superposed coherent state by a photon subtraction is actually very close to the implementation of the proposed Hadamard gate for a known coherent-state input.

The experimental implementation of the proposed gates should be straightforward. The most difficult part of the gates is the photon subtraction, which can be implemented by a strongly unbalanced beam splitter and an on-off photodetector—the avalanche photodiode. In this form the photon subtraction is becoming a staple of continuous variables quantum optical experiments and it is widely used to generate superposed coherent states [4,5], or to manipulate and concentrate entanglement [7,8].

To summarize, we have proposed a feasible implementation of several elementary gates for superposed coherent-state qubits. The main benefit of the proposed approach, which is based on using single-photon subtractions, is that it allows achieving strong nonlinearities even with the currently available small cat-like states exhibiting $|\alpha| \approx 1$, much unlike the proposal of Ref. [3]. The experimental feasibility, together with the ability to produce strong nonlinearities, makes these gates suitable for immediate tests of quantum-information processing with coherent-state qubits.

[1] E. Knill, L. Laflamme, and G. J. Milburn, Nature (London) **409**, 46 (2001); R. Raussendorf and H. J. Briegel, Phys. Rev. Lett. **86**, 5188 (2001); H. J. Briegel, D. E. Browne, W. Dür, R. Raussendorf, and M. V. den Nest, Nature Physics **5**, 19 (2009).

[2] H. Jeong and M. S. Kim, Phys. Rev. A **65**, 042305 (2002).

[3] T. C. Ralph, A. Gilchrist, G. J. Milburn, W. J. Munro, and S. Glancy, Phys. Rev. A **68**, 042319 (2003).

[4] A. Ourjoumtsev, H. Jeong, R. Tualle-Brouri, and P. Grangier, Nature (London) **448**, 784 (2007); J. S. Neergaard-Nielsen, B. M. Nielsen, C. Hettich, K. Mølmer, and E. S. Polzik, Phys. Rev. Lett. **97**, 083604 (2006); H. Takahashi, K. Wakui, S. Suzuki, M. Takeoka, K. Hayasaka, A. Furusawa, and M. Sasaki,

ibid. **101**, 233605 (2008); T. Gerrits, S. Glancy, T. S. Clement, B. Calkins, A. E. Lita, A. J. Miller, A. L. Migdall, S. W. Nam, R. P. Mirin, and E. Knill, e-print arXiv:1004.2727.

[5] J. S. Neergaard-Nielsen, M. Takeuchi, K. Wakui, H. Takahashi, K. Hayasaka, M. Takeoka, and M. Sasaki, e-print arXiv:1002.3211v1 [quant-ph].

[6] M. G. A. Paris, Phys. Lett. A **217**, 78 (1996).

[7] T. Opatrný, G. Kurizki, and D.-G. Welsch, Phys. Rev. A **61**, 032302 (2000).

[8] H. Takahashi, J. S. Neergaard-Nielsen, M. Takeuchi, M. Takeoka, K. Hayasaka, A. Furusawa, and M. Sasaki, Nature Photonics **4**, 178 (2010).

Experimental demonstration of a Hadamard gate for coherent state qubits

Anders Tipsmark,[1,*] Ruifang Dong,[2,1] Amine Laghaout,[1] Petr Marek,[3] Miroslav Ježek,[3,1] and Ulrik L. Andersen[1]

[1]*Department of Physics, Technical University of Denmark, Fysikvej, DK-2800 Kgs. Lyngby, Denmark*
[2]*Quantum Frequency Standards Division, National Time Service Center (NTSC), Chinese Academy of Sciences,*
710600 Lintong, Shaanxi, China
[3]*Department of Optics, Palacký University, 17. listopadu 12, CZ-77146 Olomouc, Czech Republic*

We discuss and make an experimental test of a probabilistic Hadamard gate for coherent state qubits. The scheme is based on linear optical components, nonclassical resources, and the joint projective action of a photon counter and a homodyne detector. We experimentally characterize the gate for the coherent states of the computational basis by full tomographic reconstruction of the transformed output states. Based on the parameters of the experiment, we simulate the fidelity for all coherent state qubits on the Bloch sphere.

Measurement-based, linear optical quantum processors rely on offline prepared resources, linear optical transformations, and measurement-induced operations [1]. Among all measurement-based protocols, the most famous ones are the cluster state quantum processor where universal operations are executed by measuring a large entangled cluster state [2], and the linear quantum computer approach proposed by Knill, Laflamme, and Milburn [3]. The latter method is based on single-photon resources that interfere in a linear optical network and subsequently are measured to enforce the desired operation. Despite its seeming simplicity, the implementation of a fault tolerant operating algorithm is complex as it requires a very large overhead.

An alternative approach to measurement-based linear quantum computing has been put forward by Ralph *et al.* [4]. Rather than using discrete degrees of freedom (e.g., the polarization) of a single photon as the computational basis, it was suggested to use two mesoscopic coherent states $|\alpha\rangle$ and $|-\alpha\rangle$, where α is the amplitude. Although these states are only approximately orthogonal ($\langle\alpha|-\alpha\rangle \neq 0$), resource-efficient and fault-tolerant quantum gates can be implemented: For a large coherent amplitude, that is, $\alpha > 2$, deterministic gates can in principle be realized, although the experimental implementation is very challenging [5]. On the other hand, by employing a simpler physical implementation, nondeterministic gates can be realized for any value of α, and for $\alpha > 1.2$, the scheme was theoretically shown to be fault tolerant and resource efficient [6].

An even simpler implementation of a universal set of nondeterministic quantum gates was recently suggested by Marek and Fiurášek [7]. They proposed the physical realization of a single-mode and a two-mode phase gate as well as the Hadamard gate. In this Rapid Communication we present a proof of principle experiment of the probabilistic Hadamard gate for coherent state qubits. The implemented protocol is based on a squeezed state resource, linear operations as well as two projective measurements of discrete and continuous variable types. By injecting the computational basis states ($|\alpha\rangle$ and $|-\alpha\rangle$) into the gate we partially characterize

───────
*Corresponding author: anders.tipsmark@fysik.dtu.dk

its function by reconstructing the Wigner functions of the transformed output states and calculate the fidelity with an ideally transformed state. Based on these results we perform a simulation of the gate performance for arbitrary coherent state qubits.

A Hadamard gate transforms the computational basis states $|\pm\alpha\rangle$ into the diagonal basis states $(|\alpha\rangle \pm |-\alpha\rangle)/\sqrt{N_\pm}$, which we refer to as the even and odd coherent state qubits (CSQs) [8–15]. Such a transformation can be performed probabilistically using the circuit shown in Fig. 1(a). The gate is based on a supply of coherent state superposition resources which are assumed to have the same amplitude as the coherent states of the computational basis. The gate works by displacing the arbitrary CSQ input state $|\psi_{\rm in}\rangle = (u|\alpha\rangle + v|-\alpha\rangle)/\sqrt{N}$, followed by a nondistinguishable subtraction of a single photon, from either the displaced input or the resource state. Physically, this can be done by reflecting a small part of either state using highly asymmetric beam splitters (ABS1,ABS2), interfering the resulting beams on a beam splitter (BS) with transmittivity t and reflectivity r, and detecting one photon at the output with a single-photon detector. Theoretically this is described by the operator $r\hat{a} + t\hat{b}$, where $\hat{a}$ and $\hat{b}$ are annihilation operators corresponding to the subtraction of a photon from the displaced input and the coherent state superposition resource, respectively. As a final step the two-mode state is projected onto the single-mode quadrature eigenstate $|x\rangle$, where x is the amplitude quadrature, by using a homodyne detector (HD). The resulting output state is

$$u\frac{|\alpha\rangle + |-\alpha\rangle}{\sqrt{N_+}} + Y_1(u + vZ)\frac{|\alpha\rangle - |-\alpha\rangle}{\sqrt{N_-}}, \qquad (1)$$

where

$$Y_1 = \frac{t}{2r}\sqrt{\frac{N_-}{N_+}}, \quad Z = \frac{\langle x|0\rangle}{\langle x|2\alpha\rangle}. \qquad (2)$$

By using a beam splitter (BS) with $t \ll r$ and setting the x quadrature such that $Z \gg 1$ and $ZY_1 = 1$, the Hadamard transform is implemented. The gate is probabilistic, and implemented by a hybrid detection system, using both discrete and continuous variable projections [16,17]. Its success is conditioned on the joint measurement of a photon and a quadrature measurement outcome with the value x.
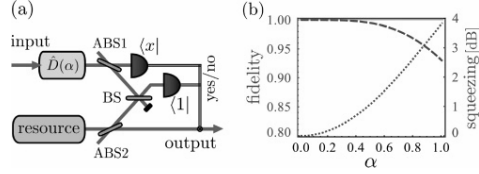
FIG. 1. (Color online) (a) Schematic of the Hadamard gate. The input coherent state qubit (CSQ) is displaced ($\hat{D}$) and mixed with a resource state at a beam splitter (BS). The output of the gate is conditioned by a single-photon detection ($\langle 1|$) and a homodyne measurement ($\langle x|$). (b) Gate fidelity as a function of the CSQ amplitude for an ideal coherent state superposition resource (solid green/light gray) and the squeezed state resource (dashed red/gray). The degree of squeezing that optimizes the fidelity is represented by the dotted blue/dark gray curve.

As an even coherent state superposition with small amplitude is reminiscent of a squeezed vacuum state, and this latter state is experimentally easier to prepare, we will in the following consider the replacement of the ideal resource with a squeezed vacuum state. With this substitution, the transformed state will have the following form:

$$u\hat{S}(s)|0\rangle + Y_2(u + vZ)\hat{S}(s)\hat{a}^\dagger|0\rangle, \qquad (3)$$

where s is the squeezing parameter which is related to the squeezing variance by $V = e^{-2s}$, and the parameter Y_2 is now given by

$$Y_2 = -t \sinh(s)/(2r\alpha). \qquad (4)$$

Again, the requirement for optimal implementation of the Hadamard transform is $Z \gg 1$ and $ZY_2 = 1$. Using this result we calculate the expected gate fidelity for various amplitudes α as shown by the dashed red/gray curve in Fig. 1(b). For the squeezed vacuum resource, we optimize the squeezing degree (shown by the dotted blue/dark gray curve) to obtain the highest fidelity which reaches unity for $\alpha = 0$. At higher amplitudes, the resource deviates from the ideal coherent state superposition and thus the fidelity decreases. For comparison, we also plot the expected gate fidelity for the case of an ideal resource (the solid green/light gray line). In the experiment described below we use $\alpha = 0.8$, which gives a reasonable trade-off between fidelity ($F = 0.97$), required squeezing ($V = 2.6$ dB), and success probability.

The experimental setup is presented in Fig. 2. Nearly Fourier-limited picosecond pulses (4.6 ps) generated by a cavity-dumped Ti:sapphire laser with a repetition rate of 815 kHz and a central wavelength of 830 nm are frequency doubled [second-harmonic generation (SHG)] by single passing a 3-mm-long periodically poled KTiOPO$_4$ nonlinear crystal (PPKTP1). Up-converted pulses at 415 nm pumps a second crystal (PPKTP2) which is phase matched for degenerate collinear optical parametric amplification (OPA), thus yielding up to 3 dB of vacuum squeezing, in the vertical polarization. This state is used as a resource for the Hadamard gate. An adjustable fraction of a horizontally polarized mode at 830 nm passes the OPA crystal unchanged and serves as the input coherent state to the gate. Approximately 7.5% and
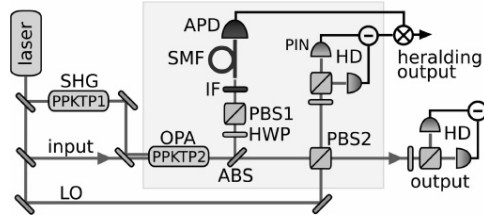

FIG. 2. (Color online) Experimental setup for the coherent state qubit Hadamard gate.

1.5% of the coaxially propagating resource and input modes, respectively, are reflected off an asymmetric beam splitter (ABS) and transmitted through a half-wave plate (HWP) and a polarizing beam splitter (PBS1), which in combination acts as a variable beam splitter (BS), thus mixing the input mode and the resource mode. The transmittance $|t|^2$ of the BS is set to 25%. The output is spatially and spectrally filtered by a single-mode optical fiber (SMF) and a narrow interference filter (IF) with a bandwidth of 0.05 nm and detected by a single-photon counting module based on a silicon avalanche photodiode (APD) with a dark count rate of 20 ± 4 per second. The total efficiency of the APD arm reaches $25 \pm 4\%$.

The transmitted fraction of the modes after the asymmetric beam splitter is superimposed with a bright local oscillator (LO) at a polarizing beam splitter (PBS2). The amplitude quadrature is measured on the reflected mode by homodyne detection with a fixed relative phase set to zero. The recording of the measurement results was done by correlating the APD detection events with a synchronization signal from the laser cavity dumper through a coincidence circuit to decrease the probability of dark events. Every time a photon was detected by the APD within the accepted time slot, the homodyne signal was sampled by an oscilloscope running in a memory segmentation regime and fed to a computer where the corresponding quadrature value was processed. The state at the output of the gate is measured with another homodyne detector with the relative phase of the LO scanned over a period and then reconstructed using maximum-likelihood-based quantum state tomography [18]. In the reconstruction we corrected for the total detection efficiency of the homodyne detector, which was estimated to be $77 \pm 2\%$, including efficiency of the photodiodes ($93 \pm 1\%$), visibility ($95 \pm 1\%$), and transmission efficiency ($93 \pm 1\%$).

Making a full experimental investigation of the gate performance would require access to states in the diagonal basis. In our experiment we did not have access to these diagonal states, which prevents us from performing a full characterization of the gate performance. The gate was solely tested for the computational basis states $|\pm\alpha\rangle$, which after the displacement operation $\hat{D}(\alpha)$ corresponds to the injection of $|0\rangle$ and $|2\alpha\rangle$, where $\alpha = 0.8 \pm 0.2$ in our case. The uncertainty is due to the imperfect calibration of total losses of the whole setup. As described, the gate is heralded by conditioning on two different measurement outcomes—the APD detection event and a certain outcome of the first homodyne detector. It can be seen that the conditional homodyning only plays a role

when we inject a CSQ into the gate, i.e., when $u,v \neq 0$. With coherent states as the input, the solution is to choose a narrow heralding window that would balance the success probabilities of the gate for those basis states. For the input state $|-\alpha\rangle$ the APD detection probability was of the order of 10^{-3} while for the $|\alpha\rangle$ input state, the probability was of the order of 10^{-2}. From this we can see that we need to choose a heralding window that will balance out the factor of 10. Based on the experimental data we found its optimal position $x = 0.4$ and the width of 0.02 that would give us an overall success probability of the order of 10^{-5}.

The reconstructed output states for both input states $|-\alpha\rangle$ and $|\alpha\rangle$ can be seen in Fig. 3. For the $|-\alpha\rangle$ input, the gate yields a state which closely resembles a small odd cat state, which is what we expect from the gate operation. We found the fidelity between the prepared state and the ideal CSQ, $(|\alpha\rangle - |-\alpha\rangle)/\sqrt{N_-}$, is maximized for $\alpha = 0.75$ and reaches a value of $F_{-\alpha} = 0.65 \pm 0.04$. The nonclassicality of the superposition state produced by the Hadamard gate can be seen from the negativity of the corresponding Wigner function, which is $W(0,0) = -0.11 \pm 0.02$, which is comparable to previous experiments where photon subtraction has been used to prepare non-Gaussian states [9–15]. The nonclassical effects were also observable without correction, with a fidelity of $F_{-\alpha} = 0.55 \pm 0.04$ and a value at the origin of $W(0,0) = -0.05 \pm 0.02$. For the $|\alpha\rangle$ input, the output state closely resembles a squeezed state, approximating a small even CSQ, $(|\alpha\rangle + |-\alpha\rangle)/\sqrt{N_+}$. The fidelity between the prepared state and the ideal CSQ for $\alpha = 0.75$ was found to be $F_\alpha = 0.94 \pm 0.02$.

The experimental results shown in Fig. 3 only provide a partial test of the Hadamard gate. In order to gain insight into its action on an arbitrary CSQ input, we conducted a numerical simulation of the gate, taking into account all important experimental imperfections, including realistic splitting ratios of ABS1, ABS2, and BS, losses in APD and HD channels, and the impurity of our resource squeezed state.

Our simulation starts with an arbitrary qubit in the coherent state basis $|\psi_{in}\rangle$ for which the global input state reads

$$\hat{\rho}_{in} = |\psi_{in}\rangle_1 \langle\psi_{in}| \otimes |0\rangle_2\langle 0| \otimes |0\rangle_3\langle 0| \otimes \hat{\rho}_4^A, \quad (5)$$

where the subscripts are used to label the four participating modes and $\hat{\rho}^A$ represents the density matrix of a squeezed thermal state used as the ancillary resource. The action of the gate can now be represented by a unitary evolution of the linear optical elements $\hat{U}$, followed by positive operator-valued measure (POVM) elements of successful heralding events $\hat{\Pi}$, with the output state given by

$$\rho_{out} = \frac{1}{P_S} \text{Tr}_{123}(\hat{U}\hat{\rho}_{in}\hat{U}^\dagger\hat{\Pi}), \quad (6)$$

where $P_S = \text{Tr}(\hat{U}\rho_{in}\hat{U}^\dagger\hat{\Pi})$ is the success rate. $\hat{U} = \hat{U}_{23}(t_{BS})\hat{U}_{12}(t_{ABS1})\hat{U}_{34}(t_{ABS2})$ is composed of unitary beam-splitter operations coupling the respective modes, and $\hat{\Pi} = \hat{\Pi}_1^{HD} \otimes \hat{\Pi}_3^{APD}$ describes the inefficient homodyne and APD measurements. To parametrize a Bloch sphere of input CSQ states, we denote $u = \cos\theta$ and $v = \sin\theta \exp(i\phi)$, where $\theta \in [0,\pi/2]$ and $\phi \in [0,2\pi]$. The north and south poles correspond to the pseudo-orthogonal states $|\alpha\rangle$ and $|-\alpha\rangle$, respectively.
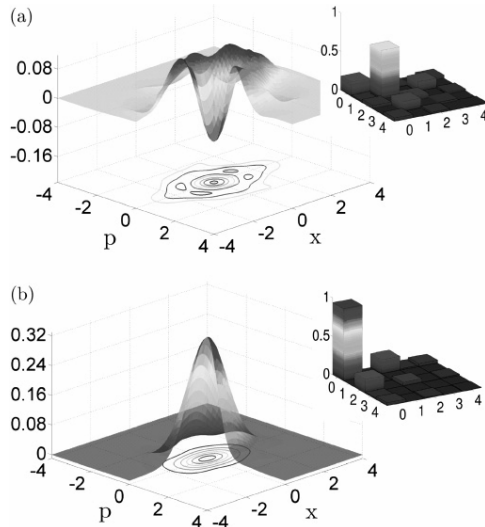

FIG. 3. (Color online) Reconstructed density matrices (insets) and calculated Wigner functions of the output states for (a) $|-\alpha\rangle$ input and (b) $|\alpha\rangle$ input.
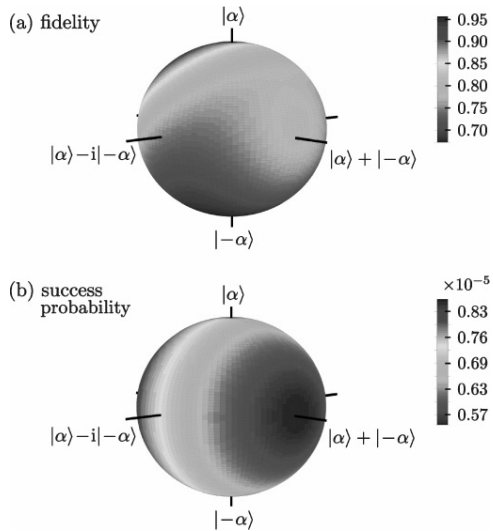

FIG. 4. (Color online) The overall quality of the gate is visualized by mapping the Bloch sphere of input CSQ onto the fidelity F of the output states (a) and their corresponding success probabilities P_S (b).

A mapping of this Bloch sphere onto the corresponding fidelities and success probabilities at the output is shown in Fig. 4. The fidelity spans the interval of $F \in [0.67, 0.96]$ with an average value of $\bar{F} = 0.78$. Particularly, for coherent states $|\alpha\rangle$ and $|-\alpha\rangle$ at the input, the fidelities of 0.88 and 0.67 are predicted, respectively, which agrees well with the actually measured values. The success probabilities associated with $|\alpha\rangle$ and $|-\alpha\rangle$ are almost equal, which confirms the correct value of the amplitude quadrature used at the HD for conditioning. The average success probability is $\bar{P}_S = 7.2 \times 10^{-6}$.

Alternatively, we quantify the performance of the gate by employing the process fidelity. This quantity is based on the elegant notion that any operation can be implemented through teleportation: The desired operation is conducted onto an entangled state which is subsequently used to teleport the state on which the operation should be imparted [19]. The quality of such an operation is given by the quality of the actually transformed entangled state, which can be quantified by the fidelity with respect to the ideally transformed entangled state. We have performed a numerical simulation of the transformation of the entangled state $|\alpha, \alpha\rangle + |-\alpha, -\alpha\rangle$ and compared it to the ideally transformed state $|\alpha\rangle(|\alpha\rangle + |-\alpha\rangle)/\sqrt{N_+} + |-\alpha\rangle(|\alpha\rangle - |-\alpha\rangle)/\sqrt{N_-}$. The process fidelity resulting from this simulation reaches $\mathcal{F} = 0.70$.

In conclusion, we have demonstrated a single-mode Hadamard gate for coherent state qubits on the computational basis, by using a hybrid projector consisting of a conditional homodyne detector and a photon counter. Its performance has been characterized by a set of basis states and from this we derived a model which could be used to simulate its performance for an arbitrary qubit. This implementation constitutes an important step toward the demonstration of quantum computing with macroscopic qubit states. To implement universal quantum computing, the Hadamard gate must be supplemented with a single-mode phase gate (a special case—the sign-flip gate—was recently implemented [20]) and a two-mode controlled phase gate. In addition to the implementation of these gates, another outlook is to refine the experimental techniques or propose alternate schemes that may increase the gate fidelity, and thus eventually may allow for fault-tolerant operation.

[1] P. Kok *et al.*, Rev. Mod. Phys. **79**, 135 (2007).

[2] R. Raussendorf, D. E. Browne, and H. J. Briegel, Phys. Rev. A **68**, 022312 (2003).

[3] E. Knill, R. Laflamme, and G. Milburn, Nature (London) **409**, 46 (2001).

[4] T. C. Ralph, A. Gilchrist, G. J. Milburn, W. J. Munro, and S. Glancy, Phys. Rev. A **68**, 042319 (2003).

[5] H. Jeong and T. Ralph, in *Quantum Information With Continuous Variables of Atoms and Light*, edited by N. J. Cerf, G. Leuchs, and E. S. Polzik (Imperial College Press, London, 2007).

[6] A. P. Lund, T. C. Ralph, and H. L. Haselgrove, Phys. Rev. Lett. **100**, 030503 (2008).

[7] P. Marek and J. Fiurášek, Phys. Rev. A **82**, 014304 (2010).

[8] The Hadamard transform is the unitary operation defined as $\hat{H}(x|0\rangle + y|1\rangle) \rightarrow x(|0\rangle + |1\rangle) + y(|0\rangle - |1\rangle)$, assuming $\langle 0|1\rangle = 0$. In our case the coherent basis states $|\alpha\rangle$ and $|-\alpha\rangle$ are only approximately orthogonal, which opens a question of the normalization of the corresponding CSQ states. Our choice of the normalized transformations (in contrast to $|\pm\alpha\rangle \rightarrow |\alpha\rangle \pm |-\alpha\rangle$) has the benefit of all states being physically sound and, consequently, fidelities for $\alpha \rightarrow 0$ approaching unity. On the other hand, it is true that for these small amplitudes the gate does not behave exactly as the Hadamard gate. However, this is a general problem caused by the nonorthogonality of the coherent

states, and we are avoiding it by choosing reasonably large α. Furthermore, our gate implements both the transformations (the normalized as well as the unnormalized one), switching between them just by a suitable choice of the quadrature value used at the HD for heralding of the gate.

[9] J. S. Neergaard-Nielsen *et al.*, Phys. Rev. Lett. **105**, 053602 (2010).

[10] J. Wenger, R. Tualle-Brouri, and P. Grangier, Phys. Rev. Lett. **92**, 153601 (2004).

[11] J. S. Neergaard-Nielsen, B. M. Nielsen, C. Hettich, K. Molmer, and E. S. Polzik, Phys. Rev. Lett. **97**, 083604 (2006).

[12] A. Ourjoumtsev *et al.*, Science **312**, 83 (2006).

[13] K. Wakui *et al.*, Opt. Express **15**, 3568 (2007).

[14] N. Namekata *et al.*, Nat. Photonics **4**, 655 (2010).

[15] T. Gerrits *et al.*, Phys. Rev. A **82**, 031802(R) (2010).

[16] S. A. Babichev, B. Brezger, and A. I. Lvovsky, Phys. Rev. Lett. **92**, 047903 (2004).

[17] A. Ourjoumtsev *et al.*, Nature (London) **448**, 784 (2007).

[18] Z. Hradil, Phys. Rev. A **55**, R1561 (1997); M. Ježek, J. Fiurasek, and Z. Hradil, *ibid.* **68**, 012305 (2003); A. I. Lvovsky, J. Opt. B: Quantum Semiclassical Opt. **6**, S556 (2004).

[19] D. Gottesman and I. L. Chuang, Nature (London) **402**, 390 (1999); L. Slodička, M. Jezek, and J. Fiurasek, Phys. Rev. A **79**, 050304(R) (2009).

[20] R. Blandino *et al.*, e-print arXiv:1105.5510.

Resources for universal quantum-state manipulation and engineering

Petr Marek and Jaromír Fiurášek

Department of Optics, Palacký University, 17. listopadu 50, 77200 Olomouc, Czech Republic

(Received 30 March 2009; published 23 June 2009)

We investigate which non-Gaussian resources are needed, in addition to Gaussian operations and measurements, for implementation of arbitrary quantum gates on multimode quantum states of light. We show that an arbitrary set of pure non-Gaussian states with finite expansion in Fock basis is sufficient for this task. As an illustration we present an explicit scheme for probabilistic implementation of the nonlinear sign gate using resource non-Gaussian states and Gaussian operations.

PACS number(s): 03.67.Lx, 42.50.Ex, 42.50.Dv

I. INTRODUCTION

The ability to perform an arbitrary operation on a quantum system is a crucial prerequisite for advanced quantum information processing and quantum computing [1]. In optical implementations, quantum states of light are manipulated mainly with passive and active linear optical elements such as beam splitters and squeezers. The resulting state transformations preserve the Gaussian form of the Wigner function and are thus referred to as Gaussian operations. It is readily apparent that such operations alone are not sufficient for universal continuous-variable (CV) quantum computation [2–4] and must be supplemented by access to some other resources such as nonlinear dynamics [2], single-photon detectors [5,6], or non-Gaussian states [7,8]. While several schemes for generation of highly nonclassical states of light and implementation of various non-Gaussian operations have been suggested [9–11], a systematic study of usefulness of non-Gaussian states for universal quantum state manipulation and engineering has been missing.

In the present paper we focus on implementation of quantum gates using off-line generated ancilla states and Gaussian measurements and operations [8,12,13]. The ancilla states represent the only non-Gaussian ingredient and can thus be seen as a resource that is converted into a non-Gaussian CV quantum gate. It is our aim to investigate what non-Gaussian ancilla states are sufficient for realization of arbitrary CV quantum gate within this approach. We shall prove that arbitrary pure single-mode non-Gaussian state $|\psi\rangle$ possessing finite expansion in Fock-state basis is sufficient for (probabilistic) implementation of any n-mode quantum gate on Hilbert-space $\mathcal{H}_N^{\otimes n}$, where $\mathcal{H}_N$ is spanned by the first $N+1$ Fock states and both N and n are finite but otherwise arbitrary. The formulation in terms of truncated finite-dimensional Hilbert spaces is necessary in order to ensure that a scheme with finite number of components can be constructed that (conditionally) implements the requested gate.

The core of our argument is the reduction of the problem to generation of single-photon Fock states $|1\rangle$ from the resource state $|\psi\rangle$. We provide explicit scheme for this latter task and assess its performance. For the sake of presentation clarity we explain the protocol on the example of traveling light modes, but the scheme is applicable also to other physical platforms such as atomic ensembles or optomechanical systems.

II. SUFFICIENCY OF SINGLE-PHOTON STATES

We start by demonstrating that only single-photon states, apart from Gaussian operations and measurements, are required for probabilistic implementation of arbitrary quantum operation on $\mathcal{H}_N^{\otimes n}$. A crucial observation is that the projection on a single-photon state can be performed with the help of an ancillary single-photon state, a balanced beam splitter, and a pair of homodyne detectors measuring amplitude quadrature x_1 and phase quadrature p_2, respectively, cf. Fig. 1(a). Successful projection is heralded by outcomes $x_1=0$ and $p_2=0$. In this case, the two input modes impinging on the balanced beam splitter are projected on the maximally entangled Einstein-Podolsky-Rosen (EPR) state $|\Psi_{\text{EPR}}\rangle=\Sigma_{n=0}^{\infty}|n,n\rangle$. This in conjunction with the ancillary single-photon state implements the probabilistic projection on a single-photon state, $_{12}\langle\Psi_{\text{EPR}}|1\rangle_1=_2\langle1|$. To achieve a nonzero success probability, a finite acceptance window for the measurement outcomes x_1 and p_2 has to be introduced, which reduces the fidelity of the projection and leads to a trade-off between operation quality and its success probability. This is an unavoidable feature of our protocol arising from involvement of only Gaussian measurements.

Single-photon states and single-photon measurements combined with Gaussian operations are sufficient for probabilistic preparation of arbitrary multimode quantum state
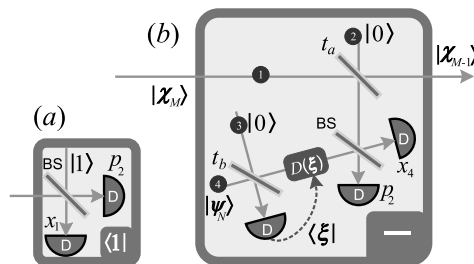

FIG. 1. (Color online) (a) Setup for projective measurement on a single-photon state. D—Homodyne detectors, BS—balanced beam splitter. (b) Setup for approximate photon subtraction. D—homodyne detector, BS—balanced beam splitter, $t_{a,b}$—beam splitter with transmittance $t_{a,b}$, $D(\xi)$—displacement driven by detected value ξ.

[10] and implementation of arbitrary transformation on $\mathcal{H}_N^{\otimes n}$, e.g., by exploiting the scheme described in Ref. [9] or simply by quantum teleportation [14]. The whole question about the nature of non-Gaussian resources sufficient for universal quantum state manipulation is thereby reduced to finding a class of states from which a single-photon state can be generated with the help of only Gaussian operations and measurements. We are going to show that any collection of non-Gaussian pure states possessing finite expansion in the Fock-state basis is sufficient for this.

III. GENERALIZED PHOTON SUBTRACTION

Let us consider a steady supply of states of the form

$$|\psi_N\rangle = \sum_{k=0}^{N} c_k |k\rangle. \tag{1}$$

An essential ingredient of our protocol is the setup depicted in Fig. 1(b) which employs one auxiliary state $|\psi_N\rangle$ and Gaussian operations to remove the highest Fock-state $|M\rangle$ from the input state $|\chi_M\rangle = \sum_{m=0}^{M} b_m |m\rangle$. This produces a state $|\chi_{M-1}\rangle = \sum_{m=0}^{M-1} b_m' |m\rangle$ and this operation can be thus seen as a version of approximative photon subtraction.

First part of the process lies in a deterministic transformation of $|\psi_N\rangle$ into a state

$$|\phi_{\bar{0}}\rangle = \sum_{k=1}^{\infty} d_k |k\rangle, \quad \sum_{k=1}^{\infty} |d_k|^2 = 1, \tag{2}$$

with $d_1 \neq 0$ and missing vacuum term, $d_0 = 0$. This can be achieved by coherent displacement of the state $|\psi_N\rangle$ if the displacement amplitude α satisfies

$$\langle 0|D(\alpha)|\psi_N\rangle = e^{-|\alpha|^2/2} \sum_{k=0}^{N} c_k \frac{(-\alpha^*)^k}{\sqrt{k!}} = 0. \tag{3}$$

Such α exists for all finite N. However, for a particular set of scenarios, e.g., when $|\psi_N\rangle = |N\rangle$, this approach does not work as the required displacement is $\alpha = 0$ corresponding to no action at all and the scheme in Fig. 1(b) would produce vacuum state from input $|\psi_N\rangle$. This problem can be fortunately circumvented using an ancillary vacuum mode, a beam splitter, a single homodyne detection, and feed-forward [see Fig. 1(b)]. After passing through the beam splitter with transmittance t_b, the homodyne detection of the amplitude quadrature $\hat{x}_3$ yielding a value x, and the displacement α, the state $|N\rangle$ transforms into

$$|\phi\rangle = D(\alpha) \sum_{k=0}^{N} \sqrt{\binom{N}{k}} t_b^k r_b^{N-k} \langle x|N-k\rangle |k\rangle, \tag{4}$$

where $r_j = \sqrt{1-t_j^2}$ for any j. By employing the relation for an overlap of a quadrature eigenstate and a Fock-state

$$\langle x|n\rangle = \frac{H_n(x)}{\pi^{1/4}\sqrt{n!\,2^n}} e^{-x^2/2}, \tag{5}$$

where $H_n(x)$ stands for the Hermite polynomial, we can see that to arrive at form (2) with $d_0 = 0$ and $d_1 \neq 0$ for an arbi-
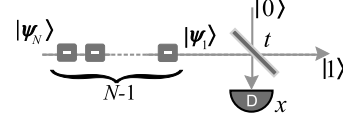

FIG. 2. (Color online) Complete setup for generation of a single-photon state.

trary measured value x, the real displacement α must satisfy

$$H_N(\tilde{x}) = 0, \quad N t_a \sqrt{2} H_{N-1}(\tilde{x}) \neq \alpha r_a H_N(\tilde{x}), \tag{6}$$

where $\tilde{x} = x - \alpha t_a/(\sqrt{2}r_a)$. The first condition can be for all values of x fulfilled by a suitable choice of α, while the second condition is in these cases satisfied automatically, as Hermite polynomials of unequal orders have different roots. To summarize, the universal setup for deterministic generation of state (2) from a completely arbitrary state $|\psi_N\rangle$ consists of a beam splitter, homodyne detection, and a suitable displacement operation, where the specific values of parameters have to be adjusted according to the state employed. Also note that the displacement operation could be replaced by a suitable postselection—allowing only states for which no displacement is necessary and discarding the rest. Thus, experimental feasibility can be gained at the cost of a reduced success rate.

To perform the approximate photon subtraction on the input state $|\chi_M\rangle$, this state in mode 1 is combined with vacuum in mode 2 on a beam splitter with transmittance t_a yielding a two-mode entangled state at the output. A balanced beam splitter and a pair of homodyne detectors are then used to project the mode 2 and the mode 4 prepared in auxiliary state $|\phi_{\bar{0}}\rangle$ onto the EPR state $|\Psi_{\text{EPR}}\rangle$, cf. Fig. 1(b). This conditionally prepares the remaining output mode 1 in the state $|\chi_{M-1}\rangle = \sum_{m=0}^{M-1} b_m' |m\rangle$, where

$$b_m' = \sum_{k=m+1}^{M} d_{k-m} b_k \sqrt{\binom{k}{m}} t_a^m r_a^{k-m}. \tag{7}$$

IV. PREPARATION OF SINGLE-PHOTON STATE

The complete scheme for preparation of single-photon state from N copies of state $|\psi_N\rangle$ is shown in Fig. 2. By repeated application of the approximate photon subtraction we can transform any state $|\psi_N\rangle$ to state

$$|\psi_1\rangle = a_0 |0\rangle + a_1 |1\rangle, \tag{8}$$

with $|a_1| > 0$. The parameters a_0 and a_1 can be made real by a suitable phase shift. This state is then combined with vacuum on a beam splitter with transmittance t, after which a homodyne detection of the amplitude quadrature x of one output mode is performed, projecting the state onto

$$|\psi_{\text{out}}\rangle \propto (a_0 + \sqrt{2}xr a_1)|0\rangle + t a_1 |1\rangle. \tag{9}$$

If we postselect the events when the measurement outcome is $x = -a_0/(\sqrt{2}r a_1)$, we remove the vacuum term by destructive quantum interference and obtain the desired single-photon state.
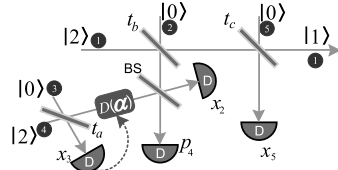
FIG. 3. (Color online) Complete setup for generation of a single-photon state from a pair of two-photon states. t_a, t_b, and t_c denote transmittances of the respective beam splitters, while BS stands for a balanced beam splitter. Numbers 1–5 are used to label the modes involved.

As a demonstration, let us now explicitly show the procedure to create a single-photon state from a pair of two-photon states $|2\rangle$. The full scheme is presented in Fig. 3. It can be easily shown that to generate the single-photon state the feed-forward displacement α should read

$$\alpha = \frac{r_a}{t_a}(x_3\sqrt{2} - 1), \tag{10}$$

where x_3 represents a value obtained by the homodyne measurement of the amplitude quadrature x_3 of mode 3. The other three homodyne detectors measure amplitude quadratures x_2 and x_5 of modes 2 and 5, respectively, and phase quadrature p_4 of mode 4. Successful preparation of state $|1\rangle$ is heralded by the measurement outcomes

$$x_2 = 0, \quad p_4 = 0, \quad x_5 = -r_b\frac{t_a^2 + 2(x_3\sqrt{2} - 1)r_a^2}{t_a r_a t_b r_c 2\sqrt{2}}. \tag{11}$$

In real experimental practice we cannot condition on the projection on a single quadrature eigenstate $|x = \xi\rangle$, as this corresponds to an event with zero probability of success. Instead, we have to accept all events when the measured value falls within a narrow interval centered at ξ, thus realizing a positive-operator-valued measure (POVM) element

$$\Pi_{k,x=\xi} = \int_{-X}^{X} |x = \xi + q\rangle_k \langle x = \xi + q| dq, \tag{12}$$

where the parameter X determines the half width of the postselection interval and k labels the mode that is measured. This of course effects the output state. The global input state encompassing five modes, as can be seen in Fig. 3, can be expressed as

$$|\psi_{\text{in}}\rangle = |2\rangle_1|0\rangle_2|0\rangle_3|2\rangle_4|0\rangle_5. \tag{13}$$

After interactions on all beam splitters and the feed-forward loop the output state for a single particular measured value x_3 reads

$$|\psi_{\text{out}}(x_3)\rangle = U_{c,15}U_{\text{BS},24}U_{b,12}D_4(\alpha)\langle x_3|_3 U_{a,34}|\psi_{\text{in}}\rangle. \tag{14}$$

Here, $U_{j,kl}$ represents a unitary transformation of a beam splitter $j = a, b, c$, BS coupling a pair of modes k and l. $D_4(\alpha)$ represents the displacement performed on mode 4 and α is given by Eq. (10). The final state is given by
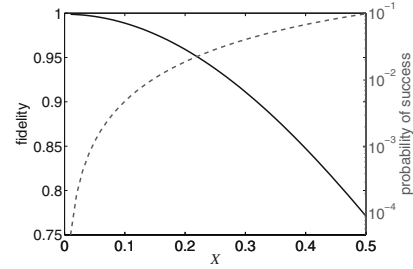

FIG. 4. (Color online) Fidelity (left, blue solid line) and probability of success (right, green dashed line) of the preparation of the single-photon state from a pair of two-photon states with respect to the postselection threshold X.

$$\rho_1(x_3) = \frac{\text{Tr}_{2345}[\Pi_{2,x=0}\Pi_{4,p=0}\Pi_{5,x=x_5}|\psi_{\text{out}}\rangle\langle\psi_{\text{out}}|]}{P_S(x_3)},$$

where x_5 is given by Eq. (11) and we have avoided to explicitly mark the dependence of $|\psi_{\text{out}}\rangle$ on the value x_3 for the sake of brevity. Tr_{2345} stands for the partial trace over all modes other than mode 1 and $P_S(x_3)$ denotes the probability of success

$$P_S(x_3) = \text{Tr}[\Pi_{2,x=0}\Pi_{4,p=0}\Pi_{5,x=x_5}|\psi_{\text{out}}\rangle\langle\psi_{\text{out}}|]. \tag{15}$$

This, however, still corresponds only to the scenario when a particular value x_3 was detected. To obtain the final result, we need to average state (15) over all possible experimental outcomes, arriving at

$$\rho_1 = \frac{1}{P_S}\int_{-\infty}^{\infty} P_S(x_3)\rho_1(x_3)dx_3, \tag{16}$$

with a probability of success $P_S = \int_{-\infty}^{\infty}P_S(x_3)dx_3$.

Figure 4 shows the performance of the procedure with respect to homodyne detection with nonzero threshold X. As the measure of quality we employ the fidelity, $F = \langle 1|\rho_1|1\rangle$, which in this case reliably quantifies the content of the single-photon state in the overall mixture. The transmittances of the beam splitters were optimized as to maximize the probability of success P_S in the limit of very narrow acceptance windows ($X \to 0$): $t_a = 0.62$, $t_b = 0.79$, and $t_c = 0.90$. The trade-off between fidelity and the success probability is clearly visible in Fig. 4.

V. EXAMPLE: NONLINEAR SIGN GATE

Finally we are going to present a full implementation of a non-Gaussian operation using only Gaussian operations and measurements and ancillary states $|\psi_N\rangle$. The resource states are again going to be the two-photon states $|2\rangle$ from which the single-photon states are extracted by means of procedure depicted in Fig. 3. The non-Gaussian operation under consideration is the nonlinear sign gate [5] which transforms a generic state $|\psi_{\text{in}}\rangle = c_0|0\rangle + c_1|1\rangle + c_2|2\rangle$ into $|\psi_{\text{out}}\rangle = c_0|0\rangle + c_1|1\rangle - c_2|2\rangle$. This represents a unitary evolution induced by
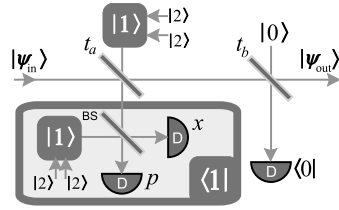
FIG. 5. (Color online) Complete setup for implementation of the nonlinear sign gate using only Gaussian operations and two-photon states as a resource. t_a and t_b transmittances of the respective beam splitters, while BS stands for a balanced beam splitter.

a Kerr-type Hamiltonian $\hat{H} = \frac{\pi}{2}\hat{n}(\hat{n}-1)$ on a three-dimensional Hilbert space spanned by $|0\rangle, |1\rangle, |2\rangle$.

A celebrated result in linear-optics quantum computing is that this gate can be implemented with help of only beam splitters, one ancillary single-photon state, and two measurements, one projecting on a single-photon state, the other on the vacuum state [15] (see Fig. 5). The single-photon state projection can be performed with help of a scheme in Fig. 1(a) while the projection on the vacuum state is a Gaussian operation. The transmittances of the beam splitter must satisfy $t_a^2 = (3-\sqrt{2})/7 \approx 0.23$ and $t_b = t_a/(1-2t_a^2) \approx 0.87$ [15].

The performance of the gate can be evaluated by using the quantum process fidelity. Consider a maximally entangled state on the Hilbert-space $\mathcal{H}_{N=2}^{\otimes 2}$, $|\Phi_{012}\rangle = (|00\rangle + |11\rangle + |22\rangle)/\sqrt{3}$. Applying the nonlinear sign gate on one of the modes transforms the state into $|\Phi'_{012}\rangle = (|00\rangle + |11\rangle - |22\rangle)/\sqrt{3}$. With the help of this state the gate could be applied by means of teleportation to an arbitrary unknown state [14]. In this sense, the measure of quality of the state $|\Phi'_{012}\rangle$ can serve as a tool to evaluate the quality of operation.

Using similar calculations as before, we can determine the mixed two-mode state ρ_{012} produced by the scheme and the success probability of the scheme for finite acceptance windows on homodyne detections. The fidelity of the operation can now be expressed as $F = \langle \Phi'_{012} | \rho_{012} | \Phi'_{012} \rangle$. Figure 6 shows the resulting relations between the fidelity, the postselection threshold X, and the probability of success.
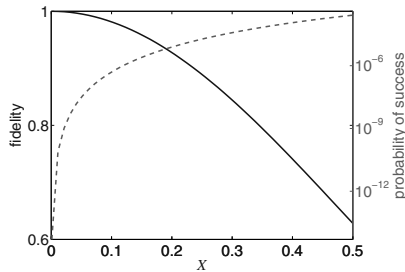

FIG. 6. (Color online) Fidelity (left, blue solid line) and probability of success (right, green dashed line) for implementation of the nonlinear sign gate with respect to the postselection threshold X.

VI. CONCLUSIONS

In summary, we have demonstrated that a steady supply of pure non-Gaussian states possessing finite expansion in the Fock-state basis, together with the experimentally readily accessible Gaussian operations and Gaussian measurements, is sufficient for universal quantum state manipulation and engineering. The required ancilla non-Gaussian states could be generated, e.g., using squeezing operations, coherent displacements, and conditional single-photon subtraction [11]. The conditional photon subtraction can be performed reliably with avalanche photo-diode detectors even though their overall detection efficiency is on the order of 50% or even lower [16]. The low efficiency only reduces the success probability of the state-preparation scheme but not the fidelity of the prepared state [11]. In contrast, such detectors are unsuitable for direct implementation of measurement-induced non-Gaussian operations using the schemes proposed in Refs. [9,10] because the low efficiency would imply reduced fidelity of the gate. In our approach we thus replace direct single-photon detection by an indirect detection relying on off-line-produced non-Gaussian states and homodyne detection. In this way it is possible to achieve high fidelity at the expense of the probabilistic nature of the scheme. Our generic scheme involves several optimization possibilities and its efficiency can be improved by tuning the transmittances of beam splitters and the widths of the acceptance windows of homodyne measurements. Moreover, it is likely that for each particular task the efficiency can be improved significantly by using a specific dedicated scheme tailored to a given resource state $|\psi_N\rangle$.

Besides states with finite Fock-state expansion also other classes of states could be sufficient for universal CV quantum gate engineering. However, dealing with completely generic states in infinite-dimensional Hilbert space of the quantized electromagnetic field is extremely difficult due to the *a priori* infinite number of parameters. It is unlikely that the question of sufficiency of a given state for universal CV quantum gate engineering could be decided in a completely general way. Instead, partial *ad hoc* solutions could be provided for certain finite-parametric classes of states (e.g., the cubic phase state proposed in Ref. [7]). Identifying such potentially useful classes of states is an interesting open problem which, however, is beyond the scope of our present work.

Our findings shall find applications in advanced optical quantum information processing and quantum state engineering. On more fundamental side, our results shed more light on the quantum information processing power of non-Gaussian states and they help to bridge the gap between single-photon and continuous-variable approaches.

[1] S. L. Braunstein and P. van Loock, Rev. Mod. Phys. **77**, 513 (2005).

[2] S. Lloyd and S. L. Braunstein, Phys. Rev. Lett. **82**, 1784 (1999).

[3] S. D. Bartlett, B. C. Sanders, S. L. Braunstein, and K. Nemoto, Phys. Rev. Lett. **88**, 097904 (2002).

[4] S. D. Bartlett and B. C. Sanders, Phys. Rev. Lett. **89**, 207903 (2002).

[5] E. Knill, R. Laflamme, and G. J. Milburn, Nature (London) **409**, 46 (2001).

[6] M. Gu, C. Weedbrook, N. Menicucci, T. Ralph, and P. van Loock, e-print arXiv:0903.3233.

[7] D. Gottesman, A. Kitaev, and J. Preskill, Phys. Rev. A **64**, 012310 (2001).

[8] S. D. Bartlett and W. J. Munro, Phys. Rev. Lett. **90**, 117901 (2003).

[9] J. Clausen, L. Knöll, and D.-G. Welsch, Phys. Rev. A **68**, 043822 (2003).

[10] J. Fiurášek, S. Massar, and N. J. Cerf, Phys. Rev. A **68**, 042325 (2003).

[11] J. Fiurášek, R. Garcia-Patrón, and N. J. Cerf, Phys. Rev. A **72**, 033822 (2005).

[12] R. Filip, P. Marek, and U. L. Andersen, Phys. Rev. A **71**, 042308 (2005).

[13] J. I. Yoshikawa, Y. Miwa, A. Huck, U. L. Andersen, P. van Loock, and A. Furusawa, Phys. Rev. Lett. **101**, 250501 (2008).

[14] D. Gottesman and I. L. Chuang, Nature (London) **402**, 390 (1999).

[15] T. C. Ralph, A. G. White, W. J. Munro, and G. J. Milburn, Phys. Rev. A **65**, 012314 (2001).

[16] A. Ourjoumtsev, R. Tualle-Brouri, J. Laurat, and P. Grangier, Science **312**, 83 (2006).

Nonlinear potential of a quantum oscillator induced by single photons

Kimin Park,* Petr Marek, and Radim Filip

Department of Optics, Palacký University, 17. listopadu 1192/12, 77146 Olomouc, Czech Republic

Experimental investigation of the nonlinear dynamics of a quantum oscillator is a long-standing goal of quantum physics. We propose a conditional method for inducing an arbitrary nonlinear potential on a quantum oscillator weakly interacting with light. Such an arbitrary nonlinear potential can be implemented by sequential repetition of an elementary conditional X gate. To implement the X gate, a single photon is linearly coupled to the oscillator and is subsequently detected by optical homodyne detection.

I. INTRODUCTION

In quantum physics it is crucial to be able to precisely manipulate quantum systems. This ability is the key both to experimental tests of fundamental natural principles and to the actual development of quantum technology. The ultimate aim in this direction is the implementation of a variety of nonlinear transformations. One way of approaching this daunting task lies in disassembling general operations into elementary building blocks. For two-level (qubit) quantum systems, such building blocks are the single-qubit rotations and the two-qubit controlled NOT operation [1]. In a similar vein, the basic building blocks for continuous-variable harmonic oscillator systems [2,3] are the operations imposing quadratic and cubic potentials [4,5]. The quadratic potential inducing Gaussian operations can be considered readily available. A general method of achieving any form of quadratic potential uses squeezed states of light which interact with the oscillator and are subsequently measured by an optical homodyne detection [6–9].

However, squeezed states of light and optical homodyne detections are not sufficient resources to induce highly nonlinear potentials, such as the cubic one. Since fully deterministic implementation of cubic nonlinearity is a very challenging task [10], it is important to be able to induce a nonlinear potential on a quantum oscillator at least conditionally, as it is currently the only feasible way for studying the nonlinear quantum dynamics. A straightforward, but complicated, way is to use the typical decomposition of quantum operations relying on annihilation $\hat{a}$ and creation $a^\dagger$ operators [11–16]. These operators with clear Fock-state interpretation play an important role in phase-insensitive applications [17], such as entanglement distillation [18,19] or a version of the noiseless amplification [20–22].

In this article we present a complementary approach which allows inducing an arbitrary nonlinear potential $V(\hat{X})$ on a quantum oscillator by sequential application of the position operator $\hat{X} = (\hat{a} + \hat{a}^\dagger)/\sqrt{2}$, which was also denoted as the orthogonalizer [23], by an operation which we will call the X gate. An optical scheme to achieve an operation $m^*\hat{a} + n^*\hat{a}^\dagger$ was also proposed in [24] using a standard approach with nonlinear resources, while our scheme is more compact and suitable for sequential application. The main benefit of using

X gate instead of the annihilation or creation operators is that the former can be naturally extended to physical systems other than light, such as mechanical oscillators or clouds of atoms, and that the exact form of the potential can be adjusted at will. As the resource for the X gate we are going to use single-photon guns [25–32], which were recently extensively developed for a broad class of applications. We analyze the performance and feasibility of this methodology with regard to realistic experimental tools and emphasize two exemplary applications: generation of the cubic nonlinearity and efficient state preparation of non-Gaussian states.

In Sec. II, we analyze how to implement the X gate in various ways. We investigate the performance of our gate in realistic situations in Sec. III. Applications of our gates are summarized in Sec. IV. In Sec. V we conclude.

II. IMPLEMENTATION OF X GATE

A. Oscillator in a nonlinear potential

The quantum oscillator with a Hamiltonian operator $\hat{H} = \hbar\omega(\hat{a}^\dagger\hat{a} + \frac{1}{2}) + V(\hat{X})$, where $\hat{X}$ is the position operator and $V(\hat{X})$ is a nonlinear potential, contains a mixture of free linear evolution with frequency ω and nonlinear dynamics induced by $V(\hat{X})$. To obtain the pure effect of a nonlinear potential on a quantum system, we assume the limit $\omega \to 0$ of a low-frequency oscillator evolving very slowly. In this limit, the unitary evolution operator $U(\hat{X},\tau) = e^{-\frac{i}{\hbar}V(\hat{X})\tau}$, where τ is the time duration of evolution in the potential, preserves the statistics of position and affects only the statistics of the complementary variable described by the momentum operator $\hat{P} = (\hat{a} - \hat{a}^\dagger)/\sqrt{2}i$.

The evolution operator can be approximated by a Taylor series $U(\hat{X},\tau) = \sum_{k=0}^{\infty} \frac{U^{(k)}(\bar{X})}{k!}(\hat{X} - \bar{X})^k$ around the initial mean position $\bar{X}$ of the oscillator. The finite truncation of this Taylor series can be expanded as $U(\hat{X},\tau) = \prod_{k=0}^{N}(1 + \lambda_k\hat{X})$ using the general theorem of algebra, where λ_k are related to the complex roots of the polynomial, $U(-\lambda_k^{-1},\tau) = 0$. Any dynamics imposed purely by the nonlinear potential can therefore be decomposed to a sequence of the *nonunitary X gates* $\hat{A}_X(\lambda_k) = 1 + \lambda_k\hat{X}$ controlled by *complex* parameters λ_k. For a purely imaginary λ_k with the magnitude close to zero, the operation $\hat{A}_X(\lambda_k)$ is close to a unitary displacement operator. For a larger magnitude of purely imaginary or real λ_k, however, the X gate is inherently probabilistic, and its action is nontrivial. Our approach suggests how to implement

---

*park@optics.upol.cz

the individual X gates which are applied sequentially with variable complex parameters λ_k to mimic the behavior of slowly evolving quantum oscillators in the nonlinear potential.

B. Coupling an oscillator to light

Implementation of an individual X gate exploits one of two kinds of coupling between a quantum oscillator and a single mode of electromagnetic radiation. Under the approximation of weak coupling for which the time duration is short enough, the interaction can be represented by a unitary operator derived from one of two possible interaction Hamiltonians. The beam splitter (BS) interaction with $\hat{H}_{\mathrm{BS}} = i\kappa_{\mathrm{BS}}(\hat{a}^{\dagger}\hat{b}_L - \hat{b}_L^{\dagger}\hat{a})$, where $\hat{a}$ is the annihilation operator of the quantum oscillator and $\hat{b}_L$ is the annihilation operator of the single mode L of radiation, represents a natural coupling between different modes of radiation varying in polarization, spatial properties, or frequency [33]. It can also be used to describe coupling with a continuous-wave or semicontinuous-wave regime of a mechanical oscillator [34,35]. The second kind of coupling is the quantum nondemolition (QND) coupling given by $\hat{H}_{\mathrm{QND}} = i\kappa_{\mathrm{QND}}(\hat{a}^{\dagger} + \hat{a})(\hat{b}_L^{\dagger} - \hat{b}_L)/2$. This type of interaction naturally appears for the coupling with spin ensembles [36,37] and the pulsed regime of mechanical oscillators [23,38,39].

C. Elementary X gate based on BS coupling

We shall start by explaining the implementation of the X gate for the BS coupling because it plays a prominent role in all-optical implementations, which are in turn a natural platform for experimental tests of the method. For reasons which will become clear later, we generalize the X gate $\hat{A}_X(\lambda) = 1 + \lambda \hat{X}_\theta$ to a more general class of operations:

$$\hat{A}(\lambda_-, \lambda_+) = 1 + \lambda_-\hat{a} + \lambda_+\hat{a}^{\dagger}, \qquad (1)$$

where $\hat{a}$ and $\hat{a}^{\dagger}$ are the annihilation and creation operators, respectively. Here λ_+ and λ_- are complex numbers which can be adjusted at will. The conceptual scheme for implementing the ideal operation (1) is depicted in Fig. 1. This scheme is a measurement-induced operation which is composed of the main implementation step and the correction step. In the first step, the input oscillator mode interacts with the ancillary mode L in the single-photon state $|1\rangle_L$. The ancillary mode L is subsequently measured by a setup which contains beam splitters and homodyne detectors, and the state of the oscillator mode is postselected when specific values are detected. This process can be expressed as the projection onto a Gaussian state $|\zeta\rangle$, which is represented by an operator $_L\langle\zeta|U_{\mathrm{BS}}|1\rangle_L$. Here $\hat{U}_{\mathrm{BS}} = \exp(-i\hat{H}_{\mathrm{BS}}t) = T^{\hat{n}}e^{-R^*\hat{b}_L^{\dagger}\hat{a}}e^{R\hat{b}_L\hat{a}^{\dagger}}T^{-\hat{n}_L}$ stands for the unitary operator of the beam splitter with transmission coefficient $T = \cos\kappa_{\mathrm{BS}}t$, which couples the ancillary mode to the oscillator. Here $\hat{n} = \hat{a}^{\dagger}\hat{a}$ and $\hat{n}_L = \hat{b}_L^{\dagger}\hat{b}_L$.

The projection $|\zeta\rangle_L\langle\zeta|$ can be implemented by an unbalanced heterodyne detection: the ancillary mode L is split at an unbalanced beam splitter with transmission and reflection coefficients $\mathcal{T}$ and $\mathcal{R}$, and optical homodyne detections of complementary quadratures $\hat{X}_L = (\hat{b}_L + \hat{b}_L^{\dagger})/\sqrt{2}$ and $\hat{P}_L = (\hat{b}_L - \hat{b}_L^{\dagger})/\sqrt{2}i$ are performed on each output port. Such a
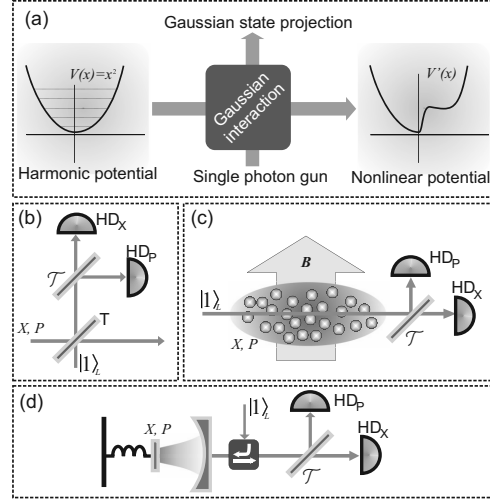

FIG. 1. (Color online) (a) Concept of the implementation of a nonlinear potential by single-photon guns, (b) X gate for a single mode of light using BS-type coupling, (c) X gate for a collective spin of cloud of atoms in magnetic field, and (d) X gate for the vibration mode of a mechanical oscillator.

measurement can be represented by the projection onto a state:

$$
\begin{aligned}
&_L\langle x|_{L'}\langle p|U_{\mathrm{BS}}|0\rangle_L' \\
&= {}_L\langle 0|\exp\left[-\frac{x^2 + p^2}{2} + \sqrt{2}(x\mathcal{T} + ip\mathcal{R}^*)b_L\right. \\
&\qquad\left. + \frac{\mathcal{R}^{*2} - \mathcal{T}^2}{2}b_L^2\right] \\
&\propto {}_L\langle 0|\exp\left[A^*b_L + B^*b_L^2\right] \equiv {}_L\langle A, B|, \qquad (2)
\end{aligned}
$$

where $A = \sqrt{2}(x\mathcal{T} - ip\mathcal{R})$ and $B = 2^{-1}(\mathcal{R}^2 - \mathcal{T}^2)$ are complex measurement parameters with $-1/2 < |B| < 1/2$, whose phases $\arg A$ and $\arg B$ can be chosen arbitrarily.

The full operation by the homodyne detection looks like

$$
\begin{aligned}
_L\langle x_\theta|U_{\mathrm{BS}}|1\rangle_L &\propto T^{\hat{n}}\exp\left[-\sqrt{2}x_\theta e^{-i\theta}R^*\hat{a} - \frac{R^{*2}e^{-2i\theta}\hat{a}^2}{2}\right] \\
&\quad \times\left(\frac{\sqrt{2}}{T}x_\theta + \frac{R^*e^{-i\theta}}{T}\hat{a} + \frac{Re^{i\theta}}{T}\hat{a}^{\dagger}\right), \qquad (3)
\end{aligned}
$$

and the complete operation by the heterodyne measurement is summarized as

$$
\begin{aligned}
_L\langle A, B|U_{\mathrm{BS}}|1\rangle_L &= \exp\left[A^*\frac{R}{T}\hat{a} + B^*\frac{R^2}{T^2}\hat{a}^2\right] \\
&\quad \times T^{\hat{n}-1}(A^* + 2B^*R^*\hat{a} + R\hat{a}^{\dagger}). \qquad (4)
\end{aligned}
$$

The operator (4) is composed of three parts: the ideal operation $A^* + 2B^*R^*\hat{a} + R\hat{a}^{\dagger}$ consisting of the proper

superposition of annihilation and creation operators, the error operator $\exp[A^*R\hat{a} + B^*R^2\hat{a}^2]$, and another error operator $T^{\hat{n}-1}$, which we will denote as pure attenuation. These two sources of error need to be considered separately, as each of them possesses very different properties. The error term $\exp[A^*R\hat{a} + B^*R^2\hat{a}^2]$ can be compensated by a correction operation using optical ancilla L' in the vacuum state:

$$_{L'}\left\langle A',B'\right|U_{\rm BS}|0\rangle_{L'} = T'^{\hat{n}}\exp[A'^*R'\hat{a} + B'^*R'^2\hat{a}^2], \quad (5)$$

which is implemented in the same way as the main gate in Eq. (4), only with a replacement of a single photon by the vacuum state in the ancillary mode. With $A' = -A/T$, $B' = -B/T^2$, and $R' = R$ we can erase the error and obtain an approximate version,

$$\hat{A}_{\rm BS} = (T'T)^{\hat{n}}(A^* + 2B^*R^*\hat{a} + R\hat{a}^\dagger), \quad (6)$$

of the generalized X gate (1) using the BS coupling. The desired gate is accompanied by an increased noiseless attenuation $(T'T)^{\hat{n}}$ as an unavoidable cost of transforming an ill-behaved error into a well-behaved one. It should be noted that in the case of a highly transmissive beam splitter $R \ll 1$, all sorts of errors become less prominent even up to the point when the correction step is not necessary. The cost of this strategy is the diminished success rate and a high sensitivity to the quality of ancilla.

The noiseless attenuation error caused by $(T'T)^{\hat{n}}$ becomes significant when the elementary X gates are combined into a more complicated function. For this purpose we have to apply the relations $T^{\hat{n}}\hat{a} = \hat{a}T^{\hat{n}-1}$ and $T^{\hat{n}}\hat{a}^\dagger = \hat{a}^\dagger T^{\hat{n}+1}$ to move the attenuation term. As a consequence, an arbitrary polynomial $\prod_{i=0}^{N}(1 + \lambda_i\hat{X})$ needs to be implemented as

$$\prod_i T_i^{\hat{n}}\left(1 + \lambda_i\frac{\mathbb{T}_i\hat{a} + \mathbb{T}_i^{-1}\hat{a}^\dagger}{\sqrt{2}}\right) = \left[\prod_i^N(1 + \lambda_i\hat{X})\right]\mathbb{T}_N^{\hat{n}}, \quad (7)$$

where $\mathbb{T}_i = \prod_{j=1}^{i}T_j$. As can be seen, the noiseless attenuation is effectively applied only once, solely on the initial state. In principle it can be approximatively compensated by the noiseless amplification conditionally approaching operation $G^{\hat{n}}$ with $G > 1$ [40]. On the other hand, the noiseless attenuation has a very clear Fock space interpretation, and it is always acting in a predictable manner. In many experiments it can therefore be taken into account and compensated by manipulating the measured data.

D. Elementary X gate based on QND coupling

Although the QND coupling can be established between different modes of radiation [6,8], it is much more important in experiments with atomic spin ensembles [36,37] or a pulsed regime of mechanical oscillators [23,38,39], where it appears naturally. Adapting the X gate for this coupling therefore allows expanding the methods of quantum optics even to these systems. For the QND coupling, represented by the unitary operator $\hat{U}_{\rm QND} = e^{-i\kappa\hat{X}\hat{P}_L}$, where $\hat{X} = (\hat{a} + \hat{a}^\dagger)/\sqrt{2}$ and $\hat{P}_L = (\hat{b}_L - \hat{b}_L^\dagger)/\sqrt{2}i$, of optical mode L to the oscillator

the complete gate can again be expressed as

$$_L\langle A,B|U_{\rm QND}|1\rangle_L \propto \exp\left[\frac{A\kappa}{\sqrt{2}}\hat{X} + \left(\frac{B}{2} - \frac{1}{4}\right)\kappa^2\hat{X}^2\right]$$
$$\times \left\{A + \kappa\left(2B - \frac{1}{\sqrt{2}}\right)\hat{X}\right\}, \quad (8)$$

where A and B are the same as before and $\kappa = \kappa_{\rm QND}t$. In a similar manner as for the BS interaction, the correction operation required to eliminate the error term $\exp[\frac{A\kappa}{\sqrt{2}}\hat{X} + (\frac{B}{2} - \frac{1}{4})\kappa^2\hat{X}^2]$ is $_L\langle -A, -B|\hat{U}_{QND}|0\rangle_L = \exp[-A\frac{\kappa}{\sqrt{2}}\hat{X} - (B/2 + 1/4)\kappa^2\hat{X}^2]$, which is implemented using another QND interaction with the optical mode being in vacuum state. The redundant $\exp[-\kappa^2\hat{X}^2/4]$ can be in part compensated by squeezing the ancillary state, whose effect can be described by $\exp[\tanh r\kappa^2\hat{X}^2/4]$. In contrast to the BS type of coupling to the optical mode, after erasing the error term, we approach the ideal X gate without the noiseless attenuation errors. Moreover, the X gate can also be implemented by replacing the homodyne detection by a photon-number-resolving detector and changing the ancilla. The resulting gate,

$$_L\langle 0|U_{\rm QND}(|0\rangle_L + c_1|1\rangle_L) = \exp\left[-\frac{\kappa^2\hat{X}^2}{4}\right]\left(1 + c_1\frac{\kappa}{\sqrt{2}}X_A\right)$$
$$(9)$$

always has a nonzero probability of success. This approach will become fully feasible with the advent of efficient photon-number-resolving detectors.

III. REALISTIC CONSIDERATIONS

A. Requirements on the quality of single photons

The single photons employed by the X gate are an experimental resource sensitive to imperfections. They usually do not appear in the pure form $|1\rangle_L$, but rather in a mixture $\eta|1\rangle_L\langle 1| + (1 - \eta)|0\rangle_L\langle 0|$ [41], which may reduce the quality of the gate. To quantify the quality of a single photon that is necessary for successful implementation of the X gate, we compare the performance of the gate with methods using coherent-state ancillae. The required quality of the single-photon gun is then characterized by the critical efficiency η_c, the value of η for which the fidelity of the gate is equal to the classical threshold.

B. Performance analysis and the classical threshold

For the analysis of performance, we apply the X gate to a set of quantum states and compare their fidelities. For this analysis it is advantageous to consider quantum states which are orthogonalized by the X operation because then the operation $1 + \lambda X$ effectively creates a qubit whose fidelity has a good operational meaning. The states which satisfy this criterion are the coherent states with purely imaginary amplitudes $|\beta\rangle$, with $\beta = i|\beta|$; single-photon state $|1\rangle$; and the squeezed state $|\xi\rangle = \exp[-\xi/2\hat{a}^{2\dagger} + \xi/2\hat{a}^2]|0\rangle$. For these states, the fidelities are compared to the classical benchmark which is obtained by considering the gate with only a classical state used as an ancilla. As any classical state can be represented as a mixture of coherent states, it is sufficient to consider a coherent state

as the ancilla and maximize over its amplitude. The operation with the classical resource can be written as

$$
\begin{aligned}
{}_2\langle x = 0|\hat{U}_{\mathrm{BS}}|\alpha\rangle_2 \\
\propto T^{\hat{n}} \exp[\alpha R T^{-1}\hat{a}^\dagger] \exp\left[-\frac{R^2}{2}\hat{a}^2\right] \exp[\alpha R T \hat{a}] \\
= \exp[\alpha R \hat{a}^\dagger] \exp[\alpha R \hat{a}] \exp\left[-\frac{R^2}{2T^2}\hat{a}^2\right] T^{\hat{n}}.
\end{aligned}
\tag{10}
$$

Note that it is simply impossible to obtain the desired X operation perfectly with a classical resource regardless of any correction we may apply.

Another benchmark is obtained by trying to achieve the target operation by using only unitary Gaussian operations: displacement and squeezing. These operations are experimentally feasible, but on their own they are not sufficient for obtaining any kind of higher-order nonlinearity. For the target single-photon input state, the Gaussian benchmark is 0.82, which leads to $\eta_c \approx 0.7$ for $T = 0.734$. For the other input states we are considering, these unitary Gaussian operations give a lower benchmark and do not need to be considered.

With a realistic resource single photon, the full gate (with the correction) transforms the input state $|\psi\rangle$ into

$$
\begin{aligned}
\rho \propto T^{\hat{n}}[\eta R^2/\lambda^2 T^2 (1 + \lambda \hat{a} \pm \lambda a^\dagger)|\psi\rangle\langle\psi|(1 + \lambda \hat{a}^\dagger \pm \lambda a) \\
+ (1 - \eta)|\psi\rangle\langle\psi|]T^{\hat{n}}.
\end{aligned}
\tag{11}
$$

We notice that for a very small $T \ll 1$, the effect of lower η in single-photon generation can be completely ignored, and a perfect target operation is achieved regardless of η, but only at the cost of a significant noiseless attenuation. This can be seen as a conditional transformation of the resource state's impurity to noiseless attenuation, which does not significantly reduce the purity of the state. This is a valuable strategy if the noiseless attenuation does not play an important role. However, if this is not the case or if the attenuation cannot be very well compensated by a suitable noiseless amplification, the efficiency η remains important.

In Fig. 2 we show the analysis of a trial gate operation $1 + \lambda\hat{a} - \lambda\hat{a}^\dagger$ applied to selected quantum states for various levels of quality of the single-photon ancilla, where their fidelities with the ideal states are compared to the classical threshold. When λ is as small as 0.1, the operation is generally well simulated by a displacement operator, and the classical threshold fidelity is typically as high as 0.99. For large $\lambda = 1.5$, on the other hand, $\eta_c \approx 0.55$ for a coherent state $|\beta = 0.1\rangle$, and $\eta_c \approx 0.35$ for a coherent state $|\beta = 1\rangle$. For a single-mode squeezed vacuum state input $|\xi\rangle = \hat{S}(\xi)|0\rangle$, $\eta_c \approx 0.7$ for $|\xi = 0.1\rangle$, and $\eta_c \approx 0.6$ for $|\xi = 1\rangle$. For single-photon input $|1\rangle$, for $T \approx 0.45$ we can achieve $\eta_c = 0.12$. Therefore, with the current quality of the single-photon gun our scheme can surpass classical resources rather easily. It is therefore feasible to experimentally observe the nonclassical performance of
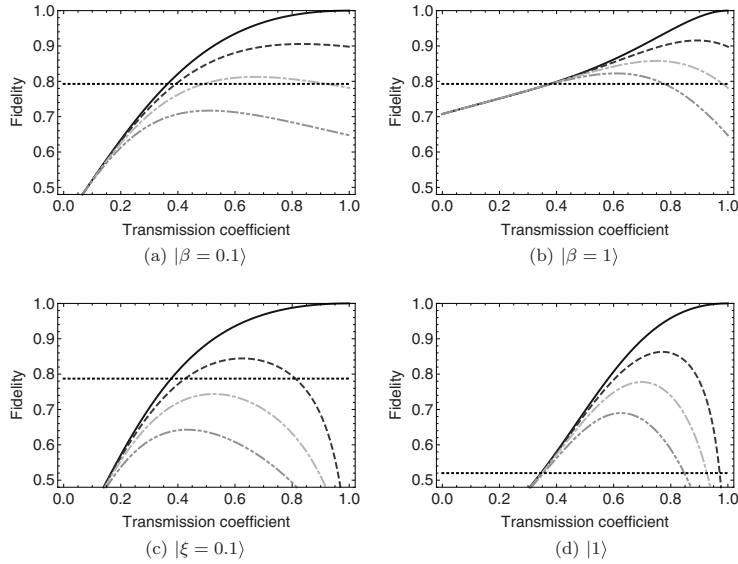

FIG. 2. (Color online) Fidelity vs transmission coefficient T for operation $1 + 1.5\hat{a} - 1.5\hat{a}^\dagger$ on coherent-state inputs (a) $|\beta = 0.1\rangle$ and (b) $|\beta = 1\rangle$, squeezed state inputs (c) $|\xi = 0.1\rangle$, and (d) single photon $|1\rangle$, with imperfect single-photon ancilla $\eta|1\rangle_L\langle 1| + (1 - \eta)|0\rangle_L\langle 0|$. Near $T \approx 1$, the fidelity is high for $\eta = 1$ (blue solid line) but drops rapidly when the ancilla is imperfect [$\eta = 0.8$ (red dashed line), 0.6 (green dot-dashed line) and 0.4 (orange double-dot-dashed line)] below the classical benchmark (black dotted line). The values for the classical benchmark are 0.79 for coherent states and squeezed states and 0.52 for the single-photon state.
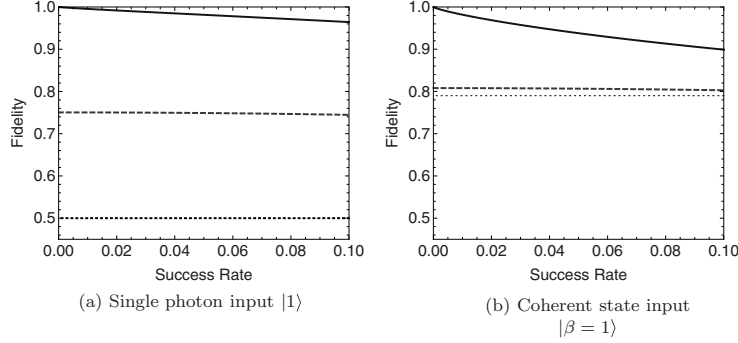
(a) Single photon input $|1\rangle$

(b) Coherent state input
$|\beta = 1\rangle$

FIG. 3. (Color online) $F(\epsilon)$ vs $P(\epsilon)$ for (a) single-photon input $|1\rangle$ and (b) coherent-state input $|\beta = 1\rangle$ for the operation $1 + 1.5\hat{a} - 1.5\hat{a}^\dagger$ with (blue solid line) a perfect single-photon ancilla and (red dashed line) an imperfect single photon with $\eta = 0.8$ for the homodyne measurement window $10^{-3} \leqslant \epsilon \leqslant 1$. The setup is optimized for the largest F. Here no correction is considered. $F = 0.95$ and $P = 0.10$ are achieved for a perfect single-photon input, and $F = 0.91$ and $P = 0.10$ are achieved for a coherent-state input.

the elementary X gate with limited $|\lambda|$. Note that the performance of the gate for large λ can be used as a very strict operational measure of single-photon states, as in this case even resource states with significant negativity in the Wigner function [41] might not be sufficient to beat the classical threshold.

C. Success rate vs fidelity

So far we have been concerned with ideal projections onto quadrature eigenstates. This is just an idealization, and in practice such a projection onto a quadrature eigenstates has a zero probability of success. In practice it needs to be approximated by performing a homodyne detection and postselecting upon detecting a value which falls closely into a small interval ϵ around the sharp target value x_0, which necessarily reduces the quality of the gate as a cost. The fidelity with the target state $|\psi_t\rangle$ of this realistic gate applied to state ρ_{IN} can be expressed as $F(\epsilon) = \int_{x_0-\epsilon}^{x_0+\epsilon} dx \mathrm{Tr}[(|\psi_t\rangle\langle\psi_t| \otimes |x\rangle_L \langle x|) U_{\mathrm{BS}} \rho_{\mathrm{IN}} \otimes |1\rangle_L \langle 1| U_{\mathrm{BS}}^\dagger]/P(\epsilon)$, where the probability of success is $P(\epsilon) = \int_{x_0-\epsilon}^{x_0+\epsilon} dx \mathrm{Tr}_L[_L\langle x| U_{\mathrm{BS}} \rho_{\mathrm{IN}} \otimes |1\rangle_L \langle 1| U_{\mathrm{BS}}^\dagger |x\rangle_L]$. In Fig. 3, the fidelity and the probability of success of the operation $1 + 1.5\hat{a} - 1.5\hat{a}^\dagger$ applied to a single photon and to a coherent state are plotted both for a perfect ancilla $\eta = 1$ and a realistic ancilla $\eta = 0.8$. We can see that although there is a visible drop of fidelity for a perfect single-photon ancilla when we increase ϵ, the fidelity still remains quite high and obviously above the classical threshold. Furthermore, the reduction of fidelity is less prominent for the imperfect ancilla, which is very promising for the eventual experimental implementation.

Our scheme can be compared to the previous one proposed in [24], which employs inline coupling into a parametric downconverter, interferometer, and two single-photon detectors. Apart from the feasibility, our scheme can exhibit success rates of around 0.05, while the previous proposal did not surpass 10^{-12}, mainly due to the low rate of the downconversion process.

IV. MULTIPLE GATES FOR APPLICATIONS

A. Conditional generation of cubic nonlinearity

As a prominent example, a non-Gaussian cubic Hamiltonian up to the quadratic expansion can be achieved as

$$\exp[i\chi\hat{X}^3] \approx 1 + i\chi\hat{X}^3 - \frac{\chi^2}{2}\hat{X}^6$$

$$\propto \left[1 - \left(\frac{\chi}{-1+i}\right)^{1/3}\hat{X}\right]\left[1 + \left(\frac{\chi}{1-i}\right)^{1/3}\hat{X}\right]$$

$$\times \left[1 - (-1)^{-2/3}\left(\frac{\chi}{-1+i}\right)^{1/3}\hat{X}\right]\left[1 - \left(\frac{\chi}{1+i}\right)^{1/3}\hat{X}\right]$$

$$\times \left[1 + \left(\frac{\chi}{-1-i}\right)^{1/3}\hat{X}\right]\left[1 - (-1)^{-2/3}\left(\frac{\chi}{1+i}\right)^{1/3}\hat{X}\right],$$

$$(12)$$

where χ is the nonlinearity strength and the attenuation is omitted for simplicity. This second-order expansion is sufficient to achieve the cubic nonlinearity for a general purpose [10]. Exploiting the emerging single-photon guns, it will be the first step towards controlled nonlinear dynamics of a quantum oscillator. The identification of hidden nonclassical features of quantum states produced by the cubic nonlinearity has been proposed [42].

B. Arbitrary wave-function generation

It is well known that any quantum state can be approximated with an arbitrarily high precision by a finite superposition of Fock states up to Nth order as $|\psi\rangle = \sum_{n=0}^{N} c_n \hat{a}^{\dagger n}/\sqrt{n!}|0\rangle$. We observe that this state can be constructed by a polynomial of $\hat{a}^\dagger$ applied to the vacuum state [12]. This operation is achieved by the repeated application of the elementary operation $1 + \lambda\hat{a}^\dagger$, which is a special case of Eq. (6) with $B = 0$. Complementary to this approach, we can also use the continuous-variable operators to build not the discrete Fock state expansion of the state but rather the continuous-variable wave function of
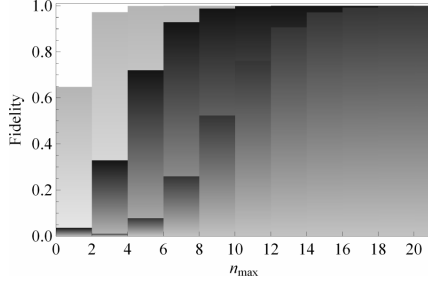
FIG. 4. (Color online) Fidelity of the ideal coherent-state superposition $N_c(|\beta\rangle + |-\beta\rangle)$ with the generated cat states. Depending on the highest photon number n_{max} which coincides the repetition number of the X gate, we can achieve the approximate cat state very efficiently. Green (light gray), blue (dark gray), and red (medium gray) bars correspond to $\beta = 1, 2, 3$, respectively.

the state. The wave function of the general state in the coordinate representation can be simply expressed as

$$\psi(x) = \langle x|\psi\rangle = \sum_{n=0}^{N} \frac{c_n H_n(x)}{\pi^{1/4}\sqrt{2^n n!}} e^{-x^2/2} \equiv G(x)\langle x|0\rangle, \quad (13)$$

where $G(x) = \sum_{n=0}^{N} \frac{c_n H_n(x)}{\sqrt{2^n n!}}$ and $H_n(x)$ are Hermitian polynomials. Therefore, we can write $|\psi\rangle = G(\hat{X})|0\rangle$. This is simply a wave function of the vacuum state multiplied by an Nth-order polynomial of x, which is exactly obtained by N-fold application of the X gates. The number of required operations can be reduced by attempting to generate a suitably squeezed version of the target state and then manipulating the Gaussian envelope by another squeezing operation [43]. Therefore, the X gate can be seen as a universal elementary gate sufficient for general state preparation, the continuous counterpart of the particle-like single-photon addition.

To demonstrate the state generation aspect of our scheme, let us attempt to generate an equal superposition of coherent states, $N_c(|\beta\rangle + |-\beta\rangle)$, where $N_c = (2 + 2e^{-2\beta^2})^{-1/2}$ is the normalization factor. This quantum state is an important resource in quantum information processing and fundamental tests of quantum mechanics [44–47] and has been realized experimentally for $\beta \lesssim 2$ [48–51]. It alternatively can be written as $N_c e^{-\beta^2/2}(\exp[\beta\hat{a}^\dagger] + \exp[-\beta\hat{a}^\dagger])|0\rangle = N_c'(n_{max}) \sum_{n=\text{even}}^{n_{max}} 2(\beta\hat{a}^\dagger)^n/n!|0\rangle$, where $N_c'(n_{max})$ is a normalization factor for a finite expansion up to the maximum photon number n_{max} in a truncated form. This state is generated

by the following polynomial of $\hat{a}^\dagger$ on the vacuum state: $\sum_{n=\text{even}}^{n_{max}} 2(\beta\hat{a}^\dagger)^n/n!$. The dependence of the fidelities on n_{max} with the exact even cat state is drawn in Fig. 4. We note that for $n_{max} = 16$, we can achieve the fidelity of 0.993 for $\beta = 3$. An odd cat state can be constructed in a completely equivalent way. We also note that no attenuation effect exists in the state generation due to the initial vacuum state the scheme acts on.

C. Multiple X gates in a single-shot operation

Implementing a potential $F(\hat{x})$ by the sequential application of X gates is accompanied by an exponential decrease of the probability of success. This issue can be overcome by applying the total potential consisting of several X gates directly in a single step. First, a specific ancillary state $f(\hat{X}_L)|0\rangle_L$, where $f(\hat{x}) = F(-\hat{x}/\kappa)$, can be generated off-line using X gates, as in [10]. After a QND coupling between the ancilla and the oscillator, the ancillary mode is measured by homodyne detection, and the target operation is achieved:

$$_L\langle x_0 = 0|U_{QND}f(\hat{X}_L)|0\rangle_L =_L \langle x_0 = 0|f(-\kappa\hat{X})U_{QND}|0\rangle$$
$$= f(-\kappa\hat{X})_L\langle x_0 = 0|U_{QND}|0\rangle = F(\hat{X})\exp\left[-\frac{1}{2}\kappa^2\hat{X}^2\right]. \quad (14)$$

The factor $\exp[-\kappa^2\hat{X}^2/2]$ can be compensated by a suitable squeezing of the ancilla as before. The same approach can be applied to the operations based on the beam splitter interaction. In this scheme the unavoidable attenuation is suppressed as a side benefit.

V. CONCLUSIONS

We have presented a methodology for the conditional induction of various nonlinear potentials in quantum oscillators and conditional preparation of wave functions of the quantum oscillators. This method is based on the sequential application of the elementary X gates supplied by the single-photon guns. Based on a wide class of emerging single-photon guns [25–32], it is broadly applicable for various quantum oscillators (optical, atomic, or mechanical). The presented operation will therefore open a broad area of very anticipated investigation of controllable nonlinear dynamics of quantum oscillators.

ACKNOWLEDGMENTS

[1] M. A. Nielsen and I. L. Chuang, *Quantum Computation and Quantum Information* (Cambridge University Press, Cambridge, 2000).

[2] N. J. Cerf, G. Leuchs, and E. S. Polzik, *Quantum Information with Continuous Variables of Atoms and Light* (Imperial College Press, London, 2007).

[3] A. Furusawa and P. van Loock, *Quantum Teleportation and Entanglement: A Hybrid Approach to Optical*

Quantum Information Processing (Wiley VCH, Berlin, 2011).

[4] D. Gottesman, A. Kitaev, and J. Preskill, Phys. Rev. A **64**, 012310 (2001).

[5] S. D. Bartlett and B. C. Sanders, Phys. Rev. A **65**, 042304 (2002).

[6] R. Filip, P. Marek, and U. L. Andersen, Phys. Rev. A **71**, 042308 (2005).

[7] J. I. Yoshikawa, T. Hayashi, T. Akiyama, N. Takei, A. Huck, U. L. Andersen, and A. Furusawa, Phys. Rev. A **76**, 060301(R) (2007).

[8] J. I. Yoshikawa, Y. Miwa, A. Huck, U. L. Andersen, P. van Loock, and A. Furusawa, Phys. Rev. Lett. **101**, 250501 (2008).

[9] J. I. Yoshikawa, Y. Miwa, R. Filip, and A. Furusawa, Phys. Rev. A **83**, 052307 (2011).

[10] P. Marek, R. Filip, and A. Furusawa, Phys. Rev. A **84**, 053802 (2011).

[11] M. Dakna, T. Anhut, T. Opatrný, L. Knoll, and D.-G. Welsch, Phys. Rev. A **55**, 3184 (1997).

[12] M. Dakna, L. Knoll, and D. G. Welsch, Opt. Commun. **145**, 309 (1998).

[13] M. Dakna, J. Clausen, L. Knöll, and D.-G. Welsch, Phys. Rev. A **59**, 1658 (1999).

[14] A. Ourjoumtsev, R. Tualle-Brouri, J. Laurat, and P. Grangier, Science **312**, 83 (2006).

[15] J. S. Neergaard-Nielsen, B. M. Nielsen, C. Hettich, K. Molmer, and E. S. Polzik, Phys. Rev. Lett. **97**, 083604 (2006).

[16] V. Parigi, A. Zavatta, M. Kim, and M. Bellini, Science **317**, 1890 (2007).

[17] J. Fiurášek, Phys. Rev. A **80**, 053822 (2009).

[18] T. Opatrny, G. Kurizki, and D.-G. Welsch, Phys. Rev. A **61**, 032302 (2000).

[19] H. Takahashi, J. S. Neergaard-Nielsen, M. Takeuchi, M. Takeoka, K. Hayasaka, A. Furusawa, and M. Sasaki, Nat. Photonics **4**, 178 (2010).

[20] P. Marek and R. Filip, Phys. Rev. A **81**, 022302 (2010).

[21] M. A. Usuga, Ch. R. Müller, Ch. Wittmann, P. Marek, R. Filip, Ch. Marquardt, G. Leuchs, and U. L. Andersen, Nat. Phys. **6**, 767 (2010).

[22] A. Zavatta, J. Fiurášek, and M. Bellini, Nat. Photonics **5**, 52 (2011).

[23] M. R. Vanner, M. Aspelmeyer, and M. S. Kim, Phys. Rev. Lett. **110**, 010504 (2013).

[24] S. Y. Lee and H. Nha, Phys. Rev. A **82**, 053812 (2010).

[25] A. Kuhn, M. Hennrich, and G. Rempe, Phys. Rev. Lett. **89**, 067901 (2002); see also H. J. Kimble, *ibid.* **90**, 249801 (2003); A. Kuhn, M. Hennrich, and G. Rempe, *ibid.* **90**, 249802 (2003).

[26] T. Legero, T. Wilk, M. Hennrich, G. Rempe, and A. Kuhn, Phys. Rev. Lett. **93**, 070503 (2004).

[27] S. Chen, Y.-A. Chen, T. Strassel, Z.-S. Yuan, B. Zhao, J. Schmiedmayer, and J.-W. Pan, Phys. Rev. Lett. **97**, 173004 (2006).

[28] M. Hijlkema, B. Weber, H. P. Specht, S. C. Webster, A. Kuhn, and G. Rempe, Nat. Phys. **3**, 253 (2007).

[29] D. Bozyigit, C. Lang, L. Steffen, J. M. Fink, M. Baur, R. Bianchetti, P. J. Leek, S. Filipp, M. P. da Silva, A. Blais, and A. Wallraff, Nat. Phys. **7**, 154 (2011).

[30] M. Förtsch, J. Fürst, Ch. Wittmann, D. Strekalov, A. Aiello, M. V. Chekhova, Ch. Silberhorn, G. Leuchs, and Ch. Marquardt, Nat. Commun. **4**, 1818 (2013).

[31] M. J. Collins, Ch. Xiong, I. H. Rey, T. D. Vo, J. He, S. Shahnia, Ch. Reardon, M. J. Steel, T. F. Krauss, A. S. Clark, and B. J. Eggleton, Nat. Commun. **4**, 2582 (2013).

[32] Y.-M. He, Y. He, Y.-J. Wei, D. Wu, M. Atatre, Ch. Schneider, S. Hfling, M. Kamp, C.-Y. Lu, and J.-W. Pan, Nat. Nanotechnol. **8**, 213 (2013).

[33] S. Zaske, A. Lenhard, Ch. A. Kessler, J. Kettler, Ch. Hepp, C. Arend, R. Albrecht, W.-M. Schulz, M. Jetter, P. Michler, and Ch. Becher, Phys. Rev. Lett. **109**, 147404 (2012).

[34] S. G. Hofer, W. Wieczorek, M. Aspelmeyer, and K. Hammerer, Phys. Rev. A **84**, 052327 (2011).

[35] E. Verhagen, S. Delglise, S. Weis, A. Schliesser, and T. J. Kippenberg, Nature (London) **482**, 63 (2012).

[36] K. Hammerer, A. S. Sorensen, and E. S. Polzik, Rev. Mod. Phys. **82**, 1041 (2010).

[37] R. J. Sewell, M. Napolitano, N. Behbood, G. Colangelo, and M. W. Mitchell, Nat. Photonics **7**, 517 (2013).

[38] M. R. Vanner, I. Pikovski, G. D. Cole, M. S. Kim, C. Brukner, K. Hammerer, G. J. Milburn, and M. Aspelmeyer, Proc. Natl. Acad. Sci. USA **108**, 16182 (2011).

[39] M. R. Vanner, J. Hofer, G. D. Cole, and M. Aspelmeyer, Nat. Commun. **4**, 2295 (2013).

[40] T. C. Ralph and A. B. Lund, in *Quantum Communication Measurement and Computing: Proceedings of the 9th International Conference*, edited by A. Lvovsky (AIP, New York, 2009), pp. 155–160.

[41] A. I. Lvovsky, H. Hansen, T. Aichele, O. Benson, J. Mlynek, and S. Schiller, Phys. Rev. Lett. **87**, 050402 (2001).

[42] M. Yukawa, K. Miyata, H. Yonezawa, P. Marek, R. Filip, and A. Furusawa, Phys. Rev. A **88**, 053816 (2013).

[43] D. Menzies and R. Filip, Phys. Rev. A **79**, 012313 (2009).

[44] P. T. Cochrane, G. J. Milburn, and W. J. Munro, Phys. Rev. A **59**, 2631 (1999).

[45] H. Jeong and M. S. Kim, Phys. Rev. A **65**, 042305 (2002).

[46] T. C. Ralph, A. Gilchrist, G. J. Milburn, W. J. Munro, and S. Glancy, Phys. Rev. A **68**, 042319 (2003).

[47] C. C. Gerry and R. Grobe, Phys. Rev. A **51**, 1698 (1995).

[48] B. Yurke and D. Stoler, Phys. Rev. Lett. **57**, 13 (1986).

[49] A. Ourjoumtsev, F. Ferreyrol, R. Tualle-Brouri, and Ph. Grangier, Nat. Phys. **5**, 189 (2009).

[50] H. Takahashi, K. Wakui, S. Suzuki, M. Takeoka, K. Hayasaka, A. Furusawa, and M. Sasaki, Phys. Rev. Lett. **101**, 233605 (2008).

[51] A. Ourjoumtsev, H. Jeong, R. Tualle-Brouri, and P. Grangier, Nature (London) **448**, 784 (2007).

Deterministic implementation of weak quantum cubic nonlinearity

Petr Marek and Radim Filip

Department of Optics, Palacký University, 17. listopadu 1192/12, CZ-771 46 Olomouc, Czech Republic

Akira Furusawa

Department of Applied Physics, School of Engineering, The University of Tokyo, 7-3-1 Hongo, Bunkyo-ku, Tokyo 113-8656, Japan

We propose a deterministic implementation of weak cubic nonlinearity, which is a basic building block of a full-scale continuous-variable quantum computation. Our proposal relies on preparation of a specific ancillary state and transferring its nonlinear properties onto the desired target by means of deterministic Gaussian operations and feed forward. We show that, despite the imperfections arising from the deterministic nature of the operation, the weak quantum nonlinearity can be implemented and verified with the current level of technology.

I. INTRODUCTION

Ever since it has been first mentioned by Feynman [1], quantum computation has been the holy grail of quantum-information theory, because the exponential speedup it offers promises to tackle certain computational problems much faster than any classical computer could [2]. The original approach to quantum computing relied on manipulation of discrete quantum systems [3], but later it was shown that the same speedup can be achieved by computing with continuous-variable (CV) quantum systems, and that CV systems may be even more effective [4,5].

Besides the readily available operations with Hamiltonians composed of first (linear) and second (quadratic) powers of quadrature operators $\hat{x}$ and $\hat{p}$, CV quantum computation requires a single kind of nontrivial resource—a single operation with a Hamiltonian at least cubic (third power) in quadrature operators [4]. Unfortunately, the currently achievable experimental interaction strengths are too low compared to noise to be of use.

Fortunately, the need for currently unavailable cubic unitary evolution may not be so dire. Let us recall the original statement of Lloyd and Braunstein [4]: If one has access to Hamiltonians $\hat{A}$ and $\hat{B}$, one can approximatively implement an operation with Hamiltonian $i[\hat{A},\hat{B}]$. *Approximatively* is the key term here, meaning that the desired operation is engineered only as a quadratic polynomial of the interaction time:

$$e^{i\hat{A}t}e^{i\hat{B}t}e^{-i\hat{A}t}e^{-i\hat{B}t} \approx e^{-[\hat{A},\hat{B}]t^2} + O(t^3). \quad (1)$$

Consequently, even the initial operations need not be unitary—their quadratic approximations are fully sufficient. What this means is that if we take interest in a sample cubic interaction with Hamiltonian $\hat{H} \propto \hat{x}^3$, we need not implement the unitary $e^{i\chi\hat{x}^3}$, where χ is a real parameter, but it is enough to be able to perform operation

$$\mathcal{O}_6(\hat{x}) = 1 + i\chi\hat{x}^3 - \chi^2\hat{x}^6/2. \quad (2)$$

This is the lowest order expansion for which the commutator trick (1) works, but let us start with the real lowest order expansion, $1 + \beta\hat{x}^3$, where β is a complex number. This expansion behaves as a weak cubic coupling if β is imaginary and has the added benefit that it can be used to compose (2) when the respective values of β are complex and chosen properly. In principle, even this gate can be further decomposed into series of $1 + \gamma\hat{x}$ ($\gamma \in \mathbb{C}$) operations [6]. These phase sensitive gates can be implemented probabilistically on a traveling beam of light by subsequent application of photon subtraction and photon addition, represented by operators $\hat{a} = (\hat{x} + i\hat{p})/\sqrt{2}$ and $\hat{a}^\dagger$ [7–9]. They are very useful for preparing various ancillary states, but for use in a full-fledged information processing we are interested in their *deterministic* implementation.

II. IDEAL IMPLEMENTATION

To this end we employ the approach of [10], thoroughly discussed in [11], where it was suggested that a unitary operation acting on a state can be deterministically implemented with the help of a proper resource state, a quantum nondemolition (QND) coupling, a suitable measurement, and a feed-forward loop. Explicitly, for operation $\mathcal{O}(\hat{x})$ acting on the pure state $|\psi\rangle = \int \psi(x)|x\rangle dx$, the resource state is $\mathcal{O}(\hat{x})|p = 0\rangle$. After QND coupling, represented by the unitary $\hat{U}_{QND}(\lambda) = e^{i\lambda\hat{x}_2\hat{p}_1}$, is employed and the overall state is transformed to

$$\int \psi(x)\mathcal{O}(y)|y - \lambda x, x\rangle dx dy, \quad (3)$$

the ancillary resource mode gets measured by a homodyne detection. We can for now assume $\lambda = 1$, as the overall message remains unchanged. For any detected value q the output state is

$$\int \psi(x)\mathcal{O}(x + q)|x\rangle dx. \quad (4)$$

To obtain the desired result, one either postselects only for situations when $q = 0$ was detected, or applies a feed forward which would compensate for $x + q$ in the argument of the operator. It has been shown in [10] that if the desired operation $\mathcal{O}(x)$ is a unitary operation driven by a Hamiltonian of order n, the feed-forward operation requires a Hamiltonian of order $n - 1$. Explicitly, imperfections in the operator $\mathcal{O}(\hat{x} + q) = \exp[i\chi(\hat{x} + q)^3]$ can be compensated by the unitary operator $\hat{U}_{FF} = \exp[-i\chi(3q\hat{x}^2 + 3q^2\hat{x})]$, which is a combination of displacement, squeezing, and phase shifts. The operation (2) we are interested in is not unitary, but since it is an

approximation of a unitary driven by a cubic Hamiltonian, a feed forward of squeezing and displacements should perform adequately, up to some error. We'll get to this issue later. In fact, the operations available for feed forward limit us in what we can do. With squeezing and displacement we can implement only cubic operations. Of course, with them we could also tackle Hamiltonians of the fourth order, and so on. And there is another limitation—since the feed forward must be deterministic and noiseless, and therefore unitary, it can be only used to deterministically compensate unitary (at least approximatively) operations whose Hamiltonian is Hermitian. Therefore we cannot use the trick of implementing a series of $1 + \gamma \hat{x}$ operations; we have to implement operation (2) in one go. Consequently, we need a sufficiently complex resource state.

III. RESOURCE STATE GENERATION

Let us now shift our attention to the required resource state. In realistic, even if idealized, considerations, one has to, instead of a position eigenstate, use a squeezed state $S|0\rangle = [\int \exp(-x^2/g)|x\rangle dx]/(\pi g)^{1/4}$, which approaches the ideal form as $g \to \infty$. The resource state can now be expressed as $\mathcal{O}(\hat{x})\hat{S}|0\rangle = \hat{S}\mathcal{O}(\hat{x}/\sqrt{g})|0\rangle$ which is a state finite in a Fock basis with a superficial layer of squeezing. As it has a finite structure, the state can be engineered by a sequence of six photon additions [12] or photon subtractions [13]. This is an extremely challenging task; let us therefore first focus at the lowest nontrivial cubic Hamiltonian expansion, $\mathcal{O}_3(\hat{x}) = 1 + \chi x^3$, which is a feasible extension of recent experimental works [14]. The appropriate resource state looks like

$$\hat{S}(1 + \chi' \hat{x}^3)|0\rangle = \hat{S}\left(|0\rangle + \chi'\frac{3}{2\sqrt{2}}|1\rangle + \chi'\frac{\sqrt{3}}{2}|3\rangle\right), \quad (5)$$

with $\chi' = \chi g^{-3/2}$. This state can be generated from a squeezed state by a proper sequence of photon subtractions and displacements [13], which acts as $(\hat{a} - \alpha)(\hat{a} - \beta)(\hat{a} - \gamma)\hat{S}|0\rangle$. Since the squeezing operation transforms the annihilation operator as $\hat{S}^\dagger \hat{a}\hat{S} = \mu\hat{a} - \nu\hat{a}^\dagger$, where $\mu = \cosh(\ln\sqrt{g})$ and $\nu = \sinh(\ln\sqrt{g})$, the required displacements can be obtained as a solution of the set of equations:

$$A = \alpha\beta\gamma, \quad \alpha + \beta + \gamma = 0,$$
$$2\sqrt{2}\nu^3 = A\chi', \quad 3\nu^2 + 3\mu\nu = (\alpha\beta + \alpha\gamma + \beta\gamma), \quad (6)$$

where A is a constant parameter related to normalization. The solution exists and it can be found analytically as

$$\alpha = \frac{\xi + \sqrt{\xi^2 - 4\zeta}}{2},$$
$$\beta = \frac{\xi - \sqrt{\xi^2 - 4\zeta}}{2}, \quad (7)$$
$$\gamma = -(\alpha + \beta).$$

Here ξ and ζ are solutions of the set of equations

$$xy + C_1 = 0, \quad y - x^2 - C_2 = 0, \quad (8)$$

where $C_1 = \nu^3 2\sqrt{2}\chi'^{-1}$ and $C_2 = 3\nu^2 + 3\mu\nu$. The solutions of (8) always exist and they can be obtained analytically

using the Cardan formula. The squeezing used in the state generation can be in general different from the squeezing in (5). However, squeezing can be considered to be a well accessible operation, and we shall therefore not deal with this in detail. It should be noted that an alternative way of preparing the state (5) lies in performing a suitable projection onto a single mode of a two-mode squeezed vacuum state. Engineering of the proper measurement, which too requires three avalanche photodiodes (APDs) and three displacements, leads to similar equations as in the previous case (6) with the solution of the same form.

IV. REALISTIC IMPLEMENTATION

With the resource state at our disposal we can now look more closely at the two ways to implement the gate, the probabilistic and the deterministic, in order to compare them and see what is the manifestation of high order nonlinearity in the deterministic case. The probabilistic implementation is rather straightforward. Using the resource state (5) we are able to transform the initial state to

$$|\psi_0\rangle = \int \psi(x)\mathcal{O}(x)e^{-x^2/2g}|x\rangle dx, \quad (9)$$

and as the squeezing of the resource state approaches infinity, the produced state approaches its ideal form. The final state is always pure and the actual composition of the operator $\mathcal{O}_n(x)$ can be arbitrary, allowing us, for example, to implement the operator $\mathcal{O}$ in n different nonunitary steps. On the other hand, if the resource squeezing is insufficient compared to the distribution of the state in phase space, it seriously affects some properties of the state—for example, moments of x quadrature may not be preserved any more.

But let us move toward the more interesting part, the deterministic approach. In this case the operation produces a mixed state

$$\rho' = \int P(q)|\psi_q\rangle\langle\psi_q|dq. \quad (10)$$

Here, $P(q)$ represents the probability of measuring a specific outcome q, and

$$|\psi_q\rangle = \frac{1}{\sqrt{P(q)}\mathcal{N}_R} \int \psi(x)e^{-(x+q)^2/2g}\mathcal{O}(x + q)$$
$$\times e^{-i\chi q^3 - i3\chi(xq^2 + x^2q)}|x\rangle dx, \quad (11)$$

where $\mathcal{N}_R$ is the norm of the resource state, stands for the respective quantum state corrected by feed forward. Ideally, $\mathcal{O}(x + q)e^{-i3\chi(xq^2 + x^2q)} \approx \mathcal{O}(x)$, but this relation can obviously work only when both x and q are small enough for the exponent to be reasonably approximated by the finite expansion $\mathcal{O}_n$. It is, therefore, quite unfortunate that the very condition required for the operation to work flawlessly, the need for $g \to \infty$, is compatible with the feed forward only in the limit of $\chi \to 0$. To quantify these properties in greater detail we need to employ a suitable figure of merit.

V. ANALYSIS

To evaluate the quality of the approximate operation is not a straightforward task. If we want to conclusively distinguish

the cubic type nonlinear interaction from a Gaussian one, we can take advantage of the known way the quadrature operators transform: $\hat{x} \rightarrow \hat{x}$, $\hat{p} \rightarrow \hat{p} + \chi \hat{x}^2$. If we apply the operation, in form of a black box, to a set of known states, we can analyze the transformed states to see whether the operation could be implemented by a suitable Gaussian, or if it is more of what we aim for. The analysis can be as easy as checking the first two moments of the quadrature operators, because the nonlinear dependence of $\langle \hat{p} \rangle$ on $\langle \hat{x} \rangle$ can not be obtained by a Gaussian operation, unless we consider a rather elaborate detection-and-feed-forward setup, which would, however, introduce an extra noise detectable either by checking the purity of the state, or by analyzing higher moments $\langle \hat{x}^2 \rangle$ and $\langle \hat{p}^2 \rangle$.

The case with a purity of 1 is straightforward to verify—as soon as the first moments have the desired form, $\langle \hat{x}' \rangle = \langle \hat{x} \rangle$ and $\langle \hat{p}' \rangle = \langle \hat{p} \rangle + \chi \langle \hat{x}^2 \rangle$, we can be certain a form of the desired non-Gaussianity is at play. In the presence of noise, the confirmation process is more involved, and we shall deal with it in a greater detail.

It needs to be shown that, in comparison to the deterministic approximation, no Gaussian operation can provide the same values of moments $\langle \hat{x}' \rangle$, $\langle \hat{x}'^2 \rangle$, and $\langle \hat{p}' \rangle$ without also resulting in a significantly larger value of moment $\langle \hat{p}'^2 \rangle$ caused by the extra noise. The complete Gaussian scheme consists of an arbitrary Gaussian interaction of the target system with a set of ancillary modes followed by a set of measurements of these modes yielding values which are used in a suitable feed forward to finalize the operation. In the case where the approximate transformations approach the ideal scenario, i.e., when $\langle \hat{x}' \rangle = \langle \hat{x} \rangle$, $\langle \hat{x}'^2 \rangle = \langle \hat{x}^2 \rangle$, and $\langle \hat{p}' \rangle = \langle \hat{p} \rangle + \chi \langle \hat{x}^2 \rangle$, only a single ancillary mode is sufficient, the optimal Gaussian interaction is in the QND interaction with a parameter λ, and after a value of ξ is measured by a homodyne detection, the feed-forward displacement of $\kappa \xi^2$ ensures the correct form of the three moments. In the end, the Gaussian approximated state can be expressed as

$$\rho_S'' = \int dx \, \hat{D}_S(\kappa x^2)_A \langle x | \hat{U}_{QND}(\lambda) \hat{\rho}_S$$
$$\otimes |0\rangle \langle 0| \hat{U}_{QND}^{\dagger}(\lambda) | x \rangle \hat{D}_S^{\dagger}(\kappa x^2), \quad (12)$$

where the subscripts S and A denote the signal and the ancillary mode, respectively. The high order classical nonlinearity is induced by the nonlinear feed forward, represented by the displacement $\hat{D}(\alpha)$. The strength of the QND interaction λ remains a free parameter over which can the procedure be optimized to obtain the best approximation characterized by the minimal possible value of the extra noise term in $\langle \hat{p}'^2 \rangle$.

We analyze the aforementioned properties over a set of small coherent states α with $|\alpha| < 2$. We compare the state obtained by the approximative cubic interaction with the state created by the Gaussian method. In principle, this could be done for both the deterministic and the probabilistic approach, but since the probabilistic approach has the potential to work perfectly, we shall keep to deterministic methods in our comparative endeavors. For each coherent state and its cubic-gate transformed counterpart, we can, from knowledge of the first moments of quadrature operators, estimate the actual cubic nonlinear parameter and use it to construct the benchmark Gaussian-like state (12). The final step is
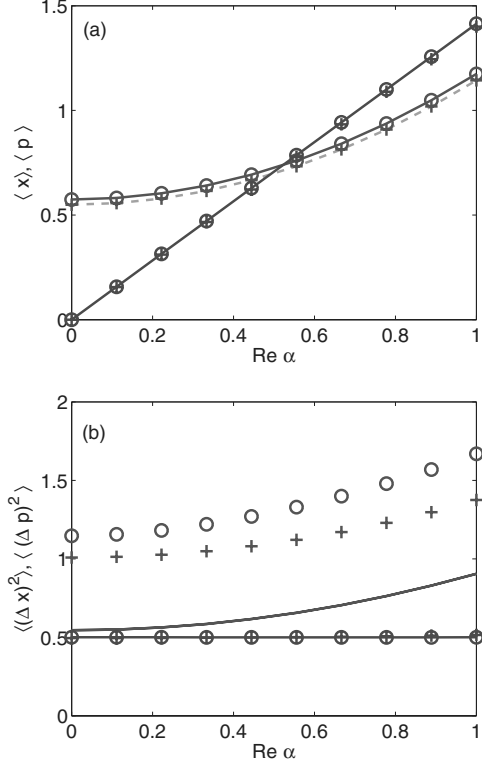

FIG. 1. (Color online) (a) First moments relative to the real part of α. Solid red and blue lines represent the ideal values of $\langle \hat{p} \rangle$ and $\langle \hat{x} \rangle$, respectively. Red and blue crosses then show these values for the deterministic non-Gaussian approximation, while red and blue circles do so for the Gaussian approximation. Dashed green line is a quadratic fit for $\langle \hat{p} \rangle$. The experimental parameters are $g = 1$ and $\chi = 0.03$. (b) Second moments relative to the real part of α. Solid red and blue lines represent the ideal values of $\langle \hat{p}^2 \rangle$ and $\langle \hat{x}^2 \rangle$, respectively. Red and blue crosses then show these values for the deterministic non-Gaussian approximation, while red and blue circles do so for the Gaussian approximation.

to compare the extra noise present in $\hat{p}$ quadrature—if the added noise for the approximate state is below the Gaussian benchmark, we can assume a non-Gaussian nature of the operation.

As an example, let us look at a particular scenario, in which the deterministic cubic gate was applied to a set of coherent states with the imaginary part of the complex amplitude constant. The effect of the operation is illustrated in Fig. 1. Figure 1(a) shows the first moments and reveals that for this purpose, effective cubic nonlinearity of $\chi_{\text{eff}} = 0.1$ can be reliably obtained for both the non-Gaussian and the Gaussian approaches. Differences arise, though, for the second moments, where the value of the Gaussian quadrature moment
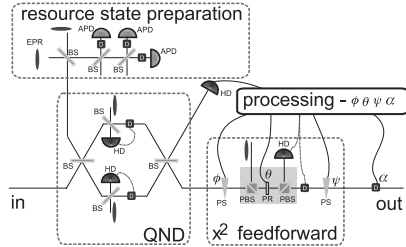
FIG. 2. (Color online) Schematic experimental setup of the deterministic x^3 gate. BS, beam splitter; PBS, polarization beam splitter; PS, phase shift; PR, polarization rotator; APD, avalanche photodiode; HD, homodyne detection; and D, displacement.

$\langle \hat{p}^2 \rangle$ is observably higher than the value of its non-Gaussian counterpart. The values of the Gaussian moment were obtained by optimizations of (12) for each particular value of Reα; it is, therefore, a stronger benchmark than a universal Gaussian operation, working over the whole range of Reα, would be. And it is still beaten by the imperfect deterministic non-Gaussian method with no squeezing in the ancillary mode.

VI. EXPERIMENTAL SETUP

The resource state generation requires three-photon subtraction from a squeezed or a two-mode squeezed light, with appropriate displacements (Fig. 2). Two photon subtractions have been already implemented [14] and three of them are within reach. The resource state is then coupled with the input using a QND gate with offline squeezing [15,16], which can be modified as to reliably manipulate the non-Gaussian resource state [17]. The final step lies in performing a sequence of feed forwards driven by a homodyne measurement of the ancilla [10]. Of those, the only nontrivial one is given by the unitary $e^{i\lambda x^2}$, where the actual value of λ depends on the measurement. This operation can be decomposed into a sequence of a phase shift by ϕ_1, squeezing with gain g_f, and another phase shift by ϕ_2, where the parameters satisfy $\tan \phi_1 \tan \phi_2 = -1$, $\tan \phi_1 = g_f$, and $(1 - g_f^4) \cos \phi_1 \sin \phi_2 = 2 g_f \lambda$. Adjusting the squeezing gain on the fly can be done by exploiting the universal squeezer [15,18], where the amount of squeezing is controlled by changing the ratio of the beam splitter, which can be done by a sequence of a polarization beam splitter, the polarization rotator, and another polarization beam splitter, where the rotator controls the splitting ratio. The nonlinear dependence of the feed-forward parameters

on the measurement results requires a sufficiently fast data processing, but that too is available today [19].

VII. CONCLUSION

We have proposed an experimentally feasible way of deterministically achieving weak nonlinearity of the third order. The procedure effectively engineers the operation on a single photon level and then deterministically cuts and pastes the properties onto the target state. This is reminiscent of the teleportation based gates presented in [20,21], but there are a few crucial differences. In the teleportation based gates, there is only a single resource state for both the teleportation and for the imparting of the nonlinear properties. As such, the state needs to be highly entangled, because otherwise the state would be transferred with too much noise to be of any further use. The need for a high entanglement then clashes with the limited-photon-number nature of the nonlinearity. In our implementation, the ancillary resource state has no squeezing at all, which allows the imparted nonlinearity to be observably large, while the Gaussian mediating interaction is driven by strong squeezing, ensuring minimal noise added during the operation. The limited number of photons still plays a role, though, and the nonlinearity can be faithfully applied only to target states which are sufficiently weak. Furthermore, since there is no such thing as a free lunch, the subsequent use of the transformed state in attempts to generate higher nonlinearities as per [4] requires higher and higher numbers of single photons used in the engineering.

The approach is not flawless. There are several sources of noise which can be simultaneously reduced only in the limit of an infinitely small (read unobservable) interaction. This is due to the finite photon approximation of the cubic gate not being unitary and therefore not perfectly correctable by the unitary feed forward. Nevertheless, we have shown that even with this noise, a demonstration of decisively non-Gaussian high order quantum deterministic nonlinearity going well beyond classical attempts, based on higher order nonlinearity in the feed-forward loop, can be observed already now.

[1] R. P. Feynman, Int. J. Theor. Phys. **21**, 467 (1982).

[2] M. A. Nielsen and I. L. Chuang, *Quantum Computation and Quantum Information* (Cambridge University Press, Cambridge, 2004).

[3] E. Knill *et al.*, Nature (London) **409**, 46 (2001).

[4] S. Lloyd and S. L. Braunstein, Phys. Rev. Lett. **82**, 1784 (1999).

[5] S. L. Braunstein and P. van Loock, Rev. Mod. Phys. **77**, 513 (2005).

[6] R. Filip and P. Marek (unpublished).

[7] A. Zavatta, V. Parigi, M. S. Kim, H. Jeong, and M. Bellini, Phys. Rev. Lett. **103**, 140406 (2009).

[8] J. Fiurášek, Phys. Rev. A **80**, 053822 (2009).

 [9] A. Zavatta *et al*., Nat. Photonics **5**, 52 (2011).

[10] D. Gottesman, A. Kitaev, and J. Preskill, Phys. Rev. A **64**, 012310 (2001).

[11] S. Ghose and B. C. Sanders, J. Mod. Opt. **54**, 855 (2007).

[12] M. Dakna J. Clausen, L. Knoll, and D.G. Welsch Phys. Rev. A **59**, 1658 (1999).

[13] J. Fiurášek, R. Garcia-Patron, and N. J. Cerf, Phys. Rev. A **72**, 033822 (2005).

[14] H. Takahashi K. Wakui, S. Suzuki, M. Takeoka, K. Hayasaka, A. Furusawa, and M. Sasaki, Phys. Rev. Lett. **101**, 233605 (2008).

[15] R. Filip, P. Marek, and U. L. Andersen, Phys. Rev. A **71**, 042308 (2005).

[16] J. I. Yoshikawa, Y. Miwa, A. Huck, U. L. Andersen, P. vanLoock, and A. Furusawa, Phys. Rev. Lett. **101**, 250501 (2008).

[17] N. Lee *et al*., Science **332**, 330 (2011).

[18] J. Yoshikawa *et al*., Phys. Rev. A **76**, 060301(R) (2007).

[19] T. A. Wheatley, D. W. Berry, H. Yonezawa, D. Nakane, H. Arao, D. T. Pope, T. C. Ralph, H. M. Wiseman, A. Furusawa, and E. H. Huntington, Phys. Rev. Lett. **104**, 093601 (2010).

[20] D. Gottesman and I. L. Chuang, Nature (London) **402**, 390 (1999).

[21] S. D. Bartlett and W. J. Munro, Phys. Rev. Lett. **90**, 117901 (2003).

Emulating quantum cubic nonlinearity

Mitsuyoshi Yukawa,[1] Kazunori Miyata,[1] Hidehiro Yonezawa,[1] Petr Marek,[2] Radim Filip,[2] and Akira Furusawa[1]

[1]*Department of Applied Physics, School of Engineering, The University of Tokyo, 7-3-1 Hongo, Bunkyo-ku, Tokyo 113-8656, Japan*
[2]*Department of Optics, Palacký University, 17 listopadu 1192/12, 77146 Olomouc, Czech Republic*

Unitary non-Gaussian nonlinearity is one of the key components required for quantum computation and other developing applications of quantum information processing. Sufficient operation of this kind is still not available, but it can be approximatively implemented with the help of a specifically engineered resource state constructed from individual photons. We present experimental realization and thorough analysis of such quantum resource states and confirm that the state does indeed possess properties of a state produced by unitary dynamics driven by cubic nonlinearity.

I. INTRODUCTION

Nonlinear interactions capable of manipulating the quantum state of the harmonic oscillators form a very challenging area of recent development in the field of modern quantum physics. Handling these interactions is necessary not only for the understanding of quantum nonlinear dynamics of the harmonic oscillators, but also for achieving the standing long-term goal of quantum information—the universal quantum computation [1,2]. The operations needed are unitary, and both Gaussian and non-Gaussian [3]. For a harmonic oscillator representing a single mode of electromagnetic radiation, Gaussian operations are relatively easy to obtain, but unitary single-mode non-Gaussian nonlinearities are either not available or are too weak to have an observable quantum effect. For other physical systems, such as cold atoms [4] or trapped ions [5], the non-Gaussian operations could be implemented using additional anharmonic potentials, but multimode Gaussian operations are hard to come by.

Quantum nonlinear operations for light can be obtained by letting the system interact with individual atoms, ions [6,7], or similar solid-state physical systems [8] and measuring the discrete system afterwards. In this way, highly nonclassical superposed coherent states were recently realized [9]. These quantum states possess strong nonlinear properties, and they were not previously observed in the trapped ions [7], the circuit cavity electrodynamics [10], and in the optical continuous variables (CV) experiments with traveling light [11,12]. However, of these systems, only the last one currently allows implementation of deterministic Gaussian operations and measurements [13–16], which are needed for deterministic measurement-induced implementation of high-order nonlinearities [17,18]. Considering that recently single-photon detectors [3] were used to prepare states with nonlinear properties at least approaching those of atomic and solid-state systems [19], the toolbox of CV quantum optics has everything it needs for tests of unitary nonlinear dynamics. Please note, there is a difference between the CV quantum optics and its discrete counterpart, relying on encoding qubits into individual photons [20,21]. In both, the desired nonlinearity can be obtained from measurements, and highly nonlinear gates have indeed been implemented for single photons [22]. However, the current level of technology does not allow discrete quantum optics experiments to be truly deterministic, as all measurements need to be performed in coincidence basis.

In principle, to realize an arbitrary unitary operation of a quantum harmonic oscillator, it is sufficient to have access to the quantum cubic nonlinearity [1,23]. Cubic nonlinearity is represented by a Hamiltonian $\hat{H} \propto \hat{x}^3$ [17], where $\hat{x} = (\hat{a} + \hat{a}^\dagger)/\sqrt{2}$ is the position operator of the quantum harmonic oscillator [$\hat{a}$ is the annihilation operator, and the momentum operator is similarly defined as $\hat{p} = (\hat{a} - \hat{a}^\dagger)/(i\sqrt{2})$]. As of now, neither quantum cubic nonlinearity, nor quantum states produced by it (cubic states), have been observed on any experimental platform. Beginning from a ground state, even the weak cubic interaction generates highly nonclassical states [24]. However, the nonclassicality of these states lies in the superposition of $|1\rangle$ and $|3\rangle$ ($|1\&3\rangle$ for shorthand), and it is unfortunately masked by the superposition of $|1\&3\rangle$ with the dominant ground state $|0\rangle$ [18], especially considering its fragility with regard to damping of the oscillator. It is therefore challenging not only to generate and detect these states, but also to understand and verify their nonclassical features.

A nonlinear gate can be deterministically implemented by coupling a specifically prepared ancillary state to the unknown target via the Gaussian quantum nondemolition coupling. The ancilla is then measured and the obtained value q is used to drive nonlinear feed forward in the form of pair of displacements proportional to q and q^2 performed on the target state. See Ref. [18] for more details. This approach was initially discussed in [17,24,25] with the ideal state, which is currently experimentally unfeasible. To remedy this issue, an *approximative* weak cubic state, described as a superposition of Fock states $|0\rangle$, $|1\rangle$, and $|3\rangle$, was recently proposed [18]. In this paper we present the experimental, completely heralded preparation of this state together with analysis of its nontrivial nonclassical properties.

II. CUBIC STATE

The ideal cubic state, which can be used as a resource for the nonlinear cubic gate, can be expressed as $\int e^{-i\chi_0 \hat{x}^3}|x\rangle \, dx$. Note that normalization factors are omitted in this paper unless otherwise noted. The cubic state can be obtained by applying cubic nonlinear interaction $\hat{U}(\chi_0) = \exp(-i\chi_0 \hat{x}^3)$ to an infinitely squeezed state. Due to general inaccessibility of

a cubic nonlinear operation, any physical realization of the state needs to be some kind of approximation. For weak cubic nonlinearity and finite energy, the state can be approximated by $\hat{S}(-r)(1 - i\chi\hat{x}^3)|0\rangle$ [18]. Here, the cubic nonlinearity χ is given by $\chi = \chi_0 e^{3r}$, and $\hat{S}(-r) = \exp[-(ir/2)(\hat{x}\hat{p} + \hat{p}\hat{x})]$ is a squeezing operation, a Gaussian operation, which can be considered feasible and highly accessible in contemporary experimental practice [13–16]. The squeezing operation does not affect the cubic behavior of the state and therefore can be omitted in our first attempts to implement the cubic operation. The approximative weak cubic state can be then expressed in the Fock space as

$$|\psi_{\mathrm{id}}\rangle = (1 - i\chi\hat{x}^3)|0\rangle = |0\rangle - i\frac{\chi\sqrt{15}}{2\sqrt{2}}|1\&3\rangle, \qquad (1)$$

where $|1\&3\rangle = (\sqrt{3}|1\rangle + \sqrt{2}|3\rangle)/\sqrt{5}$. It is a specific superposition of zero, one, and three photons, but it can also be viewed as a superposition of vacuum $|0\rangle$ with a state $|1\&3\rangle$, which in itself is an approximation of odd superposition of coherent states. The vacuum contribution results from the first term of the unitary evolution $\hat{U}(\chi) \approx 1 - i\chi\hat{x}^3$. It is an important term for the function of the deterministic cubic phase gate, but at the same time it masks the nonclassical features of the state $|1\&3\rangle$.

The cubic state (1) is generated by means of the setup depicted in Fig. 1. The nondegenerate optical parametric oscillator (NOPO) generates an entangled two-mode squeezed state $\sum_{n=0}^{\infty}\lambda^n|n\rangle_i|n\rangle_s$. The *idler* mode i is then split into three by a pair of beamsplitters, after which the states of the three modes are displaced in a phase space by amplitudes $\alpha = 1.55\lambda e^{i90°}$, $\beta = 1.19\lambda e^{i311°}$, and $\gamma = 1.19\lambda e^{i229°}$. Finally, each of the modes impinges on the avalanche photodiode (APD). Simultaneous detection of a photon by the three detectors then heralds approximative preparation of the *signal*

mode s in the state

$$\sum_{n=0}^{3}\lambda^n[\langle 1,1,1|_{\mathrm{i12}}\hat{D}_1(\alpha)\hat{D}_2(\beta)\hat{D}_\mathrm{i}(\gamma)\hat{U}_{\mathrm{BS}}^{12}\hat{U}_{\mathrm{BS}}^{1\mathrm{i}}|n,0,0\rangle_{\mathrm{i12}}]|n\rangle_\mathrm{s},$$

$$(2)$$

where $\hat{D}_k(.)$ represents the displacement operation on mode k, $\hat{U}_{\mathrm{BS}}^{kl}$ represents the beamsplitter between modes k and l, and subscripts 1 and 2 describe the ancillary modes. For the suitable choice of λ, this state turns into the required superposition (1). Please note that the state is prepared from the higher Fock number contributions of a single two-mode state, and not from several single photons as in [26]. In this sense it is actually more reminiscent of the proposal relying on repeated combinations of displacements and photon subtractions performed on a single-mode squeezed light [27]. As a consequence, the photons forming the state are indistinguishable. There are also no problems with mode structure, because the heralded state is measured by homodyne detection, the local oscillator of which perfectly defines the measured mode. Any multimode effects, arising, for example, from imperfect coincidence of the APDs, therefore directly translate to reduction of the overall quality of the produced state.

III. THE EXPERIMENT

The light source is a continuous-wave Ti:sapphire laser of 860 nm. With around 20 mW of pump beam of 430 nm, a two-mode squeezed vacuum is generated from a NOPO, which contains a periodically poled KTiOPO$_4$ crystal as an optical nonlinear medium. The pump beam is generated by second harmonic generation of the fundamental beam and frequency-shifted with an acousto-optic modulator by around 600 MHz (equal to the free spectral range of NOPO, $\Delta\omega$). As a result, photon pairs of frequency ω (signal) and $\omega + \Delta\omega$ (idler) are obtained (ω corresponds to the frequency of the fundamental beam). The output photons are spatially separated by a split cavity whose free spectral range is $2\Delta\omega$. The idler beam passing through the split cavity is sent to two frequency filtering cavities, and subsequently split into three equal-intensity beams with beamsplitters. The state of each beam is then displaced by a specific amplitude by interfering it with a displacement beam at a mirror of 99% reflectivity. The phase of the displacement is controlled by piezoelectric transducers, and the amplitude of the displacement is controlled by rotating half-wave plates followed by polarization beamsplitters. The idler photons are detected by APDs. When APDs detect photons, they output electronic pulses which are combined into an AND circuit to get threefold coincidence clicks. The signal beam is measured by homodyne detection with a local oscillator beam of 10 mW. The homodyne current is sent to an oscilloscope and stored every time coincident clicks happen. The density matrix and Wigner function of the output state are then numerically reconstructed from a set of measured quadratures and phases of the local oscillator beam.

IV. ANALYSIS OF THE EXPERIMENTAL STATE

The reconstructed quantum state, both its density matrix $\hat{\rho}_{\mathrm{exp}}$ and its Wigner function, is shown in in Fig. 2(a). The
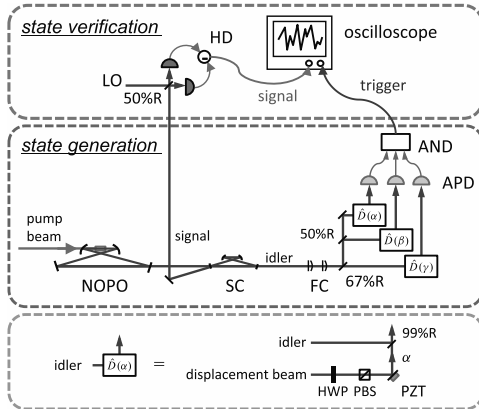

FIG. 1. (Color online) Experimental setup. NOPO, nondegenerate optical parametric oscillator; SC, split cavity; FC, filter cavity; HD, homodyne detector; APD, avalanche photodiode; HWP, half-wave plate; PBS, polarization beamsplitter; PZT, piezoelectric transducer.
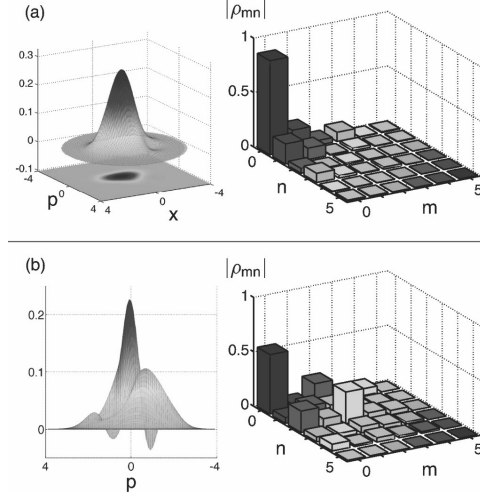
FIG. 2. (Color online) (a) Wigner function and density matrix of the experimentally generated state. (b) Wigner function and density matrix of the experimentally generated state after a single photon is numerically subtracted from the data.

traditional approach to quantifying the quality of a prepared state is by using the fidelity, $F = \langle \psi_{id} | \hat{\rho} | \psi_{id} \rangle$. In our case, the generated state has a maximal fidelity of $F_M = 0.90$ with the ideal state (1) with $\chi = 0.166$. However, due to the weak nonlinearity, the same state has fidelity $F_0 = 0.95$ with the vacuum state. This does not suggest that vacuum is a better cubic state but rather that the fidelity is not a good figure of merit in our case. In order to verify the state, we will therefore need to analyze it more thoroughly and devise new methods.

We can start by confirming the presence of nontrivial superpositions of photon numbers present in (1). The overwhelming influence of vacuum can be removed by applying a virtual single-photon subtraction $\hat{\rho}_{exp} \rightarrow \hat{\rho}_{1sub} = \hat{a}_{exp} \hat{a}^\dagger / \text{Tr}[\hat{a}_{exp} \hat{a}^\dagger]$. For the ideal resource state, $(1 - i\chi \hat{x}^3)|0\rangle$, this should result in a superposition $|0\rangle + \sqrt{2}|2\rangle$, which is a state fairly similar to an even superposition of coherent states and, as such, it should possess several regions of negativity. Thus we can convert the cubic state into a state with well-known properties, which can be easily tested. Figure 2(b) shows the Wigner function and the density matrix of the numerically photon-subtracted experimental state. Notice that two distinctive regions of negativity are indeed present. Moreover, apart from considerations involving specific states, the areas of negativity sufficiently indicate nonclassical behavior of the initial state, as they would not appear if the state was only a mixture of coherent states, which does not produce entanglement when divided on a beamsplitter [28]. The probability of two photons $p'_2 = 0.29$ is clearly dominating over $p'_1 = 0.12$ and $p'_3 = 0.03$, where $p'_i = \langle i | \hat{\rho}_{1sub} | i \rangle$. To show now that Fock states $|0\rangle$ and $|2\rangle$ appear in the superposition and not in the mixture, we use the normalized off-diagonal element for states basis $|\phi\rangle$ and $|\xi\rangle$, $\mathcal{R}_{\xi,\phi}(\hat{\rho}) = \frac{|\langle \xi | \hat{\rho} | \phi \rangle|^2}{\langle \xi | \hat{\rho} | \xi \rangle \langle \phi | \hat{\rho} | \phi \rangle}$, which

characterizes the quality of any unbalanced superposition. Since the subtraction preserves the superposition of Fock states, $\mathcal{R}_{0,2}(\hat{\rho}_{1sub}) = 0.24$ after the subtraction proves the presence of coherent superposition originating from the state $|1\&3\rangle$. In a similar way we can confirm that the three-photon element is significantly dominant over the two- and four-photon elements. Two virtual photon subtractions transform the state $\hat{\rho}_{exp} \rightarrow \hat{\rho}_{2sub} = \hat{a}^2 \hat{\rho}_{exp} \hat{a}^{\dagger 2} / \text{Tr}[\hat{a}^2 \hat{\rho}_{exp} \hat{a}^{\dagger 2}]$, where the single-photon state is present with a probability of $p''_1 = \langle 1 | \hat{\rho}_{2sub} | 1 \rangle = 0.68$. In a generated single-photon state this would be a sufficient confirmation that the state cannot be emulated by a mixture of Gaussian states. In our case it is the argument for the strong presence of the three-photon element.

Our analysis confirms presence of the highly nonclassical superposition state $|1\&3\rangle$, but we also need to demonstrate that the state appears in a superposition with the vacuum state, not just as a part of mixture. For this we look at the normalized off-diagonal element $\mathcal{R}_{0,1\&3}(\hat{\rho}_{exp})$ between the $|0\rangle$ and $|1\&3\rangle$ for the original (not photon-subtracted) experimental state, which would attain a value of one for the ideal pure state and a value of zero for a complete mixture. In our case the value is $\mathcal{R}_{0,1\&3}(\hat{\rho}_{exp}) = 0.50$, so the superposition is present, even if it is not perfectly visible due to the effects of noise. More importantly, the element is significantly larger than $\mathcal{R}_{0,1\&3^\perp}(\hat{\rho}_{exp}) = 0.11$, where $|1\&3^\perp\rangle = (\sqrt{2}|1\rangle - \sqrt{3}|3\rangle)/\sqrt{5}$ is orthogonal to $|1\&3\rangle$. This shows that the desired and theoretically expected superpositions are dominant.

V. DETECTING CUBIC NONLINEARITY

We have shown that the state contains the required superpositions, which is a strong argument about the true nature of the state. However, there is also some measure of noise present. It is a valid question, then, whether the state does indeed behave as the cubic state despite the imperfections. The cubic state should be able to drive, even at this elementary level, the cubic gate. One way the cubic gate manifests is observable even at a semiclassical level. For a given quantum state, the cubic nonlinearity transforms the first quadrature moments $\hat{x}_{in}$ and $\hat{p}_{in}$ according to $\langle \hat{x}_{out} \rangle = \langle \hat{x}_{in} \rangle$, $\langle \hat{p}_{out} \rangle = \langle \hat{p}_{in} \rangle + 3\chi \langle \hat{x}_{in}^2 \rangle$. The first moment of $\hat{x}$ should be preserved, while the first moment of $\hat{p}$ should become linearly dependent on the second moment $\langle \hat{x}^2 \rangle = \text{var}(x) + \langle \hat{x} \rangle^2$. Note that var(x) is a variance of $\hat{x}$. If we choose a set of input states with identical variances, there should be observable quadratic dependence of the first moment of $\hat{p}$ on the first moment of $\hat{x}$.

The easiest way the cubic gate can be implemented relies on mixing the prepared ancilla with the target state on a balanced beamsplitter, which is followed by projecting the ancilla onto the quadrature eigenstate $|x = 0\rangle$ by homodyne detection. This is the probabilistic version of the cubic gate [18] and it is similar to using single photons to obtain a probabilistic map [29]. As the set of target states, we will consider coherent states $|\alpha\rangle$, where $0 \leqslant \alpha \leqslant 1$, with first moments $\langle \hat{x}_{in} \rangle = \sqrt{2}\alpha$ and $\langle \hat{p}_{in} \rangle = 0$. The operation, imprinting nonlinearity from the ancillary mixed state $\hat{\rho}_A$ to the target state $\hat{\rho}_{in} = |\alpha\rangle \langle \alpha|$, can be realized by the map

$$\hat{\rho}_{out} = \text{Tr}_A[\hat{U}_{BS} \hat{\rho}_{in} \otimes \hat{\rho}_A \hat{U}_{BS}^\dagger | x = 0 \rangle_A \langle x = 0 |], \quad (3)$$
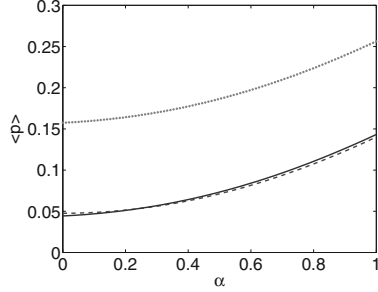
FIG. 3. (Color online) First moment of p for various coherent states: ideal state with $\chi = 0.090$ (dashed blue line), experimentally generated state (dotted green line), and experimentally generated state after the suitable displacement $\Delta p = -0.16$ (solid red line).
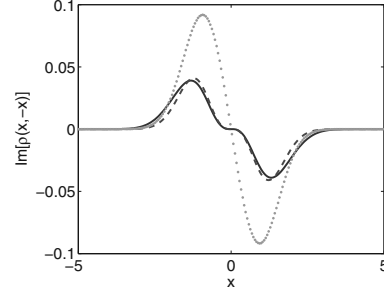

FIG. 4. (Color online) Imaginary parts of the antidiagonal values of coordinate density matrices for the ideal state with $\chi = 0.090$ (dashed blue line), the experimentally generated state (dotted green line), and the experimentally generated state after the suitable displacement $\Delta p = -0.17$ (solid red line).

where $\hat{U}_{BS}$ is a unitary operator realizing transformation by a balanced beamsplitter. This map fuses two states with wave functions $\psi_S(x_S)$ and $\psi_A(x_A)$ into a state with wave function $\psi_S(x_S/\sqrt{2})\psi_A(x_S/\sqrt{2})$. The factor $\sqrt{2}$ only introduces linear scaling of the measured data and has no influence on any nonlinear properties. Since the imprinting operation uses only Gaussian tools, any non-Gaussian nonlinearity of the transformed state needs to originate in nonlinear properties of the ancillary state $\hat{\rho}_A$. We have numerically simulated the procedure, and the behavior of the first moment of quadrature $\hat{p}$ is plotted in Fig. 3. We can see that the dependence is distinctively quadratic. This behavior is actually in a very good match with that of the ideal cubic state (1) with $\chi = 0.090$. They only differ by a constant displacement, which has probably arisen due to experimental imperfections and which can be easily compensated. This showcases our ability to prepare a quantum state capable of imposing high-order nonlinearity in a different quantum state.

We can also attempt to observe the cubic nonlinearity directly, using the density matrix in coordinate representation. In this picture, the continuous density matrix elements are defined as $\rho(x,x') = \langle x|\hat{\rho}|x'\rangle$. The cubic nonlinearity is best visible in the imaginary part of the main antidiagonal: for the ideal state $(1 - i\chi\hat{x}^3)|0\rangle\langle 0|(1 + i\chi\hat{x}^3)$, the density matrix elements are $\mathrm{Im}[\rho(x, -x)] = 2\chi x^3 e^{-x^2}$ and the cubic nonlinearity is nicely visible. One problem in this picture is that the cubic nonlinearity can be concealed by other operations. The second-order nonlinearity does not manifest in the imaginary part (not even order nonlinearities do), but a simple displacement can conceal the desired behavior. On the other hand, displacement can be quite straightforwardly

compensated by performing a virtual operation on the data. The comparison of the ideal state, the generated state, and the displaced generated state can be seen in Fig. 4. We can see that although the cubic nonlinearity is not immediately apparent, the suitable displacement can effectively reveal it. This nicely witnesses our ability to conditionally prepare a quantum state equivalent to the outcome of the required higher-order nonlinearity.

VI. SUMMARY AND OUTLOOK

In conclusion, we have generated a heralded nonclassical non-Gaussian quantum state of light, which exhibits key features of a state produced by unitary dynamics driven by cubic quantum nonlinearity. Our experimental test has demonstrated the feasibility of conditional optical preparation of the ancillary resource state for the cubic measurement-induced nonlinearity. Our analysis has contributed to general understanding of quantum states produced by the higher-order quantum nonlinearities. This understanding is a crucial step towards physically implementing these nonlinearities as a part of quantum information processing, and we expect information regarding the first attempts in this direction to appear soon.

[1] S. Lloyd and S. L. Braunstein, Phys. Rev. Lett. **82**, 1784 (1999).

[2] N. C. Menicucci, P. van Loock, M. Gu, Ch. Weedbrook, T. C. Ralph, and M. A. Nielsen, Phys. Rev. Lett. **97**, 110501 (2006).

[3] A. Furusawa and P. van Loock, *Quantum Teleportation and Entanglement: A Hybrid Approach to Optical Quantum Information Processing* (Wiley-VCH Verlag GmbH & Co. KGaA, Germany, 2011).

[4] W. K. Hensinger *et al.*, Nature (London) **412**, 52 (2001); M. Anderlini *et al.*, *ibid.* **448**, 452 (2007); S. Fölling *et al.*, *ibid.* **448**, 1029 (2007).

[5] D. Leibfried *et al.*, Phys. Rev. Lett. **89**, 247901 (2002); M. Harlander *et al.*, Nature (London) **471**, 200 (2011).

[6] S. Haroche and J.-M. Raimond, *Exploring the Quantum: Atoms, Cavities, and Photons* (Oxford University Press, New York, USA, 2006).

[7] D. Leibfried, R. Blatt, C. Monroe, and D. Wineland, Rev. Mod. Phys. **75**, 281 (2003).

[8] M. Dykman, *Fluctuating Nonlinear Oscillators: From Nanomechanics to Quantum Superconducting Circuits* (Oxford University Press, New York, USA, 2012).

[9] S. Deleglise, I. Dotsenko, C. Sayrin, J. Bernu, M. Brune, J.-M. Raimond, and S. Haroche, Nature (London) **455**, 510 (2008).

[10] M. Hofheinz, H. Wang, M. Ansmann, R. C. Bialczak, E. Lucero, M. Neeley, A. D. O'Connell, D. Sank, J. Wenner, J. M. Martinis, and A. N. Cleland, Nature (London) **459**, 546 (2009).

[11] E. Bimbard, N. Jain, A. MacRae, and A. I. Lvovsky, Nature Photon. **4**, 243 (2010).

[12] M. Cooper, L. J. Wright, Ch. Söller, and B. J. Smith, Opt. Express **21**, 5309 (2013).

[13] R. Filip, P. Marek, and U. L. Andersen, Phys. Rev. A **71**, 042308 (2005).

[14] J. Yoshikawa, T. Hayashi, T. Akiyama, N. Takei, A. Huck, U. L. Andersen, and A. Furusawa, Phys. Rev. A **76**, 060301(R) (2007).

[15] J. Yoshikawa, Y. Miwa, A. Huck, U. L. Andersen, P. van Loock, and A. Furusawa, Phys. Rev. Lett. **101**, 250501 (2008).

[16] J. Yoshikawa, Y. Miwa, R. Filip, and A. Furusawa, Phys. Rev. A **83**, 052307 (2011).

[17] D. Gottesman, A. Kitaev, and J. Preskill, Phys. Rev. A **64**, 012310 (2001); S. D. Bartlett and B. C. Sanders, *ibid.* **65**, 042304 (2002).

[18] P. Marek, R. Filip, and A. Furusawa, Phys. Rev. A **84**, 053802 (2011).

[19] M. Yukawa, K. Miyata, T. Mizuta, H. Yonezawa, P. Marek, R. Filip, and A. Furusawa, Opt. Express **21**, 5529 (2013).

[20] M. A. Nielsen and I. L. Chuang, *Quantum Computation and Quantum Information* (Cambridge University Press, Cambridge, UK, 2000).

[21] E. Knill, R. Laflamme, and G. J. Milburn, Nature (London) **409**, 46 (2001).

[22] B. P. Lanyon, M. Barbieri, M. P. Almeida, T. Jennewein, T. C. Ralph, K. J. Resch, G. J. Pryde, J. L. O'Brien, A. Gilchrist, and A. G. White, Nat. Phys. **5**, 134 (2009); R. Okamoto, J. L. O'Brien, H. F. Hofmann, and Shigeki Takeuchi, PNAS **108**, 10067 (2011); W.-B. Gao, P. Xu, X.-C. Yao, O. Gühne, A. Cabello, C.-Y. Lu, C.-Z. Peng, Z.-B. Chen, and J.-W. Pan, Phys. Rev. Lett. **104**, 020501 (2010); X.-Q. Zhou, T. C. Ralph, P. Kalasuwan, M. Zhang, A. Peruzzo, B. P. Lanyon, and J. L. O'Brien, Nat. Commun. **2**, 413 (2011).

[23] S. Sefi and P. van Loock, Phys. Rev. Lett. **107**, 170501 (2011).

[24] S. Ghose and B. C. Sanders, J. Mod. Opt. **54**, 855 (2007).

[25] M. Sasaki, K. Wakui, J. Mizuno, M. Fujiwara, and M. Akiba, *Quantum Communication, Measurement and Computing*, edited by S. M. Barnett *et al.* (American Institute of Physics, New York, 2004), pp. 44–47.

[26] N. M. VanMeter, P. Lougovski, D. B. Uskov, K. Kieling, J. Eisert, and Jonathan P. Dowling, Phys. Rev. A **76**, 063808 (2007).

[27] J. Fiurášek, R. García-Patrón, and N. J. Cerf, Phys. Rev. A **72**, 033822 (2005).

[28] M. S. Kim, W. Son, V. Bužek, and P. L. Knight, Phys. Rev. A **65**, 032323 (2002).

[29] F. Ferreyrol, N. Spagnolo, R. Blandino, M. Barbieri, and R. Tualle-Brouri, Phys. Rev. A **86**, 062327 (2012).

Generating superposition of up-to three photons for continuous variable quantum information processing

Mitsuyoshi Yukawa,[1] **Kazunori Miyata,**[1] **Takahiro Mizuta,**[1]
Hidehiro Yonezawa,[1] **Petr Marek,**[2]
Radim Filip,[2] **and Akira Furusawa**[1,*]

[1]*Department of Applied Physics, School of Engineering, The University of Tokyo,*
7-3-1 Hongo, Bunkyo-ku, Tokyo 113-8656, Japan
[2]*Department of Optics, Palacký University, 17. listopadu 1192/12,*
77146 Olomouc, Czech Republic

[*]*akiraf@ap.t.u-tokyo.ac.jp*

Abstract: We develop an experimental scheme based on a continuous-wave (cw) laser for generating arbitrary superpositions of photon number states. In this experiment, we successfully generate superposition states of zero to three photons, namely advanced versions of superpositions of two and three coherent states. They are fully compatible with developed quantum teleportation and measurement-based quantum operations with cw lasers. Due to achieved high detection efficiency, we observe, without any loss correction, multiple areas of negativity of Wigner function, which confirm strongly nonclassical nature of the generated states.

© 2013 Optical Society of America

OCIS codes: (270.0270) Quantum optics; (270.5585) Quantum information and processing.

References and links

1. W. K. Wooters and W. H. Zurek, "A single quantum cannot be cloned," Nature **299**, 802–803 (1982).
2. T. D. Ladd, F. Jelezko, R. Laflamme, Y. Nakamura, C. Monroe, and J. L. O'Brien, "Quantum computers," Nature **464**, 45–53 (2010).
3. D. Gottesman and I. L. Chuang, "Demonstrating the viability of universal quantum computation using teleportation and single-qubit operations," Nature **402**, 390–393 (1999).
4. S. D. Bartlett and W. J. Munro, "Quantum teleportation of optical quantum gates," Phys. Rev. Lett. **90**, 117901 (2003).
5. J. L. O'Brien, A. Furusawa, and J. Vučković, "Photonic quantum technologies," Nature Photon. **3**, 687–695 (2009).
6. C. Weedbrook, S. Pirandola, R. Garcia-Patron, N. J. Cerf, T. C. Ralph, J. H. Shapiro, and S. Lloyd, "Gaussian quantum information," Rev. Mod. Phys. **84**, 621–669 (2012).
7. A. I. Lvovsky, H. Hansen, T. Aichele, O. Benson, J. Mlynek, and S. Schiller, "Quantum State Reconstruction of the Single-Photon Fock State," Phys. Rev. Lett. **87**, 050402 (2001).
8. A. Ourjoumtsev, R. Tualle-Brouri, and P. Grangier, "Quantum Homodyne Tomography of a Two-Photon Fock State," Phys. Rev. Lett. **96**, 213601 (2006).
9. J. S. Neergaard-Nielsen, B. M. Nielsen, H. Takahashi, A. I. Vistnes, and E. S. Polzik, "High purity bright single photon source," Opt. Express **15**(13), 7940–7949 (2007).
10. M. Dakna, J. Clausen, L. Knöll, and D.-G. Welsch, "Generation of arbitrary quantum states of traveling fields," Phys. Rev. A **59**, 1658–1661 (1999).
11. J. Fiurášek, R. García-Patrón, and N. J. Cerf, "Conditional generation of arbitrary single-mode quantum states of light by repeated photon subtractions," Phys. Rev. A **72**, 033822 (2005).
12. P. Marek, R. Filip, and A. Furusawa, "Deterministic implementation of weak quantum cubic nonlinearity," Phys. Rev. A **84**, 053802 (2011).

13. A. I. Lvovsky and J. Mlynek, "Quantum-Optical Catalysis: Generating Nonclassical States of Light by Means of Linear Optics," Phys. Rev. Lett. **88**, 250401 (2002).
14. E. Bimbard, N. Jain, A. MacRae, and A. I. Lvovsky, "Quantum-optical state engineering up to the two-photon level," Nat. Photonics **4**, 243–247 (2010).
15. R. Filip, P. Marek, and U.L. Andersen, "Measurement-induced continuous-variable quantum interactions," Phys. Rev. A **71**, 042308 (2005).
16. J. Yoshikawa, T. Hayashi, T. Akiyama, N. Takei, A. Huck, U. L. Andersen, and A. Furusawa, "Demonstration of deterministic and high fidelity squeezing of quantum information," Phys. Rev. A **76**, 060301(R) (2007).
17. J. Yoshikawa, Y. Miwa, A. Huck, U. L. Andersen, P. van Loock, and A. Furusawa, "Demonstration of a Quantum Nondemolition Sum Gate," Phys. Rev. Lett. **101**, 250501 (2008).
18. Y. Miwa, J. Yoshikawa, N. Iwata, M. Endo, P. Marek, R. Filip, P. van Loock, and A. Furusawa, "Unconditional conversion between quantum particles and waves," arXiv: 1209.2804[quant-ph].
19. T.C. Ralph, A. Gilchrist, G.J. Milburn, W.J. Munro, and S. Glancy, "Quantum computation with optical coherent states," Phys. Rev. A **68**, 042319 (2003).
20. S. Deleglise, I. Dotsenko, C. Sayrin, J. Bernu, M. Brune, J.-M. Raimond, and S. Haroche, "Reconstruction of non-classical cavity field states with snapshots of their decoherence," Nature **455**, 510–514 (2008).
21. K. Wakui, H. Takahashi, A. Furusawa, and M. Sasaki, "Photon subtracted squeezed states generated with periodically poled KTiOPO$_4$," Opt. Express **15**, 3568–3574 (2007).
22. D. T. Smithey, M. Beck, M. G. Raymer, and A. Faridani, "Measurement of the Wigner distribution and the density matrix of a light mode using optical homodyne tomography: Application to squeezed states and the vacuum," Phys. Rev. Lett. **70**, 1244–1247 (1993).
23. A. I. Lvovsky, "Iterative maximum-likelihood reconstruction in quantum homodyne tomography," J. Opt. B **6**, S556–S559 (2004).
24. A. Ourjoumtsev, R. Tualle-Brouri, J. Laurat, and P. Grangier, "Generating Optical Schrödinger Kittens for Quantum Information Processing," Science **312**, 83–86 (2006).
25. J. S. Neergaard-Nielsen, B. M. Nielsen, C. Hettich, K. Mølmer, and E. S. Polzik, "Generation of a Superposition of Odd Photon Number States for Quantum Information Networks," Phys. Rev. Lett. **97**, 083604 (2006).
26. D. Menzies and R. Filip, "Gaussian-optimized preparation of non-Gaussian pure states," Phys. Rev. A **79**, 012313 (2009).
27. A. Ourjoumtsev, H. Jeong, R. Tualle-Brouri, and P. Grangier, "Generation of optical 'Schrödinger cats' from photon number states," Nature **448**, 784–786 (2007).
28. M. Hofheinz, H. Wang, M. Ansmann, R. C. Bialczak, E. Lucero, M. Neeley, A. D. OfConnell, D. Sank, J. Wenner, J. M. Martinis, and A. N. Cleland, "Synthesizing arbitrary quantum states in a superconducting resonator," Nature **459**, 546–549 (2009).
29. J. M. Raimond, P. Facchi, B. Peaudecerf, S. Pascazio, C. Sayrin, I. Dotsenko, S. Gleyzes, M. Brune, and S. Haroche, "Quantum Zeno dynamics of a field in a cavity," Phys. Rev. A **86**, 032120 (2012).

1. Introduction

Quantum information processing (QIP) has dramatically changed the way we view information. By tying it firmly with physical systems, the bits and pieces of information ceased to be theoretical constructs and became bound by their carriers' physical properties. In some areas this is limiting [1], but in others it has shown new ways of tackling difficult computational tasks [2]. In order to utilize quantum states for QIP, one needs to be able to effectively manipulate them. This is usually a daunting task, as any nontrivial manipulation tends to be accompanied by decoherence which deteriorates the quantum information of the states. An effective method of lessening the impact of decoherence employs the teleportation-based-QIP paradigm [3–5], in which the on-line operation is carried out deterministically with a help of a specifically prepared ancillary *resource* state, simple operations, measurement, and feedforward. In this way, the task of performing a universal quantum operation is translated to the task of generating a specific quantum state. This is usually much less of an issue, especially since the state can be, in principle, prepared by probabilistic means and then stored until it is needed.

In continuous variables (CV) quantum information processing, the currently readily available Gaussian operations [5, 6] allow us to straightforwardly prepare any Gaussian state - a state which can be described solely by Gaussian functions. However, in order to move out of this subset, a non-Gaussian operation is required. While none is available, which is deterministic, there is a probabilistic one, which has become a staple of CV quantum optics experiments.

Single-photon detection, which can be physically implemented with help of single-photon on-off detectors, conditionally induces the states with a strongly non-Gaussian behavior [7–9]. When a series of photon subtractions (or, alternatively, additions) is accompanied by suitable displacements, it can be used to generate arbitrary superpositions of Fock states up to the number of subtractions used [10, 11]. Any finite energy quantum state can be, with any desired accuracy, realized as a finite superposition of Fock states if all the required features are obtained. This approach has been suggested for deterministic implementation of highly nonlinear weak cubic quantum gate [12], which is a basic element of CV quantum information processing.

In the past, photon subtractions accompanied by displacements have been used to generate superpositions of zero and one photon [13] and superpositions of up-to two photons [14]. These experiments, however, were carried out with pulsed lasers and are therefore not compatible with the current teleportation-based quantum operations [15–18]. This is because it is difficult to apply measurement and feedforward to those generated states which have a bandwidth of more than a few GHz. In this paper, we develop an experimental scheme using a continuous-wave (cw) laser as a light source to generate arbitrary superposition states with a bandwidth of 10 MHz. In particular, we generate superposition states of up-to three photons. The generated states are applicable to the current teleportation-based quantum operations [15–18], and thus can be readily used to implement non-Gaussian gates. The generated states remarkably exhibit multiple negative areas of Wigner function, which can be not only exploited as better resource for CV quantum information processing [19], but also to completely characterize fundamental decoherence process of nonclassical states [20] from point of view of evolving system and environment.

The way the single-photon detections generate arbitrary superpositions of Fock states can be easily understood by considering an initial two-mode squeezed vacuum, which can be experimentally prepared by non-degenerate parametric process. It is expressed in the basis of photon number states $|n\rangle$ as

$$|\psi\rangle_{s,i} \propto \sum_n q^n |n\rangle_s |n\rangle_i, \tag{1}$$

where the characters s and i denote the signal and idler modes, respectively. The quantity q ($0 \leq q < 1$) depends on the pump power and the nonlinear coefficient of the nonlinear crystal. Linear optics is now used to split the idler mode into three, and to displace each of these modes i_1, i_2, and i_3 by coherent amplitudes β_1, β_2, and β_3. The idler modes are then measured by single-photon detectors and when the three-fold coincidence occurs, the signal mode is projected into the desired superposition state. In the limit of small pump power and small displacements, we can represent the projection process by

$$|\psi\rangle_s \propto \langle 0|_i \left(\frac{a}{\sqrt{3}} + \beta_1 \right) \left(\frac{a}{\sqrt{3}} + \beta_2 \right) \left(\frac{a}{\sqrt{3}} + \beta_3 \right) |\psi\rangle_{s,i}, \tag{2}$$

where a is an annihilation operator acting on the idler mode, which represents the single-photon detection. The factor $\frac{1}{\sqrt{3}}$ arises from the splitting of the initial idler mode into the three separately measured modes. The output state then looks as

$$\begin{aligned} |\psi\rangle_s \propto{} & \beta_1 \beta_2 \beta_3 |0\rangle_s + \frac{q}{\sqrt{3}} (\beta_1 \beta_2 + \beta_2 \beta_3 + \beta_3 \beta_1) |1\rangle_s \\ & + \frac{\sqrt{2}}{3} q^2 (\beta_1 + \beta_2 + \beta_3) |2\rangle_s + \frac{\sqrt{2}}{3} q^3 |3\rangle_s. \end{aligned} \tag{3}$$

We can see that generating arbitrary superpositions of Fock states from zero to three is only a matter of finding suitable values of the three displacement amplitudes. Similarly, with higher number of single-photon detectors, a superposition of higher Fock states would be viable.
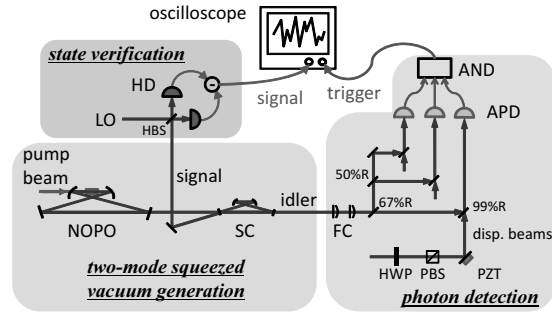
Fig. 1. Schematic of the experiment. The output of HD is recorded by a digital oscilloscope when a trigger is obtained. Triggers are obtained from an AND circuit when all of three APDs have clicks simultaneously. NOPO, non-degenerate optical parametric oscillator; SC, split cavity; FC, filter cavity; HD, homodyne detector; APD, avalanche photo diode; HBS, half beamsplitter; HWP, half-wave plate; PBS, polarization beamsplitter; PZT, piezo electric transducer.

2. Experimental setup

A schematic of the experiment is shown in Fig. 1. The light source is a cw Ti:Sapphire laser of 860 nm. In order to generate a two-mode squeezed vacuum, around 20 mW of pump beam of 430 nm is injected into a non-degenerate optical parametric oscillator (NOPO), which contains a periodically-poled $KTiOPO_4$ crystal as an optical nonlinear crystal. The pump beam is generated by second harmonic generation of the fundamental beam, and frequency-shifted with an acousto-optic modulator by around 600 MHz (equal to free spectral range of NOPO, $\Delta\omega$). As a result, photon pairs of frequency ω (signal) and $\omega + \Delta\omega$ (idler) are obtained. The output photons are spatially separated by a split cavity whose free spectral range is $2\Delta\omega$. The photons of frequency $\omega + \Delta\omega$ passing through the split cavity are sent to two frequency filtering cavities [21], and are split into three beams with beamsplitters. Each beam is interfered with displacement beams at mirrors of 99% reflectivity. Phase of displacement is controlled by piezo electric transducers, and amplitude of displacement is controlled by rotating half-wave plates followed by polarization beamsplitters. The idler beams are coupled to optical fibers to be sent to avalanche photo diodes (APDs, Perkin-Elmer, SPCM-AQRH-14 and SPCM-AQRH-16). The APDs output electronic pulses when they detect photons. The outputs are combined into an AND circuit to get three-fold coincidence clicks.

The signal beam is measured by homodyne detection with local oscillator beam of 10 mW. The homodyne current is sent to an oscilloscope and stored on every coincidence click. The density matrix and Wigner function of the output state are numerically reconstructed from a set of measured quadratures and phases of the local oscillator beam [22, 23].

The presented experimental setup is capable of generating arbitrary superpositions of up-to three photons, simply by choosing a proper array of displacement parameters. To showcase this ability, we have generated a trio of quantum states, each of them strongly dependent on its three photon component.
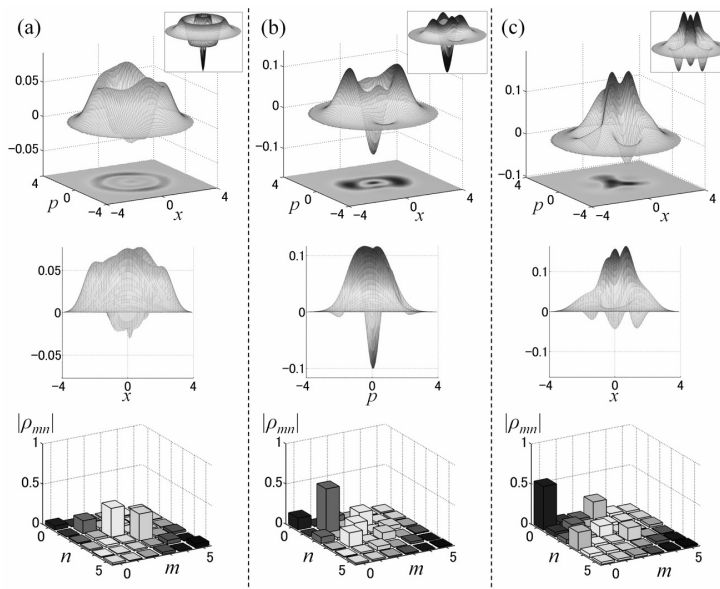
3. Results and discussions

Fig. 2. The experimentally reconstructed density matrices and Wigner functions ($\hbar = 1$). (a) Three photon state, (b) coherent state superposition, (c) superposition of zero- and three-photon state with $s = 0.86q$. The small insets of Wigner functions of the ideal states are shown for comparison.

At first, we generate the key resource, the three photon Fock state $|3\rangle$, which can be obtained without using any displacements. The defining features of this state are the distinctive presence of the three photon component, and the distinctive lack of presence of higher photon numbers. The density matrix reconstructed from 5000 data points is shown in Fig. 2(a) and it exhibits both the features mentioned. The three photon element $\rho_{33} = 0.33$ plays a significant role and the whole state is fairly well contained in the three photon subspace, with higher photon numbers populated only in 10 percent of the cases. Note that ρ_{33} is equal to the fidelity of the state, which is defined as the overlap $F = \langle \psi | \rho_{exp} | \psi \rangle$ of the experimentally generated state ρ_{exp} with the ideal state $|\psi\rangle$. The two photon and one photon contributions are caused by the experimental imperfections, such as optical losses and dark counts of the photon detectors, while the presence of higher photon numbers is caused by the strong pump power, which needed to be large enough to allow for a sufficient count rate (20 counts per minute). Despite the imperfections, the Wigner function of the three photon state, also shown in Fig. 2(a), displays all the features one would expect from the three photon Fock state: it is spherically symmetrical and along any cut in the phase space it exhibits three distinctive regions of negativity.

The second generated state is the superposition of Fock states $|1\rangle$ and $|3\rangle$, which is achieved

by using displacements $\beta_1 = -\beta_2 = \sqrt{2}q$ and $\beta_3 = 0$. For suitably selected parameters, this state is a good approximation of the coherent state superposition $|\text{CSS}\rangle \propto |\alpha\rangle - |-\alpha\rangle$, which can play a very important role in quantum information processing [19]. To be of use, the coherent state superposition needs to have a large enough amplitude. This comes with a very distinct feature: the wave function of a coherent state superposition has an infinite number of intersections with the horizontal axis. This has a consequence for the state's Wigner function - as the amplitudes of the coherent states grow, the number of regions of negativity should increase as well. In the past, approximations of odd superpositions of coherent states for travelling field of light were generated by squeezing a single photon (or by subtracting a photon from a squeezed state) [18, 21, 24, 25]. However, the states generated by this approach always have only a single region of negativity, no matter their apparent amplitude, which severely limits their potential applications. In order to obtain more regions of negativity and, consequently, more faithful approximations of coherent states superposition with higher amplitudes, one should employ higher photon numbers during the generation.

By doing exactly that, we have generated a state which is a good superposition of coherent state superposition with $\alpha = 1.3$. The fidelity with the ideal coherent state superposition was found to be $F = 0.6$. However, the state is actually a squeezed coherent state superposition - subsequent antisqueezing could increase the amplitude to $\alpha = 1.6$ while simultaneously increasing the state fidelity to $F = 0.61$. In this sense, what was actually generated was the non-Gaussian keystone for a larger coherent state superposition [26, 27]. Its density matrix and Wigner function, reconstructed from 10000 data points, can be seen in Fig. 2(b). The count rate is around 100 counts per minute. The three photon nature of the generated state is manifest in presence of three regions of negativity, which is exactly the number one would expect from a coherent state superposition with amplitude $\alpha = 1.6$. The presence of elements corresponding to Fock states 0 and 2 is again caused by losses at various stages of the experiment. By obtaining the multiple areas of negativity resulting from higher interference effects of the coherent states, we have reached a quality of state preparation previously obtained only for field in a cavity [20, 28].

The third generated state is the superposition of Fock states $|0\rangle$ and $|3\rangle$, which needs three different displacements during the state preparation stage, $\beta_1 = se^{i\frac{\pi}{6}}$, $\beta_2 = se^{i\frac{5\pi}{6}}$ and $\beta_3 = se^{i\frac{3\pi}{2}}$, where s is the displacement amplitude. Such the state is a good approximation of a different kind of coherent state superposition - $|\alpha\rangle + |\alpha e^{i\frac{2\pi}{3}}\rangle + |\alpha e^{-i\frac{2\pi}{3}}\rangle$, which can be seen as a sample qutrit state encoded in the coherent state basis. This coherent state basis is orthogonal in the limit of large α, but similarly to the coherent state qubit basis, there is also a completely orthogonal basis formed of superpositions of Fock states invariant to $2\pi/3$ phase space rotation: $|0\rangle + \frac{\alpha^3}{\sqrt{6}}|3\rangle + \cdots$, $|1\rangle + \frac{\alpha^3}{2\sqrt{6}}|4\rangle + \cdots$, and $|2\rangle + \frac{\alpha}{2\sqrt{15}}|5\rangle + \cdots$. We have succeeded in generating the first of these basis states and the density matrix, reconstructed from 4000 data points, together with the Wigner function are shown in Fig. 2(c). The count rate is 50 counts per minute. We can see that the state is strongly nonclassical, with three areas of negativity, and that it possesses distinctive rotational $2\pi/3$ symmetry, which is exactly as predicted by the theory. The fidelity with the ideal state is $F = 0.61$. Recently, an alternative procedure of similar state preparation for a field stored in a cavity has been suggested [29].

In all the presented results, there are minor contributions of photon number elements not agreeing with the idealistic expectations. Contributions of Fock states 4 and higher are generally caused by strong pumping, which was necessary in order to achieve a sufficient count rate. Undesirable photon number elements of less than three photons are caused by optical losses and dark counts of photon detectors. It should be pointed out, though, that all the states were reconstructed on a six dimensional Hilbert space without any loss correction. This is in stark contrast to previous work focused at generating superpositions of photon number states up to

two [14], where correction of 45% loss was required to counteract low quantum efficiency of the detection. In our case, the high interference visibility of homodyne detection (97%) and high quantum efficiency of photo diodes (99%) add to the overall quantum efficiency for the whole experimental setup of 78%. Consequently, the states could be reconstructed without loss correction and they are therefore suitable for use as ancillae in teleportation-based quantum operations in advanced CV quantum information processing.

4. Conclusion

We have constructed an experimental setup based on a cw laser, which is capable of generating superpositions of Fock states up to three. Since we used a cw laser as a light source, the generated states are compatible with teleportation-based CV quantum information processing [15–18]. We have tested the experimental setup by generating three characteristic states - the three photon Fock state to demonstrate the three-photon capability, and two superpositions to show that the nonclassical behavior can be also realized in a superposition. We have observed strong nonclassical features, manifesting in multiple areas of negativity, which were in good agreement with theoretical expectations, even without using any form of loss correction. This was made possible by high quantum efficiency of the experimental setup, which is indispensable for use in teleportation-based QIP. The scheme can also allow us to observe fundamental aspects of quantum decoherence of highly nonclassical states [20], giving us access to both the evolving system and the environment. The experimental setup is not limited just to the preparation of the three states - arbitrary superpositions of Fock states of up-to three can be generated by using suitable array of displacements. This, in combination with high quantum efficiency of the setup and the cw platform ready for integration with an array of CV gates, makes this scheme a strong tool in the future CV non-Gaussian quantum information processing.

Acknowledgments

Implementation of a quantum cubic gate by an adaptive non-Gaussian measurement

Kazunori Miyata,[1,*] Hisashi Ogawa,[1] Petr Marek,[2] Radim Filip,[2] Hidehiro Yonezawa,[3]
Jun-ichi Yoshikawa,[1] and Akira Furusawa[1,†]

[1]*Department of Applied Physics, School of Engineering, The University of Tokyo, 7-3-1 Hongo, Bunkyo-ku, Tokyo 113-8656, Japan*
[2]*Department of Optics, Palacký University, 17. listopadu 1192/12, 77146 Olomouc, Czech Republic*
[3]*Centre for Quantum Computation and Communication Technology, School of Engineering and Information Technology,
University of New South Wales Canberra, Australian Capital Territory 2610, Australia*

We present a concept of non-Gaussian measurement composed of a non-Gaussian ancillary state, linear optics, and adaptive heterodyne measurement, and on the basis of this we also propose a simple scheme of implementing a quantum cubic gate on a traveling light beam. In analysis of the cubic gate in the Heisenberg representation, we find that nonlinearity of the gate is independent from nonclassicality; the nonlinearity is generated solely by a classical nonlinear adaptive control in a measurement-and-feedforward process, while the nonclassicality is attached by the non-Gaussian ancilla that suppresses excess noise in the output. By exploiting the noise term as a figure of merit, we consider the optimum non-Gaussian ancilla that can be prepared within reach of current technologies and discuss performance of the gate. It is a crucial step towards experimental implementation of the quantum cubic gate.

I. INTRODUCTION

Development and application of quantum physics crucially rely on progress in quantum operations with various physical systems. For discrete-variable systems, a basic controlled-NOT nonlinear gate [1] has been already demonstrated with many systems [2–5] and the current problem is scalability of their implementations. On the other hand, for more complex continuous-variable (CV) systems [6], a full set of basic operations has not been closed yet. It was proven that in order to synthesize an arbitrary unitary operation, it is enough to add a cubic nonlinear operation to the already existing Gaussian operations [7]. Any nonlinearity can be principally obtained from a chain of the Gaussian operations, the cubic nonlinearity, and feedforward corrections [7,8]. The cubic nonlinearity is therefore a bottleneck of CV quantum physics.

Already a decade ago, Gottesman, Kitaev, and Preskill (GKP) suggested a way to implement a cubic nonlinear gate based on Gaussian operations, Gaussian measurement, quadratic feedforward correction, and an ancillary cubic state produced by the cubic nonlinearity [9]. Various approaches towards the cubic gate have followed [10–13]. Particularly in the field of quantum optics, most of the components of the cubic gate have been experimentally demonstrated, mainly because of the high quality of generating squeezed states and efficient homodyne detection. The Gaussian operations have been already mastered [14–16], utilizing a concept of measurement-induced operations [17]. Furthermore, they have been tested on non-Gaussian states of light [18] to prove their general applicability. Recently, the quadratic electro-optical feedforward control has been demonstrated [19]. In addition, to independently obtain the cubic state, a finite dimensional approximation of the cubic state has been suggested [20] and its performance in the GKP scheme has been discussed. The cubic

state has been experimentally generated as a superposition of photons and verified [21]. Potentially, such a superposition state can be stored in and retrieved from recently developed optical quantum memories [22,23]. In order to make resource nonclassical states compatible with the measurement-based scheme, real-time quadrature measurement of a single-photon state has been demonstrated [24].

A drawback of the original GKP idea is that it requires to implement the quantum nondemolition gate, i.e., the CV controlled-NOT gate [17], and a squeezing feedforward that depends on the measurement result. While each of them has been already demonstrated [15,19], the total implementation to build a unitary cubic operation demands three squeezed states as well as one non-Gaussian ancilla and is probably not the simplest arrangement. In contrast, we here use adaptability of linear optical schemes and propose a better and simpler topology with linear optics and suitable ancillary states.

Our approach is to tuck all the non-Gaussian aspects into the measurement process. The topology will be then similar to the simple one used for a measurement-induced squeezing gate [14,17–19,25]. Non-Gaussian operations can be realized by simply substituting a measurement of nonlinear combination of quadrature amplitudes for the Gaussian homodyne measurement [26,27]. We construct such a measurement in a form of a generalized non-Gaussian measurement by combining ordinary Gaussian measurement tools with non-Gaussian ancillary states that can be prepared with photon detection. In fact, we can exploit arbitrary superpositions of photon-number states up to certain photon level within reach of current technologies [21,28,29].

In this paper, we first provide an idea of non-Gaussian measurement comprising a non-Gaussian ancillary state, linear optics, and adaptive heterodyne measurement. Using the non-Gaussian measurement, we next propose a simple schematic of a quantum cubic gate based on the measurement-induced operation scheme, whose resource states are only one squeezed vacuum and one non-Gaussian state. While in previous work the input-output relation of the cubic gate has been investigated

---

*miyata@alice.t.u-tokyo.ac.jp
†akiraf@ap.t.u-tokyo.ac.jp

in the Schrödinger picture, here we analyze the gate in the Heisenberg picture to include imperfections in the scheme. We then find that nonlinearity of the gate is independent from nonclassicality. Specifically, the nonlinearity is generated solely by a classical nonlinear adaptive control in a measurement-and-feedforward process regardless of the non-Gaussian ancilla. On the other hand, the nonclassicality is attached by the ancilla that compensates residual noise in the output. Finally, we discuss an overall performance of the cubic gate in such a topology and consider non-Gaussian ancillary superposition states up to a certain photon level to investigate how well the unwanted noise can be suppressed in the gate.

II. MINIMAL IMPLEMENTATION OF MEASUREMENT-INDUCED QUANTUM OPERATIONS

A measurement-induced quantum operation scheme [17] decomposes various quadratic operations into linear optics, displacement operation, homodyne detection, and offline squeezed light beams, which are readily available in actual optical experiments. One of the realizations of the scheme is the basic squeezing gate. First we combine an input state $|\psi\rangle$ and an eigenstate $|x = 0\rangle$ of the position quadrature $\hat{x}$ at a beam splitter whose transmittance is represented by $\sqrt{T}$. We then measure the momentum quadrature $\hat{p}$ of one of the optical modes and obtain a value y. Finally, we apply displacement to the p quadrature of the remaining mode with the value $p_{\text{disp}} = \sqrt{(1 - T)/T}\, y$ and obtain a squeezed output state. Ideally the output is a pure state $\hat{S}|\psi\rangle$, where $\hat{S}$ is an x-squeezing operator defined as $\hat{S}^\dagger \hat{x} \hat{S} = \sqrt{T}\hat{x}$ and $\hat{S}^\dagger \hat{p} \hat{S} = \hat{p}/\sqrt{T}$. In the case of implementing p squeezing, it is enough to replace the ancillary x eigenstate with the p eigenstate $|p = 0\rangle$ and exchange the roles of x and p quadratures. This type of operation has been successfully demonstrated in [14,18], where the position eigenstate is replaced with the squeezed vacuum.

On the basis of one-way CV cluster computation [26,27], we can generalize the basic squeezing gate to minimal single-mode implementation of arbitrary-order quantum operations as shown in Fig. 1. The homodyne detector in the squeezing gate is now replaced with a detector that measures a general quadrature $\hat{U}_n^\dagger(\hat{x})\hat{p}\hat{U}_n(\hat{x})$, where the unitary operator $\hat{U}_n(\hat{x})$ is defined as nth-order *phase gate* $\hat{U}_n(\hat{x}) = \exp(i\gamma\hat{x}^n)$ with a real parameter γ. Hereafter we set $\hbar = 1$ for simplicity. The measured general quadrature is thus $\hat{p} + n\gamma\hat{x}^{n-1}$. In the ideal

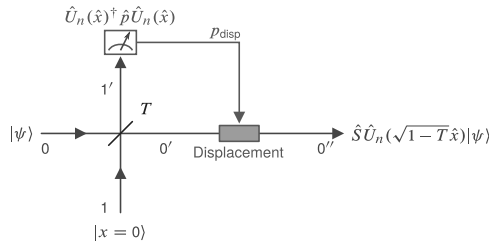

FIG. 1. Minimal single-mode implementation of measurement-induced quantum operation.

case, the output state is expressed as $\hat{S}\hat{U}_n(\sqrt{1 - T}\hat{x})|\psi\rangle$. This gate deterministically applies the phase gate to the input state with the additional constant squeezing that can be compensated by another squeezer.

It is known that an arbitrary single-mode unitary can be decomposed into the set of gates $\hat{U}_n(\hat{x})$ for $n = 1,2,3$ for all $\gamma \in \mathbb{R}$, together with the $\pi/2$ phase shift [8,27]. This also holds when we exploit the minimal implementation in Fig. 1. $\hat{U}_1(\hat{x})$ is the trivial displacement operation, and $\hat{U}_2(\hat{x})$ has been experimentally demonstrated [19,25]. The remained task is thus to realize a cubic gate $\hat{U}_3(\hat{x})$. We now consider how to construct measurement of the nonlinear quadrature $\hat{p} + 3\gamma\hat{x}^2$ with affordable apparatuses, as explained in the following sections.

III. NON-GAUSSIAN MEASUREMENT BY GENERALIZED HETERODYNE DETECTION

A. Projecting on pure states

In quantum physics, measurements are represented by operators. In the simplest case of von Neumann measurements, these operators are simply projectors on particular quantum states. In the case of the keystone measurement of CV quantum optics, the homodyne detection, each measurement result indicates that the measured state was projected on an eigenstate of the measured quadrature operator. Analogously, the heterodyne detection, which can be modeled by a pair of homodyne detectors simultaneously measuring conjugate quadratures of a mode split by a balanced beam splitter [30], implements a projection onto a coherent state. Both of these kinds of measurements are Gaussian—the measured quadrature distribution is Gaussian if the measured state is Gaussian.

One way to achieve a non-Gaussian measurement is to take advantage of non-Gaussian states in combination with the standard heterodyne detection schemes. The basic idea of the measurement is best explained in the x representation. Consider that we have a standard heterodyne detection configuration, where the idle port of the beam splitter is not injected by a vacuum but by a specifically prepared ancillary state $|\psi_A\rangle = \int \psi_A(x)|x\rangle dx$. For a particular pair of measurement results q and y, the procedure implements projection onto a state

$$\hat{D}(\sqrt{2}q + i\sqrt{2}y)\hat{\mathcal{T}}|\psi_A\rangle. \qquad (1)$$

Here $\hat{D}(\alpha) = \exp\{i\sqrt{2}\hat{x}\,\text{Im}[\alpha] - i\sqrt{2}\hat{p}\,\text{Re}[\alpha]\}$ stands for the displacement operator and $\hat{\mathcal{T}}$ is the time-reversal antiunitary operator represented by $\hat{\mathcal{T}}^\dagger\hat{x}\hat{\mathcal{T}} = \hat{x}$ and $\hat{\mathcal{T}}^\dagger\hat{p}\hat{\mathcal{T}} = -\hat{p}$. To derive the expression (1), we can start with the projection states of the pair of homodyne detectors

$$\langle x_1 = q|\langle p_2 = y|. \qquad (2)$$

If we take into account the unitary balanced beam splitter, the projection state becomes

$$\int dx_2 \left\langle \frac{q + x_2}{\sqrt{2}} \middle| \left\langle \frac{-q + x_2}{\sqrt{2}} \middle| e^{-iyx_2}. \qquad (3)$$

During the measurement, this state will be jointly projected onto the measured and the ancillary state. The measured state

is unknown, but we can already apply the ancilla in the second mode. This reduces the state to

$$\int dx \left\langle \frac{q+x}{\sqrt{2}} \middle| \psi_A\left(\frac{-q+x}{\sqrt{2}}\right) e^{-iyx}, \right. \tag{4}$$

where the subscript was dropped because it was no longer needed. After a straightforward substitution we can express the projection state as

$$\int dx\, \psi_A^*(x) e^{i\sqrt{2}xy} |x + \sqrt{2}q\rangle. \tag{5}$$

Since the time-reversal operator corresponds to complex conjugate in the x representation, the expression (5) is the same as Eq. (1). For $q = y = 0$, we obtain simple projection onto the given ancillary state $\int \psi^*(x)|x\rangle dx$. We can see that if the ancillary mode is in the vacuum or a coherent state, the measurement remains the simple heterodyne detection, as is expected. However, if the ancilla is non-Gaussian, we obtain a truly non-Gaussian measurement.

B. Projecting on impure states

In a realistic scenario, the ancillary state will be generally not pure. To take this into account, it is best to abandon the x representation and employ the formalism of Wigner functions. The basic premise, however, remains. The measurement still implements projection onto a specific state, only this time the state will be represented by a Wigner function. Specifically, for a signal two-mode state represented by a Wigner function $W_S(x_0, p_0, x_1, p_1)$, the outcome of a measurement performed on mode 1 yielding a pair of values q and y results in the Wigner function

$$W_{out}(x_0, p_0 | q, y)$$
$$\propto \int dx_1 dp_1 W_S(x_0, p_0, x_1, p_1) W_M(x_1, p_1 | q, y), \tag{6}$$

where the function $W_M(x_1, p_1 | q, y)$ represents the projector on the particular state. In our scenario, in which the pair of homodyne detectors are supplied with an ancillary state corresponding to a Wigner function $W_A(x, p)$, the projector function can be found as

$$W_M(x, p | q, y) = 2 W_A(x - \sqrt{2}q, -p + \sqrt{2}y). \tag{7}$$

We can see that this form agrees with Eq. (1) if we realize that the time-reversal operator $\hat{\mathcal{T}}$ transforms the Wigner function variables as $(x, p) \mapsto (x, -p)$. The relation (7) can be derived in the same way as relation (1). We start with the homodyne measurement projector functions, here represented by the pair of δ functions $\delta(x_1 - q)\delta(p_2 - y)$, which we then propagate through the beam splitter and apply to the ancillary state, resulting in

$$W_M(x_1, p_1 | q, y) = \int dx_2 dp_2 W_A(x_2, p_2) \delta\left(\frac{x_1 - x_2}{\sqrt{2}} - q\right)$$
$$\times \delta\left(\frac{p_1 + p_2}{\sqrt{2}} - y\right). \tag{8}$$

C. Arbitrary Gaussian operations within the measurement

One may desire to apply Gaussian operation to the non-Gaussian ancilla because some Gaussian operations (such as squeezing) enhance certain features of the state. Here we show that, instead of projecting on a raw non-Gaussian state, we can alter the measurement so it projects on a non-Gaussian state altered by an arbitrary Gaussian operation. This can be enormously useful because we do not need to implement an additional Hamiltonian that often makes the state impure in actual experiments. Note that we are disregarding displacement because that can be achieved simply by displacing the measurement results. For a pair of quadrature variables x and p, an arbitrary Gaussian operation is represented by a real two-by-two symplectic matrix S whose elements satisfy $s_{11}s_{22} - s_{12}s_{21} = 1$. If we consider that phase shift can be implemented "for free," the arbitrary Gaussian unitary transformation reduces to

$$x' = z_1 x, \quad p' = \frac{1}{z_1}p + z_2 x, \tag{9}$$

where z_1 and z_2 are arbitrary real parameters. To achieve this transformation, we must modify the measurement setup in two ways. First, the balanced beam splitter in Eq. (3) will be removed and replaced by a beam splitter with transmittance T and reflectance $R = 1 - T$. Second, instead of measuring quadrature p_2 we measure quadrature $p_2(\theta) = p_2 \cos\theta + x_2 \sin\theta$. The projection functions of the measurements themselves in Eq. (8) are then

$$\delta(x_1 - q)\delta(p_2 \cos\theta + x_2 \sin\theta - y). \tag{10}$$

Using the same steps we used to arrive at Eq. (7) we can now obtain the generalized projection function

$$W_M(x, p | q, y) = \frac{1}{|\sqrt{RT}\cos\theta|} W_A\left(\sqrt{\frac{T}{R}}x - \frac{q}{\sqrt{R}}, -\sqrt{\frac{R}{T}}p \right.$$
$$\left. -\frac{\tan\theta}{\sqrt{RT}}x + \frac{q\tan\theta}{\sqrt{R}} + \frac{y}{\sqrt{T}\cos\theta}\right). \tag{11}$$

We can immediately see that after the time-reversal operations, we have $z_1 = \sqrt{T/R}$ and $z_2 = \tan\theta/\sqrt{RT}$ and these two parameters can attain arbitrary real values. As a consequence, after addition of a phase shift the function (11) implements projection onto the ancillary state altered by an arbitrary Gaussian operation.

It is worth pointing out that the two homodyne measurements need not be independent. One of the measurements can have parameters changing based on the results of the other one, thus creating a sort of adaptive measurement scheme. For example, the measurement phase θ can depend on the measurement result q. This can be used to induce a nonlinear behavior, as we see in Sec. IV B.

IV. IMPLEMENTATION OF A CUBIC GATE

A. With nonadaptive non-Gaussian measurement

In this section we apply the non-Gaussian measurement to a particular task: the implementation of a nonlinear cubic gate $\hat{U} = e^{i\gamma\hat{x}^3}$ to an arbitrary quantum state. In terms of quadrature

operators, the gate performs transformation

$$\hat{x}' = \hat{x}, \quad \hat{p}' = \hat{p} + 3\gamma\hat{x}^2. \tag{12}$$

Before proceeding to a scheme with the adaptive heterodyne measurement, we first consider implementation with nonadaptive measurement expressed by Eq. (1).

The basic principle of the operation can be quickly explained in the x representation. The unknown input state $|\psi\rangle$ is mixed with a squeezed state on a balanced beam splitter. If we for ease of explanation consider the infinite squeezing, the resulting two-mode state can be expressed as

$$\int dx\, \psi(x) \left| \frac{x}{\sqrt{2}} \right\rangle \left| \frac{x}{\sqrt{2}} \right\rangle. \tag{13}$$

After applying non-Gaussian measurement (4) on one of the modes, we obtain the projected state in the form

$$\int dx\, \psi_{\rm A}\left(\frac{x}{\sqrt{2}} - \sqrt{2}q \right) \psi(x) e^{-ixy} \left| \frac{x}{\sqrt{2}} \right\rangle, \tag{14}$$

where q and y are again the homodyne measurement results and $\psi_{\rm A}(x)$ is the wave function of the ancillary state. For implementing the cubic gate, $\psi_{\rm A}(x)$ has to be cubically dependent on x and is ideally in a state

$$|\psi_{\rm A}\rangle = \int dx\, \exp(i\gamma x^3)|x\rangle \tag{15}$$

and the whole operation would lead to

$$\exp(-i3\sqrt{2}\gamma q\hat{x}^2) \exp[i(6\gamma q^2 - \sqrt{2}y)\hat{x}] \exp(i\gamma\hat{x}^3)$$
$$\times \int dx\, \psi(x) \left| \frac{x}{\sqrt{2}} \right\rangle. \tag{16}$$

This is almost exactly the desired output state. The only difference is a constant squeezing and two unitary operations depending on the measured values. The constant squeezing can be fully compensated either before or after the operation and the measurement-dependent unitary operations can be removed by a proper feedforward. This is exactly the same principle as employed by the CV teleportation and CV measurement-induced operations. While each particular measurement result projects on a different quantum state, these states belong to the same family and the proper operation can smear the differences and produce a quantum state independent of the measurement result. This allows the whole procedure to operate deterministically.

B. With adaptive non-Gaussian measurement

In Eq. (16) we need quadratic feedforward in the form of adjustable squeezing. Thus, the topology here is not as simple as the minimal implementation depicted in Fig. 1. To realize measurement of the nonlinear quadrature $\hat{p} + 3\gamma\hat{x}^2$, we exploit the adaptive non-Gaussian heterodyne measurement. According to the results in Sec. III C, by altering the phase of the second measurement, we can project onto a transformed
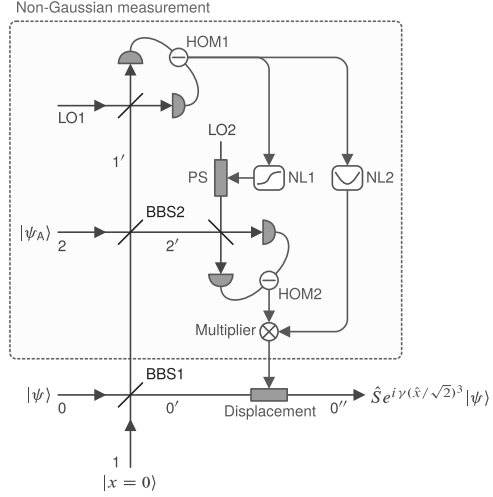

FIG. 2. Schematic of a cubic gate. BBS, balanced beam splitter; HOM, homodyne measurement; LO, local oscillator; PS, phase shift; NL, nonlinear classical calculation. While all the optics are linear, the classical circuit involves nonlinear calculations that makes the feedforward nonlinear. The nonlinear classical circuits have been already devised in the experiment of dynamic squeezing [19].

ancillary state,

$$\hat{D}\left[\sqrt{2}q + i\left(\frac{\sqrt{2}y}{\cos\theta} - \sqrt{2}q\tan\theta \right) \right] \hat{\mathcal{T}} e^{i\hat{x}^2\tan\theta} |\psi_{\rm A}\rangle. \tag{17}$$

Again, q and y are the measured values in the heterodyne detection, and $|\psi_{\rm A}\rangle$ is the cubic state (15). We then substitute $3\sqrt{2}\gamma q$ for $\tan\theta$. After simple algebras we find the projection state

$$\exp(-i\gamma\hat{x}^3)\left| p = \frac{\sqrt{2}y}{\cos\theta} \right\rangle, \tag{18}$$

which means an eigenstate of the nonlinear quadrature $\hat{p} + 3\gamma\hat{x}^2$ with the eigenvalue $\sqrt{2}y/\cos\theta$. This scheme can be illustrated as Fig. 2. Here the quadrature basis of the second homodyne detection is determined by the result of the first homodyne detection. As a result, the heterodyne detection and the classical calculation compose a module of non-Gaussian measurement, and the feedforward is now the simple displacement operation. After all, the required optical operations are displacement and beam splitters together with homodyne measurements, all of which are ubiquitous in quantum-optical experiments.

To explicitly show how this scheme works, it is instructive to employ the Heisenberg representation, which would have the added benefit of incorporating the imperfections arising from the realistic experimental implementation, e.g., finite squeezing. Let the unknown signal mode be labeled by "0" and described by quadrature operators $\hat{x}_0$ and $\hat{p}_0$. After combining

the initial state in mode "0" with the squeezed state in mode "1" and with the non-Gaussian ancilla in mode "2", the respective quadrature operators read

$$\hat{x}_0' = \frac{1}{\sqrt{2}}\hat{x}_0 - \frac{1}{\sqrt{2}}\hat{x}_1, \tag{19a}$$

$$\hat{p}_0' = \frac{1}{\sqrt{2}}\hat{p}_0 - \frac{1}{\sqrt{2}}\hat{p}_1, \tag{19b}$$

$$\hat{x}_1' = \frac{1}{2}\hat{x}_0 + \frac{1}{2}\hat{x}_1 - \frac{1}{\sqrt{2}}\hat{x}_2, \tag{20a}$$

$$\hat{p}_1' = \frac{1}{2}\hat{p}_0 + \frac{1}{2}\hat{p}_1 - \frac{1}{\sqrt{2}}\hat{p}_2, \tag{20b}$$

$$\hat{x}_2' = \frac{1}{2}\hat{x}_0 + \frac{1}{2}\hat{x}_1 + \frac{1}{\sqrt{2}}\hat{x}_2, \tag{21a}$$

$$\hat{p}_2' = \frac{1}{2}\hat{p}_0 + \frac{1}{2}\hat{p}_1 + \frac{1}{\sqrt{2}}\hat{p}_2. \tag{21b}$$

In the next step we measure the x quadrature of mode $1'$ and obtain value q. We can now use the value to adjust the measured phase of the second homodyne detector. In effect, we end up measuring the value y of quadrature operator $\hat{x}_2'\sin\theta + \hat{p}_2'\cos\theta$, where $\theta = \arctan(3\sqrt{2}\gamma q)$. Note that, since θ nonlinearly depends on q, which carries information of $\hat{x}_1$ quadrature, we can interpret this type of measurement as the origin of nonlinearity of the gate. The quadrature operators of the output mode can be now expressed in terms of the measured values as

$$\hat{x}_0' = \frac{1}{\sqrt{2}}\hat{x}_0 - \frac{1}{\sqrt{2}}\hat{x}_1, \tag{22a}$$

$$\hat{p}_0' = \sqrt{2}\hat{p}_0 + p_2 + \frac{3\gamma}{2}[(\hat{x}_0+\hat{x}_1)^2 - 2\hat{x}_2^2] - \frac{\sqrt{2}y}{\cos\theta}. \tag{22b}$$

The last term of the p quadrature, which is the only term explicitly depending on the measured values q and y, can be removed by a suitable displacement and we are then left with the final form of the operators:

$$\hat{x}_0'' = \frac{1}{\sqrt{2}}\hat{x}_0 - \frac{1}{\sqrt{2}}\hat{x}_1, \tag{23a}$$

$$\hat{p}_0'' = \sqrt{2}\left(\hat{p}_0 + \frac{3\gamma}{2\sqrt{2}}\hat{x}_0^2\right) + \left(\hat{p}_2 - 3\gamma\hat{x}_2^2\right) + 3\gamma\left(\hat{x}_0\hat{x}_1 + \frac{1}{2}\hat{x}_1^2\right). \tag{23b}$$

Both of the first terms in Eq. (23) represent the ideal cubic operation, i.e., combination of the cubic gate $e^{i\gamma(\hat{x}_0/\sqrt{2})^3}$ and the constant squeezing mentioned in Sec. II. Those terms do not depend on the quadratures of the other ancillary states. Differently from the output (16) in Sec. IV A, in the Heisenberg representation we can say that the cubic nonlinearity comes from the adaptive non-Gaussian measurement and feedforward regardless of the ancillary states.

Naturally, the ancillary states are still required to complete the operation since the outputs have residual terms. It is straightforward to find the ideal ancillary state in mode 1 as the

quadrature eigenstate $|x=0\rangle_1$ because the state affects only the last terms of Eq. (23) and they vanish when $\hat{x}_1 \to 0$. In experimental implementation, we approach the ideal state by using squeezed vacuum states.

On the other hand, the middle term of Eq. (23b), $\hat{p}_{\text{NLQ}} = \hat{p}_2 - 3\gamma\hat{x}_2^2$, depends solely on the ancilla in mode 2. This term vanishes when the ancilla is the ideal cubic state (15). This state is best approached by considering physical states that squeeze the nonlinear quadrature $\hat{p}_{\text{NLQ}}$, as discussed in the next section.

V. OPTIMAL ANCILLARY STATE

To find suitable states in mode 2, we can use the expectation value and the variance of the nonlinear quadrature $\hat{p}_{\text{NLQ}}$ as figures of merit, both of which should be approaching zero. Here we consider preparing the ancillary state that can be generated within reach of current technologies. On one hand, arbitrary superpositions of photon-number states up to the three-photon level $|\psi_{N=3}\rangle$ can be prepared [21,29], and the photon-number limit can, in principle, be incremented. On the other hand, we can perform universal Gaussian operation $\hat{U}_G$ onto any input state [14–16]. Then the ancilla best suited for our purposes can be found in a form $\hat{U}_G|\psi_N\rangle$ by optimizing over all superposition states up to N-photon level $|\psi_N\rangle$ and all Gaussian operations $\hat{U}_G$ that can be applied on the state afterwards. In this way, we are using the expensive non-Gaussian resources only for the key non-Gaussian features of the state [31].

Our goal is to find a state $\hat{U}_G|\psi_N\rangle$ that minimizes the expectation value $\langle\hat{p}_{\text{NLQ}}\rangle$ and the variance $V(\hat{p}_{\text{NLQ}}) = \langle(\hat{p}_{\text{NLQ}} - \langle\hat{p}_{\text{NLQ}}\rangle)^2\rangle$. The operator is symmetric with respect to space inversion, $\hat{x}_2 \to -\hat{x}_2$, and has a linear term of $\hat{p}_2$. Accordingly the relevant Gaussian operations are the p displacement represented by $\hat{p}_2 \to \hat{p}_2 + p_0$, and the x squeezing represented by $\hat{x}_2 \to \hat{x}_2/\lambda$ and $\hat{p}_2 \to \lambda\hat{p}_2$, where p_0 and λ are arbitrary real parameters. Thus, the nonlinear quadrature after suitable Gaussian operations is represented as

$$\hat{U}_G^\dagger\hat{p}_{\text{NLQ}}\hat{U}_G = \gamma^{1/3}\left[\lambda'\hat{p}_2 - 3\left(\frac{\hat{x}_2}{\lambda'}\right)^2\right] + p_0, \tag{24}$$

where $\lambda' = \lambda/\gamma^{1/3}$. From this point of view, we can see that the expectation value $\langle\hat{p}_{\text{NLQ}}\rangle$ vanishes when we apply suitable displacement p_0. On the other hand, the variance $V(\hat{p}_{\text{NLQ}})$ can be minimized by optimizing the state $|\psi_N\rangle$ and the parameter λ'. Furthermore, since λ' can be any real number, we can say that the optimum state does not depend on γ. We therefore use the variance of $\lambda'\hat{p}_2 - 3(\hat{x}_2/\lambda')^2$ as the actual figure of merit to derive the optimum state $|\psi_N\rangle$ and the corresponding parameter λ'.

Let V_N^{opt} be the minimum value of the variance $V(\hat{p}_{\text{NLQ}})$ with the optimum state $|\psi_N^{\text{opt}}\rangle$ and the optimal parameter λ'^{opt}. Note that V_0^{opt} represents the Gaussian limit, the minimum variances when the state is optimized over all Gaussian states. Then the relative noise $V_N^{\text{opt}}/V_0^{\text{opt}}$, as shown in Fig. 3, represents the ratio of the minimum noise to the Gaussian limit and is independent from γ. We can see that the variance decreases approaching zero with N and that even a state obtained as a superposition of zero and one photon gives
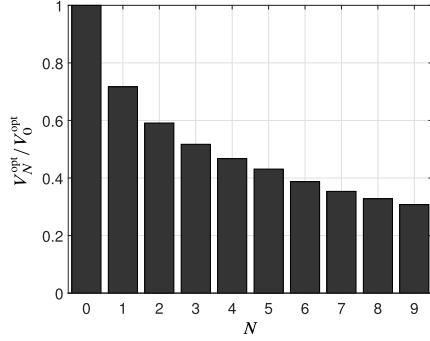
FIG. 3. Variances of the nonlinear quadrature with the optimized photon-number-state superpositions up to N photons, normalized by the Gaussian limit V_0^{opt}. The parameter λ' is optimized over to find the minimum of the variance.

a substantial benefit over the Gaussian limit. To present the optimized states, we represent the optimal approximate state up to the N-photon level by $|\psi_N^{\mathrm{opt}}\rangle = \sum_{n=0}^{N} c_n^{\mathrm{opt}}|n\rangle$ and plot absolute values of the coefficients in Fig. 4. The superposition of vacuum and single-photon states is readily available today, and generation of arbitrary superposition up to three photons has been demonstrated [21,29]. In the case of optimizing the superposition state up to three photons, the optimal
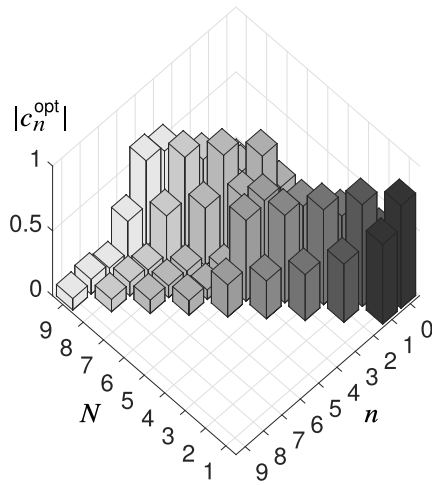

FIG. 4. Absolute values of the coefficients of the optimal finite approximation of ancillary states for various upper bounds of photon number N. Note that the coefficients of even-number photons are real and odd-number photons imaginary, due to the symmetry of the nonlinear quadrature $\hat{p} - 3\gamma\hat{x}^2$ with respect to $\hat{x} \to -\hat{x}$.

approximate state looks as

$$\left|\psi_{N=3}^{\mathrm{opt}}\right\rangle \propto 0.17|0\rangle - 0.56i|1\rangle - 0.73|2\rangle + 0.35i|3\rangle. \quad (25)$$

The state is different from the cubic state from [20] because of the different derivation of the states. In [20], the state was determined as if it was produced by applying the cubic gate to the vacuum without considering optimization over squeezing and displacement. On the other hand, the present state (25) is derived so that its overall suitability as the ancilla is maximized with suitable Gaussian operations. In either case, the state can be prepared by the same experimental method [21,29]. Note that, although the method can be adopted to generate the optimum superpositions up to arbitrary photon level, it is difficult to generate large-photon-number superposition states because the generation rate exponentially decays as the maximum photon number increases. This difficulty is expected to be remedied by exploiting a recently devised all-optical memory [22], which enables us to improve the generation rate and consequently to prepare superpositions up to four- or larger-photon-number states. Another way in the future could be to exploit quantum optomechanics with nanoparticles, which has a clear potential to produce the cubic states of mechanical oscillators in optical potential [32–34]. These mechanical states can be efficiently read out to another light mode [35] and then used as the optical cubic states.

The cubic nature of the states is also nicely visible from their Wigner functions as depicted in Fig. 5. For comparison, we check the Wigner function of the ideal cubic state [11],

$$W(x,p) = 2\pi\mathcal{N}\left|\frac{4}{3\gamma}\right|^{1/3} \mathrm{Ai}\left(\left[\frac{4}{3\gamma}\right]^{1/3}[3\gamma x^2 - p]\right), \quad (26)$$

where $\mathrm{Ai}(x)$ is the Airy function and $\mathcal{N}$ a temporary normalization factor. Since the ideal cubic state has infinite energy, it is unnormalizable. The Wigner function (26) is expediently normalized over the displayed area in Fig. 5(a). We can see that the Wigner function is symmetric with respect to the p axis and has an oscillating parabolic shape. These characteristics also appear in the approximate cubic states shown in Figs. 5(b)–5(e). We should point out that it is impossible to define meaningful fidelities between the ideal cubic state 5(a) and its approximate states 5(b)–5(e). The cubic state has infinite energy, and its Wigner function (26) has constant values along the parabolic lines on the phase space to the points at infinity. Therefore, the overlap between the ideal infinite-energy state and any finite-energy state should be zero. We can see that, however, as the upper limit of photon number becomes larger, the number of fringes along the p direction increases approaching the ideal one. Those Wigner functions of the approximate states can be considered to show core non-Gaussianity that then spreads out on the phase space by the following optimized squeezing.

So far we have not considered how to implement the optimized squeezing onto the core non-Gaussian state. Actually, instead of adding another squeezing gate, the squeezing operation can be embedded into the adaptive non-Gaussian measurement by using the results in Sec. III C. We discuss the details of it in Appendix A.

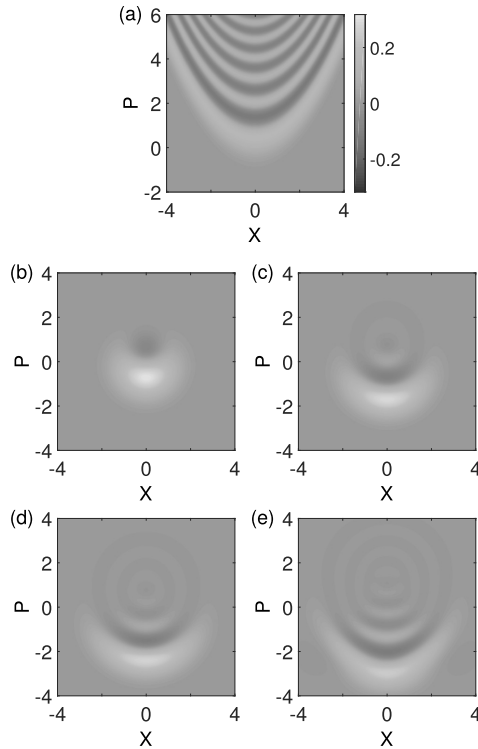Finally, we comment on determining requirements for the fidelity of the cubic gate and quality of the ancillae.

FIG. 5. Wigner functions of the optimal ancillary states. (a) The ideal cubic state for $\gamma = 0.1$ (expediently normalized over the displayed area), (b) $N = 1$, (c) $N = 3$, (d) $N = 5$, (e) $N = 9$. Note that the approximate states have offsets in the p direction, which can be compensated by p displacement.

In general, requirements for quantum gates and resources crucially depend on their applications, whose studies are still in rapid progress. One example of the requirements for resources is squeezing level of ancillary squeezed states. In CV quantum teleportation [36] of coherent states, one can confirm that the squeezing level of 20 dB in the entangled resource states results in 10^{-2} infidelity between the input and the output. While the CV regime has advantages in unconditional and deterministic quantum operations in actual experiments, this infidelity is not as good as we expect in exchange for the required energy compared to its discrete-variable (DV) counterparts. This drawback could be, however, reduced in hybrid quantum information processing where information is encoded in DV states and processed by CV operations [6]. In the case of the GKP encoding [9], it has been shown that no more than a 20.5-dB squeezing level in resource states of CV one-way quantum computing is enough to achieve a fault-tolerance threshold of 10^{-6} for a (conservative) qubit error-correction code [37,38]. Realization of the code has been

approached by 12.7-dB quantum-optical squeezing [39,40] and even 17.6-dB spin squeezing [41]. Furthermore, a recent study has shown that the fault-tolerance threshold of local depolarizing noise per qubit can be given by 13.6% [42], which is less strict. The above suggests that the same resources can result in achieving different error rates that differ by orders of magnitude depending on the applications, and more tractable requirements can be found by furthering the studies of quantum protocols. Similarly, requirements for the cubic gate are also expected to be settled in a practical way, but it is still an open question.

VI. CONCLUSION

We have introduced the concept of an adaptive non-Gaussian measurement: a CV measurement with a set of possible values, each of which is associated with a projection onto a non-Gaussian state. The measurement is realized by a pair of homodyne detectors and a supply of suitable non-Gaussian ancillary states. One particular advantage of this measurement is that an arbitrary Gaussian operation can be implemented on the soon-to-be-measured quantum system simply by tools of passive linear optics. In addition, some non-Gaussian operations can be implemented in the same way by making some of the measurement parameters dependent on already measured values.

To demonstrate this design feature, we have proposed a method of realizing the cubic gate [20]. The current proposal does not require active operations to be performed on the transformed quantum system, all of them being part of the non-Gaussian measurement, which significantly improves the feasibility of the setup. Specifically in the Heisenberg representation, it turns out that nonlinearity of the gate is created classically while the nonclassicality is given by the non-Gaussian ancilla in terms of reducing residual noise. By exploiting the noise term as a figure of merit, we have found a new class of ancillary states that promise better performance than the states of [21]. The final implementation of the complete cubic gate can be therefore expected soon.

APPENDIX A: CUBIC GATE WITH UNBALANCED ADAPTIVE NON-GAUSSIAN MEASUREMENT

By replacing BBS2 in Fig. 2 with an unbalanced beam splitter, we have another degree of freedom to effectively apply arbitrary squeezing operation onto the ancillary non-Gaussian state, as shown in Sec. III C. Thus, the Gaussian optimization discussed in Sec. V can be embedded in the cubic-gate schematic.

We explain here an input-output relationship of the cubic gate with unbalanced beam splitters. Transmittance and reflectance of the first beam splitter are represented as T_1 and $R_1 = 1 - T_1$, respectively. T_2 and R_2 are also defined in the same way for the second beam splitter. After the beam-splitter transformations, the quadratures of the output modes are

$$\hat{x}_0' = \sqrt{T_1}\hat{x}_0 - \sqrt{R_2}\hat{x}_1, \tag{A1a}$$

$$\hat{p}_0' = \sqrt{T_1}\hat{p}_0 - \sqrt{R_2}\hat{p}_1, \tag{A1b}$$

$$\hat{x}_1' = \sqrt{R_1 T_2}\hat{x}_0 + \sqrt{T_1 T_2}\hat{x}_1 - \sqrt{R_2}\hat{x}_2, \tag{A2a}$$

$$\hat{p}_1' = \sqrt{R_1 T_2}\hat{p}_0 + \sqrt{T_1 T_2}\hat{p}_1 - \sqrt{R_2}\hat{p}_2, \tag{A2b}$$

$$\hat{x}_2' = \sqrt{R_1 R_2}\hat{x}_0 + \sqrt{T_1 R_2}\hat{x}_1 + \sqrt{T_2}\hat{x}_2, \tag{A3a}$$

$$\hat{p}_2' = \sqrt{R_1 R_2}\hat{p}_0 + \sqrt{T_1 R_2}\hat{p}_1 + \sqrt{T_2}\hat{p}_2. \tag{A3b}$$

After measuring the x quadrature of mode $1'$ and obtaining value q, we set the phase factor

$$\theta = \arctan\left(\frac{6T_2\gamma}{\sqrt{R_2}}q\right). \tag{A4}$$

Then we measure the quadrature $\hat{x}_2' \sin\theta + \hat{p}_2' \cos\theta$ and obtain value y. The p quadrature of the unmeasured mode $0'$ can be expressed with the measured values q and y as

$$\begin{aligned}
\hat{p}_0' = {}& \frac{1}{\sqrt{T_1}}\hat{p}_0 - \frac{\sqrt{R_1}}{\sqrt{T_1 R_2}\cos\theta}y \\
& + \sqrt{\frac{R_1 T_2}{T_1 R_2}}\hat{p}_2 - 6\gamma\sqrt{\frac{R_1}{T_1}}\left(\frac{T_2}{R_2}\right)^{3/2}q^2 \\
& + \left(\frac{6R_1 T_2\gamma}{\sqrt{T_1}R_2^{3/2}}\hat{x}_0 + \frac{6\sqrt{R_1}T_2\gamma}{R_2^{3/2}}\hat{x}_1\right)q. \tag{A5}
\end{aligned}$$

We apply p displacement to this quadrature with value

$$p_{\text{disp}} = \frac{\sqrt{R_1}}{\sqrt{T_1 R_2}\cos\theta}y + \frac{3\gamma\sqrt{R_1 T_2}(T_2 - R_2)}{\sqrt{T_1}R_2^{3/2}}q^2 \tag{A6}$$

and obtain the output quadratures

$$\hat{x}_0'' = \sqrt{T_1}\left(\hat{x}_0 - \sqrt{\frac{R_1}{T_1}}\hat{x}_1\right), \tag{A7a}$$

$$\begin{aligned}
\hat{p}_0'' = {}& \frac{1}{\sqrt{T_1}}\left\{\left[\hat{p}_0 + 3\gamma\left(\frac{R_1 T_2}{R_2}\right)^{3/2}\hat{x}_0^2\right]\right. \\
& + \sqrt{\frac{R_1 T_2}{R_2}}\left(\hat{p}_2 - 3\gamma\hat{x}_2^2\right) \\
& \left. + 6\gamma R_1\sqrt{T_1}\left(\frac{T_2}{R_2}\right)^{3/2}\left(\hat{x}_0\hat{x}_1 + \frac{1}{2}\sqrt{\frac{T_1}{R_1}}\hat{x}_1^2\right)\right\}. \tag{A7b}
\end{aligned}$$

We can see that the outputs are equal to Eq. (23) if we set $T_1 = R_1 = T_2 = R_2 = 1/2$. Note that, if we use unbalanced beam splitters, the displacement has a quadratic term as shown in Eq. (A6).

To explicitly see how the transmittances of the beam splitters affect on the quadratures of the ancillary non-Gaussian state, we scale the strength of cubic nonlinearity γ to $(R_2/R_1 T_2)^{3/2}\gamma$. The output p quadrature (A7b) is then expressed as

$$\begin{aligned}
\hat{p}_0'' = {}& \frac{1}{\sqrt{T_1}}\left\{\left(\hat{p}_0 + 3\gamma\hat{x}_0^2\right)\right. \\
& + \left[\sqrt{\frac{R_1 T_2}{R_2}}\hat{p}_2 - 3\gamma\left(\sqrt{\frac{R_2}{R_1 T_2}}\hat{x}_2\right)^2\right] \\
& \left. + 6\gamma\sqrt{\frac{T_1}{R_1}}\left(\hat{x}_0\hat{x}_1 + \frac{1}{2}\sqrt{\frac{T_1}{R_1}}\hat{x}_1^2\right)\right\}. \tag{A8}
\end{aligned}$$

The second term represents the nonlinear noise determined by the non-Gaussian measurement. We can see that the ancilla is effectively squeezed by the squeezing factor $\sqrt{R_1 T_2/R_2}$, which can be fully controlled by choosing transmittance of the second beam splitter. While universal squeezing operation in actual experiments [14,18,19] adds non-negligible noise to the input state because of finite squeezing in its resource state, the effective squeezing in the heterodyne measurement does not require additional resource states, which helps in the preparation of the approximate cubic state with high purity.

APPENDIX B: NUMERICAL METHOD OF APPROXIMATING PHOTON-NUMBER SUPERPOSITION TO THE CUBIC STATE

In Sec. V, we considered the variance $V(\hat{p}_{\text{NLQ}})$ as a figure of merit to approximate the cubic state with photon-number-superposition states up to certain photon level and squeezing. Intuitively, the approximation can be done by numerically optimizing all of the coefficients of a superposition state and the squeezing level, but it often leads to locally optimum solutions, especially when increasing the upper limit of photon numbers. Here we reduce the problem into optimization with two variables, regardless of the size of the Hilbert space. With each set of the two variables, an optimized superposition state can be derived as an eigenstate of the minimum eigenvalue of a certain positive-semidefinite operator. By numerically creating a minimum-search map with the two variables, we can make sure that the solution is almost certainly the true optimum one. The method is a variation of the classical variance-minimization problem [43].

Suppose $\mathcal{H}_N$ is a $(N + 1)$-dimensional Hilbert space up to the N-photon level, and $|\psi\rangle$ is a state in $\mathcal{H}_N$. Our purpose is to find a set of the optimum state $|\psi\rangle$ and the optimum parameter λ' that minimizes the variance of the nonlinear quadrature $\hat{y}(\lambda') = \lambda'\hat{p} - 3(\hat{x}/\lambda')^2$. This problem can be written as

$$\min_{\substack{|\psi\rangle \in \mathcal{H}_N \\ \lambda' \in \mathbb{R}}} V(|\psi\rangle, \lambda'), \tag{B1a}$$

$$V(|\psi\rangle, \lambda') = \langle\psi|[\hat{y}(\lambda') - \langle\hat{y}(\lambda')\rangle]^2|\psi\rangle, \tag{B1b}$$

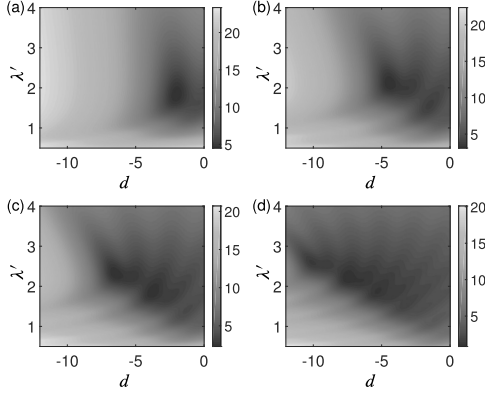where $\langle\hat{y}(\lambda')\rangle$ is the expectation value $\langle\psi|\hat{y}(\lambda')|\psi\rangle$.

FIG. 6. Minimum-search map: (a) $N = 1$, (b) $N = 3$, (c) $N = 5$, (d) $N = 9$. The values are normalized by shot noise level and shown in dB scale.

To make this problem digestible, we alternatively consider another minimization problem. Let d be a real number. We then replace the expectation value in Eq. (B1b) with d and set a new evaluation function,

$$Z(|\psi\rangle,\lambda',d) = \langle\psi|[\hat{y}(\lambda') - d]^2|\psi\rangle. \qquad (B2)$$

Next we introduce another evaluation function $W(d)$ defined as minimum of $Z(|\psi\rangle,\lambda',d)$ with respect to $|\psi\rangle \in \mathcal{H}_N$ and $\lambda' \in \mathbb{R}$. This can be expressed as

$$W(d) = \min_{\substack{|\psi\rangle \in \mathcal{H}_N \\ \lambda' \in \mathbb{R}}} Z(|\psi\rangle,\lambda',d). \qquad (B3)$$

Suppose $W(d)$ is minimum when $d = d^\star$. In addition, suppose $Z(|\psi\rangle,\lambda',d^\star)$ is minimum when $|\psi\rangle = |\psi^\star\rangle$ and $\lambda' = \lambda'^\star$. Then we can say that the set $(|\psi^\star\rangle,\lambda'^\star)$ is the true optimum set that minimizes $V(|\psi\rangle,\lambda')$. This is verified as follows. Let

$\langle\hat{y}(\lambda')\rangle^\star$ be the expectation value $\langle\psi^\star|\hat{y}(\lambda')|\psi^\star\rangle$. Then

$$Z(|\psi^\star\rangle,\lambda'^\star,d^\star) \leqslant W(\langle\hat{y}(\lambda'^\star)\rangle^\star)$$
$$\leqslant Z(|\psi^\star\rangle,\lambda'^\star,\langle\hat{y}(\lambda'^\star)\rangle^\star) \qquad (B4)$$

and consequently $(\langle\hat{y}(\lambda'^\star)\rangle^\star - d^\star)^2 \leqslant 0$, which means $d^\star = \langle\hat{y}(\lambda'^\star)\rangle^\star$. Therefore, for any $|\psi\rangle \in \mathcal{H}_N$, any $\lambda' \in \mathbb{R}$, and the corresponding expectation value $\langle\hat{y}(\lambda')\rangle = \langle\psi|\hat{y}(\lambda')|\psi\rangle$, it holds that

$$V(|\psi^\star\rangle,\lambda'^\star) = W(d^\star)$$
$$\leqslant W(\langle\hat{y}(\lambda')\rangle) \leqslant Z(|\psi\rangle,\lambda',\langle\hat{y}(\lambda')\rangle) = V(|\psi\rangle,\lambda'), \qquad (B5)$$

which means $V(|\psi^\star\rangle,\lambda'^\star)$ is minimum. As a result, the problem can be solved by searching for a state that minimizes $Z(|\psi\rangle,\lambda',d)$ with every λ' and d.

The point is that $Z(|\psi\rangle,\lambda',d)$ is a quadratic form, and therefore each optimum state is determined as an eigenstate of the minimum eigenvalue of $[\hat{y}(\lambda') - d]^2$ represented by the limited Hilbert space. In the case that we look for the optimum state up to the N-photon level, the matrix representation of $[\hat{y}(\lambda') - d]^2$ reads

$$Y(\lambda',d) = \sum_{m,n=0}^{N} Y_{mn}(\lambda',d)|m\rangle\langle n|, \qquad (B6)$$

$$Y_{mn}(\lambda',d) = \langle m|[\hat{y}(\lambda') - d]^2|n\rangle, \qquad (B7)$$

and the optimum state in terms of (λ',d) is found as the eigenstate of the minimum eigenvalue of the matrix $Y(\lambda',d)$, which can be deterministically obtained by numerical calculation. This implies that the problem is now broken down into a two-variable optimization problem. We can create a minimum-search map $\min_{|\psi\rangle \in \mathcal{H}_N} Z(|\psi\rangle,\lambda',d)$ with respect to λ' and d, which makes it easy to look for the true optimum solution.

Figure 6 shows some examples of the map used to derive the optimized superposition states in Fig. 5. We can see that the number of local minima increases as the upper limit of photon numbers becomes larger. By choosing suitable ranges and resolutions of (λ',d), we almost certainly find the true minimum and, consequently, the true optimized state.

[1] M. A. Nielsen and I. L. Chuang, *Quantum Computation and Quantum Information* (Cambridge University Press, Cambridge, UK, 2000).

[2] J. L. O'Brien, G. J. Pryde, A. G. White, T. C. Ralph, and D. Branning, Nature (London) **426**, 264 (2003).

[3] F. Schmidt-Kaler, H. Häffner, M. Riebe, S. Gulde, G. P. T. Lancaster, T. Deuschle, C. Becher, C. F. Roos, J. Eschner, and R. Blatt, Nature (London) **422**, 408 (2003).

[4] J. H. Plantenberg, P. C. de Groot, C. J. P. M. Harmans, and J. E. Mooij, Nature (London) **447**, 836 (2007).

[5] C. Zu, W. B. Wang, L. He, W. G. Zhang, C. Y. Dai, F. Wang, and L. M. Duan, Nature (London) **514**, 72 (2014).

[6] A. Furusawa and P. van Loock, *Quantum Teleportation and Entanglement: A Hybrid Approach to Optical Quantum Information Processing* (Wiley-VCH, Weinheim, 2011).

[7] S. Lloyd and S. L. Braunstein, Phys. Rev. Lett. **82**, 1784 (1999).

[8] S. Sefi and P. van Loock, Phys. Rev. Lett. **107**, 170501 (2011).

[9] D. Gottesman, A. Kitaev, and J. Preskill, Phys. Rev. A **64**, 012310 (2001).

[10] S. D. Bartlett and B. C. Sanders, Phys. Rev. A **65**, 042304 (2002).

[11] S. Ghose and B. C. Sanders, J. Mod. Opt. **54**, 855 (2007).

[12] M. Sasaki, K. Wakui, J. Mizuno, M. Fujiwara, and M. Akiba, in *Quantum Communication, Measurement and Computing*, edited by S. M. Barnett *et al.* (American Institute of Physics, New York, 2004), pp. 44–47.

[13] K. Marshall, R. Pooser, G. Siopsis, and C. Weedbrook, Phys. Rev. A **91**, 032321 (2015).

[14] J. Yoshikawa, T. Hayashi, T. Akiyama, N. Takei, A. Huck, U. L. Andersen, and A. Furusawa, Phys. Rev. A **76**, 060301(R) (2007).

[15] J. Yoshikawa, Y. Miwa, A. Huck, U. L. Andersen, P. van Loock, and A. Furusawa, Phys. Rev. Lett. **101**, 250501 (2008).

[16] J. Yoshikawa, Y. Miwa, R. Filip, and A. Furusawa, Phys. Rev. A **83**, 052307 (2011).

[17] R. Filip, P. Marek, and U. L. Andersen, Phys. Rev. A **71**, 042308 (2005).

[18] Y. Miwa, J. Yoshikawa, N. Iwata, M. Endo, P. Marek, R. Filip, P. van Loock, and A. Furusawa, Phys. Rev. Lett. **113**, 013601 (2014).

[19] K. Miyata, H. Ogawa, P. Marek, R. Filip, H. Yonezawa, J. Yoshikawa, and A. Furusawa, Phys. Rev. A **90**, 060302(R) (2014).

[20] P. Marek, R. Filip, and A. Furusawa, Phys. Rev. A **84**, 053802 (2011).

[21] M. Yukawa, K. Miyata, H. Yonezawa, P. Marek, R. Filip, and A. Furusawa, Phys. Rev. A **88**, 053816 (2013).

[22] J. Yoshikawa, K. Makino, S. Kurata, P. van Loock, and A. Furusawa, Phys. Rev. X **3**, 041028 (2013).

[23] E. Bimbard, R. Boddeda, N. Vitrant, A. Grankin, V. Parigi, J. Stanojevic, A. Ourjoumtsev, and P. Grangier, Phys. Rev. Lett. **112**, 033601 (2014).

[24] H. Ogawa, H. Ohdan, K. Miyata, M. Taguchi, K. Makino, H. Yonezawa, J. Yoshikawa, and A. Furusawa, arXiv:1507.06172.

[25] Y. Miwa, J. Yoshikawa, P. van Loock, and A. Furusawa, Phys. Rev. A **80**, 050303(R) (2009).

[26] N. C. Menicucci, P. van Loock, M. Gu, C. Weedbrook, T. C. Ralph, and M. A. Nielsen, Phys. Rev. Lett. **97**, 110501 (2006).

[27] M. Gu, C. Weedbrook, N. C. Menicucci, T. C. Ralph, and P. van Loock, Phys. Rev. A **79**, 062318 (2009).

[28] E. Bimbard, N. Jain, A. MacRae, and A. I. Lvovsky, Nat. Photon. **4**, 243 (2010).

[29] M. Yukawa, K. Miyata, T. Mizuta, H. Yonezawa, P. Marek, R. Filip, and A. Furusawa, Opt. Express **21**, 5529 (2013).

[30] C. Weedbrook, S. Pirandola, R. García-Patrón, N. J. Cerf, T. C. Ralph, J. H. Shapiro, and S. Lloyd, Rev. Mod. Phys. **84**, 621 (2012).

[31] D. Menzies and R. Filip, Phys. Rev. A **79**, 012313 (2009).

[32] S. Singh, G. A. Phelps, D. S. Goldbaum, E. M. Wright, and P. Meystre, Phys. Rev. Lett. **105**, 213602 (2010).

[33] O. Romero-Isart, M. L. Juan, R. Quidant, and J. I. Cirac, New J. Phys. **12**, 033015 (2010).

[34] O. Romero-Isart, A. C. Pflanzer, M. L. Juan, R. Quidant, N. Kiesel, M. Aspelmeyer, and J. I. Cirac, Phys. Rev. A **83**, 013803 (2011).

[35] R. Filip and A. A. Rakhubovsky, Phys. Rev. A **92**, 053804 (2015).

[36] S. Pirandola, J. Eisert, C. Weedbrook, A. Furusawa, and S. L. Braunstein, Nat. Photon. **9**, 641 (2015).

[37] N. C. Menicucci, Phys. Rev. Lett. **112**, 120504 (2014).

[38] J. Preskill, Proc. R. Soc. London, Ser. A **454**, 385 (1998).

[39] T. Eberle, S. Steinlechner, J. Bauchrowitz, V. Händchen, H. Vahlbruch, M. Mehmet, H. Müller-Ebhardt, and R. Schnabel, Phys. Rev. Lett. **104**, 251102 (2010).

[40] M. Mehmet, S. Ast, T. Eberle, S. Steinlechner, H. Vahlbruch, and R. Schnabel, Opt. Express **19**, 25763 (2011).

[41] J. Thompson, in *12th US-Japan Seminar* (Madison, Wisconsin, 2015).

[42] M. Zwerger, H. J. Briegel, and W. Dür, J. Sci. Rep. **4**, 5364 (2014).

[43] X. Cai, Appl. Math. Lett. **6**, 97 (1993).